Profiling Purification Dependent Sample Composition and Phosphorylation of the CNG Ion Channel

Inaugural-Dissertation
zur Erlangung des Doktorgrades
der Mathematisch-Naturwissenschaftlichen Fakultät
der Universität zu Köln

vorgelegt von

Christoph Klatt
aus Eckernförde, Deutschland

Bonn, September 2021

Aus dem Institut für Biochemie
der Universität zu Köln

1. Gutachter: **Professor Dr. Elmar Behrmann**

2. Gutachter: **Professor Dr. Günter Schwarz**

Vorsitzende: **Professorin Dr. Stephanie Kath-Schorr**

Tag der mündlichen Prüfung: 03.12.2021

Eidesstattliche Erklärung:

Hiermit versichere ich an Eides statt, dass ich die vorliegende Dissertation selbstständig und ohne die Benutzung anderer als der angegebenen Hilfsmittel und Literatur angefertigt habe. Alle Stellen, die wörtlich oder sinngemäß aus veröffentlichten und nicht veröffentlichten Werken dem Wortlaut oder dem Sinn nach entnommen wurden, sind als solche kenntlich gemacht. Ich versichere an Eides statt, dass diese Dissertation noch keiner anderen Fakultät oder Universität zur Prüfung vorgelegen hat; dass sie - abgesehen von unten angegebenen Teilpublikationen und eingebundenen Artikeln und Manuskripten - noch nicht veröffentlicht worden ist sowie, dass ich eine Veröffentlichung der Dissertation vor Abschluss der Promotion nicht ohne Genehmigung des Promotionsausschusses vornehmen werde. Die Bestimmungen dieser Ordnung sind mir bekannt. Darüber hinaus erkläre ich hiermit, dass ich die Ordnung zur Sicherung guter wissenschaftlicher Praxis und zum Umgang mit wissenschaftlichem Fehlverhalten der Universität zu Köln gelesen und sie bei der Durchführung der Dissertation zugrundeliegenden Arbeiten und der schriftlich verfassten Dissertation beachtet habe und verpflichte mich hiermit, die dort genannten Vorgaben bei allen wissenschaftlichen Tätigkeiten zu beachten und umzusetzen. Ich versichere, dass die eingereichte elektronische Fassung der eingereichten Druckfassung vollständig entspricht.

Christoph Klatt
Bonn, den 21.09.2021

Contents

Summary

The flow of ions across the plasma membrane is one of the fundamental processes in living cells. Ion channels aid in regulating the flow of ions along the electrochemical gradient and are essential for sensory signal transduction events. In the retina of the eye, Cyclic Nucleotide Gated (CNG) ion channels are located in rod photoreceptors, where they are crucial for vertebrate vision by producing a dark-current that ceases upon light detection. Unlike most ion channels of the voltage-gated ion channel superfamily, CNG channel cation conductance is primarily activated upon binding of cyclic nucleotides (e.g. cyclic Guanosine Monophosphate).

The heterotetrameric CNG channel in bovine rod outer segments comprises three A1 and one B1 subunit. The downregulation of CNG channel activity via the Ca^{2+}-dependent Calmodulin (CaM) binding to the B1 subunit is evident, but not all underlying structural mechanisms are understood. Although phosphorylations have been shown to modulate the activity of other related ion channels, only few studies have attempted to investigate potential phosphorylation sites in CNG channels, and information on the phosphorylation of endogenous CNG channels is particularly sparse.

We used two orthogonal affinity-based strategies to purify endogenous CNG channels from bovine rod outer segments and performed Mass Spectrometry (MS) to analyse sample composition and localise phosphorylation sites in CNG channels. Moreover, we employed Negative Staining-Electron Microscopy (Negative Staining-EM) to evaluate the purified protein regarding sample quality and structural integrity.

We have successfully characterised the purified CNG channels and show subunit composition, stoichiometry, and tetrameric organisation in line with our expectations. Protein identification and quantification in MS-driven analysis revealed distinct protein populations obtained by the two purification strategies, with about a third of proteins unique to either purification strategy. Among the common proteins, we identified several known or suspected interaction partners. The presence of these proteins in relatively high abundance suggests a fraction of CNG channels is purified in a multimeric protein assembly.

In addition, we present the first comprehensive phosphorylation analysis of endogenous bovine CNG channels from rod photoreceptors. We observed phosphorylations that may be relevant in the heterotetrameric assembly, interaction with other proteins, and characteristic modulation mechanism of the CNG ion channels.

Zusammenfassung

Der Fluss verschiedener Ionen durch die Zellmembran stellt einen fundamentalen Prozess in lebenden Zellen dar. Ionenkanäle helfen dabei, den Fluss von Ionen entlang des elektrochemischen Gradienten zu regulieren und sind für die Signaltransduktion von wesentlicher Bedeutung. In der Netzhaut des Auges befinden sich die CNG (Cyclic Nucleotide Gated) Ionenkanäle in den Stäbchenzellen und sind dort für das Sehvermögen von Wirbeltieren entscheidend. In der Dunkelheit erlauben die CNG-Kanäle einen kontinuierlichen Einstrom von Kationen, der bei Lichteinfall unterbrochen wird. Entgegen des Großteils der Familienmitglieder spannungsaktivierter Ionenkanäle, werden CNG-Kanäle durch zyklische Nukleotide (z. B. zyklisches Guanosinmonophosphat) für den Einstrom von Kationen geöffnet.

Die CNG-Kanäle in den Stäbchenzellen von Rindern sind Heterotetramere und setzen sich aus drei A1- und einer B1-Untereinheit zusammen. Die reduzierte Aktivität des CNG Kanals in Folge der kalziumabhängigen Bindung von Calmodulin an die B1 Untereinheit ist bekannt, aber die zugrunde liegenden strukturellen Mechanismen sind nicht vollständig verstanden. Obwohl gezeigt wurde, dass Phosphorylierungen die Aktivität verwandter Proteine modulieren, thematisieren nur wenige Studien die mögliche Phosphorylierung von CNG-Kanälen und insbesondere für endogene CNG-Kanäle sind Informationen nicht verfügbar.

Wir haben zwei orthogonale affinitätsbasierte Strategien verwendet, um CNG-Kanäle aus den Außensegmenten der Stäbchen aufzureinigen. Des Weiteren haben wir Massenspektrometrie (MS) verwendet, um die Zusammensetzung der aufgereinigten Probe zu analysieren und Orte der Phosphorylierung in CNG-Kanälen zu lokalisieren. Außerdem haben wir, unter anderem mit Hilfe der Negativkontrast-Elektronenmikroskopie, das gereinigte Protein im Hinblick auf Probenqualität und strukturelle Integrität evaluiert.

Unsere Charakterisierungen zeigen, dass die von uns aufgereinigten CNG-Kanäle unsere Erwartungen an Zusammensetzung, Stöchiometrie und Organisation der Untereinheiten als Tetramer erfüllen. Die Identifizierung und Quantifizierung von Proteinen im Rahmen unserer MS-basierten Analyse ergab zwei charakteristische Proteinpopulationen, die durch die beiden Aufreinigungsstrategien gewonnen wurden, wobei je etwa ein Drittel aller Proteine in nur einer der Aufreinigungsstrategien präsent ist. Unter den gemeinsamen Proteinen finden sich bekannte und mutmaßliche Interaktionspartner von CNG-Kanälen. Die Anwesenheit dieser Proteine in relativ großer Menge deutet darauf hin, dass ein Teil der CNG-Kanäle in einem multimeren Proteinverbund aufgereinigt wird.

Darüber hinaus präsentieren wir die erste umfassende Analyse von Phosphorylierungen der endogenen CNG-Kanäle aus Stäbchenzellen der Netzhaut. Wir haben dabei Phosphorylierungen identifiziert, die möglicherweise für den Aufbau des heterotetrameren Ionenkanals, die Interaktion mit anderen Proteinen und den charakteristischen Modulationsmechanismus von Bedeutung sein könnten.

1 Introduction

Members of the Voltage-Gated Ion Channel (VGIC) superfamily are present in neuronal, muscular, or sensory tissue membranes. They generally conduct ions in response to a change in membrane potential and range from Voltage-Gated Potassium (K_v), Sodium (Na_v), and Calcium (Ca_v) channels to Transient Receptor Potential (TRP) channels (Catterall, 2000; F. H. Yu & Catterall, 2004). Cyclic Nucleotide-Gated ion channels (CNG channels) are a VGIC family member distinguished by a diverging activation/gating mechanism (Z. Wang et al., 2007). CNG channels are characterised by an activation mechanism that depends on the direct binding of the cyclic nucleotides cyclic Guanosine Monophosphate (cGMP) or cyclic Adenosine Monophosphate (cAMP) (Fesenko et al., 1985). They can be found in vertebrates and some invertebrate species like *Caenorhabditis elegans* (Coburn & Bargmann, 1996; Kaupp & Seifert, 2002; Komatsu et al., 1996). CNG channels have been best studied in neuronal tissue, such as Olfactory Sensory Neurons (OSN) and photoreceptors (Ahmad et al., 1994; Bönigk et al., 1999; Bradley et al., 1997; Kaupp & Seifert, 2002; Körschen et al., 1995; Strijbos et al., 1999).

1.1 CNG Channels of the Vertebrate Rod Photoreceptors

Photoreceptors are the photosensitive part of the nervous tissue in the retina of the eye. The two main types of photoreceptors are rods and cones. Cones distinguish between light of different wavelengths and are responsible for vision in bright light. On the other hand, rods are more sensitive to light and are responsible for vision in dim light (Luo et al., 2009; Yau, 1994). A rod photoreceptor can be divided into at least four morphologically distinct areas, namely the cell body, the synaptic terminal, the Inner Segment (IS), and the Outer Segment (OS) (Figure 1 A). The cell body contains the nucleus and is the place of biosynthesis. As part of the neurological tissue, rods have a synaptic terminal that projects onto bipolar cells. The IS is adjacent to the cell body and is filled with mitochondria, providing energy for the cell. Finally, the OS contains a stack of ordered discs encompassed by the plasma membrane. Each disc membrane is filled with Rhodopsin and other proteins relevant for sensing photons (Biel & Michalakis, 2009; Fesenko et al., 1985; Kaupp & Seifert, 2002; Matulef & Zagotta, 2003; Wensel et al., 2016). While CNG expression and translation occur in the cell body, the mature CNG channel is located in the plasma membrane of the Rod Outer Segment (ROS) (Maity et al., 2015; Wohlfart et al., 1992).

The overall function of CNG channels is to translate changes in intracellular cGMP concentrations into a change in membrane potential. In the absence of light, the secondary messenger cGMP is present in relatively high concentrations because it is generated by the constantly active Guanylate Cyclase (GC). cGMP binds directly to CNG channels, thereby maintains their open state, and facilitates a nonselective influx of cations. Due to the concentration gradients, mostly Na^+ and Ca^{2+} ions flow into the cell. As a result, the plasma

membrane is depolarized, and the photoreceptor releases neurotransmitters at the synaptic terminal (Figure 1 B, dark state). The light-induced activation of Rhodopsin is the starting point of the phototransduction cascade, which results in a drop in the local cGMP concentration by activation of Phosphodiesterases (PDE6). Consequently, the low cGMP concentration leads to an inactivation of CNG channels, ceasing the ion influx, and the rod photoreceptor hyperpolarizes, ceasing the neurotransmitter release (Figure 1 B, light state).

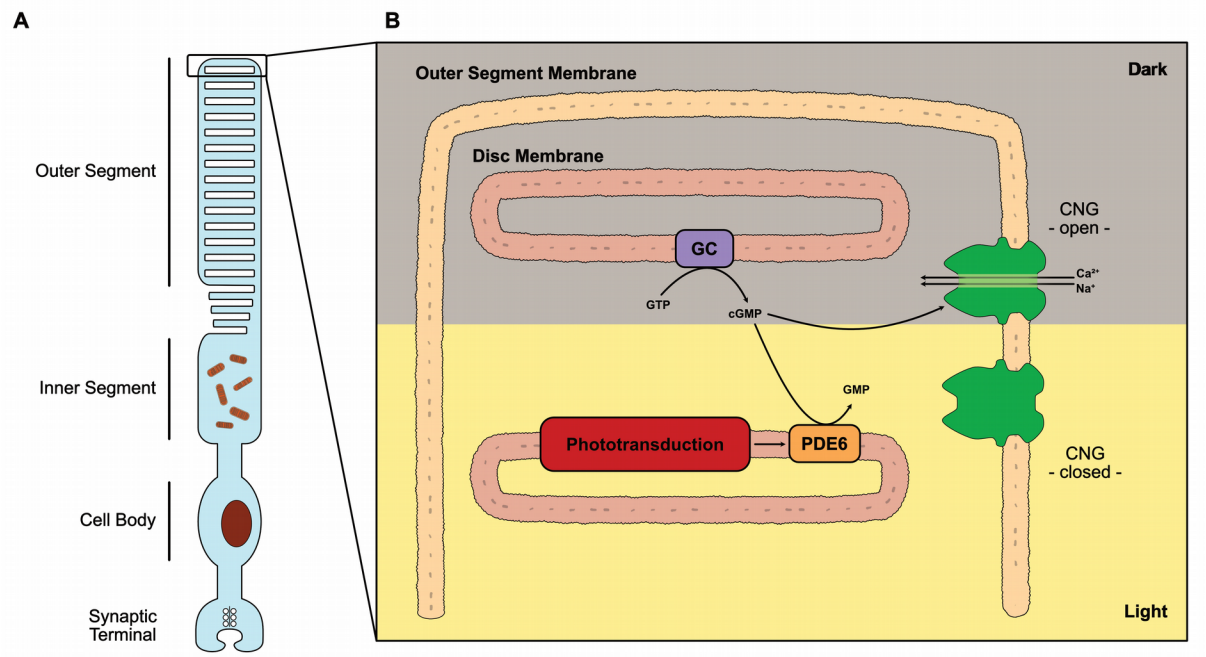

Figure 1: Localisation and cellular context of CNG channels in rod photoreceptors

(A) Morphology of rod photoreceptors. Outer Segment (OS) with discs, Inner Segment (IS) containing mitochondria, cell body with nucleus and synaptic terminal. (B) Simplified mechanism depicting the flow of dark current in photoreceptors and the closing of Cyclic Nucleotide-Gated ion channel (CNG) upon activation of the phototransduction cascade. In the dark, the Guanylate Cyclase (GC) in the disc membrane produces the cyclic nucleotide cGMP from Guanosine Triphosphate (GTP). cGMP binds to CNG channels in the plasma membrane and keeps them open. The cation influx depolarizes the plasma membrane, and neurotransmitter is released. In the presence of light, the phototransduction cascade is activated, which in turn activates Phosphodiesterases 6 (PDE6), and cGMP is hydrolysed. The reduced cGMP concentration is insufficient to keep CNG channels open, the cation influx is stopped and the plasma membrane hyperpolarises.

The role of CNG channels is understood to a degree where the primary function and mechanisms are known, but open questions remain. For example, the structural arrangement of subunits of the native channel is yet to be established. A structural investigation by neither X-ray crystallography nor cryo-EM has successfully revealed the atomic model and interactions of the A1 and B1 subunit. Furthermore, the intricacies of CNG channel modulation are not yet clear. Although CNG channels are reasonably well characterised, they still hold some mystery in crucial aspects of function - a situation presenting challenges and worthwhile explorations alike.

1.2 Biochemistry of Protein Purification

Proteins are one of the major groups of macromolecules that living organisms rely upon. They consist of a string of covalently linked amino acids, and this sequence defines the primary structure of a protein (or peptide). Secondary-, tertiary- and in some cases a quarternary- structural organisation rely on interactions such as hydrogen bonds, ionic bonds, or van der Waals forces and are usually reversible (Berg et al., 2018). These non-covalent interactions in higher order structural organisations allow for conformational changes. Proteins can be found in all compartments of an organism, and the majority are soluble in aqueous solutions due to hydrophilic amino acids on the protein surface. Soluble proteins can diffuse freely, be held in place by an anchor or interaction partner, subjected to directional transport through the cell, or be part of the cytoskeleton. The membrane proteins (MP) represent the other fraction besides soluble proteins. They account for about one-third of the total proteins in the cell and are associated with (peripheral MP) - or spanning the double layer of lipids (integral MP) (Wallin & Von Heijne, 1998). As part of biological membranes, MPs may exercise functions similar to soluble proteins or have unique functions directly tied to the properties of a membrane. Being part of a membrane also comes with unique requirements to the MPs. The hydrophobic area inside the membrane dictates some hydrophobic domains on the surface of the protein.

The primary motivation in protein purification is to separate a specific protein or protein complex from other proteins and other cellular components. Depending on further experimental requirements, the activity and structure of the purified protein may have to be maintained. The beginnings of protein purification were of academic motivation, but latest in the 1940s, the purification of proteins from blood serum was of importance beyond scientific curiosity (Cohn et al., 1946; R.K. Scopes, 2002). The unifying principle of all protein purifications lies in obtaining protein in a sufficient amount and adequate purity for the intended use. Preparative purifications of proteins are usually used in an industrial context when a large volume of protein has to be prepared with high purity and few limitations to the time scale. Analytical purifications usually follow a limited time frame and aim at a relatively low volume of protein because the primary purpose is to provide material for analytical techniques (Ward, 2012a). Many principles find use in both approaches. In the context of this thesis, however, the focus will be on analytical purification techniques. Downstream analytical studies may characterise the function under different circumstances, identify variances and modifications, determine the atomic structure, or map interaction partners (ions, ligands, proteins). Such analytical techniques may have their specific prerequisites, such as sufficient protein concentration, that must be considered when setting up the purification.

Hundreds of fully sequenced genomes and thousands of genes were discovered in projects such as the “human genome project” (Shendure & Aiden, 2012). With the vast genetic

information at hand, molecular biology emerged to describe and understand three-dimensional structures. Computational methods develop rapidly but still fail to predict atomic models for the more challenging proteins (Callaway, 2020). For the experimental characterisation and determination of a protein structure, the presence of purified protein is mandatory, and challenging proteins also elude the experimental approaches.

1.2.1 Expression Systems

DNA contains genes that encode for the sequence of proteins and further information relevant for the transcription. For example, a promoter controls the transcription of a gene and determines the amount of protein produced. Some proteins lead to a specific phenotype that defines the properties of an organism. The term “gene expression” is used to describe the process of obtaining a product from a gene, which may be a protein. When messenger RNA (mRNA) is the result of transcription, then a protein is produced in a process called translation. In higher organisms, additional steps increase the diversity of proteins, often in response to the cellular environment. Alternative splicing takes place between transcription and translation that enables the production of multiple proteins from one gene. After translation, folding (possibly supported by chaperones or in parallel to translation) and post-translational modifications (PTM), like phosphorylations, are established (Figure 2).

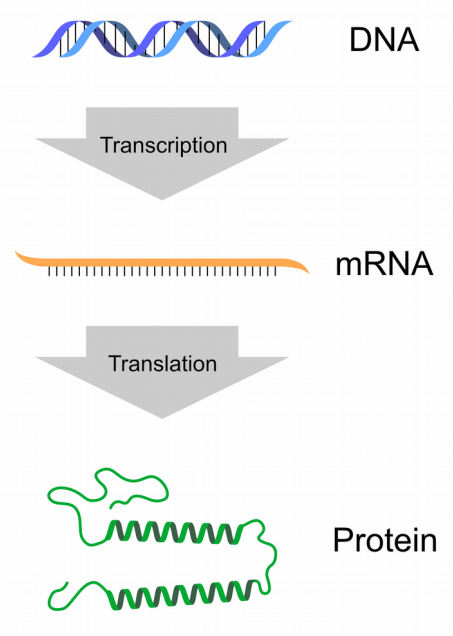

Figure 2: Principle of protein biosynthesis

DNA contains genetic instructions required for building proteins, and protein synthesis starts with transcription of the respective gene into messenger RNA (mRNA) (RNA synthesis). Subsequently, mRNA may undergo post-transcriptional modifications (e.g., alternative splicing). In the following translation, the mRNA sequence is translated into a chain of amino acids (protein synthesis). Finally, the protein typically undergoes folding and may be subject to post-translational modifications (e.g., phosphorylation).

The first (native) proteins that were purified were easily accessible due to their abundance and resilience. For functional and structural studies this is advantageous because of the inherent mechanisms present in the cell supporting protein folding and systems executing quality control (Mogk & Bukau, 2006). Nevertheless, most proteins are characterised by low expression levels in the cell and are consequently less accessible. Molecular cloning techniques enable changes in the DNA sequence (recombinant DNA), thereby increasing the accessibility of proteins in different ways. On the one hand, immediate changes in a gene encoding a protein modifies the protein sequence (recombinant protein). On the other hand, changes in the upstream or downstream of the gene can be used to control the protein expression. Furthermore, due to molecular cloning techniques the expression host is not limited to the original host cell, tissue, or organism. The combination of molecular cloning techniques and improved purification techniques increased the number of accessible proteins significantly (Gräslund et al., 2008; Pandey et al., 2016).

The following sections introduce the major approaches for obtaining proteins briefly, and their respective main advantages and disadvantages are discussed. Furthermore, Figure 3 illustrates the distribution of proteins used in structural biology (PDB, rcsb.org), including the source (native source or non-native expression, Figure 3 A) and details the host organism for each of the sources (Figure 3 B and C) (Berman et al., 2000).

1.2.1.1 Recombinant Proteins and their Expression

DNA can be modified in many ways, and “molecular cloning” is a collective term for techniques that can create recombinant DNA. The discovery of the CRISPR/Cas9 system from bacteria and the subsequent development of techniques that utilize this system improved the ability to edit the genome significantly. This development was revolutionary for modifying the genetics of mammalian organisms (Doudna & Charpentier, 2014; Manghwar et al., 2019).

Changes in the genome can be limited to parts of the DNA outside the protein sequence (Hunter et al., 2019). This way, specific promoters can enhance the expression levels (and patterns), and inducible gene expression bestows scientists even more control. However, the over-expression will eventually become a burden for the host cell, and specialised systems, such as the restrained expression, are required to balance the impact of toxic proteins (Eguchi et al., 2018; Narayanan et al., 2011). Especially membrane proteins and ion channels are often toxic to a cell when expression levels are elevated (Bernaudat et al., 2011; Stoebel et al., 2008).

If a gene sequence is modified, leading to a change in the protein sequence, then the protein is referred to as “recombinant protein”. Changes in the gene allow for mutational studies (Morbœuf et al., 2000) or the analysis of domains or truncated proteins (Novák, 1994). However, adding tags, functional groups, or reporters grants the protein with additional interesting characteristics used in the purification or as tools in functional studies

(Gileadi, 2017; P. Lee & Hruby, 1997; Y. Wang et al., 2019; Young et al., 2012). Even the fusion of the Protein Of Interest (POI) with another protein is possible and can be used, for example, in protein-protein interaction studies (Kaniyappan et al., 2020; Yao et al., 2018).

Another aspect that recombinant methods can influence is the localisation of a protein. Peptides near the amino terminus of a synthesized protein often act as a signal that defines the localisation within a cell by inducing insertion into a membrane or transport into a specific cell organelle. Thus, the location of a protein impacts accessibility and determines the purification steps that follow. In secretion, the proteins can be harvested from the media resulting in lower costs or reduced cell toxicity (Lodish et al., 2000; Mergulhão et al., 2005; Rapoport, 2007).

1.2.1.2 Homologous Expression

The phrase homologous expression is used as long as the POI is (over-) expressed in the original host organism. Apparent advantages of homologous expression are the potential to increase the expression level while relying on all the established mechanisms such as folding or maturation. However, as valid for all other expression techniques, eventually, over-expression leads to an increased risk of aggregation, misfolding, and finally exhaustion of the cells.

Homologous expression is performed under specific circumstances when the native POI lacks a desired characteristic and a recombinant protein is needed, but switching the host organism would impact an essential attribute of the analysed POI. One example of such an attribute that requires expression in a specific host is glycosylation (Chung et al., 2015).

1.2.1.3 Heterologous Expression

Changing the host organism requires the gene of interest to be inserted into the new cell, either for a limited period for transient expression or as part of the genome for a permanent expression and creation of a stable cell line. Naturally, it requires molecular cloning of the DNA to achieve such a transient or transgenic transfer of the (recombinant) DNA to a new host cell (C. Y. Chen et al., 1984). Such systems where a gene is expressed in a foreign host are heterologous expressions (Duquesne et al., 2016). One significant advantage of heterologous expression systems is the transition from an animal (as a host) to cell cultures that are often well characterised. This transition boosts accessibility and control of the system while often reducing the financial cost of upkeep and improving animal welfare. Most eukaryotic cell lines used as expression systems are derived from tumors or have been intentionally immortalised to circumvent the limited self-renewal. However, one must consider that the similarity with the original cell phenotype they have been derived from is reduced, potentially impacting the folding of proteins.

A plethora of hosts have been successfully used for heterologous expression, but only a few will be briefly introduced in the following section, according to the most common expression systems used in structural biology (Figure 3 B and C; Berman et al., 2000).

1.2.1.4 Hosts for Recombinant Protein Expression

Mammalian Cells

Proteins from higher eukaryotic organisms require specific folding and post-translational modifications for their activity. Furthermore, membrane proteins rely on additional specific mechanisms for their membrane insertion. Mammalian cell lines (HEK, HeLa, CHO) can provide the right environment to obtain functional proteins and are commonly used, despite the high cost of mammalian cell cultures and low expression levels. Although transient transfections of mammalian cells are less time-consuming, even for non-commercial studies, establishing stable cell lines is often the procedure of choice due to higher safety, reproducibility, and expression levels (Camponova et al., 2007; Chelikani et al., 2006; Pandey et al., 2016). Virus-based transfection of mammalian cells requires caution as they can transfect target cell lines and researchers alike.

Insect

A way to circumvent virus-based methodologies that pose a threat to humans is using insect cells (e.g., *Spodeptera frugiperda* or *Trichoplusia ni*). Here the most commonly used *Baculovirus* is specialised on transfecting insect cells, but a high virus load is required for this system, which will eventually cause cell lysis and degradation of the POI. However, insect cells also support chaperone-assisted protein folding and have been used successfully for membrane proteins and structural characterizations (Hitchman et al., 2011; Shi & Jarvis, 2007; Sitarska et al., 2015).

Yeast

The use of yeast has many practical advantages, including the lower cost for cell culture media, high growth rates, and expression levels in well-studied organisms. In addition, in the most commonly used yeast species (*Saccharaomyces cerevisiae* and *Pichia pastoris)*, a solid basis for protein folding, membrane insertion, and most PTMs is present (Böer et al., 2007; Bornert et al., 2012). However, the glycosylations are likely different for native mammalian proteins, and even genetically engineered strains are not necessarily able to produce the correctly modified and functional protein (Hamilton et al., 2003; Pandey et al., 2016).

E. coli

Escherichia coli is a prokaryote and the most frequently used host for protein expression (Figure 3) (Gold, 1990; Pandey et al., 2016). Like yeast, *E. coli* combines low costs with high growth and protein production rates (Shiloach & Fass, 2005). Furthermore, the simple construction of the extensively studied bacteria enables genetic modifications that provide

tools and solutions for many situations (Gileadi, 2017) or push the biological boundaries even more (T7 RNA polymerase) (Iost et al., 1992). Prokaryotic protein production in *E. coli* benefits from these advantages, but the unprecedented performance also entails severe limitations to the production of eukaryotic proteins. Mostly, protein folding, PTM, and membrane insertion are insufficient (Duquesne et al., 2016; Pandey et al., 2016).

In vitro translation/cell-free expressions

A way to circumvent the limitations of a cell-based expression system is to create a specialised environment focused on producing the POI. As a result, only the parts required for the translation process are isolated from the metabolic machinery. The *in vitro* translation system enables control over parameters such as the lipid environment that defines mechanical and electrostatic characteristics crucial for the correct folding of membrane proteins (Corin & Bowie, 2020). Even though the approaches are technically cell-free, they still rely on the cell extracts of various descent. There are systems based on *E. coli*, plant cells, mammalian cells, and more (Endo & Sawasaki, 2006; Jewett & Swartz, 2004; Mikami et al., 2008). However, post-translational modifications depend on several proteins that need to be introduced specifically, limiting the fitness of the *in vitro* protein production.

1.2.1.5 The Choice of Expression System

With all these parameters selecting an expression host often boils down to the best guess followed by a trial and error procedure. The scale of production and complexity of the POI and recombinant modifications are the main parameters to consider. The analysis of published structures for the protein source illustrates the dominance of heterologous expression in *E. coli* for structural studies (Figure 3). However, membrane proteins demonstrate the need for expression in more complex hosts and also the native environment.

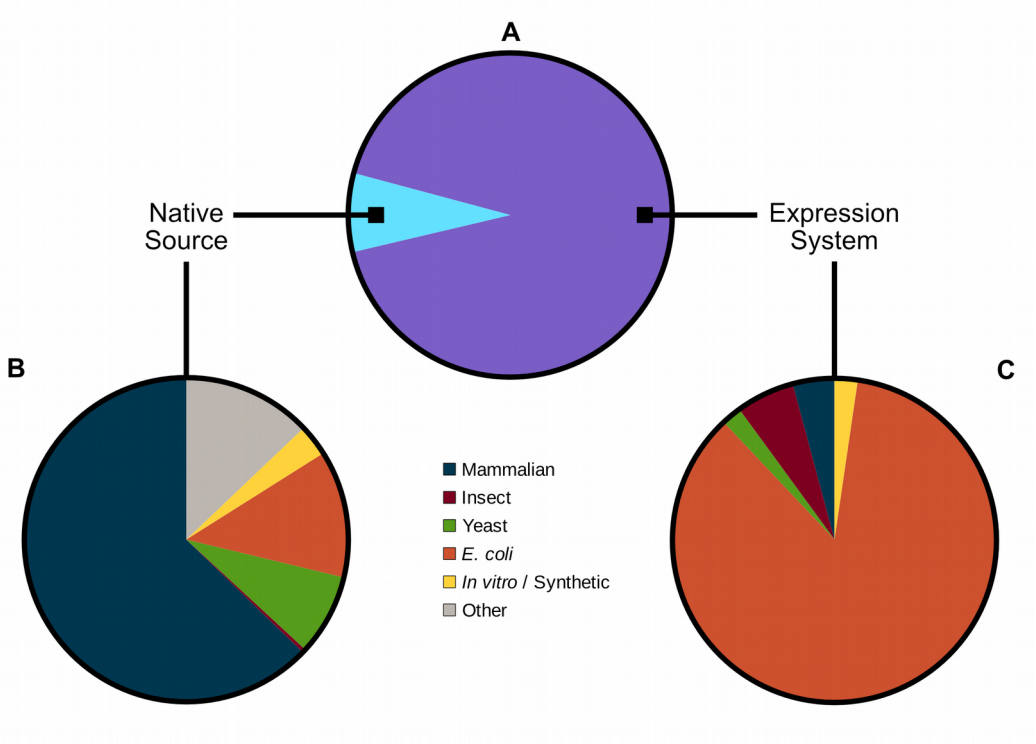

Figure 3: Protein sources for the structures deposited in the protein data bank (PDB)

(A) Proportions of proteins from native source and expression systems. The “expression system” category includes all proteins with modifications to the sequence or promoter or host organism (or any combination thereof). (B) Proteins from a native source are sorted by phylogenetic affiliation of the source organism. (C) Phylogenetic affiliation of the host organism for the non-native expression of proteins. Color code as provided in the center. Data was fetched in April 2021 from the PDB website (https://www.rcsb.org; Berman et al., 2000).

1.2.2 Purification Strategies

This chapter will provide an overview of the general protein purification strategy and introduce concepts required to appreciate the upcoming chapters.

Protein purification aims to separate a target protein or complex from other biomolecules to obtain a sample of sufficient purity for further use. Plenty of biochemical concepts and methods have been developed over the years to purify a given protein. However, there is no universal method, as proteins are molecules with a broad diversity of properties, such as size, surface/net charge, hydrophobicity, binding affinities, and more. Individual methods have specific advantages, disadvantages, and limitations. The sequential combination of several techniques allows for purification according to the protein requirements and the intended downstream application. Every combination of purification techniques results in an overall purification strategy with a more or less balanced outcome regarding resolution, capacity, recovery, concentration, and speed. Furthermore, many methods in protein purification can be of use in various stages and for different reasons.

1.2.2.1 General Considerations and Strategy for Setting Up a Purification

Even though methods are available to characterise a protein in a crude context, a preceding purification is usually required. However, excessive purification can reduce the protein activity and yield, for example, by removing stabilising co-factors or adsorption of the POI to a resin. Therefore, it is advised to reduce the number of purification stages, select quick procedures, and combine stages with compatible buffer systems to minimize additional buffer exchange steps (Labrou, 2014; Rehm & Letzel, 2016; R.K. Scopes, 1995; Ward, 2012b). A commonly used strategy consists of three phases called 1) capture, 2) intermediate purification, and 3) polishing (collectively referred to as CIPP) (Ersson et al., 2011; Haslbeck et al., 2003). While the overall procedure is analogous, variations in terminology are in use as well (e.g., 1) initial fractionation, 2) enhancement, 3) polishing). In recent times this triplet is often reduced to two phases because the middle phase can be combined with either the capture or the polishing step, for example, due to increasingly potent affinity resins (Robert K. Scopes, 1994). Purification of recombinant protein is considered less complicated due to the high concentration or an additional tag designed for a simplified capturing process (Sassenfeld, 1990; Ward, 2012b).

A purification strategy is often subject to change throughout the POIs characterisation because the conditions and procedure can be refined with every information gained. Nevertheless, the following topics summarize some essential prerequisites that require attention as preliminary literature- or laboratory research.

The source material has an impact on the purification procedure that follows. For example, in some cases, the POI is expressed in several organisms or tissues by nature, some of which are more accessible, abundant, or express a desired variant. Alternatively, as discussed previously, with molecular cloning, the POI could be expressed heterologously.

Another prerequisite is the awareness of basic physical and chemical features. These POI features include general characteristics like the size and oligomeric state and the existence of hydrophilic and hydrophobic domains, charge/isoelectric point, or even metal- or ligand-binding capabilities (Labrou, 2014).

For a targeted development and monitoring of the purification, an assay to identify the POI is required. Basic methods like SDS-PAGE or immunoblot will suffice, but assays based on (enzymatic) activity are superior because they also provide insight into the condition/state of the protein. Some proteins, such as fluorophores, exhibit unique properties that can be leveraged for their identification.

Several previously mentioned topics are relevant for the stability of the POI. The buffer system, salts, pH, and temperature limits must be the center of attention and be defined in advance. As a comprehensive list of measures is beyond the scope of this work, only some relevant examples will be mentioned.

During the initial stages, protease inhibitor cocktails are often used to protect the POI against the enzymatic breakdown, and at the later stages, proteases will most likely be separated from the POI.

Similarly, phosphatase inhibitors can be administered to maintain phosphorylation patterns by blocking kinase and phosphatase activity. Moreover, reducing agents like DTT are often used to prevent the formation of disulfide bridges, and chelating agents like EDTA are either in use to inhibit metalloproteases or avoided if metal ions are required to maintain folding or function. Besides the chemical integrity, the functional status of the protein has to be maintained in many cases as well. For this reason, additional molecules like ligands and ions can be provided throughout the purification. Furthermore, membrane proteins require a specialised environment for stabilisation and functionality, as explained further below.

1.2.2.2 Overview of Methods and Corresponding Goals in Purification

The extraction and separation are the two main objectives of protein purification procedures. For poorly soluble proteins like MPs, solubilisation is an additional main objective.

The extraction is the initial step in protein purification. Then, the POI is made accessible to further steps by disrupting the cells (and connective tissue) in the source material. The method of choice depends on the localisation of the proteins. For example, in the purification of membrane-associated proteins, detergent-driven lysis may be harmful to the POI. Standard methods are homogenization by compression and expansion upon discharge (French press), or grinding (homogenizer), freeze-thaw cycles, sonication, hypotonic pressure, and the application of lysozyme or detergent (Ersson et al., 2011; R.K. Scopes, 1995, 2001; Ward, 2012a). The hydrophobic areas of MPs and poorly soluble proteins require shielding from a hydrophilic environment to become stable in aqueous solutions and thereby accessible for later stages of purification. Usually, this additional objective is approached after the extraction to enclose the exposed hydrophobic residues at the surface with an amphipathic molecule. A variety of detergents with variable characteristics (CMC, (non-) denaturing, and so on) is available, and they are the most commonly used approach (Ersson et al., 2011; Popot, 2010). However, often the detergent solubilised POI does not suffice for more intricate studies because the stability is affected by detergents, and the POI is devoid of any interactions with specific lipids. Alternative systems primarily rely on detergents for the initial solubilisation of the POI and replace the detergent with surfactants, for example, amphipathic polymers (Amphipols), or with the native-like environment, such as Membrane Scaffolding Proteins (MSP, nanodisc), Saposin-lipoprotein (Salipro, nanoparticles), or amphipathic bi-helical peptides (NSP, peptidisc) (Carlson et al., 2018; Frauenfeld et al., 2016; Nath et al., 2007; Tribet et al., 1996). Another system uses Styrene-Maleic Acid (SMA) or SMA-derivates to form polymer stabilised native nanodiscs. These SMA polymers do not rely on detergents for an initial step. Instead, they can self-insert into a

membrane and form nanodiscs, including the native lipid environment. However, all these systems come with their specific limitations. For example, the SMA polymer can only be used in a specific pH range and requires the absence of divalent cations (Dörr et al., 2014; Knowles et al., 2009; Popot, 2010).

The essence of the purification is isolating the POI. The methods available use various physical and chemical (including structural and functional) characteristics of the POI to achieve this goal. The more specific/rare the exploited characteristic is, the higher the resolution (specificity) will be, and the fewer purification steps are necessary overall. However, specific properties that exhibit low affinity may not be practical. The first part is often called capture or initial fractionation. These methods often split the sample into two fractions, separating the POI from a large body of contaminants. Typical approaches are centrifugation, precipitation, filtration, or two-phase partitioning (Burgess, 2009; Labrou, 2014; R.K. Scopes, 1995).

Further purification steps aim to separate the POI from contaminants, but utilize successively more unique POI properties to achieve the required purity. For these intermediate steps, usually chromatographic methods like Ion-Exchange Chromatography (IEX, exploits surface charge) or Hydrophobic Interaction Chromatography (HIC, exploits hydrophobic surface) are used (Ersson et al., 2011; Lucy, 2003; R.K. Scopes, 1995).

In the final polishing steps, specific/unique properties of the POI are utilized. Again chromatography-based procedures are commonly employed. Affinity Chromatography (AC) is the preferred option in purifications of limited protein volume because it exploits the inherent binding affinity and selectivity of the POI (Labrou, 2014; Roque et al., 2007). With more knowledge about the ligand, it is possible to design a synthetic ligand. The synthetic ligand is usually cheaper, and exhibits increased binding affinity and selectivity (Matos et al., 2021). Besides AC, size exclusion chromatography (gel filtration, HPLC), which exploits the hydrodynamic radius, is also a frequently used method. In the purification of recombinant protein, the appropriate method is used. A typical example is Immobilized Metal Affinity Chromatography (IMAC) for recombinant proteins equipped with a His-tag (Kallberg et al., 2012; Labrou, 2014).

Within the course of the purification, the following secondary objectives have to be considered for a well-functioning procedure. The high viscosity of a cell extract will harm chromatography methods. One reason for such a high viscosity can be DNA, and adding DNase will help with this problem effectively. Alternative methods precipitate the nucleic acids (Ersson et al., 2011). Another secondary objective is volume reduction to increase the final concentration of the purified POI. In most cases, this is addressed automatically because methods typical for early stages reduce viscosity and increase concentration. Such methods typical for the early stages of the purification are (ultra) centrifugation, precipitation, or chromatography. Several characteristics can be monitored throughout the

purification to guide the design and inspect the process. As mentioned above, SDS-PAGE, Immunoblot, and concentration measurement of the POI are commonly employed methods for this purpose.

1.2.3 Conformational and Compositional Heterogeneity

Many characterisations and analysis methods, like structural investigations, require homogenous protein samples. Proteins from native context can exhibit higher heterogeneity, both conformational and compositional, and thereby complicate investigations. Also, the purification procedure and method of structural investigation may increase the heterogeneity as aggregation or dissociation of the protein complex sometimes is induced. While a homogenous protein sample is simpler to analyse and describe, it may lack functional dimensions, such as dynamic interactions in living cells. (Haurowitz, 1979). In biochemical terms, protein heterogeneity describes the uniformity of proteins concerning a specific property. Therefore, the proteins in a sample can be homogenous in one aspect and heterogeneous in another. Sources of proteins exhibiting a non-uniform appearance are multiple, and the manifestation can be classified as conformational and compositional heterogeneity (McNaught & Wilkinson, 2019), which are not mutually exclusive. Both conformational and compositional heterogeneity can be observed in proteins to represent the physiological variations and the dynamic processes occurring throughout the life cycle of a functional protein.

1.2.3.1 Conformational Heterogeneity

Conformational heterogeneity describes variations in the spatial arrangement of the molecule resulting in different secondary and tertiary structures (McNaught & Wilkinson, 2019). As a result, rotations around the single bonds in the protein backbone are of high relevance. For each amino acid in the protein, the torsion angles phi (φ) and psi (ψ) are used to describe the arrangement. Ramachandran plots are widely used to visualise these torsion angles for each amino acid in a protein. In theory, the combination of all possible rotations creates a plethora of arrangements, but conformations are limited due to the van-der-Waals radii of atoms. As clashes (steric collisions) between atoms are not allowed, a set of common structural elements, like alpha-helices, beta-sheets, turns, and coils can be widely observed (Hovmöller et al., 2002; Ramachandran et al., 1963).

Every conformation is associated with a state of potential energy with specific arrangements that require less energy to reach and maintain. The energy is determined by attractive and repulsive forces between atoms of the protein. The possible arrangements and corresponding energy can be represented in a conformational energy landscape. A (local) minimum marks a conformation with low free energy where the protein fold is stable in this landscape. These stable conformations are favored, but the conformation can shift to a different state when energy is provided. Iso-energetic movements, for example, rotation of side chains, are often not relevant for meaningful conformational changes. Required energy

can be, for example, introduced by binding of a ligand. Some of the low energy minima represent native conformations associated with the protein functions, such as active and inactive states or states of high and low interaction/binding affinity. Other states with low free energy may represent aggregates that tend to be very stable while lacking function (Frauenfelder et al., 1991).

Intrinsically Disordered Proteins (IDP) are an example of proteins with extreme conformational heterogeneity. However, most IDPs will adopt a specific structure upon binding to a substrate (Uversky, 2016). Thisillustrates how important it is to consider the structure obtained in an experiment in the context of the environment and the availability of interacting molecules. Also, flexible domains or regions that connect structured domains are common in ordered proteins (Radivojac et al., 2004). However, the impact of dynamic conformational changes upon protein-protein interactions is still hard to resolve with certainty. Nevertheless, combined studies of experimental and computational approaches show progress in understanding, for example, the complex dynamics of G protein-coupled receptors (Kharche & Sengupta, 2020). And the recent improvements of cryo-EM (see section 1.4) enable the analysis of heterogeneous samples and details of structural dynamics, as shown by Soung-Hun Roh and colleagues for the bacterial chaperone GroEL (Roh et al., 2017).

1.2.3.2 Compositional Heterogeneity

Compositional heterogeneity describes in broad terms variations in elemental composition. Variations of the protein's primary structure, including post-translational modifications and variations in the composition of protein complexes or heteromeric proteins (stoichiometry) can result in compositional heterogeneity (Baumann & Meri, 2004; McNaught & Wilkinson, 2019). Furthermore, computational models may (currently) not replace experimental investigations of the protein structure but can inform about statistical relevance and implications of specific residues in the polypeptide chain. Small changes in composition can significantly impact secondary and tertiary structural elements (Kuhlman & Bradley, 2019; Radivojac et al., 2004).

The genome contains the information for the primary structure of a protein and provides additional instructions that may or may not influence the composition. One example of such genetically determined variations are splicing variants. Alternative splicing allows for increased diversity of proteins because the number of (potentially) produced proteins exceeds the number of genes (Graveley, 2001). However, the resulting variants of a protein differ in structure and, in many cases, also in function (Black, 2000).

Another way to create compositional heterogeneity lies in Post-Translational Modifications (PTM). Phosphorylations are the most frequent PTMs, but Acetylations, Glycosylations, and more are also widely observed (Khoury et al., 2011). Moreover, the diversity of modifications is enhanced by a temporal component. PTMs can be attached throughout the whole lifespan

of the protein to mark the maturation status, induce transportation to the intended localization, or initiate degradation and recycling. Furthermore, they can be transient, as PTMs can be reversible (Baumann & Meri, 2004; Jensen, 2004).

The ratio of essential components is taken into account when considering the compositional heterogeneity that occurs based on stoichiometry. While some proteins are functional as a single strand of amino acids, others assemble from separate polypeptide chains to form a protein complex. The association in protein complexes can range from transient protein complexes to stable assemblies.

As long as all subunits in a protein complex have the same sequence, the homomeric protein complex composition is simple, as only the number of subunits has to be analysed. Nevertheless, the stoichiometry and identity of involved subunits matter in heteromeric complexes with different subunits because the composition will influence the function (Emmott et al., 2019). For example, among VGIC such as CNG channels, the most common assemblies consist of four subunits with two subunits of one type and two of a different type (Kaupp & Seifert, 2002). However, variations of three plus one or other permutations of more than two different subunits have been observed (Bönigk et al., 1999; Kaupp & Seifert, 2002; Zhong et al., 2002). Therefore, the analysis of stoichiometry is an essential step in the characterisation of the POI.

1.2.3.3 How to Study Heterogenous Protein Samples

A complicated protein complex, such as the Ribosome, combines several varieties of heterogeneity. The heterogeneity of Ribosomes and their dynamic changes throughout the life cycle have been studied extensively. Here both, conformational and compositional heterogeneity are orchestrated carefully (J. Chen et al., 2013). One driving force in these studies has been the ability of cryo-EM to examine Ribosomes in their close-to-native state and environment. Furthermore, cryo-EM is well-equipped to deal with the heterogeneity likely to be encountered in such samples. Computational approaches like 3D classification can identify certain structural variations and contribute to the characterisation of protein dynamics. Besides, intrinsically disordered proteins have also been studied using cryo-EM (Nwanochie & Uversky, 2019). X-ray crystallography tends to suppress heterogeneity because the crystallization forces the protein into a particular arrangement. However, the resulting structure may not truly represent the functional or active state of the native protein (DePristo et al., 2004). Another concept to approach a heterogeneous protein sample is the use of recombinant techniques to express a single variant, remove a flexible domain, analyse a domain by itself, or introduce mutations to study their impact on the structure.

1.2.4 Current State of Scientific Knowledge on CNG Channels

CNG channels have been studied for several decades, and different purification protocols have been established to support different experimental approaches and corresponding requirements. In this section, the main approaches will be discussed, focusing on CNG channels from rod photoreceptors. In 1985 Fesenko and colleagues conducted the first (electrophysiological) studies on excised plasma membrane patches of the rod outer segment (Fesenko et al., 1985). Since then, various purifications have been established over the years, using native sources (Haynes et al., 1986; Taylor & Baylor, 1995; Torre et al., 1992), heterologous expression systems to express one subunit (Kaupp et al., 1989a), or to co-express various combinations of different subunits (T. Y. Chen et al., 1993; Körschen et al., 1999).

Independent of the types of subunits, CNG channels always consist of four subunits, and all known native channels are heterotetramers. The genome of mammals contains a total of six genes coding for CNG subunits. The four genes for alpha subunits are *CNGA1*, *CNGA2*, *CNGA3*, *CNGA4*, and the two genes for beta subunits are *CNGB1 CNGB3*. Furthermore, two splicing variants of the *CNGB1* gene have been reported. The CNGB1a subunit (B1a or B1) is present in the rod photoreceptors, and the CNGB1b (B1b) is present in the olfactory sensory neurons and lacks the Glutamic-Acid Rich Part (GARP) (Bönigk et al., 1999; Körschen et al., 1995). As proposed by Kaupp and Seifert in their 2002 review, a three CNGA1 (A1) to one B1 stoichiometry in rod photoreceptors explains the characteristics best. Also, a study by H Zhong and colleagues verifies this stoichiometry, and it is considered scientifically accepted (Biel & Michalakis, 2009; Giblin et al., 2016; Matulef & Zagotta, 2003; Weitz et al., 2002; Zhong et al., 2002). However, to date, direct proof of stoichiometry has not been published. Experimental determination by direct structural investigations, or techniques equipped to analyse a complex composition such as mass spectrometry, would confirm the stoichiometry. The CNG channel assembly is highly dependent on the tissue, and even cell type, as illustrated by the channels of rod and cone photoreceptors. In rod photoreceptors, most CNG channels are composed of three A1 and one B1a subunit, while in cone photoreceptors, most CNG channels are composed of two A2, one A3, and one B1b subunit. Along with the composition, CNG channels vary among themselves in conductivity, modulation, and other properties.

While CNGB1 subunits cannot assemble into functional tetrameric ion channels independently, the expression of CNGA1 subunits results in the assembly of active homomeric channels (T. Y. Chen et al., 1993; Körschen et al., 1995). However, characteristic properties such as modulation of the channel activity by Ca^{2+}/CaM are absent in CNGA1 homomeric channels (Kaupp & Seifert, 2002). The co-expression of CNGA and CNGB subunits results in heteromeric proteins, and these channels resemble the native CNG channels more closely (Körschen et al., 1995). They reported that a stoichiometry of three A1 to one B1 subunit is crucial for all functional aspects of CNG channels in rod

photoreceptors. However, the CNGB1 subunit is not only responsible for the modulation and functional characteristics. In experiments with CNGB1 deficient mice, the animals turn out to be virtually blind. Although expression of CNGA1 subunits results in the formation of functional channels, *in vivo*, these homomeric channels were not present in ROS of the knockout mice. It suggests that CNGB1 is required for the correct localisation of heteromeric channels to the ROS plasma membrane. It may be a safety mechanism to ensure that only heteromeric channels reach the ROS (Biel & Michalakis, 2009; Hüttl et al., 2005).

No expression system has been published that faithfully reproduces the three A1 and one B1 assembly until now. However, depending on the scientific question, expression systems can be successfully used to characterise aspects of the CNG channels (Xue et al., 2021). When native sources are used, bovine rod outer segments from dark-adapted animals are the most prominent choice. CNG channels show a high sequence and structural similarity across various organisms, from mammalians to vertebrates and invertebrates (Kaupp & Seifert, 2002; Robert S. Molday & Molday, 1999). Even prokaryotic channels such as SthK feature a high sequence homology (Rheinberger et al., 2018). Transferring knowledge from one organism to another is not applicable as long as no atomic structure of the native CNG channel is available.

The main objective of purifying CNG channels is solubilisation followed by separation from the highly abundant Rhodopsin. Furthermore, as long as Rhodopsin is present, (ROS-) purification steps must be performed in the dark or dim red light ($\lambda > 650$ nm). In the beginning, ROS from the bovine retina were prepared via sucrose gradient centrifugation (Schnetkamp & Kaupp, 1985), and until now, only minor adjustments were introduced into this step (Okada et al., 1998). The choice of detergent for the following CNG channel purification is a critical parameter, and CHAPS has been determined to be gentle end efficient for solubilisation. This choice was recently confirmed when competing against modern detergents (Jeyasankar, 2019). The exact CHAPS concentration varies over the decades, but overall a concentration slightly above the Critical Micelle Concentration (CMC) of 8 to 10 mM is required. The long dialysis steps and ion exchange chromatography approaches of early purifications were replaced by combinations of immunoaffinity chromatography and ion exchange or affinity chromatography (AC) and later transitioned to the exclusive use of AC (Cook et al., 1986, 1987; Hsu & Molday, 1994; Hurwitz & Holcombe, 1991; Jeyasankar, 2019; Robert S. Molday & Molday, 1999). This development is an exemplary illustration of the impact on the improvement of resins. Furthermore, using the affinity towards cGMP and Ca^{2+}/CaM could also potentially allow the purification of different CNG channel populations. Ca^{2+} and phospholipids were already used in early protocols to support the stability (Cook et al., 1986, 1987), and while the lipid concentration was reduced by a factor of 100, Ca^{2+} concentration was increased to facilitate the transition to AC. Furthermore, current protocols introduce Glycerol and feature other optimizations (Jeyasankar, 2019).

As mentioned above in section 1.2.2, a prerequisite for successful purification is the existence of an assay to follow and identify the POI and determine the concentration (preferably throughout the purification). With CNG channels, several approaches are present, but only a few utilize the CNG channel directly. Most significant are electrophysiological experiments, as they assess the activity and function of the purified protein. Also, the presence and purity can be determined by immunoblot and SDS-PAGE. However, these approaches are not fit for immediate evaluation. Furthermore, the Rhodopsin concentration is often used to guide the dilution factor in early purification steps (Robert S. Molday & Molday, 1999). Thus, a direct and fast verification method is still missing to assess the CNG channel stability and functionality throughout the purification procedure.

1.3 Mass Spectrometry

For an extensive characterisation, a protein has to be studied from different perspectives. There are many research disciplines in biology, and the collection of methods to understand biological molecules within a cell or tissue is referred to as “Omics Technologies”. The major branches are Genomics, Transcriptomics, Proteomics, and Metabolomics (Martens, 2011; Schneider & Orchard, 2011).

Genomics reveal the basic building blocks in the form of a genetic blueprint for proteins. Although computational approaches are available that predict the structural features of a protein from the corresponding DNA sequence of the gene, they often fail to elucidate the functional mechanisms (Baker & Sali, 2001; Sułkowska et al., 2012). Transcriptomics shed light on the expression and inform about the active cellular processes (Lowe et al., 2017). The function and role of an uncharacterised gene (and resulting protein) may be deduced by the circumstances at the time of transcription and by the context of other known genes that are co-expressed (Moffitt et al., 2018). Transcriptomics are an important aspect in understanding protein-protein interactions as they inform about the temporal dimension of whether two proteins are present in the cell simultaneously. However, it is challenging to link the transcription to translation and the resulting proteome (Chalmel & Rolland, 2015). Proteomics study the entire proteome regarding identity, abundance, localisation, and interaction of proteins. The structure, modifications, function, and physiological role of the given protein are analysed (Anderson & Anderson, 1998). Finally, in metabolomics, the biomolecules that are subject to anabolic and catabolic processes are studied. The resulting metabolite network also includes the intermediate steps of the chemical reactions (Hollywood et al., 2006).

In proteomics, methods like gel electrophoresis, interaction assays, antibody-based techniques, and Mass Spectrometry (MS) are used (Aebersold & Mann, 2003; Uhlen & Ponten, 2005; Yarmush & Jayaraman, 2002). However, MS stands out because the method provides information on the proteome in a given sample and can also analyse a POI in detail. The foundation for MS has been established in the early 20th century. The resulting mass

spectrometers were used for physical and chemical analysis, for example, of characterisation of electrons (Kaufmann, 1906) and the discovery and identification of isotopes (Thomson, 1912). Further development resulted in the commercial availability of mass spectrometers in the 1960s. The novel accessibility of information about the mass of small molecules led to a surge of studies published using MS (Griffiths, 2008). In the 1980s, different ionizing techniques (Fenn et al., 1989; Karas et al., 1985) that enabled the analysis of biomolecules were developed, and MS became a powerful tool in biochemistry and proteomics. As a result, today, MS is a widely used, versatile, and accessible technique.

The critical element in MS is the ionization of the sample and the determination of the mass-to-charge ratio (*m/z*) of molecules. Based on this, it is possible to calculate the mass of a molecule, as the charge is a known value. This information of mass is crucial for all analytical approaches of MS in biological studies. The mass spectrum can be visualized in combination with the signal intensity (Figure 4). As described previously, there are plenty of ways to use the knowledge of the mass of a component in order to study it, may it be a sub-atomic particle, atom, or molecule. This thesis will focus on the description of mass spectrometry in the study of proteins.

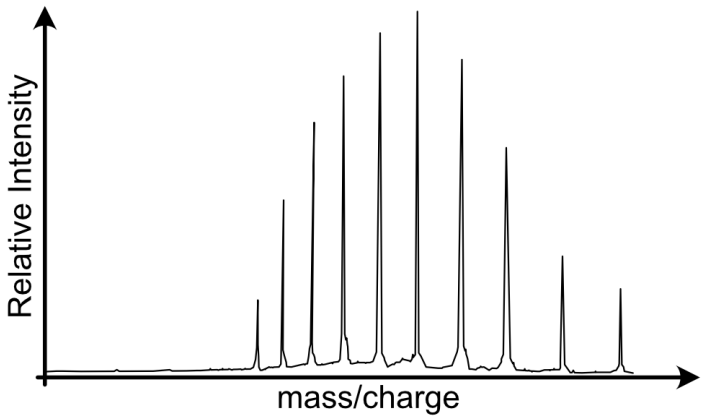

Figure 4: Schematic representation of a mass spectrum

The (relative) intensity of detected ions is plotted against the mass/charge. Each peak represents the accumulated signal of a specific ion. The molecular formula has to be determined computationally.

1.3.1 Principles of Mass Spectrometry

The general assembly of a mass spectrometer consists of an ion source, a mass analyser, and a detector (Figure 7). Every component achieves a crucial goal in the mass analysis of molecules, and a plethora of specific designs are available for each of the three main components as well as for the optional expansions and combinations thereof. Further instrumentation like a vacuum pump, electrostatic lenses, or C-traps are required to operate a mass spectrometer, but their operating principle will not be covered.

At first, the sample is ionized, i.e., charging the molecules and converting the liquid into a gas. These two attributes are crucial for further analysis because, in MS, the analytes have to be in the gas phase and require a charge to be susceptible to magnetic or electric fields. The peptides must be in a gas phase to enable the separation of single molecules in the mass analyser. Due to the charge, the molecules avoid collapsing into droplets and are susceptible to magnetic or electric fields. Therefore, electromagnetic lenses can guide the ionised analyte through the mass spectrometer or hold a cloud of molecules in a specific place until use. Soft ionisation methods are used for biological samples because hard ionisation leads to uncontrolled fragmentation that is often not desired at this stage. Several ionization methods have been developed, and the most frequently used are Matrix-assisted Laser Desorption Ionization (MALDI) (Karas & Hillenkamp, 1988), Electrospray Ionization (ESI) (Fenn et al., 1989; Zeleny, 1917), Atmospheric Pressure Chemical Ionization (APCI) (Carroll et al., 1975), and Atmospheric Pressure Photoionization Ionization (APPI) (Syage et al., 2008; Zhang et al., 2016). Each method achieves the ionisation differently, and the sample preparation is coordinated with the ionisation method.

For example, in ESI, acid is added to provide a source of positive charge (protons). At the beginning of the ionisation process, electrons are removed from the liquid sample. Then the liquid is dispensed into small drops, and the solvent evaporates. As the amount of protons is constant while the droplet size decreases, the charge of molecules in the droplet increases to a point at which surface tension is no longer strong enough to maintain the shape of a droplet. The dissociation of liquid droplets into a gas phase of charged molecules marks the successful ionisation of the analyte. The ionised peptides are the ion source, and acceleration via a charged metal plate (counter electrode) removes non-ionised droplets and creates a steady stream of ions (Simon J. Gaskell, 1997). Electromagnetic lenses are used to focus the ions into an ion beam and are required to manipulate the beam throughout the analysis. A vacuum continuously removes non-ionic molecules and thereby prevent collisions and contaminations.

In the mass analyser, the ionized molecules are sorted for their *m/z*. The ionized peptides enter the mass analyser at an equal velocity, and the electromagnetic field is used to deflect the ions. Equations that describe how charged particles move in an electromagnetic field also apply to the motion of ionised peptides in the mass analyser. Therefore, Newton’s

second law and the Lorenz force can be used to understand acceleration and trajectory of the ionised peptides in the mass analyser. Peptides with a lower *m/z* accelerate faster than those with a higher *m/z*, and a higher mass results in a lower deflection compared to lighter molecules (Haag, 2016). The main designs of the mass analysers are time-of-flight (TOF), quadrupole, and ion trap (including the enhanced Orbitrap design). Each design differs in resolution (mass resolving power), mass accuracy, and mass range, and when choosing a design, the characteristics of the protein sample have to be considered.

For example, Quadrupole mass analysers are characterised by their fast scan speeds and low resolution. They are very common in tandem MS where they are used to select a specific range of *m/z* values for further analysis. Quadrupole mass analysers consist of four parallel rods that are arranged around a central space with a direct current, as indicated in (Figure 5 A). Furthermore, a current alternating at high frequency is applied to each of the rods (radio frequency, RF). Only ions with a specific *m/z* will resonate with the electric fields at a given radio frequency, and only these ions have a trajectory that allows them to pass through the quadrupole (Figure 5 B green line). Ions with *m/z* that do not allow a stable trajectory collide with the rods or escape the central area. A range of ions with different *m/z* values can be detected or selected for further analysis by tuning the radio frequency (Paul, 1990).

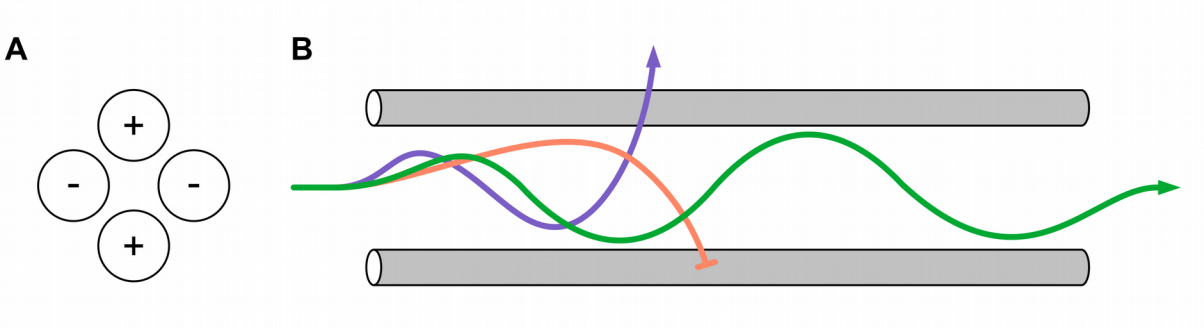

Figure 5: Illustration of a Quadrupole mass analyser

(A) depicts the cross-section of a Quadrupole, the opposite polarity is applied to adjacent rods. (B) Longitudinal view of ion trajectories shown for three exemplary cases: 1) ions leave the chamber (purple), 2) ions collide with a rod (orange), and 3) resonance ions move successfully through the mass analyser.

Subsequently, the detector counts the ions with a specific *m/z*. As the signal of incident ions is small, electron multipliers and photomultipliers are most common in modern MS. Both designs can convert the incident ion into secondary electrons at the conversion dynode. The electron signal is further amplified, and the resulting electron current is finally converted into a voltage by an electrode. One example of such a detector is the discrete dynode electron multiplier. In this type of detector, the conversion of the ion and the following amplification cascade occurs in a series of discrete dynodes (Figure 6). All dynodes are held at progressively positive potentials, and therefore the secondary electrons move towards the next dynode until they reach the anode (Benedikt et al., 2012; Tao et al., 2016).

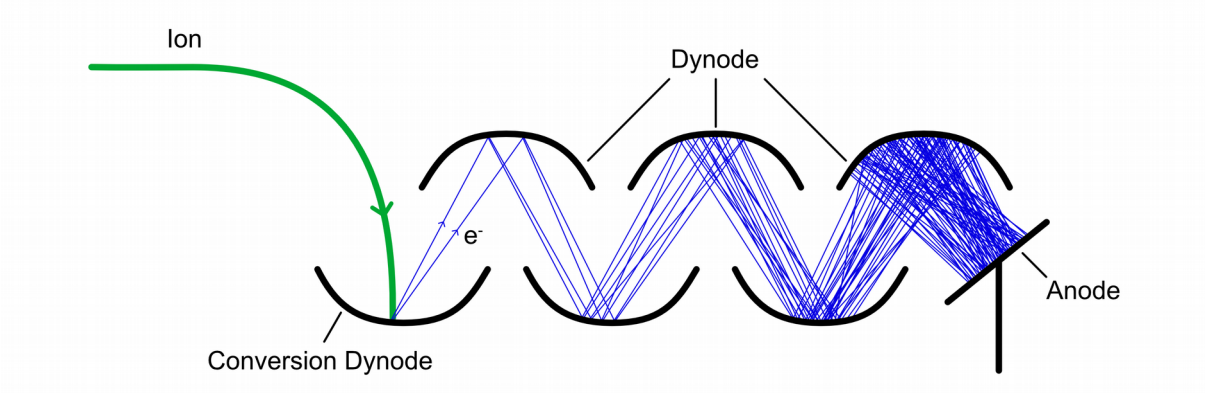

Figure 6: Illustration of a mass spectrometry detector

Discrete electron multiplier design, as used in mass spectrometry detectors. The incident ion (green) hits the conversion dynode (cathode), and secondary electrons (blue) are emitted. The following distinct dynodes facilitate the cascade of electron multiplication. Finally, the electrons induce a current at the anode that results in the mass spectrum.

1.3.1.1 Tandem MS (MS/MS)

Following the development of crucial components, like the LC-MS, triple quadrupole mass spectrometers, and advancements in computerization, another extension of MS was developed and termed “Tandem Mass Spectrometry” (Tandem MS or MS/MS) (D. S. Millington et al., 1990; David S. Millington et al., 1989). In tandem MS, the analysis of peptides is performed in two coupled mass analysis events, referred to as MS1 and MS2 (Figure 7). This sequential analysis yields not only the *m/z* of the peptides but also informs about more detailed structural features, such as the sequence of a peptide (Biemann, 2015; Büyükköroğlu et al., 2018). Tandem MS is possible with the two mass analysis events being separated by time or separated in space. For this thesis, the latter approach was used. The first MS analysis selects precisely the peptides of interest, which will be passed into a collision chamber, where the peptide collides with a gas (e.g., nitrogen) to further dissociate into smaller fragments (Collision-Induced Dissociation, CID). The resulting molecules subsequently pass to the second mass analyser, where the *m/z* of the fragments is analysed (Büyükköroğlu et al., 2018; Olsen et al., 2007; Zhang et al., 2016).

1.3.1.2 Liquid Chromatography MS (LC-MS)

Frequently, proteomics uses a combination of MS or tandem MS with liquid chromatography (LC-MS or LC-MS/MS). When crude samples or samples with a low abundance of protein are analysed, the LC-MS or LC-MS/MS approach enhances the resolution, signal-to-noise ratio (SNR), versatility, and throughput (Glish & Vachet, 2003; Zhang et al., 2016). With the capability of ESI to ionize liquids, an apparent link between LC and MS is also available.

1.3.2 Mass Spectrometry Guided Characterisation of Proteins

As previously elaborated, MS is a powerful technique in proteomics and the analysis of proteins. Combining the AC-based purification and LC-MS/MS enables a thorough analysis of the protein sample. With the *m/z* of peptides and peptide fragments, the amino acid sequence and the identity of the proteins present in the sample can be determined. The introduction of LC increases the sensitivity of the MS analysis and supports ionization because current methods cannot ionize all peptides at once. The development of analysis methods allows for label-free quantitative analysis of the proteins (Sandin et al., 2014).

Furthermore, the tandem MS approach aids in determining the presence, localisation, and identity of post-translational modifications. In general, the protein concentration and abundance are limitations to the MS experiments. In addition, the limitations in ionization technology demand the digestion of proteins. Thus, while the analysis of macromolecules is possible, the identification of proteins depends on the successful matching of the peptides to a protein database. Also, the sequence coverage of an identified protein is limited, and information on relevant parts of the protein may be missing. Orbitrap mass analysers are the latest development and stand out due to their high resolving power and mass accuracy. Therefore, Orbitraps are often used in LC-MS/MS analysis of fragmented peptides (Makarov, 2000; Perry et al., 2008).

The combination of quadrupole (MS1) and Orbitrap (MS2) analysers allows for a specific selection of precursor peptides followed by fragmentation and accurate determination of *m/z* of the fragmented peptides. This approach could be used for *de-novo* protein sequence determination and an automated identification (Michalski et al., 2012).

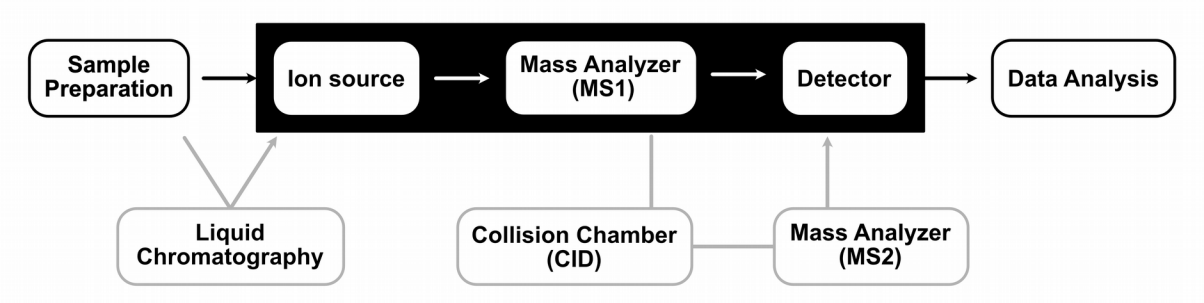

Figure 7: Schematic overview of basic components in a mass spectrometer

After initial preparation of the sample, the analysis in the mass spectrometer follows. Three main components (ion source, mass analyser, and detector) constitute a functional mass spectrometer (black box). Subsequent data analysis is required for the interpretation of mass spectra. Two common optional modifications are indicated (grey arrows and boxes) that introduce liquid chromatography MS (LC-MS) and collision-induced dissociation (CID) followed by a second mass analyser (Tandem MS or MS/MS).

1.3.3 Sample Requirements for MS

In this thesis, the purification approach is affinity chromatography, and for the subsequent MS analysis, the LC-MS/MS approach is used. While the technical details can be found in the materials and Methods section 3.2.21, the general information regarding sample preparation is outlined in this chapter.

MS has high sensitivity, and therefore, the contamination from handling samples and equipment has to be minimized. One of the most prominent sources of contamination is human hair. While low amounts of (human) Keratin, for example, are easily identified and not considered during data analysis, strong contaminations may obscure the signal from the actual sample. After the purification, the protein sample needs to be cleaned from chemical contaminations like lipids and detergents. The two widely used protocols are the filter-aided sample preparation (FASP) (Wiśniewski & Rakus, 2014) and the Single-Pot Solid-Phase-enhanced Sample Preparation (SP3) protocol (Hughes et al., 2014). Following the purification, the protein sample is subject to tryptic digestion, allowing for the bottom-up approach. The two main reasons for this step are the heterogeneous size distribution of proteins in the sample and the limitations in ionizing more large proteins. Furthermore, the complexity of the sample is reduced. The final cleaning step removes the remaining acidic, basic, and neutral compounds. Here a solid phase cleanup is used due to its simplicity, reproducibility, and rapid processing. The resulting cleaned protein sample can be loaded into the LC system.

1.3.4 Analyses of the Mass Spectrometry Data

Mass Spectrometry is characterised by high accuracy and sensitivity. Therefore, high sample quality is crucial, as even trace amounts of contaminations may stem from sample handling or imperfections in the (biochemical) purification process and interfere with the analysis of the protein of interest. In the biochemical characterisation of protein, MS can retrieve several essential information. The four topics relevant to this thesis (identification, quantification, complex analysis, and post-translational modifications) will be reviewed in the following sections.

Identification

The first step in MS sample analysis is the detection and identification of all proteins. Unlike sequencing methods in genomics, MS cannot directly establish the protein sequence. Instead, the indirect mass Peptide Mass Finger-Printing (PMF) approach uses the *m/z* information of peptides (or fragmented peptides in MS/MS). A theoretical digest of the proteins in the search database followed by calculating a theoretical mass spectrum of each peptide is the basis for the analysis. Next, a score is calculated based on the Peptide-Spectrum Matches (PSM) between the experimental and theoretical spectra (Figure 8). Scores above a certain threshold indicate protein identifications with significant certainty. In tandem MS, specific precursor peptides are selected for fragmentation and *m/z* analysis. The selection of precursor peptides depends on the scientific aim and could, for example, be based on the highest intensity or a predefined *m/z*. In the Data-Dependent Acquisition mode (DDA), MS1 scans a range of range *m/z* that contains most precursor peptides and feeds the ions with the highest intensity (limit is determined by the speed of the system) into the collision chamber and MS2 (Figure 5) (Michalski et al., 2012).

Various software has been developed to analyse the recorded mass spectra and match the peptides to protein databases. As the thresholds applied for the PSM scores depend on the experimental data (see DDA) and the software (search parameters and scoring algorithms), the results cannot necessarily be compared between datasets (Fenyö & Beavis, 2003).

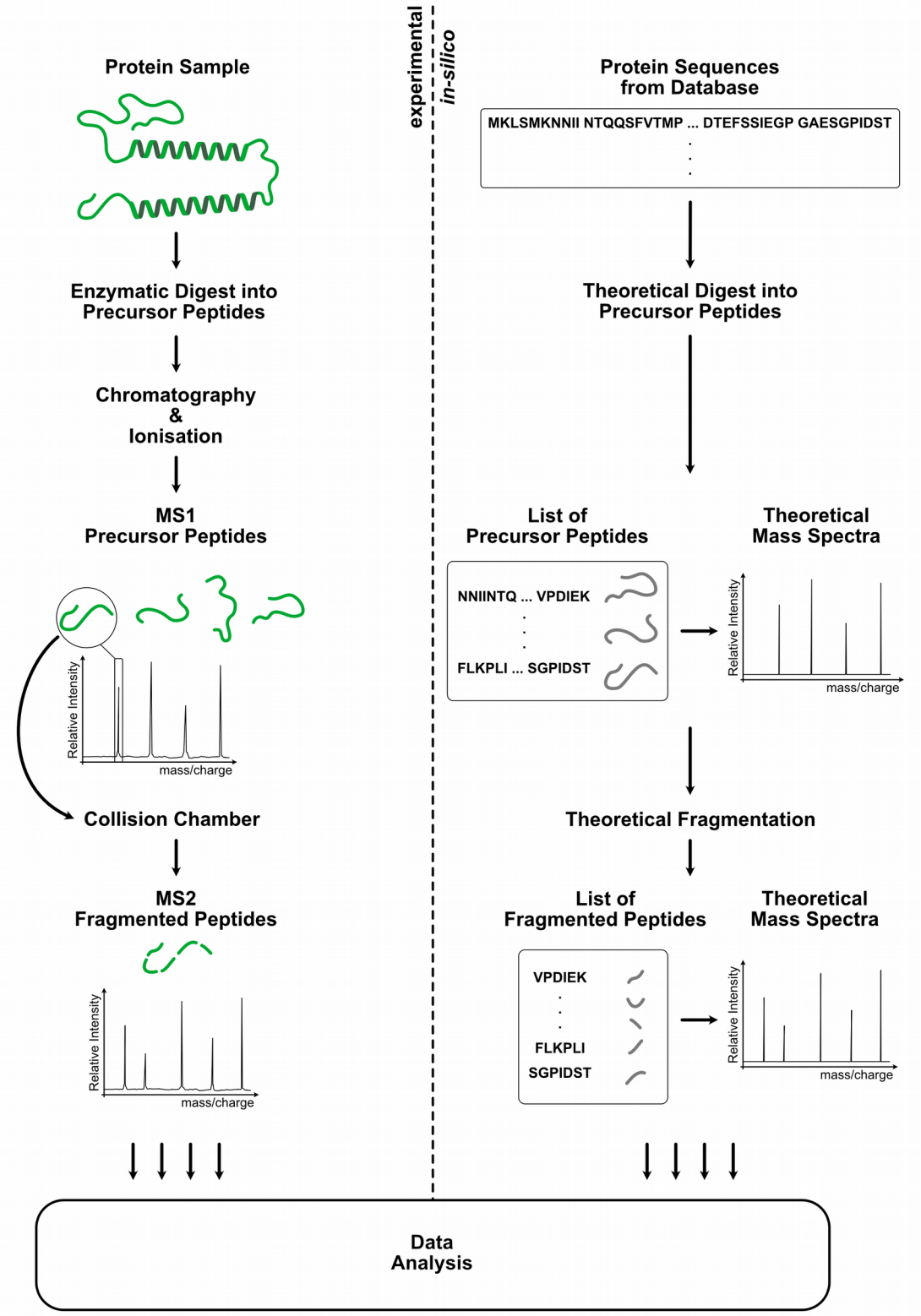

Figure 8: Overview of tandem mass spectrometry protein identification

For protein identification, experimental and *in-silico* mass spectra are compared. All steps of the experiment (left panel) with an impact on protein/peptide length (enzymatic digest, collision-induced dissociation) are theoretically calculated (right panel) by the data analysis software. Peptide-Spectrum Matches (PSM) between observed and predicted spectra indicate the presence of a protein.

Quantification

Quantitative MS is an extension of the identification and aims at analysing the abundance of all proteins in a sample. The mass spectrum provides an intensity for each ion, leading to an inherent ability to compare protein abundance within a sample/run. However, the proteome-wide abundance cannot directly be deduced from these values because the size and composition of peptides influence ionisation efficiency and detection rate. Moreover, the comparison of samples across experiments is complicated. Overall, quantitative analysis by MS can determine the relative (compare quantities within a proteome or relative abundance between proteomes) or absolute abundance (calculation of concentration) of proteins. Furthermore, the quantification may indicate false-positive identifications and highlight what proteins are significantly present and what proteins are background contaminants. As indicated previously, the modular assembly and extensions of mass spectrometers allow consideration of sample requirements and limitations and lead to a plethora of experimental setups and analysis approaches (Matthiesen, 2020; Nikolov et al., 2012).

While quantification was originally performed with stable isotope labelling, newer approaches have emerged that also allow reliable quantification in label-free approaches. However, the label-free approach is generally less accurate between these two main branches, as it is more sensitive to experimental bias (e.g., digest or ionisation efficiency) (Dunham et al., 2012; Sandin et al., 2014; Werner et al., 2014).

In Stable Isotope Labelling (SIL) based approaches, a defined amount of heavy carbon or nitrogen isotopes are introduced into the sample, either as a component during metabolic processes (e.g., Stable Isotope Labelling by Amino acids in Cell culture, SILAC) or attached to the protein during purification (e.g., an Isotope Coded Affinity Tag, ICAT) (D. K. Han et al., 2001; Ong et al., 2002). Often two proteomes of different conditions are compared, one of the conditions labelled with heavy isotopes and the other with light isotopes. The two proteomes have to be combined into one sample before preparation and analysis by MS to minimize technical variances. The shift in mass for each heavy isotope in a molecule is used to distinguish the two conditions, and the intensity peak can be used to compare the relative abundance of the same peptide.

For absolute quantification, samples are, for example, spiked with a specific amount of isotopically labelled reporter protein or synthetic peptides. The defined concentration and stoichiometry allow the labelled protein to be used as a standard (e.g., QconCAT, Pratt et al., 2006). However, with this approach, only a few proteins can be quantified absolutely. With the development of the isobaric mass tags, labelling approaches were refined, and due to the amine-specific reactive cross-linker, all peptides containing a compatible amino acid could be labelled and quantified (Dunham et al., 2012; Ross et al., 2004; Werner et al., 2014).

While quantification initially relied on labelling techniques, newer approaches have emerged that also allow quantification by label-free approaches, for example, the quantification of endogenous proteins (Sandin et al., 2014). However, the label-free approaches are less accurate. The most straightforward approach in label-free quantification uses the number of peptides that match a protein. This "spectra counting" quantification assumes a linear correlation of protein concentration in the sample and peptide-spectrum matches. However, several factors, like ambiguous peptide sequence, incomplete digest, and low sequence coverage, impact this correlation and render this approach inaccurate. Another approach is based on the precursor ion current area under the curve (AUC). Here the peak area (not only the peak height) in the mass spectrum is taken into account (Arike et al., 2012).

In a study, Schwanhüusser and colleagues showed that the AUC could be used in a label-free approach for the global (relative) quantification using software initially developed to quantify labelled protein (Cox & Mann, 2008; Schwanhüusser et al., 2011). In this process, for each protein, the cleavage sites, ionization success, and more features are considered in the theoretical estimation of observable peptides. The intensity-Based Absolute Quantification (iBAQ) compares the sum of measured peak intensities for all peptides of a protein to the theoretically observable peptides (Schwanhüusser et al., 2011). The resulting value was reported to represent the protein level of the proteins over at least five orders of magnitude accurately (Schwanhüusser et al., 2011). Furthermore, it follows the minimum set cover rule (following the concept of Ockham's Razor), where only the lowest and most likely number of proteins that would explain all peptides is considered (Cox et al., 2014). This approach provides a more precise and robust quantification analysis than the standard technique (Cox & Mann, 2008). While this label-free approach is not used to determine an absolute abundance of protein, the relative abundance can be compared between experiments.

Complex Analysis

In the analysis of oligomeric proteins and protein complexes, the composition and stoichiometry of constituents is an important characteristic. Similar to the quantification, the stoichiometry of a complex can be determined by MS. Isotopic labelling of the constituents results in the most accurate determination because precise quantification is available. In label-free analysis, well-purified complex or supportive measures like cross-linking resulted in an accurate determination of complex stoichiometry (Gingras et al., 2007).

Post-translational Modifications

Another feature that gives insight into the biological protein function are post-translational modifications (PTM). As the name suggests, these modifications are the result of enzymatic modifications happening after the protein synthesis. The most common modifications occur at the side chains of amino acids in the form of oxidations of cysteines, phosphorylations of Serine, Threonine or Tyrosines, or acetylations of the C- or N-terminus (Berg et al., 2018;

Khoury et al., 2011). In addition, glycosylation, hydroxylation, lipidation, methylation, and ubiquitination are possible. Several unintentional chemical modifications exist besides the PTMs introduced as a consequence of cellular processes in the native tissue. One example are oxidations introduced during the purification. Another artificial modification that is often introduced intentionally is cysteine derivatives. Modification sites can be predicted using genomics, but experimental analysis of the protein itself is mandatory to identify actual PTMs.

Serine, Threonine, and Tyrosine together account for 16% of amino acids in proteins and can be phosphorylated. Hence, determining a peptide containing phosphorylation does not necessarily inform about the specific phosphorylation site. Tandem MS increases the site analysis precision because the peptide is further fragmented. It has been reported that analysis tools, such as the Mascot database search and IsobarQuant, are suitable to identify variable modifications if combined with statistical analysis and experimental validation of software and scoring procedures (Franken et al., 2015).

1.3.5 Current State of Scientific Knowledge on CNG Channels Based on Mass Spectrometry

Only a few studies have been published that use MS and provide information about CNG channels in photoreceptors. Moreover, the available information stems from studies that have a narrow focus on a specific set of proteins or functions. The following section will highlight publications that used MS as a tool to investigate composition (identification), give insight into the abundance of proteins, and detail protein complexes formation in ROS.

The ROS consists of the plasma membrane that is wrapped around the stacked discs. While Rhodopsin is the most abundant protein in the ROS (Milo et al., 2009; Nathans, 1992), its majority is confined to the discs. In 1987 Molday and Molday reported on the proteins present in the disc rim and plasma membrane, including Rhodopsin and three glycoproteins (110, 160, and 230 kDa in size) besides minor populations of other proteins (R. S. Molday & Molday, 1987).

Additional studies used MS-based approaches to characterise the outer segment proteome. Kwok and colleagues focused on the structure and renewal of rod photoreceptors (Kwok et al., 2008), while Bruschi and colleagues reported the presence of mitochondrial proteins involved in oxidative phosphorylation outside of mitochondria (Bruschi et al., 2018).

Moreover, interaction studies focused on specific proteins of the ROS report an intrinsic disordered Glutamic Acid-Rich Protein (GARP) that is relevant for linking CNG channels to Peripherin-2 proteins in the disk rim (Batra-Safferling et al., 2006) and several other interactions (Körschen et al., 1999). Beicivoric and colleagues support this interaction using several methods (including MS) to report a complex formation of Peripherin-2, Rhodopsin, and CNG channels *in-vitro* and *in-vivo* (Becirovic et al., 2014). These studies highlight the

relevance of the GARP domain in CNGB1 subunits for the correct localisation of CNG channels. Further interaction studies using cross-linking MS described the interaction of PDE6 with Transducin subunits (Irwin et al., 2019). While XQ Ding and colleagues focused on the CNG channel from cones (Ding et al., 2014), Cheng and Molday conducted a study in (bovine) rods and found a splice variant of the protein 4.1G, another interaction partner of CNG channels. In their study using (co-) immunoprecipitation followed by MS, Cheng and Molday report that the 4.1G binds CNG channels to possibly support arrangement of CNG in the plasma membrane and complex formation with other proteins such as Peripherin-2 (C. L. Cheng & Molday, 2013).

As previously described, the CNG channel in bovine rod photoreceptors is a heterotetramer, consisting of three CNGA1 and one CNGB1 subunit. From the available data on CNGA1 and CNGB1 subunits identified and quantified by MS, no conclusive stoichiometry can be deduced (Becirovic et al., 2014; Bruschi et al., 2018; C. L. Cheng & Molday, 2013; Kwok et al., 2008). However, none of the publications analysed the data with a CNG stoichiometry investigation in mind.

Phosphorylation is a known way to modulate the CNG channel activity. It was first indicated in a study in 1992 by SE Gordon and colleagues. The increase of CNG channel sensitivity over prolonged cGMP presence could be slowed by Ser/Thr phosphatase inhibitors and promoted by type 1 phosphatases (Gordon et al., 1992). In a similar experiment, the increase in sensitivity was observed to be a result of Tyrosine phosphorylation (Molokanova et al., 1997), and Jeffrey L. Krajewski and colleagues described the process in more detail as a switch that allows (dephosphorylation) or suppresses (phosphorylation) Ca^{2+}/CaM inhibition of CNG channels (Krajewski et al., 2003). Warren and Molday showed phosphorylation of the CNGB1 subunit that is not affecting the sensitivity, and therefore, might be connected at a different position or mechanism (Warren & Molday, 2002). However, these functional studies were only able to highlight the existence, diversity, and relevance of the phosphorylations but did not identify the position of the phosphorylation site.

A different series of papers identified two Tyrosine residues in CNG channels using mutational studies. The residues Y498 of CNGA1 subunit and Y1097 of CNGB1 subunit were determined to be the target of phosphorylations (Molokanova et al., 1997, 1999, 2003). Furthermore, these two phosphorylation sites were associated with the previously described toggling mechanism of Ca^{2+}/CaM inhibition of CNG channels in a proposed mechanism (Krajewski et al., 2003). However, a direct examination of the phosphorylation in native channels never followed (Bright et al., 2007).

1.4 Structural Biology using Single Particle EM

Besides the biochemical characterisation, investigation of the three-dimensional structure is another crucial step towards understanding the functional mechanism of a protein. Structural biology is the domain of three-dimensional investigations of a protein structure and informs about various aspects of the protein, such as its assembly, function, and interactions.

While there is only one type of chemical bond connecting individual amino acids, the complexity of proteins arises due to the variety of amino acid side chains and the vast amount of possible combinations thereof. A functional protein (or peptide) is characterised by its amino acid sequence (primary structure), structural arrangement (secondary and tertiary structure), and additional chemical modifications. The genetic code determines the amino acid sequence and can be resolved by genomic methods that do not necessarily require the protein to be present. For the following structural organisation, accurate *in silico* predictions have been successful in some cases (Mesdaghi et al., 2021). However, even with continuous hardware and software improvements, the *de novo* structure prediction is challenging (Kuhlman & Bradley, 2019).

Protein structures cannot be resolved with conventional microscopy methods because the wavelength of visible light is larger than the details to be determined. Therefore, specialized tools and techniques are required for visualization and structure determination.

Historically, X-ray crystallography and nuclear magnetic resonance spectroscopy (NMR) are used in structural biology. X-ray crystallography is considered the dominant method because it reliably produces density maps with atomic resolution and accounts for 88 % of the published structures in the protein data bank (PDB, Figure 9). The number of structures solved by NMR reached a plateau, and only 7.5 % of the published structures in the protein data bank have been determined by NMR (PDB, Figure 9). While X-ray crystallography is severely limited by the requirement of obtaining a crystal lattice of POI, NMR is limited by the size of the protein that can be studied (Nwanochie & Uversky, 2019).

Due to technological advancements, additional approaches became more suitable for structural biology. The electron microscopy-based approaches, single particle (cryo-) EM and (cryo-) electron tomography, both benefit from developments of direct electron detectors and improvement of detective quantum efficiency (Y. Cheng, 2015; Kuhlbrandt, 2014). A series of 2D images of the POI is recorded from various angles to determine 3D structures using electron microscopy. Recently, it has been shown that atomic resolution can be reached by single particle cryo-EM (Hamdi et al., 2020; Yip et al., 2020). The recent advancements lead to a clear trend of increasing numbers of structures solved each year by EM (green line Figure 9).

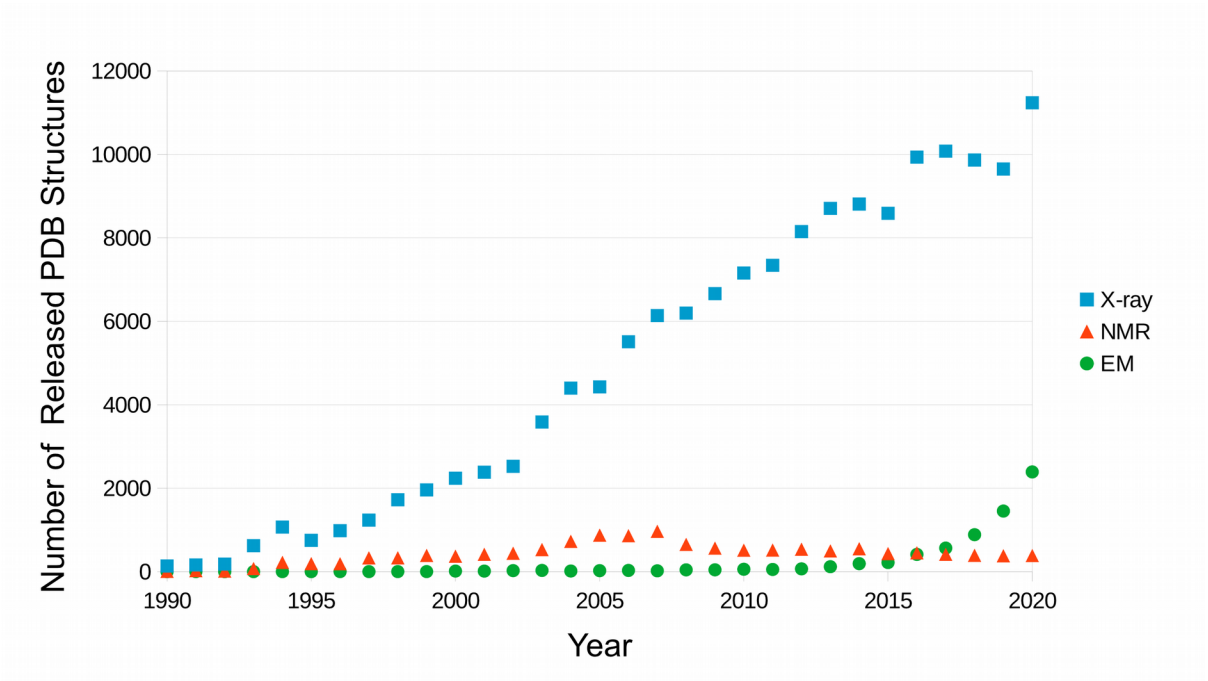

Figure 9: Methods in structural biology

Structures released in the PDB database for each year from 1990 to 2020. Data are shown for X-ray crystallography (X-ray, blue squares), nuclear magnetic resonance spectroscopy (NMR, orange triangles), and electron microscopy (EM, green circles). Data was fetched in April 2021 from the PDB website (https://www.rcsb.org; Berman et al., 2000).

More techniques in structural biology are available, such as neutron diffraction, electron crystallography, electron paramagnetic resonance, and small-angle X-ray scattering. However, these are used on rare occasions where the previously mentioned approaches fail or where the scientific question requires a specific approach.

Although MS is an established method in biochemical characterisation and a powerful tool in determining the primary structure of a protein, the variation called cross-linking MS (CX-MS) is also relevant in the realm of structural biology. However, cross-linking MS is predominately used to study the topology and interfaces in protein complexes. Therefore, the emphasis of CX-MS in structural biology lies in supporting other methods such as modelling after cryo-EM (Leitner et al., 2016).

Bioinformatics uses an interdisciplinary approach to analyse biological structures and molecular dynamics *in silico*. Depending on the scientific question, bioinformatics may involve integrating the experimental information, predicting or analysing the structural features, preparing a (mechanistic) model, and testing the resulting model (Bayat, 2002; Can, 2014; Nussinov et al., 2019). Especially the field of structural dynamics benefits from bioinformatic approaches to understand how the protein's structural arrangement translates into its function.

1.4.1 Introduction to Single Particle Cryo-EM

As powerful as X-ray crystallography is, the investigation of membrane proteins is not one of its strengths. On the contrary, the crystallisation of MPs is a major restrain (Carpenter et al., 2008; Y. Cheng, 2018; Kwan et al., 2020). Conversely, single particle cryo-EM proves capable in the structural investigation of challenging proteins, including MPs (Y. Cheng, 2018). The technological achievements in the design of the detector, resulting in the direct detection of electrons and high readout speed, have accelerated the number of protein structures determined by single particle cryo-EM. This chapter presents the basic principles of Transmission Electron Microscopy (TEM) and an overview of available methods associated with it.

An electron microscope is similar to a light microscope because both create a magnified image of an object. While the wavelength of visible light is the limiting factor of resolution achieved in light microscopy, the aberrations introduced by lenses limit the resolution in EM. Nevertheless, the much smaller wavelength of electrons allows for resolutions that are magnitudes better than light microscopes and grants access to investigations on the molecular scale. In TEM, an electron beam is directed at the specimen using electromagnetic lenses. Using the lenses, the diffraction pattern of the 3D Coulomb field of the atoms that make up the specimen can be used to form a 2D transmission image in the image plane. The detector positioned behind the specimen records the electrons and converts the signal into a digital image termed a micrograph.

Similar to light, electrons exhibit a wave-particle duality where the electrons display properties of both waves and particles. The electron beam interacts with the specimen in several ways that result in the image formation. As the specimens used for TEM are very thin and composed of soft matter, only a fraction of the electron beam interacts with the sample (weak-phase approximation) (Glaeser, 2013). The two modes of interaction that occur are scattering and diffraction.

When considering the particle properties of the electron beam, electron scattering describes the interactions of single electrons with parts of the atoms. The electron’s negative charge, mass, and velocity are required to describe its interactions with the specimen. In EM the majority of interactions occur between the electron beam and the outer shell electrons of the atoms in a specimen in the form of elastic scattering and a minority occur in form of inelastic scattering. Interactions of electrons and the atomic nucleus generally result in inelastic scattering. Elastic scattering events diverge the path of electrons from the beam while maintaining their energy and inelastic scattering events lead to the transfer of a part of the electron’s energy to the atom of the specimen. This energy transferred to the atom has a damaging effect on the sample and is commonly referred to as radiation damage that could break covalent bonds. The mass of atoms and thickness of the specimen affects the amplitude contrast. Moreover, the specimen thickness determines the likelihood of single

scattering events (mean free path) that are required for a correct reconstruction of the Coulomb potential map (often referred to as “electron density map”) (Y. Cheng et al., 2015; Peter J. Goodhew et al., 2001).

When considering the wave properties of the electron beam, electron diffraction describes the interactions with the sample as a whole. Here, the moving electrons are described by their wavelength and momentum, and the *de Broglie hypothesis* states the relation between these properties. Modern electron sources like field emission guns create a spacial coherent electron beam (Zemlin, 1994). The electron diffraction results in a phase shift of the coherent beam due to interactions with the specimen. This eventually becomes apparent in the micrograph due to the interference of the electron waves and is termed “phase contrast” (Peter J. Goodhew et al., 2001). Phase contrast also depends on the atomic composition, and soft matter samples such as biological material (weak-phase objects) induce only small diffraction. However, the phase contrast is most important in TEM because it allows for atomic resolution (Ludwig Reimer & Helmut Kohl, 2008).

In recent years, electron microscopy developed from producing low-resolution blobs to a robust approach in determining high-resolution 3D structures of biological molecules. This “resolution revolution” resulted from significant hardware and software improvements and opened the field of structural biology for smaller and challenging proteins, such as average-sized MPs or heterogeneous proteins (Kuhlbrandt, 2014). Single particle analysis is the most common method using EM to determine protein structure. Besides structure determination, this technique allows the visualization of the protein samples, and therefore, by inspecting individual micrographs, the purification and sample quality can also be assessed. For screening purposes, the room temperature (RT) technique, negative staining-EM, is used unless the preparation of samples for high-resolution is an immediate aim. High-resolution structural investigations require superior preservation of the specimen, and therefore, cryo-EM is used. However, the low-resolution structural investigations by negative staining-EM can answer specific scientific questions (Takizawa et al., 2017).

As previously described, the micrographs in electron microscopy are 2D projections of the specimen, and therefore, do contain the 3D information. However, currently available technologies cannot determine the 3D protein structure based on a single biological molecule but require multiple representations or viewing angles of the POI. Furthermore, the signal-to-noise ratio (SNR), especially of unstained samples, introduces an uncertainty of the high resolution information. In the single particle approach, additional information is obtained by combining information from several molecules of the POI and several viewing angles (of single particles). An electron density map is reconstructed upon determining the particle orientations for all the available single particles (Penczek, 2010). The single particle acquisition strategy and reconstruction workflow is the general approach towards structure determination, but single particle cryo-electron tomography is also increasingly used. Throughout the reconstruction process, six parameters have to be identified for each

particle. The in-plane position (*x* and *y* coordinates) and the defocus (shift along the z-axis) describe the particle's position in the 3D space of a cartesian coordinate system. Three corresponding Euler angles ψ (psi), θ (theta), and φ (phi) describe the rotation around any of the three axes. Here, the direction of the electron beam is defined along the z-axis; therefore, rotation around *z* is simply an in-plane rotation (Bartesaghi et al., 2012; Penczek, 2010).

Single particle electron tomography entails tilting the specimen around a fixed axis (referred to as y-axis), and the acquisition of micrographs occurs at regular spacing throughout the tilting. As the tilt angles of micrographs are known, the Euler angles can be more easily established. Each micrograph of the tilt series is acquired with a low electron dose to avoid excessive radiation damage to the specimen. Consequently, sub-volume alignment and averaging are performed to compensate for the resulting low SNR (De Rosier & Klug, 1968; Koster et al., 1997; Walz et al., 1997).

For classic single particle electron microscopy, micrographs of randomly oriented particles are taken without tilting the specimen. Similar 2D projections are aligned with each other and are classified to create class averages with an improved SNR. For the following reconstruction, the common line of two intersecting 2D projections is used to establish projection angles and reconstruct the volume (Crowther et al., 1970; Penczek et al., 1996; Sigworth, 2015). In brief, the following steps define the course of reconstruction in single particle EM: identification and picking of particles, 2D alignment and classification, generation of the 3D initial model, and 3D refinement/polishing.

1.4.2 Sample Preparation for Electron Microscopy

No matter how powerful the method is, the quality of the input sample directly influences the quality of the results – and 3D EM is no exception to this rule of thumb. Due to the harsh environment inside the TEM, specimens need to be prepared in a specific manner. This section outlines the sample preparation techniques suited for negative staining-EM and cryo-EM.

The EM grid supports the specimen and aids in the delivery of the samples into a TEM. Grids are comprised of a metal mesh carrying a thin film to support the sample. The typical materials of EM grids consist of copper as the metal, although other materials like gold are also in use. Similarly, various films are available that span the grid, and the grid preparation method influences the selection. Due to the hydrophobic properties of the EM grids, a chemical or plasma treatment is required before its usage with biological specimens.

Negative staining preserves the sample chemically for analysis at ambient temperature using heavy metal salts. The sample is fixed by cross-linking to preserve the biological structure during the necessary specimen drying process. Furthermore, the contrast of biological samples is relatively low due to the low mass of the atoms making up the biological matter.

Therefore, embedding the sample in a heavy-metal solution enhances the contrast of the specimen in TEM. With negative staining-EM the resolution that can be reached is limited to 18 - 20 Å, which is sufficient to identify the shape of a protein and global structural assembly at best (Brenner & Horne, 1959; Fabre et al., 2017; Ohi et al., 2004; Scarff et al., 2018).

In the cryo-fixation, the aim is to trap the POI in its respective aqueous solution/buffer into vitrified ice, ensuring a (close to-) native preparation. Vitrified ice is characterized by an amorphous arrangement of water molecules in a solid form. This amorphous solid state can be achieved by cooling the sample rapidly enough to pass through the glass transition temperature. The qualities of the sample and the vitrified ice are critical for successful sample preparation. On the one hand, crystalline ice is not transparent for the electron beam due to the high diffraction contrast. On the other hand, slow freezing water can result in drastic changes of buffer composition regarding salt concentration and pH which likely damages the POI or leads to formation of salt crystals. This concept of ice vitrification for cryo-EM was developed by Dubochet and McDowall in 1981 and was further developed in the following years to achieve the vitrification of biological samples (J. Dubochet & McDowall, 1981; Jacques Dubochet et al., 1988). Cryo-EM did not reach atomic resolution of biological samples until Yip and colleagues could identify accurate atomic positions of a symmetric protein (Yip et al., 2020). Current techniques for sample vitrification often cannot be reproduced and do not result in sufficient sample quality. Therefore, new emerging freezing methods and diversification of existing approaches address these flaws (Weissenberger et al., 2021).

Comparing these two approaches, negative staining techniques results in an easy and fast assessment of sample quality and even low-resolution structural information, and the vitrification of proteins is superior in several qualitative aspects. First and foremost, the samples are well preserved by the vitrification process because drying the sample, even in the presence of cross-linking agents, results in deformation. Furthermore, the heavy-metal contrast cannot represent the fine details in protein structure due to the grain size of the stain (Scarff et al., 2018), even though Uranyl Formate has a finer grain size compared to Uranyl Acetate (Ohi et al., 2004). Another problem with the negative staining is the poor representation of the interior structure because the stain does not penetrate the outer area of the protein.

1.4.3 Indicators of Pitfalls and Challenging Projects for Single Particle EM

Structural investigations by electron microscopy and especially single particle cryo-EM are constantly in development. Cryo-EM is a method established to a degree where the technique can contribute to structural insights inaccessible by other techniques in an ongoing global pandemic (Wrapp et al., 2020). Furthermore, commercial availability of cryo-EM systems enables access to a large group of scientists. However, severe limitations and

challenges are in place, some valid for all samples alike, others specific to the method of investigation, and others again specific to the POI. This section describes major pitfalls and challenges. While some challenges may be out of the researcher's reach, awareness of as many parameters as possible is key to reaching the final goal of the structural investigation of a protein.

General concerns in single particle EM are lack of contrast, SNR, and radiation damage. These issues can be traded off for each other but are not mutually exclusive; trading off on one comes with a price on another. For example, an increase in SNR comes at the expense of radiation damage due to increased exposure.

Sample specific challenges include the size and dynamic behaviour of the POI and biochemical composition of the sample buffer. Large globular proteins are advantageous independent of the sample preparation method and yield high contrast, supporting high-resolution (Henderson et al., 2011). Thanks to recombinant techniques, the size of the protein can be increased by fusion to a large protein that serves as a scaffold or supports alignment. For small native proteins, structural analysis in the context of a complex or known interaction partner(s) may be advantageous (Liu et al., 2019; Uchański et al., 2021). Low protein concentration can be tolerated to a certain extent, and extended acquisition sessions will result in reasonable particle numbers. However, purification optimisation may be appreciated in the spirit of effective use of beam time.

Glycerol or sugars are commonly used in buffers to support protein integrity or act as a cryo-protectant. However, in EM, they may interfere with the tight coat of heavy metal stains or equalize the density difference between the ice and protein, thereby lowering the SNR (Y. Cheng et al., 2015). Similarly, sample buffers containing high salt concentrations cause precipitation, and nucleotides or detergents present in the buffers can also impact sample quality. The latter will negatively impact both negative staining and vitrification because a change of surface tension impacts the sample preparation and should be kept at a minimal concentration if required for protein solubility. The air-water interface affects many proteins, causing aggregation or disintegration of the protein complex or particles arranging in a preferential orientation. Throughout the purification, foam formation or beads running dry are known sources of protein degradation, and similarly, exposure to air has to be avoided during the sample preparation process on the EM grid. Quick handling, faster freezing procedures, and intentional use of surfactants are the most common approaches to deal with these kinds of challenges (Alvarez et al., 2017; Noble et al., 2018). Interactions with the support film may also induce preferential orientation of the proteins on the EM grid. In that case, coating of the surface (E. Kang et al., 2007; G. Yu et al., 2014), tilted acquisition (Zi Tan et al., 2017), or use of megabodies might act as solutions (Uchański et al., 2021). However, each of these methods comes with additional challenges and also advantages.

Even though dynamic and heterogenous samples are tolerated in EM, they pose a computational challenge and should be limited to a minimum (Kuhlbrandt, 2014). A homogenous purification (Takizawa et al., 2017) or on-grid affinity purification and enrichment strategies (G. Yu et al., 2014) may improve the homogeneity of the sample. 3D classification serves as a proven approach to analysing dynamic and heterogeneous samples without prior knowledge (S. H.W. Scheres, 2016). Structural insights from preceding studies, such as symmetry, are advantageous for protein reconstruction.

Membrane proteins are demanding in purification and an example for samples accumulating several challenging factors, such as the use of detergents, the requirement for salts, and they are often only present in a low concentration. Besides, with the current deficit of structural information for membrane proteins, an important fraction of potential drug targets is inaccessible for developing targeted drugs and basic research. Membrane proteins of the plasma membrane are a major target for therapeutic drugs because they are accessible and are involved in most cellular processes, strikingly demonstrated by the G protein-coupled receptors and ion channels (Lundstrom, 2004). While there are constant advancements in biochemical methods and techniques to solve protein structures, single particle cryo-EM developed into an essential driver of progress for membrane protein structures (Bill et al., 2011; Y. Cheng, 2018). General technical concerns for structural studies are expression, solubilisation, and concentration steps of the membrane proteins because all of these may interfere with the structural integrity. Furthermore, detergents or membrane mimetic systems are driving the complexity and requirements of the sample.

The close-to-native imaging conditions of cryo-EM are an advantage in contrast to other approaches. However, considerations and compromises are required to accommodate the wide variety and complexity of samples. It becomes apparent that a successful sample preparation hinges on the biochemical optimisation of the sample and the grid preparation. Both factors severely depend on the time restrictions of the POI’s stability.

1.4.4 Current State of Knowledge on Structure of CNG Channels

Biochemical studies could characterise the CNG channels from ROS with respect to their functional domains and local motifs. As previously elaborated, the accepted hypothesis describes that the two subunits CNGA1 and CNGB1 are present in a three-to-one stoichiometry, and the four subunits are arranged around a central pore.

Regarding their basic domain organisation, CNGA1 (Figure 10 A) and CNGB1 (Figure 10 B) subunits are similar, except for additional domains present in CNGB1. The common features of CNG subunits are that the amino-terminus (-NH_2) is located in the cytoplasm, and six transmembrane helices (S1 to S6) are located in the plasma membrane. Four of these transmembrane helices (S1 to S4) form the voltage-sensor-like domain (VSLD). The last two (S5 and S6) are connected via a loop (Pore-loop) and form the pore domain (Kaupp et al., 1989b; Kaupp & Seifert, 2002; R. S. Molday et al., 1991). The C-linker connects the

transmembrane domain to the cyclic nucleotide-binding domain (CNBD) (Kaupp et al., 1989b; Zagotta et al., 2003). Finally, the carboxy-terminus is located in the cytoplasm as well. While the overall topology of CNGA1 and CNGB1 subunits are similar regarding the mentioned domains, minor differences have been observed. For example, the pore region of CNGA1 binds extracellular divalent cations (Ca^{2+} and Mg^{2+}) well, but in CNGB1, a crucial glutamate amino acid is not present (Root & MacKinnon, 1993; Seifert et al., 1999). It is an important characteristic of the selectivity filter, as binding divalent cations block a current of monovalent ions. The resulting low noise is a requirement for the single-photon sensitivity (Yau & Baylor, 1989).

Additional domains are present in the CNGB1 subunit (Figure 10 B). The glutamic acid-rich domain (GARP) is located close to the amino terminus and introduces a substantial negative charge to the molecule. This region is elongated but appears to be intrinsically disordered (Körschen et al., 1995). Between CNBD and S1 helix, a site that could bind Calmodulin in the presence of Ca^{2+}has been identified and was termed “CaM1”. A second Calmodulin-binding site (CaM2) is located near the carboxy-terminus (Grunwald et al., 1998; Weitz et al., 1998). The CNGB1 specific domains are relevant for the localisation of the assembled hetero-tetrameric channel in the plasma membrane and interaction with other proteins in the ROS (GARP) and mediate modulation of the channel (CaM1) (Poetsch et al., 2001; Weitz et al., 1998).

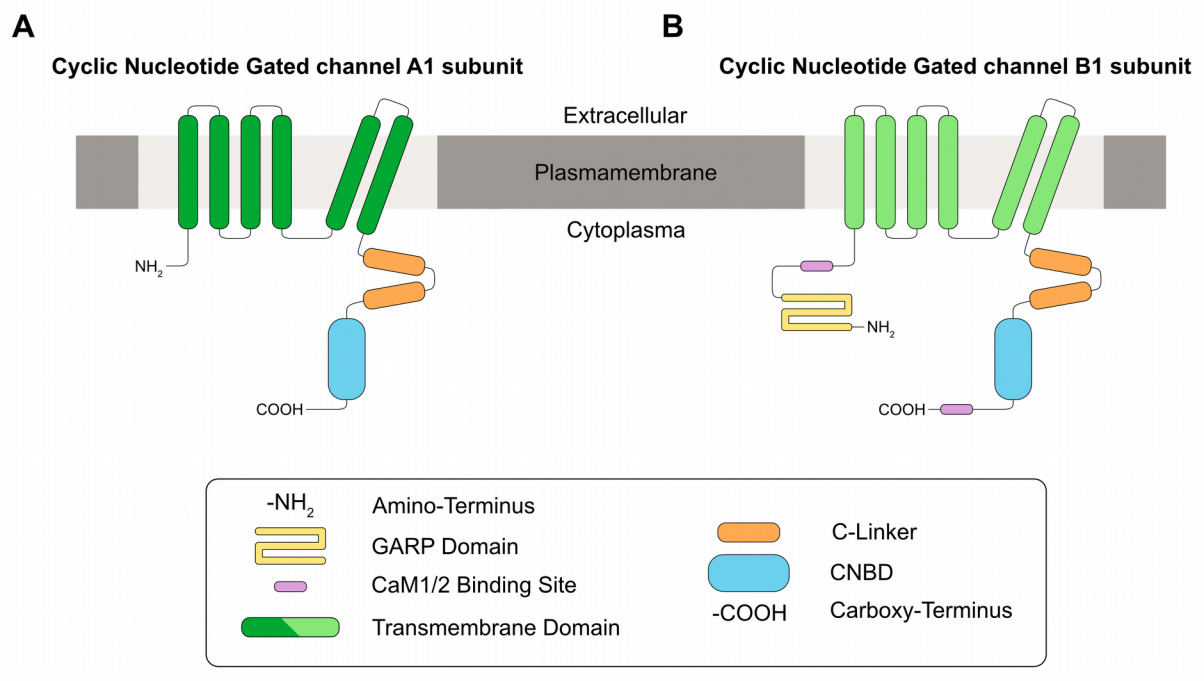

Figure 10: Schematic overview of CNG channel subunit domain composition

The domains in the schematic overview are used in this thesis, as mentioned below. Dark green is the colour used for CNGA1 subunits and light green for CNGB1 subunits throughout the thesis. Composition of CNGA1 subunit (A) and CNGB1 subunit (B).

The hetero-tetrameric composition and stoichiometry of CNG channels were established almost two decades ago and are the basis for their functional understanding (Kaupp et al., 1989b; Zhong et al., 2002). Further biochemical and electrophysiological studies, often exploiting cloning techniques for truncated or mutated protein, contributed significantly to understanding CNG channels (overviews in Biel & Michalakis, 2009; Kaupp & Seifert, 2002; Matulef & Zagotta, 2003). Crystallisation of MPs is notoriously difficult, but the structural understanding of individual domains has been achieved for the CNBD (Scott et al., 2001). However, a comprehensive atomic model and a complete understanding of the channel modulation are not yet available.

For the native CNG channel from ROS, only a structural investigation based on negative staining-EM has been published. Here, the channel was obtained from bovine ROS, solubilised in CHAPS, and purified via CaM affinity chromatography. The architecture was described as a tetrameric transmembrane part connected by two thin protrusions to a slim cytosolic part. This study suggested a “hanging gondola” architecture to describe the appearance of the CNG channel, similar to other channels known at the time (e.g., Shaker potassium channel, Sokolova et al., 2001). The ion conducting pore was speculated to be located at the central region of the tetramer but could not be resolved clearly. Furthermore, the subunits are suspected of forming a “dimer of dimers” with the cytosolic part two subunits closely associated.

A subset of views of the reconstruction from the publication is shown in Figure 11. As expected, the resolution of this structural investigation is severely limited (35 Å) and the description rather generic, as internal details and the non-symmetric stoichiometry could not be identified (Higgins et al., 2002).

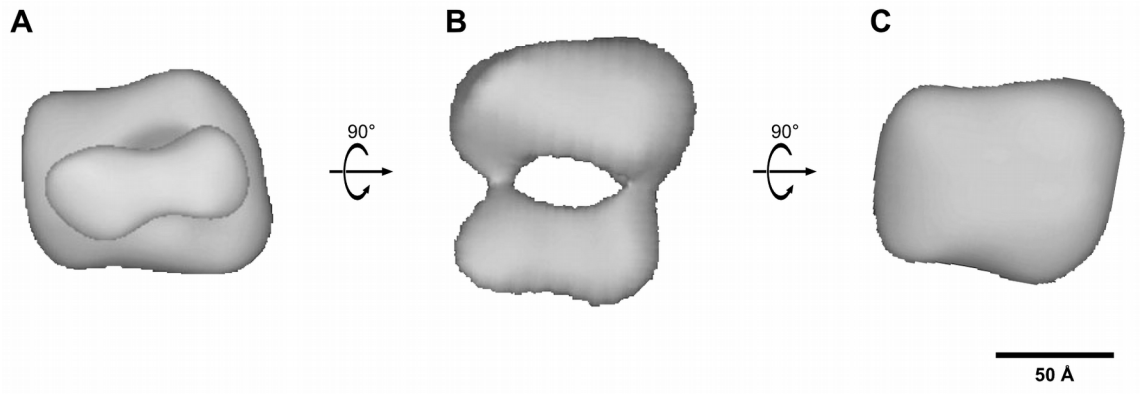

Figure 11: CNG density map obtained by negative-stain EM single particle analysis

Reconstructed density map of the hetero-tetrameric CNG channel from bovine rod outer segments obtained by negative-stain EM and single particle analysis. Channel is in an cGMP unbound state and solubilised in CHAPS. (A) view from the cytosol (B) view parallel to the membrane and (C) view from extracellular space. Scale bar is 50 Å. Figure modified after Higgins et al., 2002.

While the atomic structure of the native CNG hetero-tetramer is not known, several related ion channel structures are available and can be used as a reference to understand the possible structural architecture of the CNG channels. However, channels from the VGIC superfamily that could serve as reference are heterogeneous in their functional and structural nature (see Figure 12 for the phylogenetic family tree). They exhibit a common topology but significantly differ in minimal pore regions and functional traits.

The first insights were gained from the structures of K^+ channels where preliminary results based on mutational studies (L. Heginbotham et al., 1994; Lise Heginbotham et al., 1992) could be evaluated by the X-ray structure published in 1998 (Doyle et al., 1998). Understanding the structure of selectivity filters in the K^+ channel led to theories and investigations that explain differences in the selectivity filter of CNG channels causing the non-selective gating behaviour in them (Hackos & Korenbrot, 1999; Y. Zhou et al., 2001). However, also indications of the subdomain architecture were gathered, for example, by analysing structures of the *Ether-à-go-go* 1 channel (EAG1 or Kv10.1). EAG1 channels are not activated by changes in the membrane potential but are regulated by endogenous signals (B. Han et al., 2017). The non-domain swapped architecture featured in EAG1 channels is suggested for CNG channels (W. Wang & MacKinnon, 2017; Whicher & MacKinnon, 2016). CNG and Hyperpolarization-activated Cyclic Nucleotide-modulated (HCN) channels are a subgroup within the superfamily and modulated by cyclic nucleotides. They are present in a wide variety of organisms ranging from prokaryotes to eukaryotes and across several tissues. Investigations in C-linker/CNBD domain (Zagotta et al., 2003) deepened the understanding of cyclic nucleotide-binding and potential mechanisms propagating the signal towards the channel pore. When structures of cyclic nucleotide (cAMP) -bound and -unbound HCN1 channels were solved by cryo-EM (C. H. Lee & MacKinnon, 2017), the C-linker arrangement could be analysed in context. However, apparent differences due to the activation by hyperpolarisation still necessitated structural investigations of the CNG channels.

Prokaryotic CNG channels are overall more simple than their eukaryotic counterparts, and structural investigations prove fruitful. For example, the low-resolution structure of detergent-solubilized MloK1, a cyclic nucleotide-modulated K^+ channel from *Mesorhizobium loti*, is characterised by a symmetric arrangement upon cAMP binding to the four CNBDs (Chiu et al., 2007). Various CNG channels were finally studied in high resolution with the accelerating momentum of structure determination driven by cryo-EM. The already mentioned MloK1 was now analysed in a lipid bilayer (Kowal et al., 2018), and Llik, a channel from *Leptospira licerasiae* (James et al., 2017), was studied in a cyclic nucleotide-bound state. In contrast to previous studies, James and colleagues suggest their structure to depict a more relevant, functional state due to the sample preservation by vitrification to explain deviations from formerly known structures. Besides, SthK (*Spirochaeta thermophila*) was reconstituted in nanodiscs and studied in open and closed states (Rheinberger et al., 2018).

The resting state was a previously unknown functional conformation and now allowing for direct comparison and discussion of implications for functional mechanisms.

Recently published structures from eukaryotic CNG channels are expected to give the best insight into the overall architecture (Figure 12). Structures of two channels were obtained using cryo-EM and featured both open and closed states.

TAX-4 is an ion channel subunit native to the nematode *C. elegans* and is related to CNGA subunits. The TAX-4 subunit was cloned and heterologously expressed as a homomeric channel in the following two studies. The TAX-4 channel was first analysed in amphipol, and the presented structure shows the open state at a resolution of 3.5 Å (Li et al., 2017). In 2020, a follow-up study analysed TAX-4 in a lipid nanodisc with resolutions of 2.7 Å and 2.6 Å in the open and closed state, respectively (Zheng et al., 2020). The overall architecture depicted the non-domain swapped configuration, and the complex conformational changes upon cGMP can also be appreciated. Local differences between HCN1 and TAX-4 channels have also been implicated in their work. The presented model explains why nucleotide-binding impacts the channels differently and how changes in membrane potential fail to activate the TAX-4 channel.

The structure of an even more closely related channel, a recombinant human rod CNGA1 homo-tetramer, was analysed and published recently. Here, a truncated CNGA1 has been expressed in *Baculovirus* transfected HEK cells. The obtained structures showed a resolution of 2.9 Å in the open and 2.6 Å in the closed state. There were also different conditions of salt concentration and targeted mutations analysed in this study (Xue et al., 2021). The non-domain swapped conformation was further confirmed, and the gating mechanism has been shown in detail. The previously suspected selectivity filter appears to be not involved in gating. Instead, a distinct area in the pore has been shown to open in response to the ligand binding. The selectivity for divalent ions was traced back to two residues in the filter region.

The increasingly detailed information available now demonstrates that technological limitations have been mostly overcome and that homomeric channels can be investigated. However, a temporal resolution showing intermediate steps in opening and closing dynamics has not yet been studied. Moreover, the absence of a CNGB subunit in all the available high-resolution structures until now illustrates that some crucial aspects of the native CNG channels remain unclear. Especially the modulation and underlying structural dynamics upon Ca^{2+}/CaM binding are of great importance. Furthermore, different phosphorylations are likely involved in the CNG channel modulation, and structural investigations of these states might also be required to understand the function thoroughly.

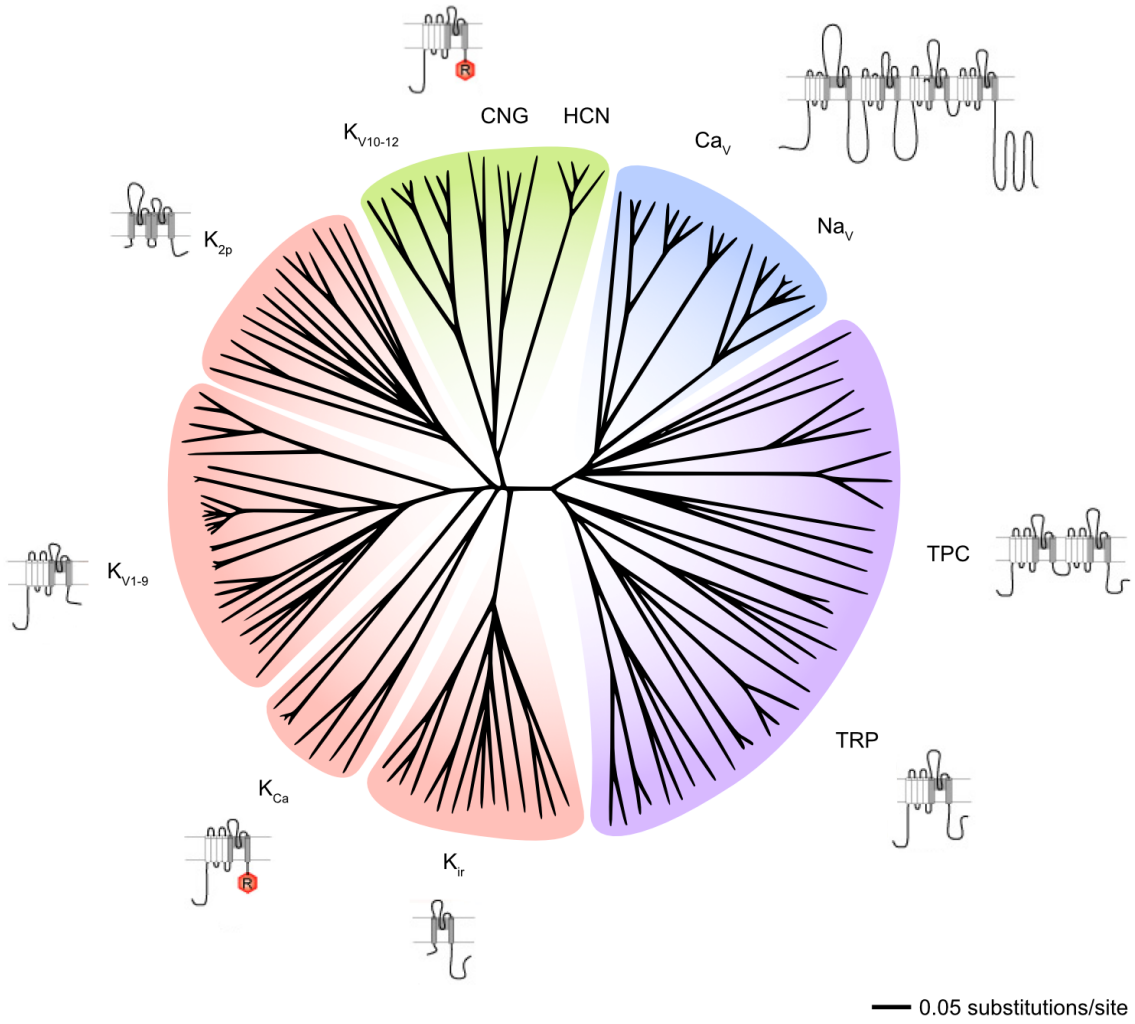

Figure 12: Phylogenetic relationships within the voltage-gated ion channel superfamily

The phylogenetic tree is based on the amino acid sequence homology of the minimal pore regions (from M1/S5 until M2/S6). It depicts 143 members of the voltage-gated ion channel superfamily, grouped into seven families of structurally related ion channels. Corresponding transmembrane topologies are shown next to the name of each family (the cytoplasmic regulatory domain indicated by a red hexagon with the letter R). The families are four-domain channels (Ca_v and Na_v, blue background colour), transient receptor potential (TRP) and the two-pore channels (TPC) (purple background colour), families of potassium selective channels (K_{ir}, K_{Ca}, K_{v1-9}, K_{2p}, red background colour), and cyclic nucleotide-binding channels (K_{v10-12}, CNG and HCN, green background colour). The image was modified after F. H. Yu & Catterall, 2004.

2 Aims and Objectives of this Study

CNG channels are heteromeric ion channels activated by the binding of cyclic nucleotides and play a significant role in the phototransduction cascade of the vertebrate rod photoreceptors. The functional role of CNG channels has been extensively studied for over two decades, which allowed the characterisation of the channel function and the interplay of heteromeric subunits. CNGA subunits are the functional backbone, allowing for cGMP activation and influence functional characteristics, such as affinity and selectivity. The CNGB subunit, on the other hand, is crucial for the modulation of the channel that is mediated by Ca^{2+}/CaM binding (Kaupp & Seifert, 2002; Matulef & Zagotta, 2003). Phosphorylation-dependent modulations are known to occur throughout the phototransduction cascade and have been suggested to be relevant in CNG channels (Gordon et al., 1992; Komolov et al., 2009; Molokanova et al., 1997, 1999, 2003; Weller et al., 1975). Identification of such phosphorylation sites in the native CNG channel would shed light on the existence and mechanism of phosphorylation-dependent (or at least -influenced) modulation. All these factors increase the heterogeneity of the native CNG channels. A complete understanding of architecture and structural states is still unknown, as the native CNG channel from rod photoreceptors so far eludes structural investigation at atomic resolution.

This thesis aims to revisit purification strategies and presents refined purification procedures that exploit the affinity towards cGMP and CaM. In addition, we strive to characterise and compare the resulting two (potentially different) populations of endogenous CNG channels to understand sample composition. Furthermore, phosphorylation is an aspect of the modulation that has not been examined in depth so far, and therefore, we also strive to investigate the phosphorylation status of the different populations.

Three methodological approaches were combined to achieve these goals. 1) Biochemical investigations were employed to provide insight into the purification and stoichiometry of purified CNG channels. 2) Mass spectrometry analysis (LC-MS/MS) was used on the proteomics level to analyse composition and abundance of (co-) purified proteins. Furthermore, the stoichiometry and phosphorylation state of CNG channels was determined. 3) Finally, electron microscopy was used to visualize the purification results and assess fitness for structural investigation.

3 Material and Methods

3.1 Materials

The following sections specify the material used in this study.

3.1.1 Instruments and Software

Type of Instrument	Name	Manufacturer
-80 Freezer	Hera Freeze	Heraeus Instruments
Analytical balance	BP211D	Sartorius
Analytical column	nanoEase™ M/Z HSS T3 column, 75 µm x 250 mm, 1.8 µm, C18, 100 Å	Waters
Balance	EWJ 3000-2	Kern
CEMOS camera	TemCam-F416	TVIPS
Centrifuge	Centrifuge 5417 R	Eppendorf
Centrifuge	Megafuge 2.0	Heraeus Instruments
Computer Workstation	Ryzen™ Threadripper™ 32 core CPU Titan V GPU	AMD Nvidia
Desktop Computer	iMac	Apple
Direct Electron Detector	Falcon 2	FEI / Thermo Fisher Scientific
Dry cabinet	Auto-Star-Desiccator, PMMA	sicco
EM Grids	R2/1 + 2 nm continous Carbon, R1.2/1.3 Holey Carbon	Quantifoil
Freezer	Liebherr comfort	Liebherr
Fridge	Unichromat 900	Uniquip
Homogenizer (40 ml)	Kontes Glas Homogenizer	Kontes Glas Co.
HPLC System	1260 Infinity II	Agilent Technologies
Imager	Licor Odyssey	Li-cor
Imager/CCD camera system	Amersham Imager 600	GE Healthcare
Magnetic stirrer	C-MAG HS7	IKA
Mass spectrometer	Fusion Lumos	Thermo Scientific
Microvolume Spectrophotometers	NanoDrop-2000c	Thermo Fisher Scientific
Nano liquid chromatography system	UltiMate 3000 RSLC	Dionex
Orbital shaker	Sky Line Digital Orbital Shaker S-3.16L	ELMI
pH meter	FiveEasy & InLab Expert Pro	Mettler Toledo
Plasma Cleaner	Med 020	Bal-Tec

Table 1: Instruments and Software

Type of Instrument	Name	Manufacturer
Plasma Cleaner	easy Glow	Pelco
Plate reader	Infinite M1000Pro	Tecan
SDS-PAGE system	PowerPac Basic	Biorad
SDS-PAGE system	Mini-PROTEAN® Tetra	Biorad
TEM	JEOL JEM2200FS	JEOL, Ltd.
TEM	Titan Krios	FEI / Thermo Fisher Scientific
Thermomixer	Thermomixer compact	Eppendorf
Trapping cartridge	µ-Precolumn PepMap™ 100, 5 µm, 300 µm i.d. x 5 mm, C18, 100 Å	Thermo Scientific
Ultracentrifuge Rotor	Ti-70	Beckman Coulter Inc.
Ultracentrifuge	Optima L-100 XP	Beckman Coulter Inc.
Ultramicrotome	Cryo EM UC7	Leica
UV Gel station	UVstar 8 312	Biometra
Wet electroblotter	Mini Trans-Blot® Cell	Biorad

3.1.2 Consumables

Name	Manufacturer
0.2 ml reaction tubes	Eppendorf
1.5 ml reaction tubes	Eppendorf
8-AET-cGMP Agarose beads	Biolog
15 ml Falcon tubes	Eppendorf
2ml reaction tubes	Eppendorf
50 ml Falcon tubes	Eppendorf
Calmodulin agarose	Sigma-Aldrich
cOmplete Protease Inhibitor Cocktail	Roche
DNase	Roche
Filter paper Whatman #2	Whatman
Gravity flow columns	Bio-Rad
Immobilon-FL polyvinylidene (PVDF) membrane	Millipore
Immobilon® Block - FL (Fluorescent Blocker)	Millipore
OASIS HLB µElution Plate	Waters
Parafilm	Bernis
Phosphatase Inhibitor Cocktail 1	Merk
Pierce BCA Protein Assay Kit	Thermo Scientific
Pipette tips	NerbePlus

Table 2: Consumables

3.1.3 Chemicals

Most standard chemicals were sourced from Sigma-Aldrich/Merck, Carl-Roth, and Thermo Fisher Scientific and at least of analytical purity. The following table lists additional chemicals.

Name	Source
3-[(3-Cholamidopropyl)dimethylammonio]-1-propanesulfonate (CHAPS)	Glycon
Soy Polar Lipid Extract	Avanti Polar Lipids
Uranyl acetate	Science Services
Uranyl formate	Science Services

Table 3: Chemicals

3.1.4 Buffers and Solutions

All buffers were prepared with double distilled water (Milli-Q, Thermo Fisher Scientific).

Buffer	Ingredients
Hypotonic Buffer (HB)	10 mM HEPES/NaOH (pH 7.4), 2 mM EDTA, 1 mM DTT, Protease Inhibitor Cocktail, Phosphatase Inhibitor Cocktail 1, DNase
Solubilisation buffer (SB)	10 mM HEPES/NaOH (pH 7.4), 150 mM NaCl, 10 mM $CaCl_2$, 1 mM $MgCl_2$, 1 mM DTT, 10 % (v/v) Glycerol, 0.1 mg/mL Soybean Polar Lipid Extract, 1.2 % (w/v) CHAPS, 0.25 % (v/v) Phosphatase Inhibitor Cocktail 1
Wash buffer (WB1, for cGMP-AC)	10 mM HEPES/NaOH (pH 7.4), 150 mM NaCl, 10 mM $CaCl_2$, 1 mM $MgCl_2$, 1 mM DTT, 10 % (v/v) Glycerol, 0.01 mg/mL Soybean Polar Lipid Extract, 0.9 % (w/v) CHAPS
Wash buffer (WB2, for CaM-AC)	10 mM HEPES/NaOH (pH 7.4), 150 mM NaCl, 1 mM $CaCl_2$, 0.5 mM $MgCl_2$, 1 mM DTT, 10 % (v/v) Glycerol, 0.01 mg/mL Soybean Polar Lipid Extract, 0.9 % (w/v) CHAPS
Elution buffer (EB1, for cGMP-AC)	10 mM HEPES/NaOH (pH 7.5), 150 mM NaCl, 10 mM $CaCl_2$, 0.5 mM $MgCl_2$, 1 mM DTT, 10 mM cGMP, 0.01 mg/mL Soybean Polar Lipid Extract, 0.9 % (w/v) CHAPS
Elution buffer (EB2, for CaM-AC)	10 mM HEPES/NaOH (pH 7.5), 150 mM NaCl, 1 mM DTT, 3 mM EDTA, 0.01 mg/mL Soybean Polar Lipid Extract, 0.9 % (w/v) CHAPS
HEPES Buffer	10 mM HEPES/NaOH (pH 7.5), 150 mM NaCl, 10 mM CaCl2, 0.5 mM $MgCl_2$
Collodial staining solution	0.08% Coomassie Brilliant Blue G250 (w/v) (CBB-G250), 10% citric acid (w/v), and 8% ammonium sulfate (w/v)
Destaining solution	5% Ethanol (v/v) and 7,5% Acetic acid (v/v)
SDS sample buffer (4x)	50 mM Tris (pH 8.9), 100 mM DTT, 2% (w/v) SDS, 0.25% (w/v) Bromophenol blue, 10% (v/v) Glycerol
Transfer buffer	25 mM Tris (pH 8.3), 192 mM Glycine, 20% EtOH, 0.037 % SDS (w/v)
TBS	25 mM Tris-HCl (pH 7.5), 137 mM NaCl, 2.6 mM KCl
TBS-T	25 mM Tris-HCl (pH 7.5), 137 mM NaCl, 2.6 mM KCl, 0.1% (v/v) Tween 20
Gel digestion buffer	50 mM NH_4HC0_3, 5 mM CaCI2, and 12.5 ng Trypsin

Table 4: Buffers and Solutions

3.1.5 Antibodies

Type	Antibody	Applied Dilution	Source
primary Antibody	Rabbit anti- Phosphoserine (ab17464)	1 : 500	abcam
primary Antibody	Rabbit anti-Phosphotyrosine (ab179530)	1 : 750	abcam
primary Antibody	Rat anti-GARP (FPc52k)	1 : 1000	Heinze Körschen
primary Antibody	Rat anti-CNGA1 (ROD E5)	1 : 50	Heinze Körschen
secondary Antibody	Goat anti-rb (926-32211)	1 : 20000	LI-COR
secondary Antibody	Goat anti-rat (926-32219)	1 : 20000	LI-COR

Table 5: Antibodies

3.1.6 Software

Type of Software	Name	Manufacturer
Camera Control	EMMENU	TVIPS
EM control software	TEMCON	JEOL Ltd.
EM processing package	Sphire	Max Plack Gesellschaft Institute of Molecular Physiology, Department Raunser
EM processing package	crYOLO 1.7.2	Max Plack Gesellschaft Institute of Molecular Physiology, Department Raunser, Thorsten Wagner
EM processing package	Relion3.1	MRC Laboratory of Molecular Biology
EM visualisation	UCSF Chimera	University of California
Image processing	EMAN2	S. Ludtke
Image processing	Fiji	J Schindelin and others
Microscope and Camera Control	SerialEM	D Mastronarde, University of Colorado, Boulder
Office software	Word, Excel, Powerpoint	Microsoft
Office software	LibreOffice Writer, Calc	The Document Foundation
Operating system	CentOS	The CentOS Project
Operating system	HighSierra	Apple
Protein Database	UniProt	European Bioinformatics Institute EMBL-EBI Swiss Institute of Bioinformatics SIB Protein Information Resource PIR
Protein interaction database	STRING	Swiss Institute of Bioinformatics European Molecular Biology Laboratory Novo Nordisk Foundation CPR University of Copenhagen, University of Zurich
Raster/Vector Graphics Editor	Affinity Designer	Serif Europe
Search engine Mass Spectrometry	Mascot	Matrix Science

Table 6: Software

3.2 Methods

3.2.1 Purification of Bovine CNG Channel

The source material for the protein purification was bovine rod outer segments (ROS) from dark-adapted animals. They were prepared under dim red light (> 650 nm) by InVision BioResources based on a previously established protocol for structural analysis of rhodopsin (Okada et al., 1998; Palczewski et al., 2000). The ROS were flash-frozen and kept at -80 °C until use. In preparation of analytical investigations, the protein purification was optimized for purity and short duration at the cost of low protein concentration and volume. The purification protocol was developed in recent years by Gayathri Jeyasankar in her dissertation, and it was based on fundamental principles and inspiration obtained from (Cook et al., 1986, 1987). Minor changes were introduced in this thesis after optimising and refining the purification procedure to increase the protein yield, shorten the preparation time, and preserve phosphorylation states. An overview of the purification steps is depicted in Figure 13. In the first sequence of steps, all membrane proteins present in ROS were isolated (see section 3.2.2) and solubilised in the detergent environment (see section 3.2.3). Subsequently, CNG channels were separated from other membrane proteins based on their inherent affinity to cyclic guanosine monophosphate (cGMP) and Calmodulin (CaM) (see sections 3.2.4 and 3.2.5). The composition of buffers used in the course of the protein purification is listed in the Materials section 3.1.4.

3.2.2 Isolation of ROS Membrane Proteins

A pellet from 50 ROS (lnVision Biosciences) was used for each purification, and all following steps were performed under dim red light until stated otherwise. Light exposure does not harm the CNG channel directly, but the light-induced activation of rhodopsin, present in abundance (~2 mg/ml) in the crude ROS input material (Cook et al., 1989; Pugh & Lamb, 2000), results in extensive protein aggregation (Okada et al., 2000). The ROS pellet was thawed upon adding 40 ml hypotonic lysis buffer (HB), resuspended, transferred into a glass homogenizer and was homogenized ten times with the glass pestle. Centrifugation at 150.000 g for 20 min at 4 °C (UC Beckman Coulter and rotor Ti-70) was performed to wash away soluble cytosolic components. The supernatant was discarded, and the pellet was resuspended as described above. The washing procedure was repeated once more.

3.2.3 Solubilisation of ROS Membrane Proteins

The solubilisation buffer (SB) contains the detergent 3-[(3-Cholamidopropyl)dimethylammonio]-1-propanesulfonate (CHAPS). CHAPS is the detergent of choice throughout protein purification because it has proven to be the most efficient solubilisation with the highest extraction rate of CNG and has resulted in stable CNG channel molecules upon reconstitution in detergent micelles (Jeyasankar, 2019). Furthermore, the SB contains soy polar lipid extract (SPLE), presenting a source of lipids for the CNG channel and

thereby stabilising it outside the native ROS membrane environment, as was established by (Jeyasankar, 2019) based on the study by (Gao et al., 2016).

After the hypotonic washes, the pellet was resuspended in 40 ml SB buffer, transferred into a glass homogenizer, and homogenized with the glass pestle. Solubilisation took place over a 60 min incubation period with head over tail rotation at 4 °C in complete darkness. In a final centrifugation step at 150.000 g, 4 °C for 30 min, the now solubilised membrane proteins were separated as supernatant from insoluble debris as a pellet.

3.2.4 Purification via cGMP Affinity Chromatography

Each of the four subunits has a cyclic nucleotide-binding domain (CNBD) with a high affinity towards cGMP, required to activate the channel (Kaupp et al., 1989a; Z. Wang et al., 2007). This binding affinity can be used to purify CNG via cGMP-agarose affinity chromatography (Hurwitz & Holcombe, 1991).

200 µl of 8-AET-cGMP agarose beads were first equilibrated with 5 ml of SB and subsequently washed with 5 ml of wash buffer 1 (WB1). The supernatant obtained after solubilisation (see section 3.2.3) was transferred to the beads and incubated for 25 min, rotating head over tail at 4 °C in complete darkness. Afterward, the unbound fraction was separated from the beads using a gravity-flow column. While the beads were washed with 20 ml WB1, the unbound fraction (UB A) was bound to fresh beads to perform a second cGMP affinity chromatography as described in the next paragraph. The following two elutions were performed under normal light conditions and consisted of incubation of the beads with 100 µl and 300 µl elution buffer 1 (EB1), respectively, for 15 min at 4 °C with gentle agitation. Finally, the samples were collected by a short spin in a centrifuge at 4 °C. The resulting samples are “Elution 1A” and “Elution 2A”.

The obtained unbound fraction (UB A) was incubated with a 400 µl aliquot of fresh, equilibrated, and washed 8-AET-cGMP agarose beads and further treated as described above, but at increased elution volumes of 200 ul (Elution 1B) and 600 ul (Elution 2B). The samples resulting from this second run are “Elution 1B” and “Elution 2B”.

3.2.5 Purification via CaM Affinity Chromatography

This purification approach is very similar to the previously described cGMP affinity chromatography but involves two domains called CaM1 and CaM2. These two domains are present on each β subunit (CNGB1) and are characterized by an affinity to CaM in the presence of Ca^{2+} (Körschen et al., 1995).

The method itself has been performed analogously to the cGMP affinity chromatography, distinguished by the requirement of Calmodulin agarose beads and buffers changed to provide Ca^{2+} ions to facilitate the interaction.

200 µl of Calmodulin agarose beads were first equilibrated with 5 ml of SB and subsequently washed with 5 ml of wash buffer 2 (WB2). The supernatant obtained after solubilisation (see section 3.2.3) was transferred to the beads and incubated for 25 min, rotating head over tail at 4 °C in complete darkness. Afterward, the unbound fraction was separated from the beads using a gravity-flow column. While the beads were washed with 20 ml WB2, the unbound fraction (UB A) was bound to fresh beads to perform a second CaM affinity chromatography as described in the next paragraph. The following two elutions were performed under normal light conditions and consisted of incubation of the beads with 100 µl and 300 µl elution buffer 2 (EB2), respectively, for 15 min at 4 °C with gentle agitation. Finally, the samples were collected by a short spin in a centrifuge at 4 °C. The resulting samples are “Elution 1A” and “Elution 2A”.

The obtained unbound fraction (UB A) was incubated with a 400 µl aliquot of fresh, equilibrated, and washed Calmodulin agarose beads and further treated as described above. Solely the elutions were performed slightly differently by increasing the elution buffer volume to 200 µl and 600 µl, respectively. The samples resulting from this second run are “Elution 1B” and “Elution 2B”.

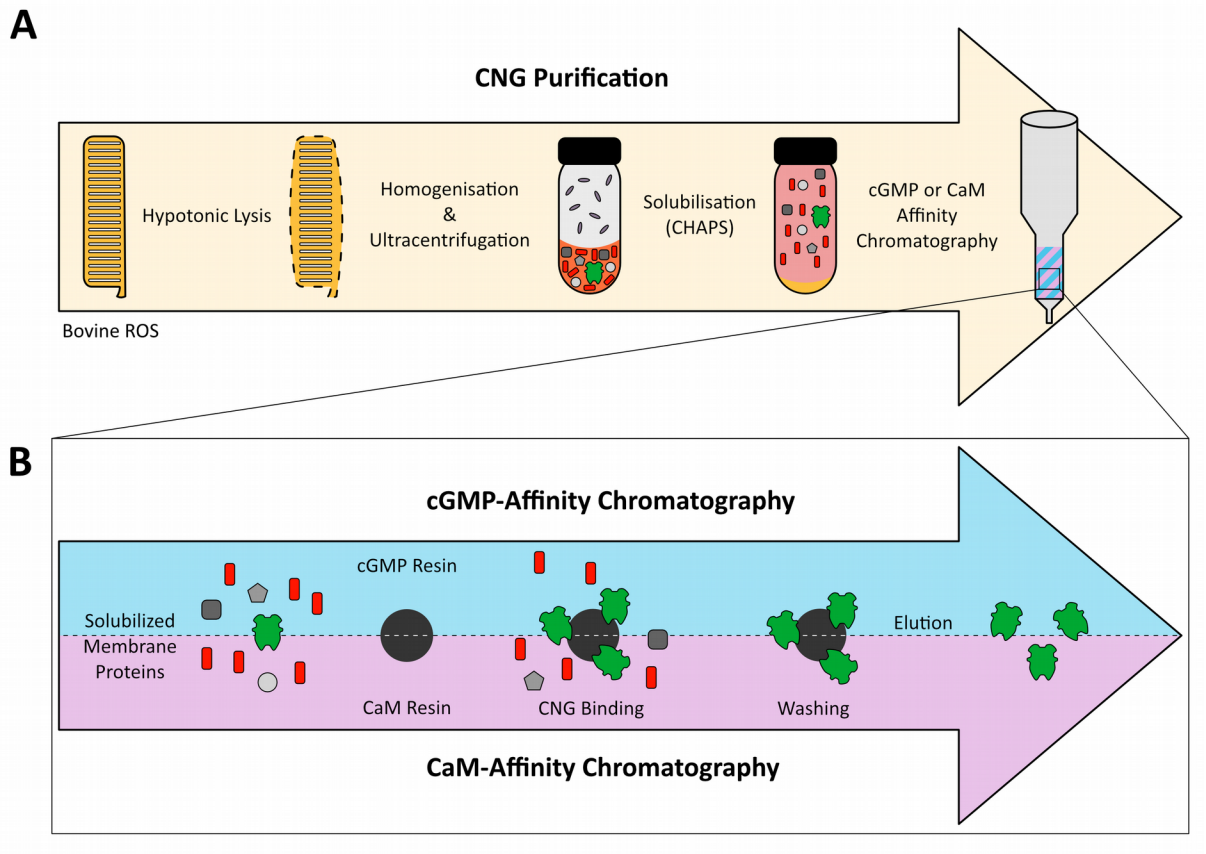

Figure 13: CNG channel purification steps

(A) Bovine rod outer segments (ROS) are subjected to hypotonic lysis, homogenized, and washed. Solubilisation of the ROS membranes was achieved by CHAPS (1.2 % w/v). CNG channels are depicted in green, Rhodopsin in red, other proteins in various grey tones and shapes and the resin as black circle. (B) The partially purified protein is subjected to either cGMP-affinity chromatography (blue) or Calmodulin (CaM)-affinity chromatography (purple).

3.2.6 Crosslinking Samples in-Solution

Glutaraldehyde is a well-studied cross-linking agent in different setups (Hayat, 1986; Migneault et al., 2004; Stark, 2010) and has been successfully used in several studies, where structural examinations by electron microscopy have been conducted (Schiffner et al., 2018; Shigematsu et al., 2010).

For the chemical cross-linking experiments 500 µl Elution 2 B was used. The CNG sample was incubated with 0.05 % (w/v) Glutaraldehyde for 60 seconds at 37 °C in a shaker. The reaction was stopped by adding 200 µl mM Tris/HCl (pH 7.5). The EM-grids were prepared immediately after the cross-linking reaction.

3.2.7 SDS-PAGE

The sodium dodecyl sulphate-polyacrylamide gel electrophoresis (SDS-PAGE) is separating proteins based on their molecular mass. The sodium salt of the detergent dodecyl sulfate denatures the protein and enables electrophoretic separation. The gels used have been prepared based on the protocol by Laemmli (Laemmli, 1970). In brief, a combination of a separation gel containing 8 % (w/v) acrylamide and a thin stacking gel containing 5 % (w/v) acrylamide was prepared. The solutions were prepared at room temperature (RT) without the oxidization agent Ammonium Persulfate (APS) and the catalyst Tetramethylethylendiamin (TEMED). The reaction of the separating gel was started by the addition of APS and TEMED to the buffer and poured into the casting chamber (Bio-Rad). A level surface was achieved by the addition of 2-propanol for the duration of the polymerization. Subsequently, the stacking gel was prepared by adding APS and TEMED to the buffer. 2-propanol was discarded, and the stacking gel was poured on top of the separation gel. A spacer comb was inserted in order to create pockets for the sample application. Again, the gel was allowed to rest at RT for the duration of the polymerization.

Samples from purification experiments were taken and immediately prepared with a denaturing SDS sample buffer (4x buffer: 50 mM Tris (pH 8.9), 100 mM DTT, 2% (w/v) SDS, 0.25% (w/v) bromophenol blue, 10% (v/v) glycerol). The gel was inserted into the Mini-Protean Tetra System (BIO-RAD), and electrophoresis was performed at 120 V until the samples entered the separation gel, followed by 180 V for 40 min.

Afterward, the gel was TCE stained (see section 3.2.8) followed by Coomassie blue staining (see section 3.2.9), or the proteins were transferred to a membrane using the western blot procedure (see section 3.2.11).

3.2.8 Trichloroethanol Stain and Imaging

2,2,2-Trichloroethanol (TCE) is used in an ultraviolet-dependent staining method for polyacrylamide gels (Chopra et al., 2019; Ladner et al., 2004). The TCE covalently binds to the Tryptophan (TRP), and to a certain extent to Tyrosine (TYR), sidechains of the protein upon illumination with ultraviolet light. This reaction leads to a shift of the fluorescent emission from 350 to 450 nm and improved quantum yield. The initial determination of CNG channel subunit stoichiometry was performed using the same approach (Zhong et al., 2002).

After running the SDS-PAGE, the gel was rinsed with double distilled water (ddH_2O) and soaked for 10 min in 10 % TCE (v/v), solved in equal parts Methanol and Water. Subsequently, the gel was rinsed with water and exposed for two minutes to UV light (UVstar 8 312, Biometra). Finally, the gel was imaged (excitation 312 nm) using an Amersham Imager 600. The subsequent analysis is described in section 3.2.10.

3.2.9 Colloidal Coomassie Brilliant Blue Staining and Imaging

Here we use a protein visualization technique with Coomassie Brilliant Blue (CBB) as the main constituent. The protocol for colloidal staining is modified after (Dyballa & Metzger, 2009; D. Kang et al., 2002) and has been reported to yield superior sensitivity over the classic CBB staining (CBS). Furthermore, CBS is compatible with mass spectrometry analysis of stained gel fragments.

The staining solution contains 0.08% Coomassie Brilliant Blue G250 (w/v) (CBB-G250), 10% citric acid (w/v), and 8% ammonium sulfate (w/v). Staining was performed by placing the gel into a plastic container and adding 50 ml staining solution, and the gel was incubated at RT, rocking for 12 h. The staining solution was discarded for destaining, the gel was washed with ddH_2O, and the destaining solution containing 5% Ethanol (v/v) and 7,5% Acetic acid (v/v) was added and incubated until the destaining was complete. Finally, the gel was imaged in the Odyssey imaging system (LI-COR), exciting at 680 nm and detecting at 700 and 800 nm.

3.2.10 Gel analysis – Stoichiometry

The protein amount in the bands was quantified using the Fiji image processing package of ImageJ (Schindelin et al., 2012) and specifically the Gel analyzer package. The signal of the bands on the digitalized SDS-PAGE gels was integrated to obtain a measure for the intensity of the bands. In the process, the background signal was removed from the final quantification value. In contrast to H Zhong and colleagues, the stoichiometry was calculated considering the amount of TRP residues in the observed protein (Zhong et al., 2002). The resulting ratios could be compared between different gels because the values were normalized according to the CNGB1 values.

The following Table 7 includes the TRP content used for the calculations, and the values have been obtained by the ProtParam database (Expasy, Gasteiger et al., 2005).

Gene Name	Protein Name	Organism	Protein accession Number	TRP Residues
CNGA1	cGMP-gated cation channel alpha-1	bovine	Q00194	10
CNGB1	cGMP-gated cation channel beta-1	bovine	Q28181	21
ALB	Albumin	bovine	P02769	3
FTL	Ferritin light chain	human	P02792	1
FTH1	Ferritin heavy chain	human	P02794	1
RHO	Rhodopsin	bovine	P02699	5

Table 7: Number of TRP residues in selected protein subunits

3.2.11 Protein Immunoblotting

Immunoblot was performed to detect specific proteins after performing gel electrophoresis (Towbin et al., 1979). The samples were transferred from the gel onto an activated Immobilon-FL polyvinylidene difluoride (PVDF) membrane (Millipore) using a wet blotting transfer cell (Bio-Rad) at 350 mA with constant Voltage set to 120 V for 1 h. For the transfer, the cell was filled to the marker with transfer buffer (25 mM Tris, pH 8.3, 192 mM Glycine, 20% EtOH, 0.037% SDS). Unspecific binding sites were blocked with Immobilon® Block – FL blocking solution (Millipore) for 60 minutes at RT. All antibodies were diluted in 10 ml equal amounts TBS-T (25 mM Tris-HCl pH 7.5, 137 mM NaCl, 2.6 mM KCl, 0.1% (v/v) Tween 20) and blocking solution at indicated concentrations (section 3.1.5). The PVDF membranes were first incubated with the primary antibody, rocking at 4°C overnight, followed by washing three times with TBS-T at RT. The secondary antibody was incubated rocking at RT for 30 minutes, followed by washing three times with TBS-T for 5 min and once with TBS for 5 min. Finally, the membranes were imaged in the Odyssey imaging system (LI-COR), exciting at 680 nm and detecting at 700 or 800 nm, depending on the secondary antibody used.

3.2.12 Protein Concentration – Bicinchoninic Acid Assay

The first assay used for the determination of protein concentration is the Bicinchoninic acid (BCA) assay. This assay is based on the color shift of the reaction components from green to purple in presence of protein. The color shift is the result of a two-step process. First, the copper ions (Cu^{2+}) from Copper (II) Sulfate are reduced by reacting with the peptide bonds of proteins. In the second step, each Cu^{+} ion reacts with BCA, leading to the colour change (Smith et al., 1985).

The procedure was performed following the manufacturer's instructions. For the BSA standard, eight samples containing 0 µg/ml, 0.02 mg/ml, 0.05 mg/ml, 0.1 mg/ml, 0.2 mg/ml, 0.3 mg/ml, 0.4 mg/ml and 0.5 mg/ml were prepared. The reagent was freshly prepared by mixing 1 ml Copper (II) Sulfate Pentahydrate (4% Solution) and 49 ml bicinchoninic acid

solution. 100 µl of the standard and each sample were mixed with 2 ml of the reagent and incubated at 37 °C for 30 minutes. The samples were allowed to cool down to room temperature before measuring the absorbance at 562 nm.

3.2.13 Protein Concentration – Absorption at 280 nm

Another assay for the determination of the protein concentration is based on the absorption at 280 nm. A micro-volume spectrophotometer measures the absorption at a wavelength of 280 nm, requiring one µL of the sample. No reaction is required because the absorbance is directly measured. While peptide bonds absorb light at about 190 - 200 nm, amino acids with aromatic rings result in an absorbance peak at 280 nm and the relationship between absorbance and protein concentration is linear (Rosenheck & Doty, 1961; R. K. Scopes, 1974). However, the composition of a protein, secondary, tertiary, or quaternary structure and even buffer components or the pH influences the absorbance and may impact the result and accuracy of this method.

Absorbance was measured in a NanoDrop photometer. The measurement was calibrated with the buffer (blank). One µl of protein sample was used to measure the absorbance. As per the previously described BCA-assay, a BSA standard was prepared and measured to calculate the protein concentration of the unknown protein samples.

3.2.14 Protein Concentration – Trichloroethanol-Assay

The reaction used to stain SDS-PAGE gels with 2,2,2-Trichloroethanol (TCE) can also be used to determine the protein concentration in a solution (Chopra et al., 2019).

90 µl of protein sample were mixed with 10 µl TCE in a microwell plate and incubated in UV light (312 nm, 18 Watt) on the glass plate of the UV Gel station for ten minutes. The fluorescent measurement took place in a microplate reader (Tecan) with an excitation at 350 nm and emission measurement at 450 nm. The analysis was performed, taking into account the amount of TRP residues of the protein in question (Table 7).

3.2.15 Electron Microscopy - Sample Preparation Negative Stain

Negative staining is a fast contrasting sample preparation method for analysing biological specimens at room temperature in an electron microscope. The staining solution fixes the proteins (Zhao & Craig, 2003) and increases the contrast by a layer of heavy metal salt crystals. While the original protocol, established by Brenner and Horne in 1959, used Uranyl Acetate as the heavy-metal salt providing the contrast, here, Uranyl Formate was used (Brenner & Horne, 1959). In this thesis, negative staining will be performed to analyse sample quality and acquire single particle datasets to gain low-resolution information about the three-dimensional structure of CNG channels.

Holey EM grids with a continuous carbon overlay on a copper mesh support (Cu R2/1 + 2 nm carbon, 200 mesh, Quantifoil) were glow discharged with an Argon plasma (Easy Glow, Pelco) before staining. 4.5 µl of the sample was incubated on the grid for 60 s and washed three times with 20 µl sample buffer, blotting excess solution from the grid with filter paper (#2, Whatman) without drying the grid entirely. The staining procedure consists of a short pre-stain with 20 µl staining solution (0.75% w/v uranyl formate), followed by a stain with 20 µl staining solution for 20 s, again blotting away excess solution from the grid with filter paper. After blotting away the final staining solution, the remaining thin film was air-dried. The samples were stored in a humidity-controlled environment (auto-star desiccator, SICCO) and protected from light until use.

3.2.16 Electron Microscopy – Screening and Acquisition Negative Stain

The optimisation of the purification protocols was guided by analysing the negative staining samples from critical steps in the procedure. Furthermore, the purified samples were used to gain structural information of the CNG channel.

The RT EM was performed in a JEOL JEM-2200 FS equipped with a Schottky field-emission gun operating at 200 kV and a 4k x 4k CMOS F416 (TVIPS) detector. Samples for screening were inserted in a JEOL Specimen Quartet Holder (EM-01070 SQH) and into the JEM-2200 FS using the dedicated side entry, following the manufacturer's procedures. The EM was controlled by the EMMENU-2 (TVIPS) software, which was also used to acquire micrographs.

To acquire micrographs for single particle analysis, the EM-grid was inserted into the high tilt specimen retainer EM-21311HTR (JEOL), which itself is clamped into the EM-21010 SCSH specimen holder (JEOL) using the spring-based mechanism. This holder is less prone to vibrations or drifting and enables tilting of the grid.

The Microscope was controlled by the SerialEM software (Mastronarde, 2005), which was also used to acquire micrographs. The micrographs were acquired in the center of the holes at a nominal magnification of 60,000 (pixel size 1.82 Å/px). Furthermore, an objective aperture was inserted (100 µm), the exposure time was set to 2 s, and the defocus ranged between -1.5 µm and -3 µm. All micrographs were acquired manually with a delay of 45 s after moving the stage.

3.2.17 Electron Microscopy – Pre-processing

Micrographs were evaluated using the contrast transfer function (CTF) estimation and CTF assessment tools from the Sparx for high-resolution electron microscopy (SPHIRE, version 1.3.2, Max Planck Gesellschaft) software package (Moriya et al., 2017).

After unstacking the micrographs into single files, the CTF values were estimated by CTER in an automated fashion with error assessment (P Penczek 2014). An acceleration voltage of

200 kV, amplitude contrast of 40 %, and pixel size of 1.82 Å/px^2 have been used for the calculation.

The calculated values for defocus, astigmatism amplitude, and astigmatism frequency were evaluated in the CTF assessment tool, and micrographs outside the set thresholds were discarded (values see Table 8). Furthermore, in a manual process, each micrograph was evaluated for major visible damages or features that negatively impact the further analysis (aggregates, carbon film integrity, apparent drift).

Parameter	Lower Threshold	Upper Threshold
Defocus [µm]	1.191	2.423
Total Amp. Contrast [%]	40.000	40.000
Astig. Amp. [µm]	0.118	0.196
Astig. Ang. [deg]	22.528	119.770
Defocus SD [µm]	0.000	0.097
Defocus Freq. Limit [1/A]	0.097	0.274
Astig. Freq. Limit [1/A]	0.090	0.274

Table 8: The parameters and thresholds used for the exemplary dataset

3.2.18 Electron Microscopy – Particle Picking

Particles were picked in an automated process using the crYOLO (version 1.7.2) software (Wagner et al., 2019). This software uses a deep-learning object detection system and can identify particles from unknown proteins in electron microscopy micrographs.

Particle picking was conducted using a box size of 110 px and the general model for negative stain data (gmodel_phosnet_negstain_200520_v1.h5). The PhosaurusNet architecture was used, but no denoising or filtering options were used.

Picking results were reviewed using the box manager from the EMAN2 (version 2.31) image processing suite (NIH), and a confidence threshold of 0.5 for picking was deemed best (Tang et al., 2007).

3.2.19 Electron Microscopy - Processing

Further processing was performed using the RELION program (version 3.1, MRC Laboratory of Molecular Biology) that contains tools for analysing single particle electron microscopy data (Sjors H.W. Scheres, 2012; Zivanov et al., 2018). The main focus of RELION is the structure determination of cryo-EM data, but it can also be used for low-resolution negative stain data. The processing in RELION is limited to the 2D classification of particles followed by the generation of a 3D model, because further steps are not advisable with low-resolution data.

In the reference-free 2D classification, similar particles are grouped. Each of the groups is representing a different viewing angle. Furthermore, particles of rare views and unrelated particles such as other proteins, contamination, or staining artifacts will be discarded. The reference-free 2D classification minimizes introducing a reference-driven bias.

The particles were classified into 75 classes in 25 iterations, with a regularization parameter T set to 2 and a mask diameter set to 200 px. A subset of particles was selected, grouped, and used as input for the following calculation of an initial 3D model. The 3D model generation was conducted *de novo*, again minimizing the introduction of a bias. Here, a stochastic gradient descent (SGD) algorithm is used to generate a 3D model from the different viewing angles (Punjani et al., 2017). The number of classes was set to 1, and a mask diameter of 200 px was used. The CNG channel contains 4 subunits, but differences between A1 and B1 subunits were not expected to be visible at this resolution; therefore, a C4 symmetry was imposed.

A detailed view of micrographs, particle numbers, 2D classes, and the 3D model is presented in the results section (see Figure 33 and Figure 34).

3.2.20 Mass Spectrometry

Mass Spectrometry (MS) is primarily able to plot the molecular mass of a given molecule. This is possible by analyzing the mass-to-charge (*m/z*) ratio of molecules while the charge is known, therefor the molecule of interest has to be ionized before the analysis. However, fully ionizing big molecules such as proteins is difficult, therefor the peptide mass fingerprinting (PMF) technique was used for the analysis in this thesis. In this PMF approach, the protein is digested into peptides using specific proteases. The peptide fragments are then identified, and the protein sequence is determined in a bottom-up approach (Henzel et al., 1993; Mann et al., 1993; Pappin et al., 1993). Unfortunately, the molecular mass alone is insufficient to identify a peptide without a doubt, because there are many proteins with the same mass and potentially heterogeneous modifications, splice variants, and other chemical changes present. By breaking the peptides further down, for example in a High energy Collision-induced Dissociation (HCD) cell, more detailed m/z information can be gathered. Here, the initial affinity chromatography-based purification is coupled to an MS system containing a nano-liquid chromatography device that directly injects into the mass spectrometer (LC-MS) that analyses the sample in a two-staged approach, called tandem mass spectrometry (MS/MS).

3.2.21 Mass Spectrometry - Sample Preparation

Elutions from the Protein Purification and SDS Gels were prepared as previously described (section 3.2.7). Gels were packed and shipped to EMBL at room temperature, while the in-solution samples were flash-frozen and shipped on dry ice.

In-Solution sample preparation and digest

Reagents were prepared in 50 mM HEPES, pH 8.5. First cysteines were reduced using 10 mM DTT at 56 °C for 30 minutes. Samples were cooled to RT and alkylated with 20 mM 2-chloroacetamide in the dark for 30 minutes. Afterward, samples were prepared for MS analysis using the Single-Pot Solid-Phase-enhanced Sample Preparation (SP3) protocol (Hughes et al., 2014), designed to separate the proteins from other components, such as detergents.

In brief, 2 µl paramagnetic beads (Sera-Mag Speed Beads A+B Thermo Scientific; CAT No. 09-981-121 and -123) with a carboxylate-modified surface were added to 100 µl sample. Afterward, 5 µl of 1% formic acid was added to acidify the solution and induce a reaction of free amines with the carboxyl groups of the beads. Subsequently, 15 µl acetonitrile was added to precipitate the proteins. After an incubation time of 8 min at RT, the reaction tube was placed on the magnetic rack for 2 min. The supernatant was discarded, and the beads washed twice with 200 µl 70 % EtOH, and once with 180 µl acetonitrile and then left to air-dry for 30 s. The beads were reconstituted in 50 mM HEPES, pH 8.5.

The proteins were digested with 300 ng trypsin for 14 h at 37°C, and finally, remaining acidic, basic, and neutral compounds were removed using an OASIS HLB µElution Plate (Waters), following the manufacturer's protocol.

In-Gel sample preparation and digest

Bands were excised as indicated (see Figure 33) and subjected to in-gel tryptic digestion (Savitski et al., 2014; Wilm et al., 1996). In brief, the gel pieces were washed with 100 mM NH_4HC0_3 and acetonitrile, the digestion buffer (50 mM NH_4HC0_3, 5 mM $CaCl_2$, and 12.5 ng trypsin) for 45 min at 4°C. The supernatant was discarded, and the gel piece was covered with 10 µl buffer (50 mM NH_4HC0_3, 5 mM $CaCl_2$) and incubated overnight at 37°C (Hellman et al., 1995; Wilm et al., 1996). Afterward, the peptides were extracted from the gel pieces by sonication for 15 min, the gel fragments were separated from the supernatant by short centrifugation, and the supernatant was collected.

For a second extraction, the gel pieces were mixed with twice their volume of a solution of 1 % formic acid (v/v), solved in equal parts water and acetonitrile. The gel pieces were again sonicated for 15 min and shortly centrifuged to separate the gel fragments from the supernatant, that was combined with the previously obtained. The supernatant was dried using a speed vacuum centrifuge and resolved in 10 µl of reconstitution buffer (96 to 4 parts water to acetonitrile, 1% formic acid (v/v)).

3.2.22 Mass Spectrometry - Data Acquisition

An UltiMate 3000 RSLC nano (Dionex) liquid chromatography (LC) system separates 2 µl of protein sample. The LC is equipped with a trapping cartridge (µ-Precolumn PepMap™, Thermo Scientific) and an analytical column (nanoEase™ M/Z HSS T3 column, Waters). A Fusion Lumos (Thermo Scientific) mass spectrometer was coupled to the LC outlet via the Proxeon Nanoflow Electrospray Ionization Source (nanoelectrospray ionization, nanoESI) in positive ion mode.

The MS1 scan was set to a resolution of 120,000, and the filling time was set to a maximum of 50 ms. The mass spectrometer was operated in a data-dependent acquisition mode (DDA). The HCD normalized collision energy was set to 34. The MS2 scan was set to a resolution of 30,000, with a fill time of 86 ms and a target of $2x10^5$ ions.

3.2.23 Mass Spectrometry - Data Processing and Analysis

The acquired data was processed to the analysis in question. A quantitative proteomics package called MaxQuant was used for the quantification and complex analysis, while the phosphorylation status was determined using the IsobarQuant. For all branches of MS data analysis the mass error tolerance for the full scan MS spectra was set to 10 ppm and for the tandem MS spectra the mass error tolerance was set to 0.02 Da. For the *in silico* tryptic digest a maximum of two missed cleavages was allowed.

Identification

The first analysis was performed using the Mascot (v2.2.07) search engine (Matrix Science, Perkins et al., 1999), searching against the UniProt (Universal Protein Resource) *Bos Taurus* database (UP000009136) containing common contaminants, reversed sequences, and the sequences of the proteins of interest (Bateman et al., 2021). For the identification only peptides longer than six amino acids were taken into account. A minimum of 2 unique peptides was required for the identification of a protein. Furthermore, a false discovery rate below 0.01 was necessary on both, the peptide and protein level.

Quantification and complex analysis

Andromeda search engine searching UniProt *Bos Taurus* database for mapping and MaxQuant (v1.6.3.4) was used to match the observed peptides against theoretical digestion of bovine proteins (Cox & Mann, 2008). Quantification was performed using iBAQ value that compare the peak intensities for all peptides to the theoretically observable peptides as a proxy for the relative protein abundances (Schwanhüusser et al., 2011). The theoretically observable peptides range from a length of 7 to 30 amino acids and missed cleavages were not considered. The iBAQ values were also used to perform the complex analysis. However, peptides were only matched to a subset of four CNG subunits (CNGA1, CNGA2 CNGA3 and CNGB1).

Determination of Post-Translational Modifications

The determination of PTMs was initiated by the Mascot search engine, matching peptides against the UniProt *Bos Taurus* proteome database. Furthermore, the charge-per-mass ratio was analysed by IsobarQuant (Franken et al., 2015) and the following modifications were searched for: Carbamidomethyl (C; fixed modification), Acetyl (N-term), Oxidation (M), and Phospho (STY). The Mascot Delta Score (MD-score or delta-mod) is a parameter that informs about the precision of a phosphorylation site analysis (Savitski et al., 2011).

In this thesis, only phosphorylations will be analysed because they are present in about a third of mammalian proteins (Vlastaridis et al., 2017) and are suspected to be involved in CNG modification (Molokanova et al., 1997, 1999). The presence of a phosphorylated residue can be detected based on the additional mass of the attached phosphate group (PO_4^{3-}) (Baumann & Meri, 2004).

The following schematic overview summarises steps taken for MS analysis of the CNG channel (Figure 14).

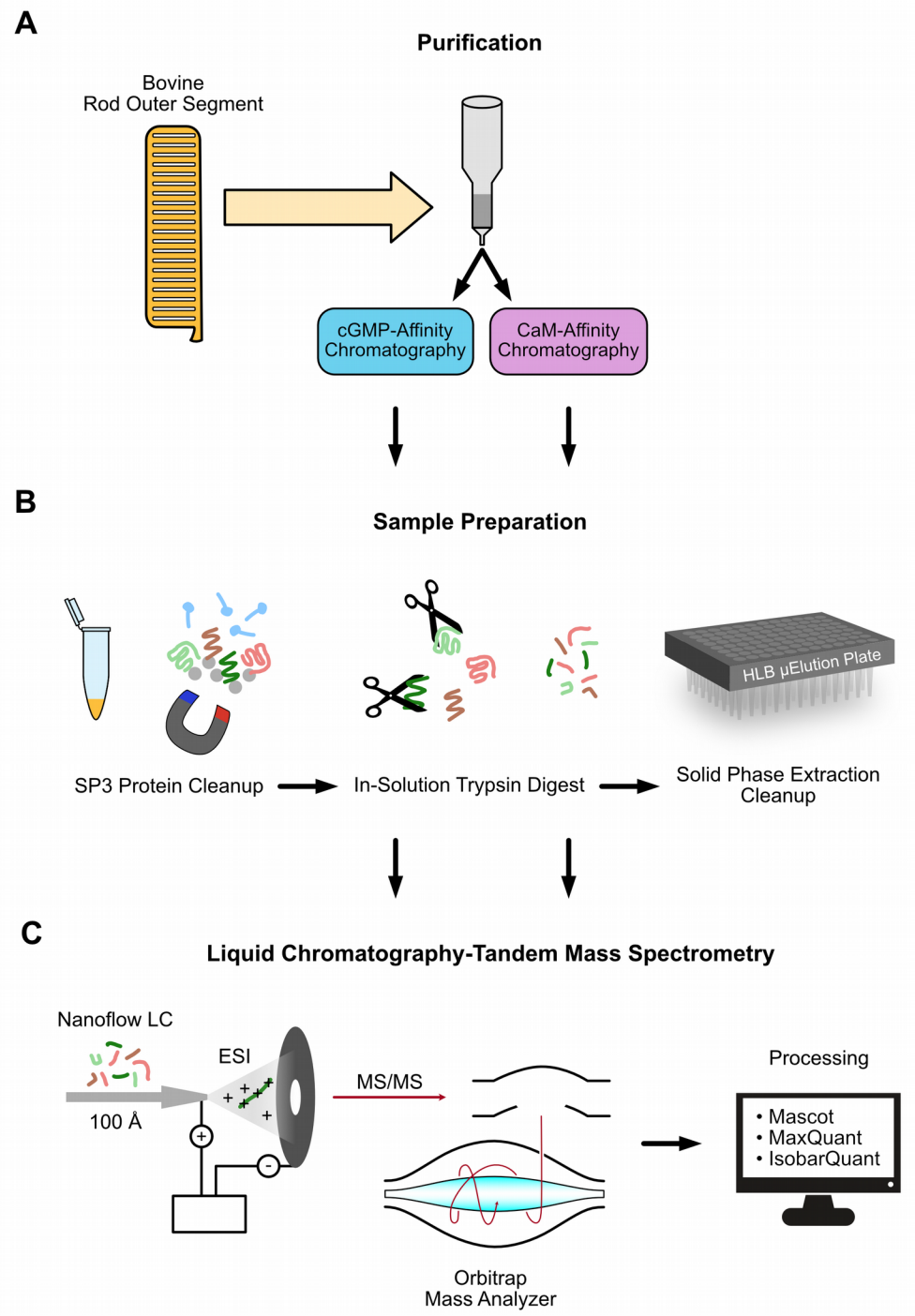

Figure 14: Illustrated overview of Mass Spectrometry workflow

(A) Purification of CNG channels via cGMP-affinity chromatography or CaM-affinity chromatography. The samples were kept separated at all times. (B) Preparation of purified protein sample. First, the sample was cleaned from compounds other than protein following the Single-Pot Solid-Phase-enhanced Sample Preparation (SP3) protocol. Afterward, the proteins were digested with trypsin, and the resulting peptides are cleaned once more (OASIS HLB µElution Plate, Waters). (C) For the mass per charge ratio analysis, the peptides were first separated by nanoflow liquid chromatography (LC). The LC was coupled to the mass spectrometer (MS) via a nanoflow electrospray ionization source (nanoESI, positive ion mode). In tandem mass spectrometry (MS/MS), the spectra were acquired and finally processed using software such as Mascot (identification), MaxQuant (quantification and complex analysis), and IsobarQuant (post-translational modifications).

4 Results

4.1 Purification of the CNG Channels from Bovine ROS

CNG channels have been known for decades and extensively studied with regard to conductivity and modulation under various conditions. The accepted subunit stoichiometry for the heteromeric channel is three CNGA1 subunits, which are mainly responsible for cGMP binding, and one CNGB1 subunit, which has a modulatory function. Nonetheless, the molecular and structural basis of the subunit interaction and the channel modulation in the presence or absence of ligands and other molecules remains unknown. The aim of the study is to analyse endogenous CNG channels from bovine ROS, and therefore endogenous tissue was used as source material for the purification. In order to allow for characterisation of the endogenous CNG channel with modern proteomics approaches, the purification procedure was optimized and streamlined. The main incentives for the optimisation are the limited availability of the endogenous material, time spent on the purification, and the resulting concentration of the purified protein.

ROS obtained from the dark-adapted bovine retina have been used as the source material. Upon hypotonic lysis, the soluble proteins in ROS have been washed away, and the remaining membrane has been solubilised using the detergent CHAPS, followed by the enrichment of the CNG channels using one of the two resins by affinity chromatography (see 3.2.4 and 3.2.5). The reasoning behind affinity chromatography over other approaches like size exclusion chromatography is discussed in chapter 5.1. Finally, the purified CNG channel was obtained as eluate from the affinity resin.

The elution is carried out in a pre-elution step (E1A) that contains only a low concentration of CNG channel, but relatively high amounts of Rhodopsin followed by the main-elution (E2A). Unless stated otherwise, elution 2A (E2A) of the respective affinity chromatography was used for further experiments.

The small elution volume is required to obtain a sufficient protein concentration but limits the number of experiments that can be performed. Therefore, the unbound fraction (UB A) was bound to fresh beads and again eluted by pre-elution (E1B) and main-elution (E2B) to obtain additional sample material that was used to establish experimental procedures.

4.1.1 Two Approaches of Affinity Chromatography

The SDS-PAGE gels followed by CBS give a stepwise overview for the purification through its different stages, with the “Input” representing the raw source material and “Elutions“ showing the final product, of which the main-elution (Elution 2A) has been used for further analysis in most cases.

The hypotonic buffer contains the chelating agent EthyleneDiamineTetraAcetic acid (EDTA) to sequester Ca^{2+} besides other di- and trivalent metal ions. Thereby proteins already bound to CNG that rely on Ca^{2+}, such as CaM, are separated from the channel. Furthermore, a protease inhibitor cocktail was added to inhibit any endogenous proteases present to prevent protein degradation over time. Similarly, the phosphatase inhibitors were added to protect the phosphorylation status of CNG for further analysis.

Figure 15 A shows the gels from a representative cGMP-AC, and Figure 15 B shows the gels from a representative CaM-AC, stained with CBB. Both figures demonstrate the successful purification of CNGA1 and CNGB1 as the Rhodopsin was strongly depleted in comparison to CNG subunits (see supplementary Table 9).

The most abundant protein in the ROS is Rhodopsin, with an estimated concentration of about 1-2 mg per ROS (Cook et al., 1989; Pugh & Lamb, 2000), running at about 36 kDa on SDS-PAGE. CNGA1 runs in the SDS-PAGE at about 64 kDa, and CNGB1 runs slightly above the 245 kDa band. The apparent running height is as expected for CNGA1 based on the molecular weight of the subunit. CNGB1 has a molecular weight of 155 kDa but runs much higher, which can be explained by the negatively charged GARP domain (Körschen et al., 1995). Supernatant 1 and 2 represent the fractions containing the soluble proteins of the ROS, while all membranes and membrane proteins are present in the samples Pellet 1 and 2. The second wash (Supernatant 2) demonstrates the successful depletion of soluble proteins.

The solubilisation was performed based on the procedure defined by (Jeyasankar, 2019), which resulted in effective solubilisation of the membrane proteins, as seen in the respective sample (Solubilisation). Three bands were observed in the samples of elutions corresponding to CNGB1, CNGA1, and Rhodopsin. The former two bands were better defined and more intense in the elutions than earlier purification steps (Input, Pellet, or Solubilisation), indicating an increase in purity and concentration, while the Rhodopsin band was only faintly observed in the elution.

Further analysis of protein concentration and composition of the bands was performed and is shown in section 4.2.2 and 4.3.2.

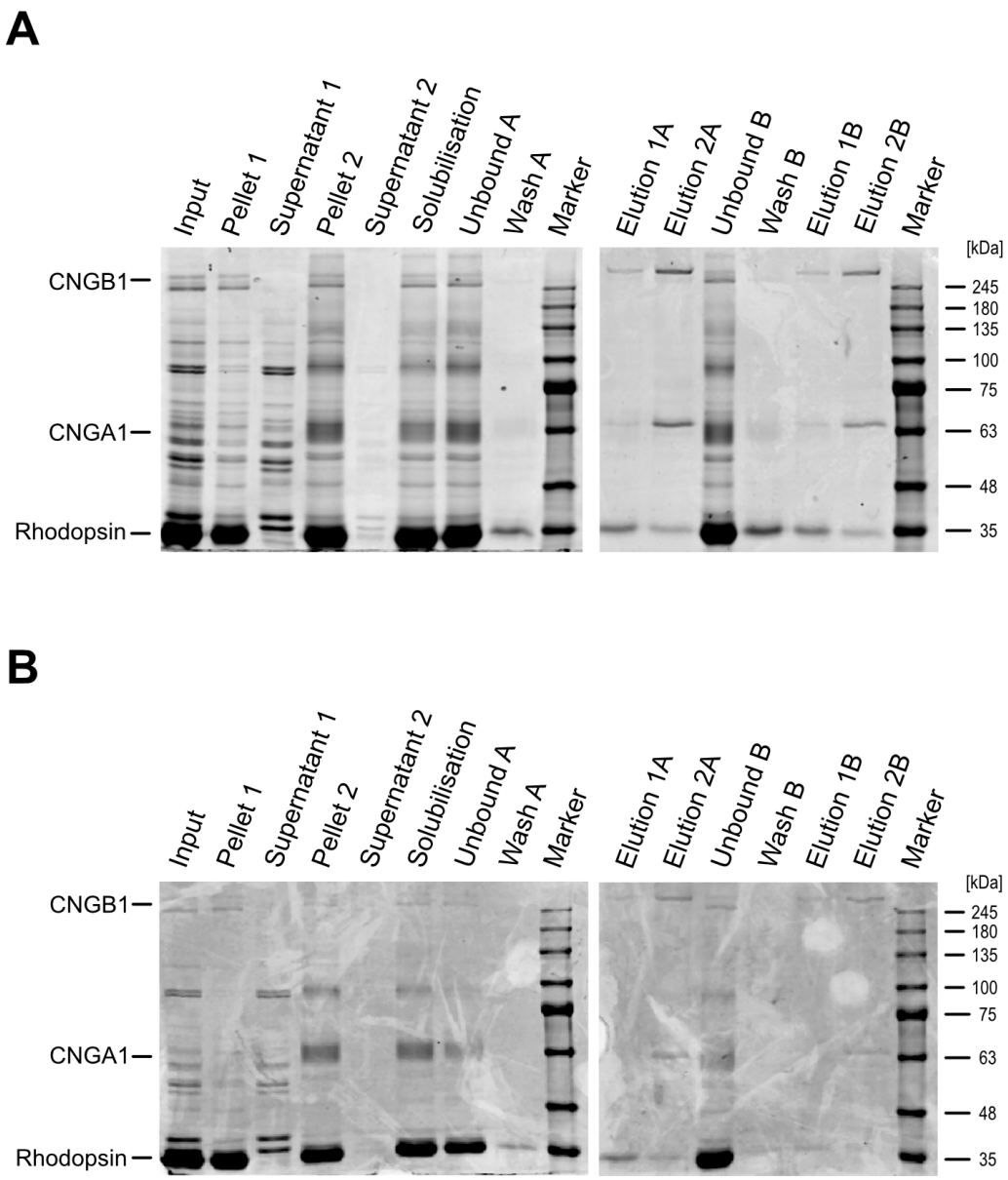

Figure 15: Purification of endogenous CNG channel from rod outer segments

Rod outer segments were harvested from 50 dark-adapted bovine retinas, and the CNG channels were obtained from it through the following steps: hypotonic lysis, membrane solubilisation with CHAPS, and purification using either (A) cGMP agarose beads or (B) CaM agarose beads. The unbound material (Unbound A) was incubated with fresh beads for a repetition (Elution 1B and 2B). An aliquot of the samples was taken throughout each step of the purification and the final elutions. SDS-PAGE was performed, followed by Coomassie Brilliant Blue staining to assess the course of purification. The typical running heights of CNGB1, CNGA1, and Rhodopsin are indicated on the left. For a detailed description of all purification steps, see section 3.2.1 to 3.2.5.

4.2 Biochemical Characterisation of CNG Channels

Following the updated purification procedure (sections 3.2.1 to 3.2.5), the quality of the resulting samples was evaluated, and further biochemical characterizations have been conducted. This section demonstrates the identification of CNGA1 and CNGB1 using immunoblotting, assessment of stoichiometry, determination of the concentration, and antibody informed characterisation of bands (WB analysis).

The immunoblot was performed with antibodies specific for the two CNG channel subunits CNGA1 and CNGB1, to confirm the identity of the bands. Furthermore, antibodies were used to inform about the presence of phosphorylation on either Serine/Threonine or Tyrosine residues in these subunits.

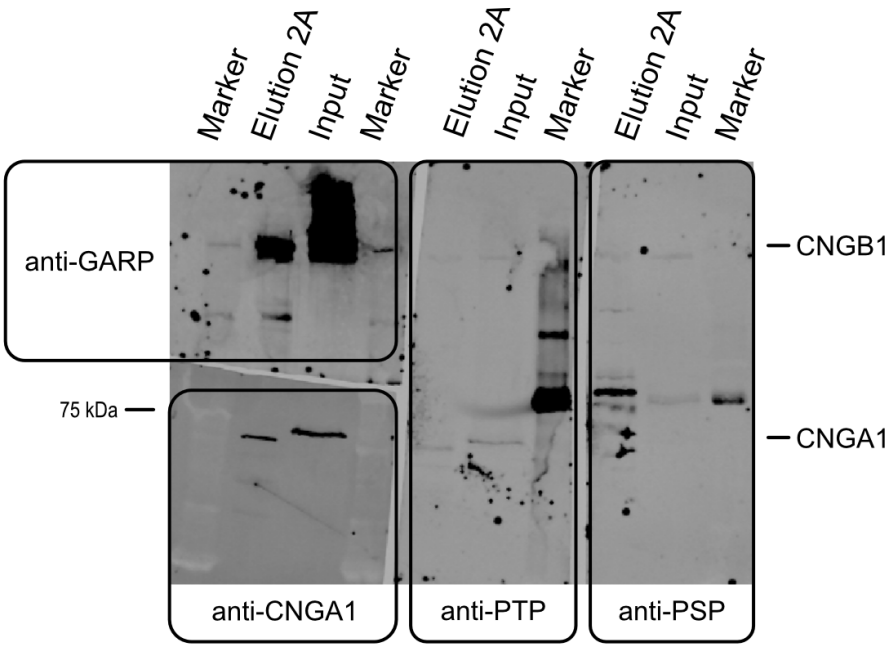

Figure 16: Immunoblot Analysis of CNG proteins from cGMP affinity chromatography

Marker, protein samples of Input and Elution 2A from cGMP-AC were subjected to SDS-PAGE analysis followed by immunoblotting. The immunoblot membrane was cut into four pieces, and each section was developed with four different antibodies as follows: anti-PSP - antibodies against phosphorylated Serine/Threonine residues, anti-PTP - antibodies against phosphorylated Tyrosine residues, anti-GARP - antibodies against the glutamic acid-rich protein of CNGB1 subunit of CNG channels, and anti-CNGA1 - antibodies against the CNGA1 domain of CNG channels. The typical running height of CNGB1 and CNGA1 are indicated on the left.

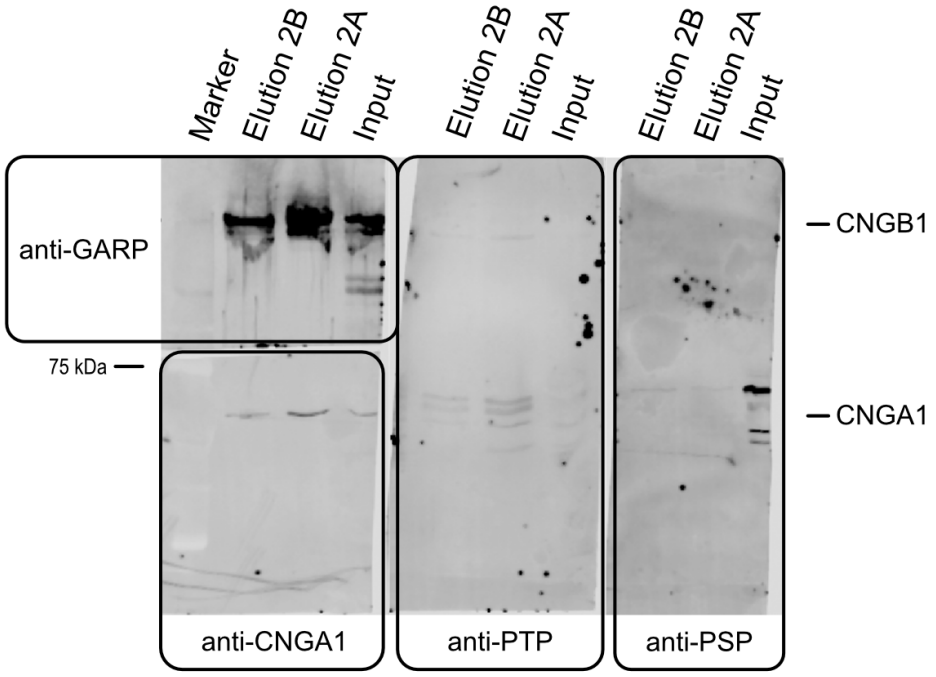

Figure 17: Immunoblot Analysis of CNG Proteins from CaM Affinity Cromatography

Marker, protein samples of Input and Elution 2A from CaM-AC were subjected to SDS-PAGE analysis followed by immunoblotting. The immunoblot membrane was cut into four pieces, and each section was developed with four different antibodies as follows: anti-PSP - antibodies against phosphorylated Serine/Threonine residues, anti-PTP - antibodies against phosphorylated Tyrosine residues, anti-GARP - antibodies against the glutamic acid-rich protein of CNGB1 subunit of CNG channels, and anti-CNGA1 - antibodies against the CNGA1 domain of CNG channels. The typical running height of CNGB1 and CNGA1 are indicated on the left.

The antibody specific for the CNGB1 subunit binds to the GARP domain. Therefore, in both purifications, a strong signal was observed in the input and elution samples, confirming the reported and previously mentioned running height of CNGB1 above the 240 kDa mark (Figure 16 and Figure 17 anti-GARP) (Körschen et al., 1995; R. S. Molday et al., 1991). The additional bands visible in the input are likely the soluble GARP 1, that runs at about 130 kDa and was also shown by Körschen and colleagues (Körschen et al., 1999). Likewise, the presence of the CNGA1 subunit was verified by the antibody specific against the CNGA1 subunit (anti-CNGA1), showing clear bands at about 66 kDa (Figure 16 and Figure 17 anti-CNGA1).

Visualisation of protein with phosphorylated residues was performed using antibodies against phosphorylated Serine/Threonine residues (anti-PSP) and antibodies against phosphorylated Tyrosine residues (anti-PTP). Phosphorylated Tyrosine residues can be observed for proteins running at about 66 kDa after cGMP-AC in the input and elution samples (Figure 17 anti-PTP), and a weak signal is visible at the corresponding running height of the CNGB1 subunit. Protein from CaM-AC (Figure 17) also shows a weak signal indicating phosphorylated Tyrosine residues running above 245 kDa. Moreover, multiple proteins contain phosphorylated Tyrosin residues, running at about 66 kDa (Figure 17 anti-PTP).

In the input and elution samples of cGMP-AC purified protein, signals corresponding to phosphorylated Serine or Threonine residues were observed in proteins running at above 245 kDa, and at 75 kDa. Additional weaker bands are visible in the elution at running eights of about 130 kDa and above and below the strong band at 75 kDa (Figure 17 anti-PSP).

With the anti-PSP antibody, the input samples and protein purified via CaM-AC show bands at 75 kDa running height and in the input three more protein bands are visible running below 75 kDa. The upper area on the SDS-PAGE gel lacks any signal for protein containing phosphorylated Serine or Threonine residues (Figure 17 anti-PSP).

For further analysis of the elution samples, it has to be noted that there are several proteins co-purified but only visible by antibody detection if they are coincidentally phosphorylated. Furthermore, the population of these co-purified proteins varies between purification approaches as most bands were specifically observed in only one of the purification approaches.

4.2.1 Quick insight into Stoichiometry of Hetero-Tetrameric Protein

For heteromeric proteins such as the CNG channel, knowing the correct stoichiometry is the basis for structural investigations or functional assays. In rods, the subunit arrangement of CNG channels was previously concluded to consist of three CNGA1 subunits and one CNGB1 subunit. When determining this arrangement, the principle behind the studies was to establish similar functional results as the native channel when modified by cross-linking or expressed heterologously (see section 1.2.4). However, a margin of error can be present in indirect approaches because both cross-linking of proteins and heterologous expression of heteromeric membrane proteins are hard to regulate and accomplish consistently.

A native composition of the channel, including potentially unknown modifications, is ensured by using an endogenous source such as ROS from the bovine retina as the source material. In this section, the purified CNG channels were characterized regarding the stoichiometry-based on SDS-PAGE gels. While the CBS is a common staining technique, it is prone to bind specific proteins better than others. Therefore, the Coomassie staining cannot determine the protein concentrations due to uncharacterized or unknown binding/staining behaviour. Band intensity after staining with Trichlorethanol (TCE), on the contrary, has been reported to represent protein abundance well (Chopra et al., 2019; Ladner et al., 2004). H Zhong and colleagues have also used TCE back in 2002 to analyse the stoichiometry of CNG channels from bovine rods (Zhong et al., 2002) (section 3.2.8). Control experiments have been performed to establish the feasibility of this approach. Known amounts of BSA and GFP have been mixed in three different ratios, and the protein mixtures were subjected to SDS-PAGE and TCE-staining. The band intensity was measured, and the ratio of the proteins was experimentally determined as shown in Figure 37.

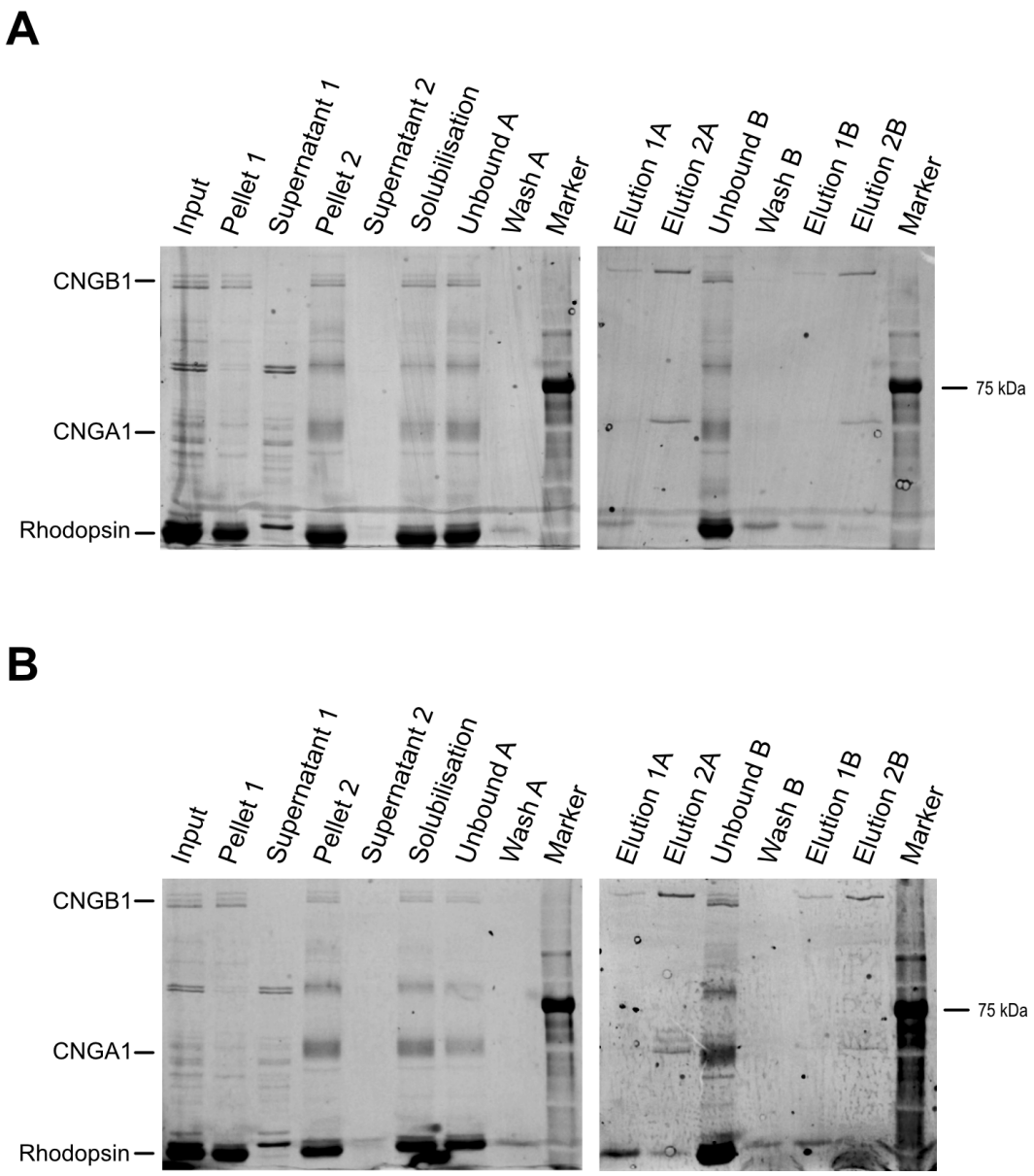

Figure 18: Trichlorethanol staining of SDS-PAGE gels from CNG channel purification

Rod outer segments were harvested from 50 dark-adapted bovine retinas, and the CNG channels were obtained from it through the following steps: hypotonic lysis, membrane solubilisation with CHAPS, and purification using either (A) cGMP agarose beads or (B) CaM agarose beads. The unbound material (Unbound A) was incubated with fresh beads for a repetition (Elution 1B and 2B). An aliquot of the samples was taken throughout each step of the purification and the final elutions. SDS-PAGE was performed, followed by TCE staining. The typical running heights of CNGB1, CNGA1, and Rhodopsin are indicated on the left. For a detailed description of all purification steps, see 3.2.1 to 3.2.5. The band intensity was measured using the gel analyzer tool in the ImageJ software package (3.2.10).

The gels containing samples of the cGMP-AC purification were stained and imaged with TCE (Figure 18 A) before the CBS shown in Figure 15 A. The same process was performed on the gels containing samples of the CaM-AC purification (Figure 18 B and Figure 15 B).

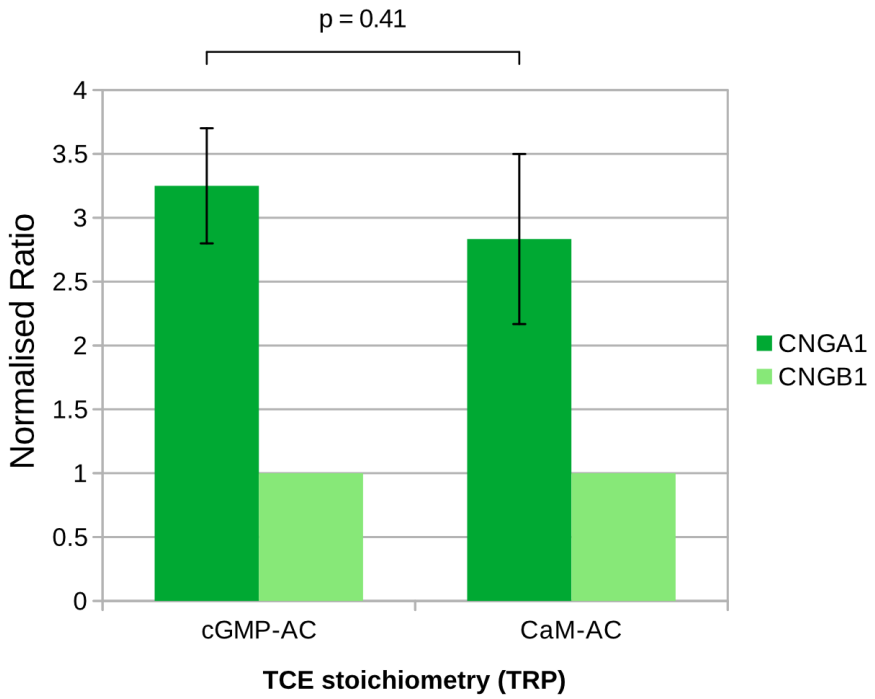

Figure 19: Stoichiometry of purified CNG channels determined by TCE

The Elution 2A sample was analysed regarding CNG subunit stoichiometry. TCE staining of SDS-PAGE gels followed by measurement of the band intensities was performed using ImageJ software package (Schindelin et al., 2012). The data was corrected for the number of Tryptophan residues in CNGA1 and CNGB1 and normalised for CNGB1 (section 3.2.10). The p-value was calculated according to student's t-test; $n_{cGMP\text{-}AC} = 4$ and $n_{CaM\text{-}AC} = 3$.

The average value for the relative amount of the CNGA1 subunit is 3.25 for cGMP-AC eluates or 2.83 for CaM-AC eluates in respect to the CNGB1 subunit (Figure 19). The p-value of 0.41 indicates no significant difference between the two purification approaches. A comprehensive comparison of the two different purification methods can be found in the discussion (section 5.1).

4.2.2 Determination of Concentration

One of the essential measures in protein purification is concentration. Conventional approaches, such as absorbance measurements at 280 nm, the Bradford assay, or the Bicinchoninic acid (BCA) assay, have been used in an attempt to determine the concentration of CNG channels. However, all of these assays failed to produce consistent results in our hands.

A less prominent method involves the trichlorinated compound 2,2,2-Trichloroethanol (TCE) and aims at visualizing proteins after shifting the emission spectrum. The method follows the principle of the stoichiometry experiments described previously, but the reaction is performed in solution instead of in the gel (Chopra et al., 2019).

As this method is not well characterized, we performed control measurements with two proteins, BSA and (human) Apoferritin, and compared the results of two established methods, absorbance at 280 nm, BCA-assay, with the new TCE-assay (Appendix 7.5).

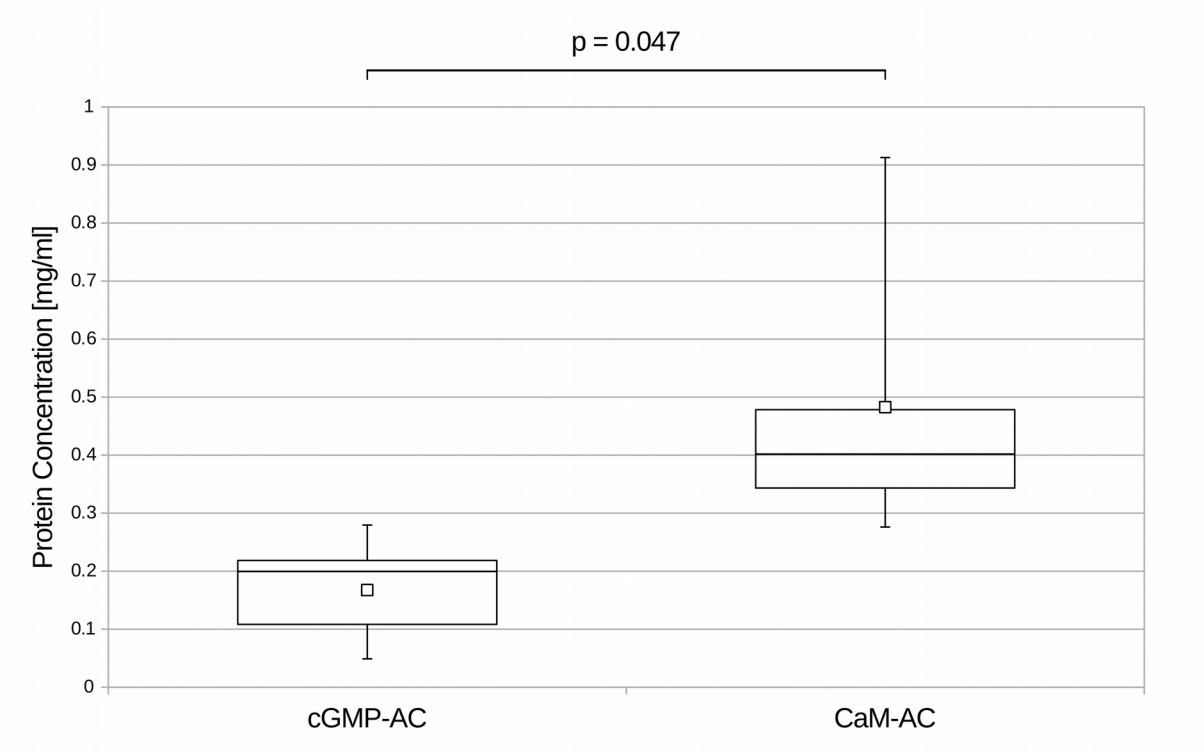

Figure 20: CNG concentration determination by TCE protein assay

The CNG channel protein concentration in Elution 2A was measured with the TCE assay, and the figure shows the distribution of three independent experiments. In this box plot representation, the whiskers indicate the 1st and 4th quartiles ranges, and the box contains the 2nd and 3rd quartiles. Within the box, the median (line) and the average (little square) are indicated. P-value was calculated according to students t-test; $n_{cGMP\text{-}AC} = 7$ and $n_{CaM\text{-}AC} = 5$.

The concentration of the CNG channel was measured immediately after the purification. The mean concentration for cGMP-AC is 0.169 mg/ml and the median is 0.199 mg/ml, whereas the mean concentration for CaM-AC is 0.48 mg/ml and the median is 0.40 mg/ml (Figure 20).

The variance of values represents an apparent difference between the two purifications. CaM-AC stands out with a much higher spread, while the interquartile is similar. The apparent differences between both samples are supported by the p-value of 0.047, calculated using the student's t-test.

4.3 Mass Spectrometry Driven Characterisation

There is a wide array of methods based on mass spectrometry that can characterize and analyse proteins. The focus of this thesis is rapid methods that do not require additional modifications of the purified proteins. Four topics will be covered in the MS section of this thesis: 1) identifying proteins in a given sample, 2) quantification of present proteins, 3) analysis of CNG channel complex composition, and 4) post-translational modifications, especially phosphorylations present in CNG channels.

4.3.1 Protein Identification

Further characterisation is aided by the identification of all proteins present in the samples. The MS data acquisition gathers information about the sequence of peptides, and these identified peptides are then matched with a database of proteins to assess the presence of proteins.

The proteins were purified using either cGMP-AC or CaM-AC, and the samples were subjected to a tryptic digest. After that, the samples were separated by liquid chromatography and transferred into the tandem MS system by nanoelectrospray ionisation, and the mass-to-charge ratio of the peptides was determined (section 3.2.23 and Figure 15).

All Proteins with an entry in the UniProt database (bovine proteins, including splicing variants), a minimum of two unique peptide matches (upm), and a total score above 100 have been considered in the following analyses.

The following Venn diagrams represent the concurrence in the proteins identified for the three biological replicates for each of the two purifications (Figure 21 A and B). Furthermore, the cumulated identified proteins were compared (Figure 21 C).

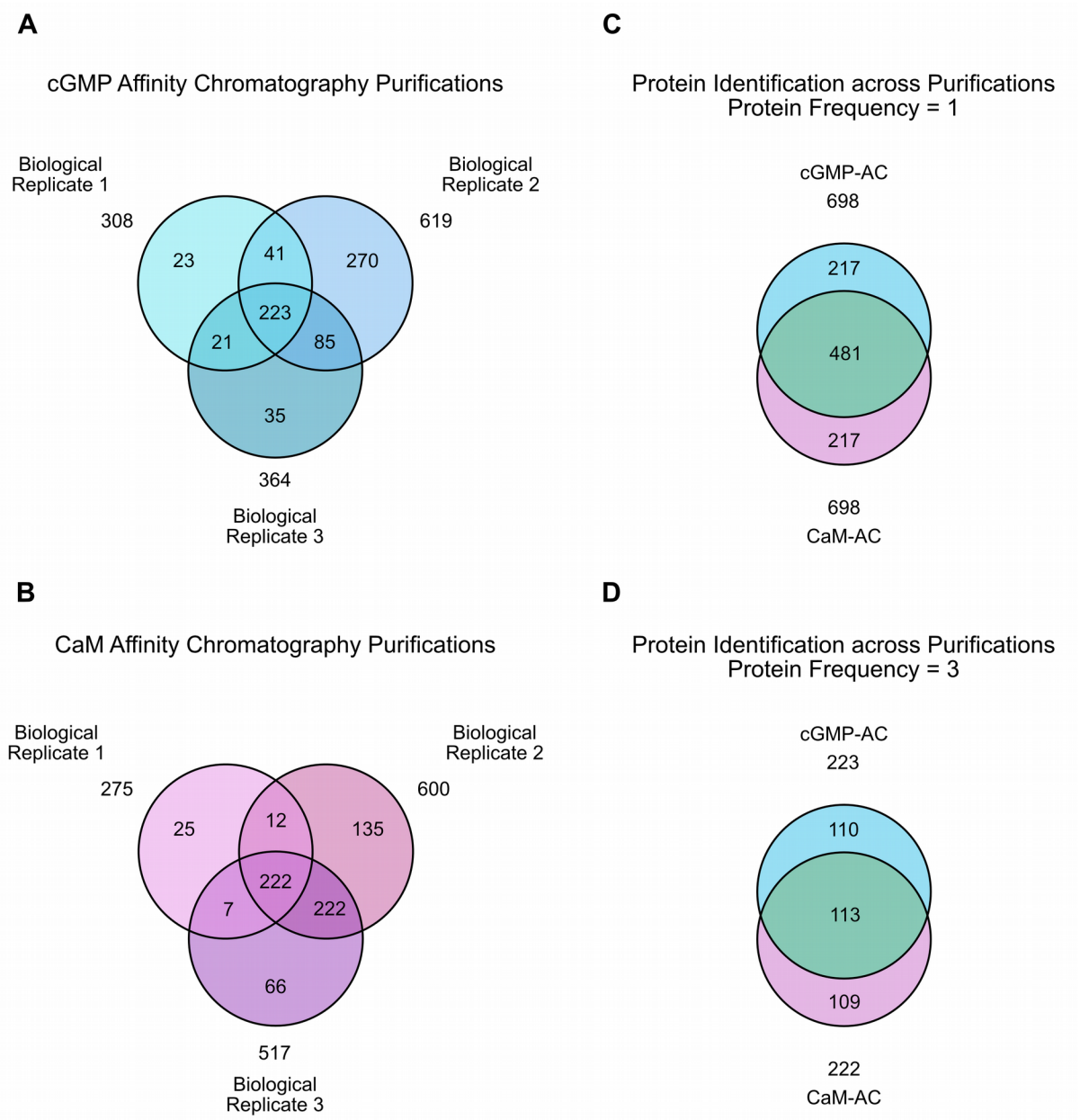

Figure 21: Number of identified proteins and congruent appearances

(A) Venn diagram of identified proteins across three biological replicates of CNG channel purifications via cGMP-AC. The total number of different proteins identified is annotated outside each circle, and values in colored areas represent the number of proteins in that section. (B) Venn diagram of identified proteins across three biological replicates of CNG channel purifications via CaM-AC. The total number of different proteins identified is annotated outside each circle, and values in colored areas represent the number of proteins in that section. (C) Venn diagram of proteins identified at least once (frequency =1) compared across purification approaches. Proteins identified in cGMP-AC are colored in blue, proteins identified in CaM-AC are colored in purple, and proteins identified in both are shown in the overlapping area (green). (D) Venn diagram of consistently identified proteins (present in all three replicates; frequency =3; equal to the center area of A and B) compared across purification approaches.

Total numbers and unique as well as overlapping proteins are annotated. In the cGMP-AC, 223 proteins were present in all experiments, and in CaM-AC purifications, 222 proteins were present in all experiments. For both cGMP-AC and CaM-AC, the total number of proteins identified is 698, and of these proteins, 481 are present in both purifications at least once (Figure 21 C). The overlap between consistently identified proteins is about half of the protein population (Figure 21 D).

The vast amount of identified proteins is hard to comprehend. The following figures focus on several key aspects and facilitate comprehension of the data. Although the following figures deal with limited selections of proteins, an extensive list can be found in the supplementary (Appendix 7.8).

At first, the five proteins with the highest total score and corresponding sequence coverage are illustrated for each experiment (Figure 23 and Figure 24). The total score is a measure for the certainty of the identification of a protein. It considers the ion scores of all peptides that make up a protein. The ion score of a peptide informs about the agreement of the observed MS/MS spectrum and the expected values based on the sequence of the stated peptide. The sequence coverage specifies the percentage of the protein sequence identified among all peptides that fit the sequence.

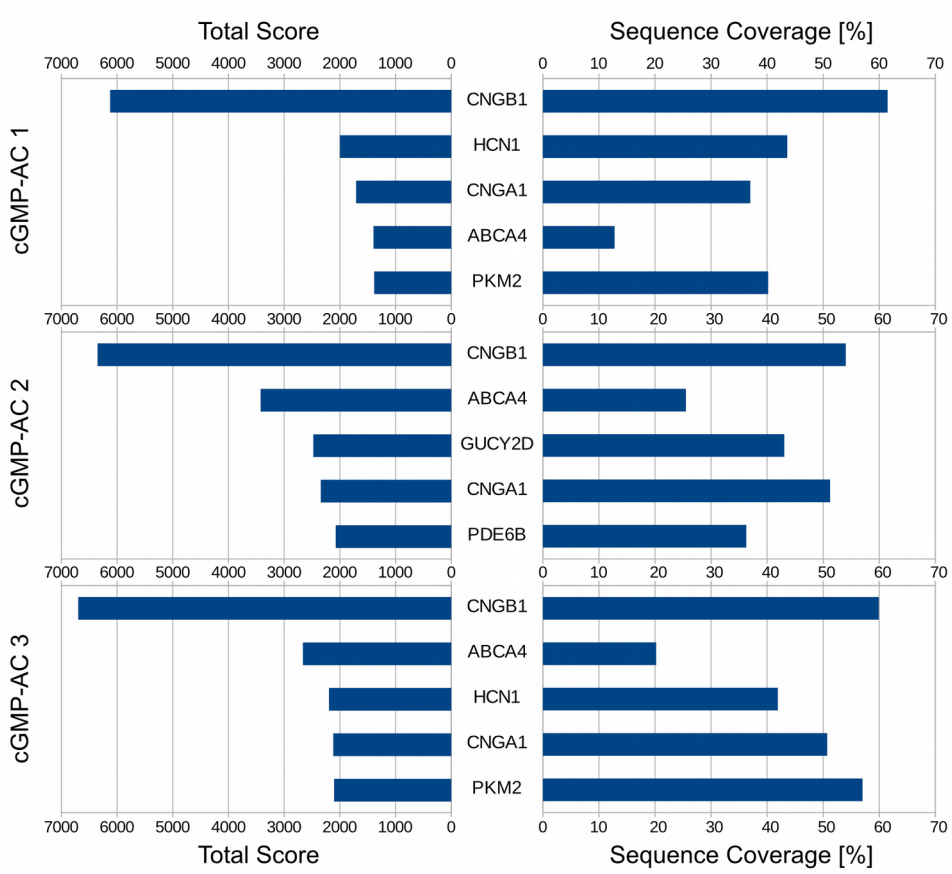

Figure 22: Proteins identified with highest total score in elution samples of cGMP affinity chromatography

The five proteins with the highest total score are listed for each of the three biological replicates purified via cGMP-AC (cGMP 1,2,3). The Gene names are listed in the center with abbreviations used are as follows CNGB1 = cyclic nucleotide-gated channel subunit beta 1; HCN1 = Potassium/sodium hyperpolarization-activated cyclic nucleotide-gated channel 1; CNGA1 = cyclic nucleotide-gated channel subunit alpha 1; ABCA4 = ATP-binding cassette, sub-family A member 4; PKM2 = Pyruvate kinase isozyme M2; GUCY2D = Retinal guanylyl cyclase 1; PDE6B = Rod cGMP-specific 3',5'-cyclic phosphodiesterase subunit beta. The bar towards the left indicates the total score, while the bar to the right indicates the sequence coverage in percent.

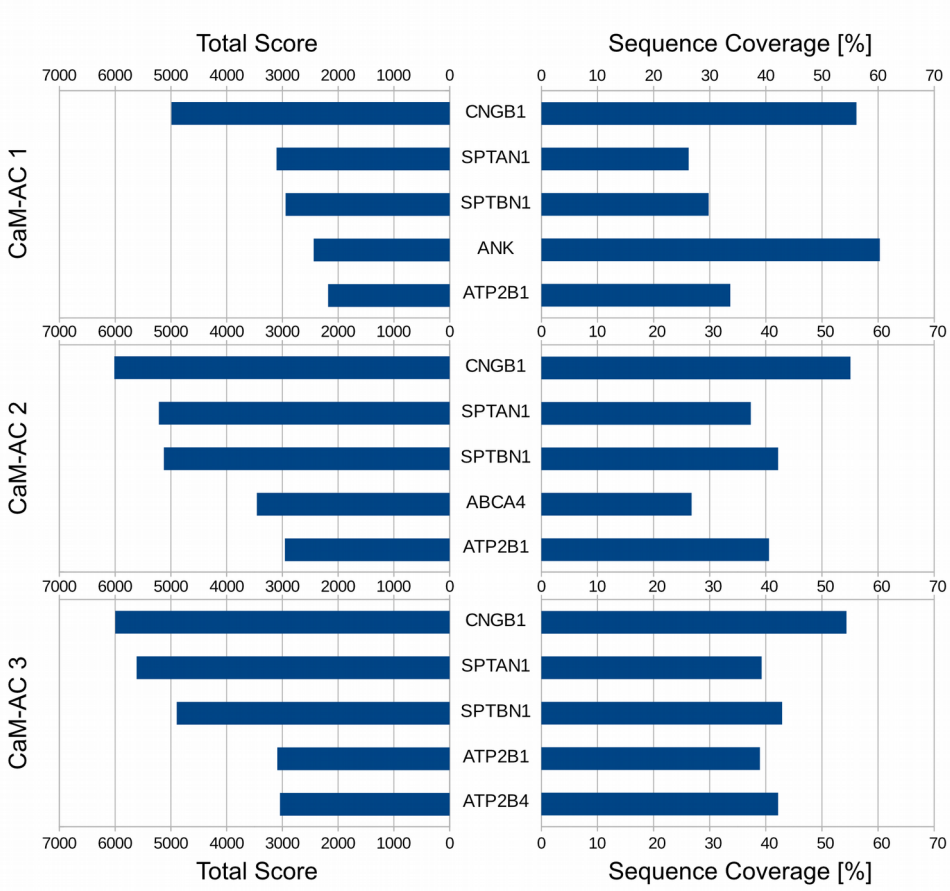

Figure 23: Proteins identified with highest total score in elution samples of cGMP affinity chromatography

The five proteins with the highest total score are listed for each of the three biological replicates purified via CaM-AC (CaM 1,2,3). The Gene names are listed in the center with abbreviations used are as follows CNGB1 = cyclic nucleotide-gated channel subunit beta 1; SPTAN1 = Spectrin alpha chain, non-erythrocytic 1; SPTBN1 = Spectrin beta chain, non-erythrocytic 1; ANK = Ankyrin repeat domain 33B; ATP2B1 = Plasma membrane calcium-transporting ATPase 1; ABCA4 = ATP-binding cassette, sub-family A member 4; ATP2B4 = Plasma membrane calcium-transporting ATPase 4. The bar towards the left indicates the total score, while the bar to the right indicates the sequence coverage in percent.

CNGB1 was identified with the highest total score in both purifications and all replicates of the experiment. CNGA1 was observed in all experiments with a total score above 1000 but not among the top 5 in CaM-AC purifications.

Besides the CNG subunits, the following proteins have reappearing presence in this top 5 ranking. In the cGMP-AC purifications, Potassium/sodium hyperpolarization-activated cyclic nucleotide-gated channel 1 (HCN1), ATP-binding cassette, sub-family A member 4 (ABCA4), and the Pyruvate kinase isozyme M2 (PKM2) were observed at least twice (Figure 22). However, in the CaM-AC purifications, Spectrin alpha chain, non-erythrocytic 1 (SPTAN1), Spectrin beta chain, non-erythrocytic 1 (SPTBN1), and Plasma membrane calcium-transporting ATPase 1 (ATP2B1) were observed more than once in this ranking (Figure 23).

Overall the figures illustrate the quality and consistency of all experiments. While the total score for CNGB1 is exceptionally high in cGMP-AC purifications, the CaM-AC is more homogeneously distributed.

4.3.2 Protein Quantification

Quantitative analysis of the identification results from before would help bringing the data in a larger context. Therefore, the data were analyzed with the MaxQuant proteomics software package, and quantification of proteins in the sample was performed. This quantification is not based on labelling the proteins because the proteins stem from a native source. Instead, the quantification considers the sequence coverage, the number of peptides, and the molecular weight of the protein. Therefore, no absolute measure can be achieved, but relative proportions of the proteins identified within a sample.

The following pie charts depict the ten most abundant proteins in cGMP-AC and CaM-AC purifications and the proportions calculated based on three independent experiments each (Figure 24). The colors for proteins are consistent between the charts.

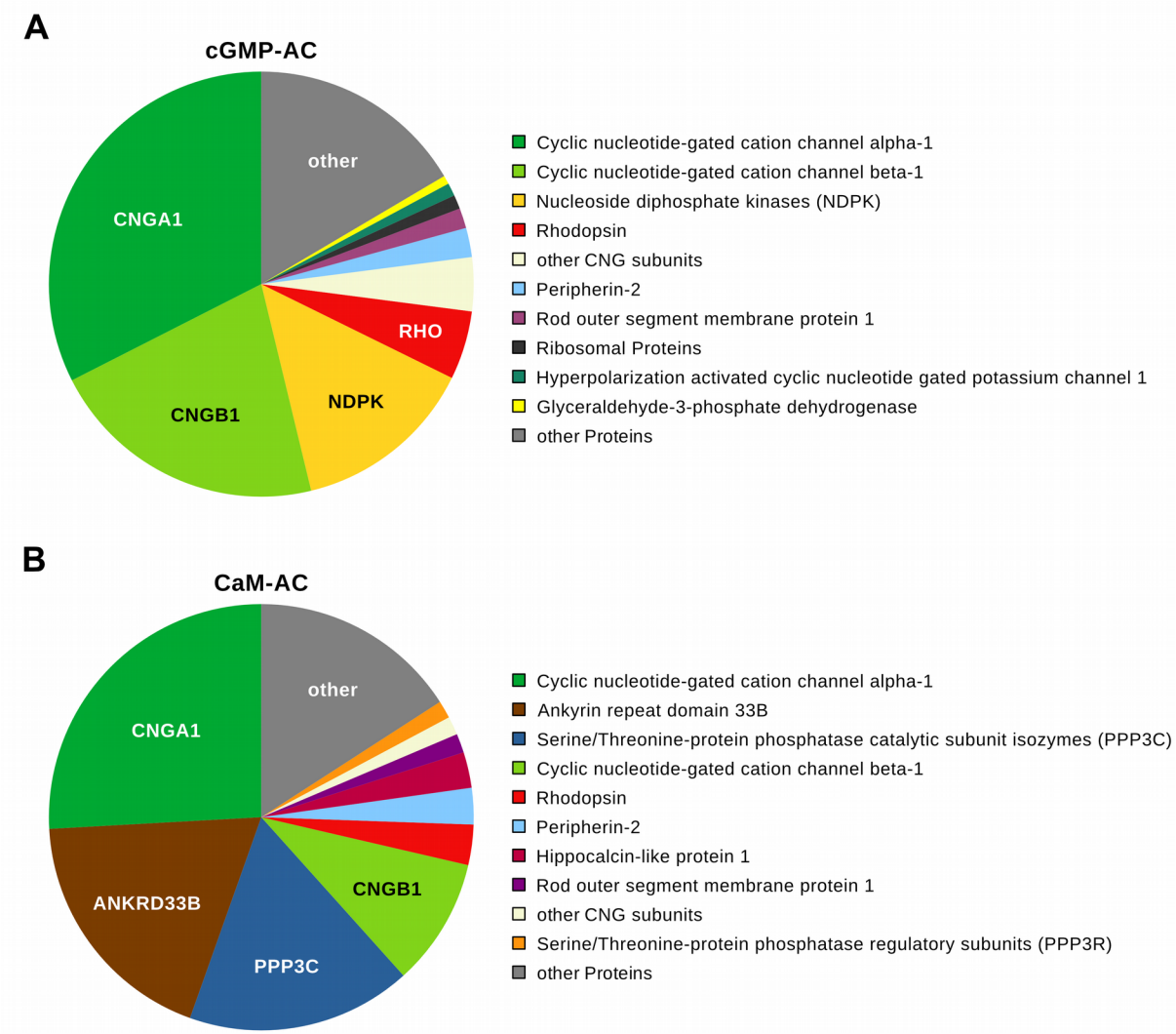

Figure 24: Relative abundance of proteins in purified CNG channel samples determined by label-free quantitative mass spectrometry
The pie charts depict the ten most abundant proteins in CNG channel purifications. (A) shows the results for cGMP affinity chromatography (cGMP-AC) purification and (B) shows the results for Calmodulin affinity chromatography (CaM-AC) purification. For both purification approaches, three independent experiments were conducted. Colors and abbreviations are specified in the corresponding legend. The following positions are protein groups of several quantification entries: NDPK (NME1-2, NME2 and NME3), PPP3C (PPP3CA, PPP3CB and PPP3CC), other CNG subunits (CNGA2 and CNGA3), Ribosomal proteins (mainly 60S ribosomal proteins RLA2, RLA18 and RLA36).

Some proteins were grouped based on affiliation to complexes or based on redundant function. The three known isozymes of the catalytic subunit from the Serine/Threonine-protein phosphatase Calcineurin (PPP3, former PP2B) were identified and grouped (PPP3CA, PPP3CB and PPPCC) because they all are able to form a functional Protein Phosphatase 3 (PPP3) together with one of the regulatory subunits (PPP3R1 or PPP3R2) (https://www.uniprot.org/uniprot/P48452). Similarly, three nucleoside-diphosphate kinases (NDPK) were grouped because they mainly catalyse the same synthesis of nucleoside triphosphates. This group contains Nucleoside diphosphate kinase A 2 (NME1-2 gene) (Abdulaev et al., 1998, https://www.uniprot.org/uniprot/P52175), Nucleoside diphosphate

kinase B (NME2 gene) (https://www.uniprot.org/uniprot/Q3T0Q4), and Nucleoside diphosphate kinase 3 (NME3 gene) (https://www.uniprot.org/uniprot/A5PK70).

In the cGMP-AC purifications, the CNG channel subunits comprised the most significant fraction of proteins, with CNGA1 accounting for an average of 32.5 % and CNGB1 for 21.3 % of the total amount of protein in the sample (Figure 24 A). Rhodopsin was the most abundant protein in the source material, but the abundance was reduced to 5.2 % by the purification.

CaM-AC differs from cGMP-AC concerning the CNG subunits representing the two predominant proteins. While CNGA1 was still the most abundant protein with 25.9 % of the total protein, CNGB1 came in fourth place with 9.7 % (Figure 24 B). Instead, the Ankyrin repeat domain 33B (18.7 %) and various catalytic subunits of the Serin/threonine-protein phosphatase (17.1 %) account for a significant fraction of the total protein. However, the Rhodopsin abundance was similar between the two purifications and accounts for 3.1 % in the CaM-AC. Besides the variations in the abundance of proteins present in both purifications, the entire sample composition varies considerably.

Using MS, we also analysed the samples taken throughout a cGMP-AC purification for the content of CNGA1 and CNGB1 subunits. This analysis gives an overview of the enrichment of CNG channels in the purified sample and the purification efficiency.

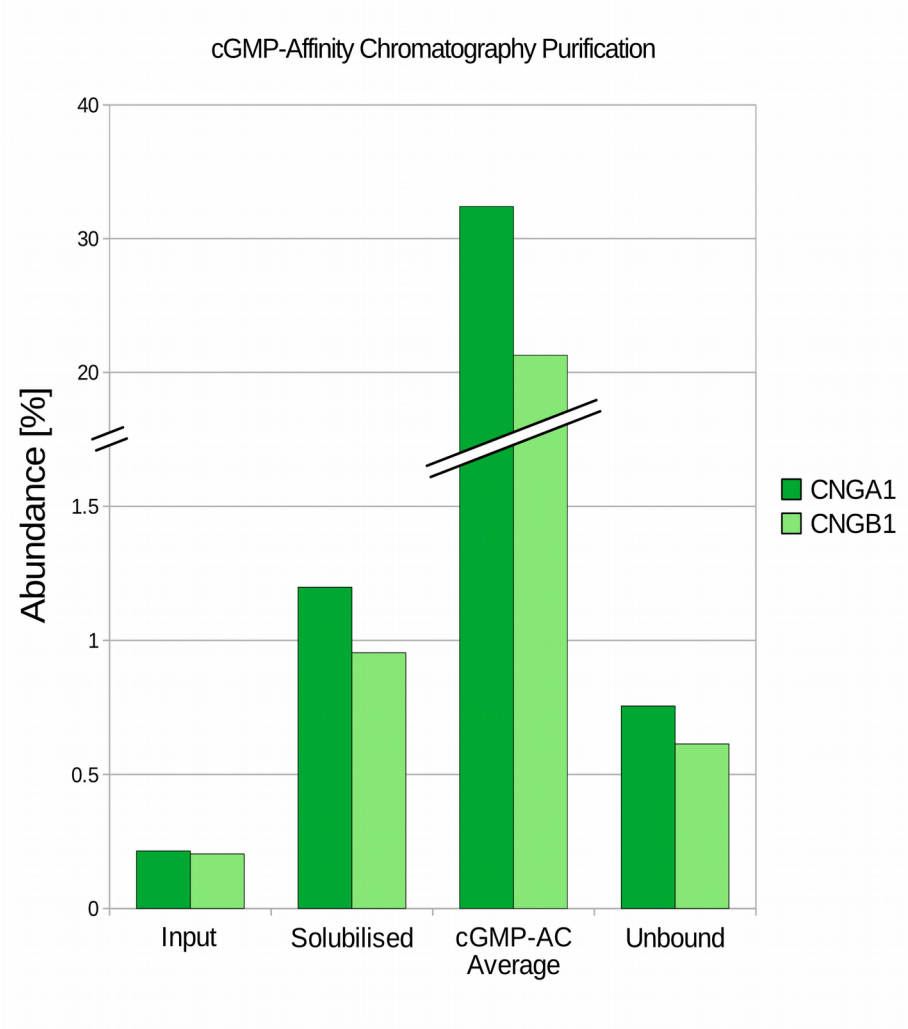

Figure 25: Relative abundance of CNG subunits throughout a cGMP-AC purification determined by label-free quantitative mass spectrometry

The bar diagram depicts the abundance of CNGA1 (dark green) and CNGB1 (light green) subunits in CNG channel cGMP-AC purifications, indicating the fraction of CNG subunits in percent. Samples were taken from the beginning of the purification (Input), after solubilisation (Solubilised), the mean value of three cGMP-AC purifications (cGMP Average), and the flow-through (Unbound A).

While the CNG subunits only account for about 0.2 % of the total protein in the input sample, washing the membranes increased this fraction to 1.2 % CNGA1 and 0.95 % CNGB1 (Figure 25). CNGA1 accounts for 32.5 %, and CNGB1 for 21.3 % of the total protein in the purified samples (average of elution 2A). After binding CNG to cGMP beads, the flow-through still contained 0.7 % CNGA1 and 0.6 % CNGB1.

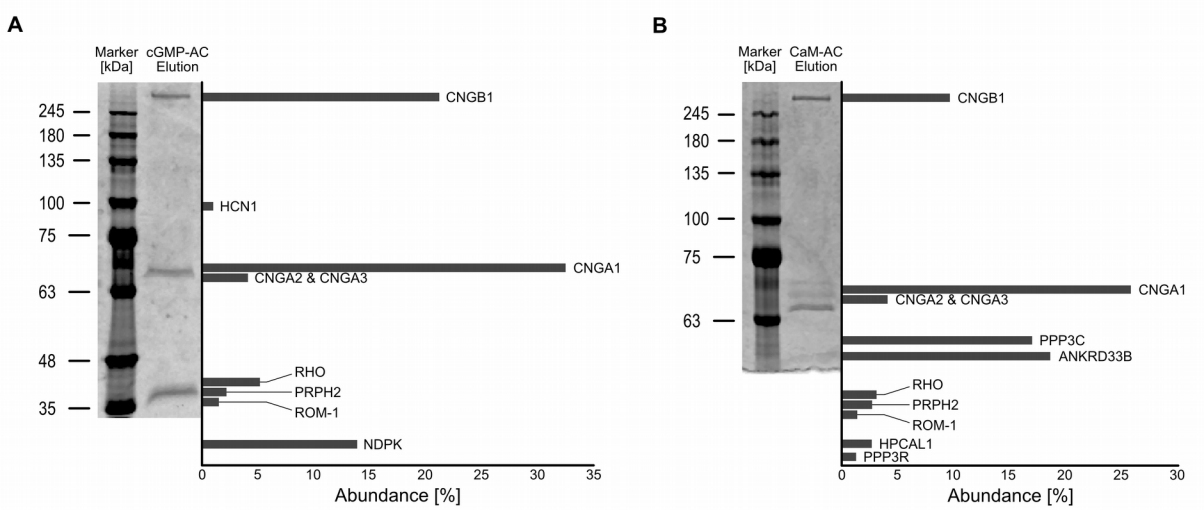

Figure 26: Comparison of results from SDS-PAGE and protein quantification by MS
Purified protein samples (elution 2A) were subjected to SDS-PAGE (representative gels shown) and a corresponding mass spectrometry quantification. In the bar diagram average data ($n_{cGMP\text{-}AC} = 3$ and $n_{CaM\text{-}AC} = 3$) for proteins accounting for ≥ 1 % of the total protein are shown. Bar data for CNGA1 and CNGB1 are shown on the height of their respective SDS-PAGE band, other proteins at a position corresponding to their molecular weight. (A) cGMP-AC purification, representative SDS-PAGE stained with CBS, and corresponding MS protein quantification (average values). CNGB1 (cyclic nucleotide-gated channel subunit beta 1), CNGA1 (cyclic nucleotide-gated channel subunit alpha 1), CNGA2 and CNGA3 (cyclic nucleotide-gated channel subunit alpha 2 and 3), HCN1 (Hyperpolarization activated cyclic nucleotide gated potassium channel 1), RHO (Rhodopsin), PRPH2 (Peripherin-2), ROM-1 (Rod outer segment membrane protein 1), NDPK (Nucleoside-diphosphate kinases NME1-2, NME2 and NME3). (B) CaM-AC purification, representative SDS-PAGE stained with CBS, and corresponding MS protein quantification. PPP3C (Serine/Threonine-protein phosphatase catalytic subunits PPP3CA, PPP3CB and PPP3CC), ANKRD33B (Ankyrin repeat domain 33B), HPCAL1 (Hippocalcin-like protein 1).

This comparison of the gel bands after SDS-PAGE and protein quantification by MS clearly shows both CNG subunits. Furthermore, it illustrates the lowest band in Figure 26 A containing Rhodopsin (RHO) and a cluster of several proteins with molecular weights ranging from 35 kDa to 48 kDa (PRPH2 and ROM-1).

In the representative gel no apparent bands are visible at the expected running height for Serine/Threonine-protein phosphatase catalytic subunits (58 kDa) and ANKRD33B (53 kDa) (Figure 26 B).

Overall, the intensity of CBB stained bands and reported abundance of protein did not appear to correlate. For further analysis, bands from an SDS-PAGE gel were excised and analysed via the in-gel digest and extraction process (section 3.2.21). Figure 26 shows the gel and the corresponding bands that were analysed.

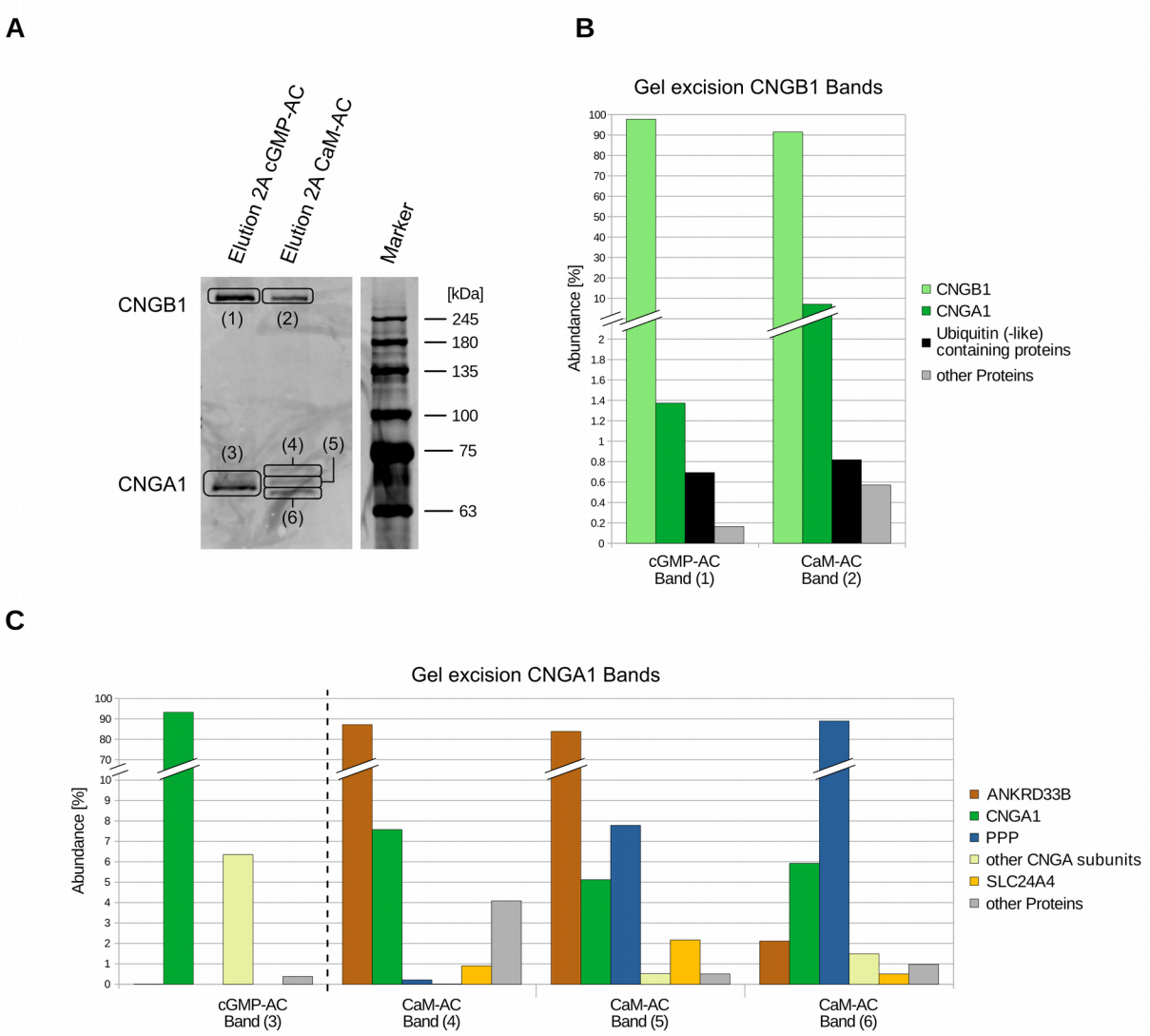

Figure 27: Relative abundance of proteins in excised gel pieces determined by label-free quantitative mass spectrometry

(A) Coomassie stained gel of cGMP affinity chromatography (Elution 2A cGMP-AC) and CaM affinity chromatography (Elution 2A CaM-AC), the typical running height of CNGA1 and CNGB1 subunits are indicated. The bands excised for analysis by LC-MS/MS are marked by numbers (1) to (6). (B) Most abundant proteins in gel pieces from CNGB1 band of cGMP-AC (1) and CaM-AC (2). Besides CNGA1 and CNGB1, several proteins that all contain Ubiquitine or Ubiquitin-like proteins are grouped. (C) Abundance of proteins that account for 2 % of the total protein in at least one of the CNGA1 bands is shown. One band was analysed for cGMP-AC (3), and three bands were analysed for CaM-AC (4), (5), and (6).

The analysis of bands from the gel electrophoresis shows that each band contains one protein that was the most abundant. In both purifications, the CNGB1 subunit accounts for more than 90 % of all proteins in the bands (1) and (2) (Figure 27 B). However, the CNGA1 subunit was present in both purifications, especially in the band (2) 7% of the total protein was identified as CNGA1. Furthermore, in both purifications, the same group of proteins was present but accounts for 0.7 and 0.8 % of the total protein, respectively. This group of small proteins is characterised by the presence of Ubiquitin or Ubiquitin-like protein domains.

There was one CNGA1 band observed in the cGMP-AC purified sample, and CNGA1 was the most abundant protein (Figure 27 C, Band 3, 93 %). CNGA2 and CNGA3 have been identified in that sample and combined account for only 6.35 %. However, the CaM-AC typically shows three bands, and the MS shows how different the composition of the bands was. CNGA1 was present in all three bands in similar quantities, varying from 5.1 % to 7.6 %. In bands (4) and (5), the most abundant protein is Ankyrin repeat domain 33B (ANKRD33B), and in band (6), Serine/Threonine-protein phosphatase subunits account for 89 % of the total protein.

4.3.3 Complex Analysis

In addition to quantifying all proteins in a sample, a more precise calculation was performed to analyse the composition of CNG complexes. In performing the complex analysis without prior cross-linking, the complex composition cannot be established directly. Therefore, the potential subunits of a complex must be defined as a basis for the calculation. All CNG subunits available in the *Bos Taurus* database were used to avoid any bias. This analysis does not reveal information about interaction but informs about the ratio of proteins in a given sample. The abundances of proteins shown in Figure 28 (CNGA1, CNGA2, CNGA3, and CNGB1 subunits) were used to calculate the ratio in a hypothetical complex containing all subunits. In all experiments, the obtained ratios were normalized after CNGB1.

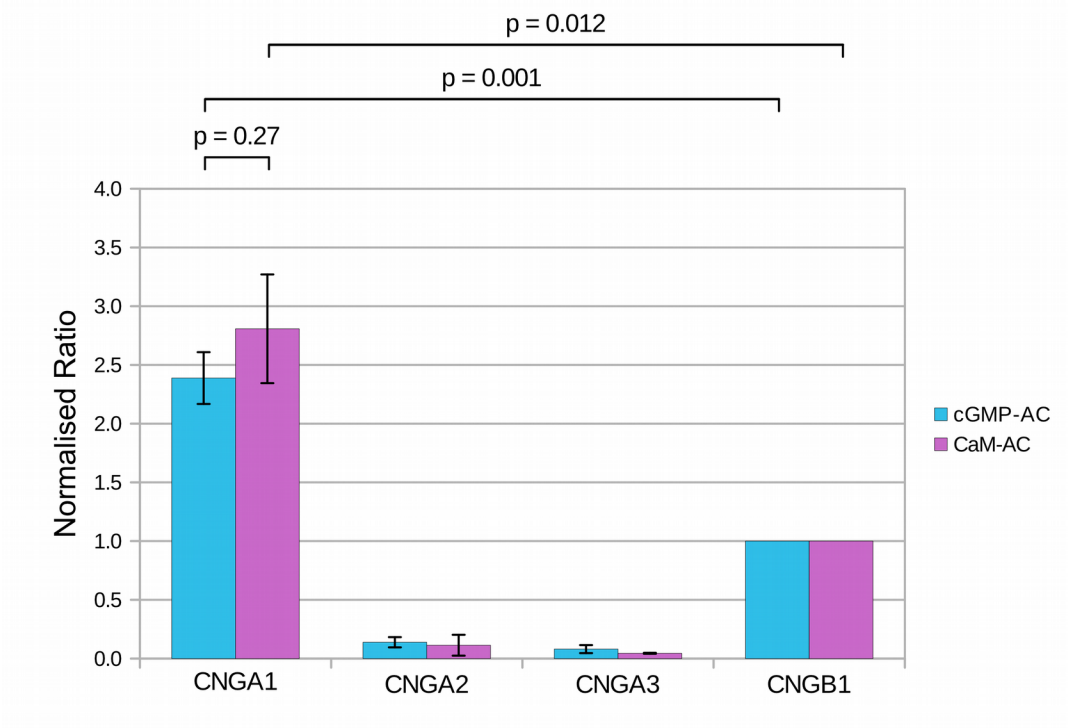

Figure 28: Complex analysis of all CNG subunits identified via mass spectrometry

The relative representation of CNG subunits in a theoretical complex, containing CNGA1, CNGA2, CNGA3, and CNGB1 subunits. Results obtained from the samples purified by cGMP-AC are shown in dark blue, and samples purified by CaM-AC in light purple. The p-values were calculated according to the student's t-test and are indicated above for selected pairings; $n_{cGMP\text{-}AC} = 2$ and $n_{CaM\text{-}AC} = 3$.

As expected, the major components were CNGA1 and CNGB1. The average ratio in cGMP-AC purifications was 2.39 CNGA1 to 1 CNGB1 and in CaM-AC purifications was 2.81 CNGA1 to 1 CNGB1. However, the difference between the cGMP-AC and CaM-AC purifications was not significant (Figure 28).

CNGA2 and CNGA3 were present in ratios below 0.2 per CNGB1 (0.14 and 0.08 in cGMP-AC, and 0.11 and 0.05 in CaM-AC, respectively).

4.3.4 Phosphorylation Sites

Phosphorylations are typical post-translational modifications and are involved in modulation of protein function. Consequently, it led us to investigate the phosphorylation state of CNGA1 and CNGB1. As mentioned before, the phosphorylations were investigated following the same bottom-up strategy of protein digestion and LC-MS/MS analysis. However, the native source of purified protein prevents a tagged approach. Therefore, the IsobarQuant software (Franken et al., 2015) was used in a label-free analysis setting.

MS can identify phosphorylations because a defined mass of 80 Da (fully protonated) is added to the peptide (Parker et al., 2009). Therefore, as long as a peptide sequence is known, deviations of the expected mass can be identified. Furthermore, it is possible to locate the modified amino acid in most cases because, in a tandem mass spectrometry setup, the peptide is further fragmented and analysed (Figure 15). Figure 29 presents an overview of all phosphorylations identified in CNGA1 and CNGB1 subunits. Along with the information of the position and identity of the amino acid, observed phosphorylations in three independent experiments are specified for cGMP-AC and CaM-AC purifications separately.

Protein	Residue	AA	cGMP 1	cGMP 2	cGMP 3	CaM 1	CaM 2	CaM 3
CNGA1	498*	Y	–	–	–	–	–	–
CNGA1	616	S	–	–	+	–	–	–
CNGA1	630	S	+	+	–	+	–	–
CNGA1	648	S	–	+	+	–	–	–
CNGB1	15	T	+	–	+	–	–	–
CNGB1	49	S	–	+	+	–	–	+
CNGB1	77	T	–	+	–	–	n.d.	–
CNGB1	131	S	+	n.d.	n.d.	+	n.d.	n.d.
CNGB1	149	S	+	n.d.	n.d.	–	n.d.	n.d.
CNGB1	478	S	–	n.d.	+	–	–	–
CNGB1	601	S	+	+	+	+	+	+
CNGB1	608	S	+	+	+	+	–	+
CNGB1	624	S	+	+	+	+	+	+
CNGB1	631	S	+	+	+	+	+	+
CNGB1	672	S	+	+	+	+	+	+
CNGB1	675	S	+	+	+	+	+	+
CNGB1	707	S	+	+	–	–	n.d.	n.d.
CNGB1	711	S	+	+	+	–	n.d.	n.d.
CNGB1	1097*	Y	–	–	–	–	–	–
CNGB1	1208	S	+	+	+	+	+	+
CNGB1	1378	T	–	+	+	–	–	+

Figure 29: Overview of CNG channel phosphorylation sites identified by Mass Spectrometry

The CNG subunit (Protein), the position of the amino acid (Residue), and the type of amino acid (AA, S = serine, T = threonine, Y = tyrosine) are specified in the first three columns. Potential phosphorylation sites indicated in the literature have been marked with an asterisk next to the amino acid position. For each purification (cGMP = cGMP-AC, CaM = CaM-AC), three biological replicates have been analysed, and observed phosphorylation (+, green), not observed phosphorylation (-, red) and not identified residue (n.d., blue) is annotated and colored correspondingly.

The previously speculated phosphorylation site in CNGA1 at Y498 could not be observed to be phosphorylated in either purification approach, even though peptides corresponding to this protein region were present in all experiments. Likewise, the previously speculated phosphorylation site in CNGB1 at Y1097 was present in all experiments, but a phosphorylation could not be detected (Krajewski et al., 2003; Molokanova et al., 1997, 1999, 2003).

While many phosphorylation sites were determined for the different purification approaches (S630 in CNGA1, six Serines between S601 and S675, and S1208 in CNGB1), some sites appear limited to one purification. Overall cGMP-AC samples are more frequently phosphorylated. The only case with phosphorylations observed in all three cGMP-AC experiments and none in CaM-AC is S711. However, S711 was not covered by peptides in all CaM-AC samples. Between the two purification approaches, the most consistent and highest average ratio of phosphorylations was observed in site S601 (Figure 31 and Figure 32). Phosphorylation in the CNGA1 subunit appears much less frequent, and if phosphorylations were observed, the ratio is low (Figure 30).

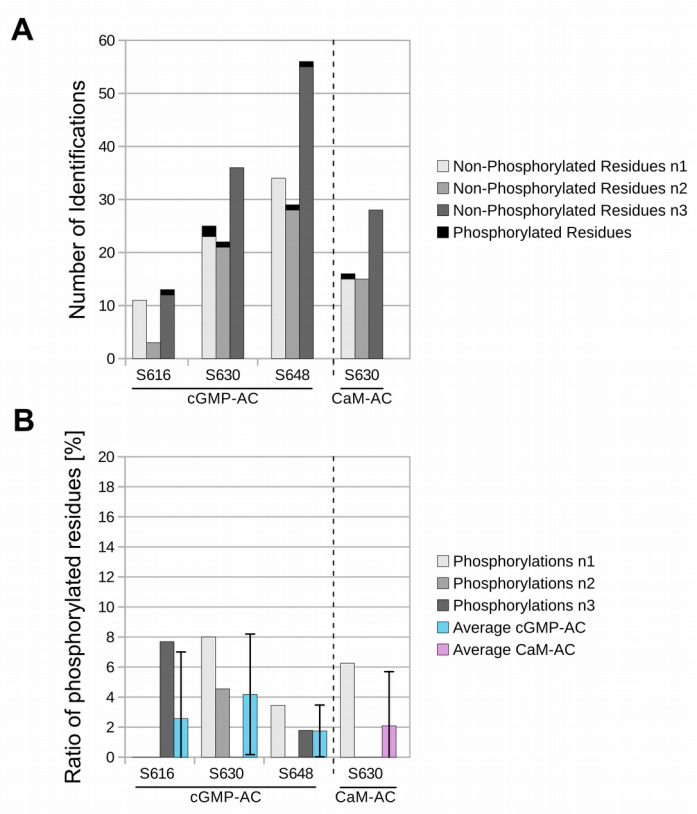

Figure 30: Detailed residue identification and phosphorylation status of CNGA1 subunits

Three independent biological replicates (n1, n2, n3) of CNG purified via cGMP-AC and CaM-AC were analysed. Mass spectrometry analysis was performed to identify and determine the phosphorylation state of CNGA1 subunits. (A) Number of identified peptides containing the specified residue (x-axis), each bar is split between the number of non-phosphorylated (grey portion of the bar) and phosphorylated (black portion of the bar) residues. (B) The ratio of phosphorylated residues of all identified residues was calculated and plotted for the three replicates (various grey values) and an average including the standard deviation, if applicable (light blue).

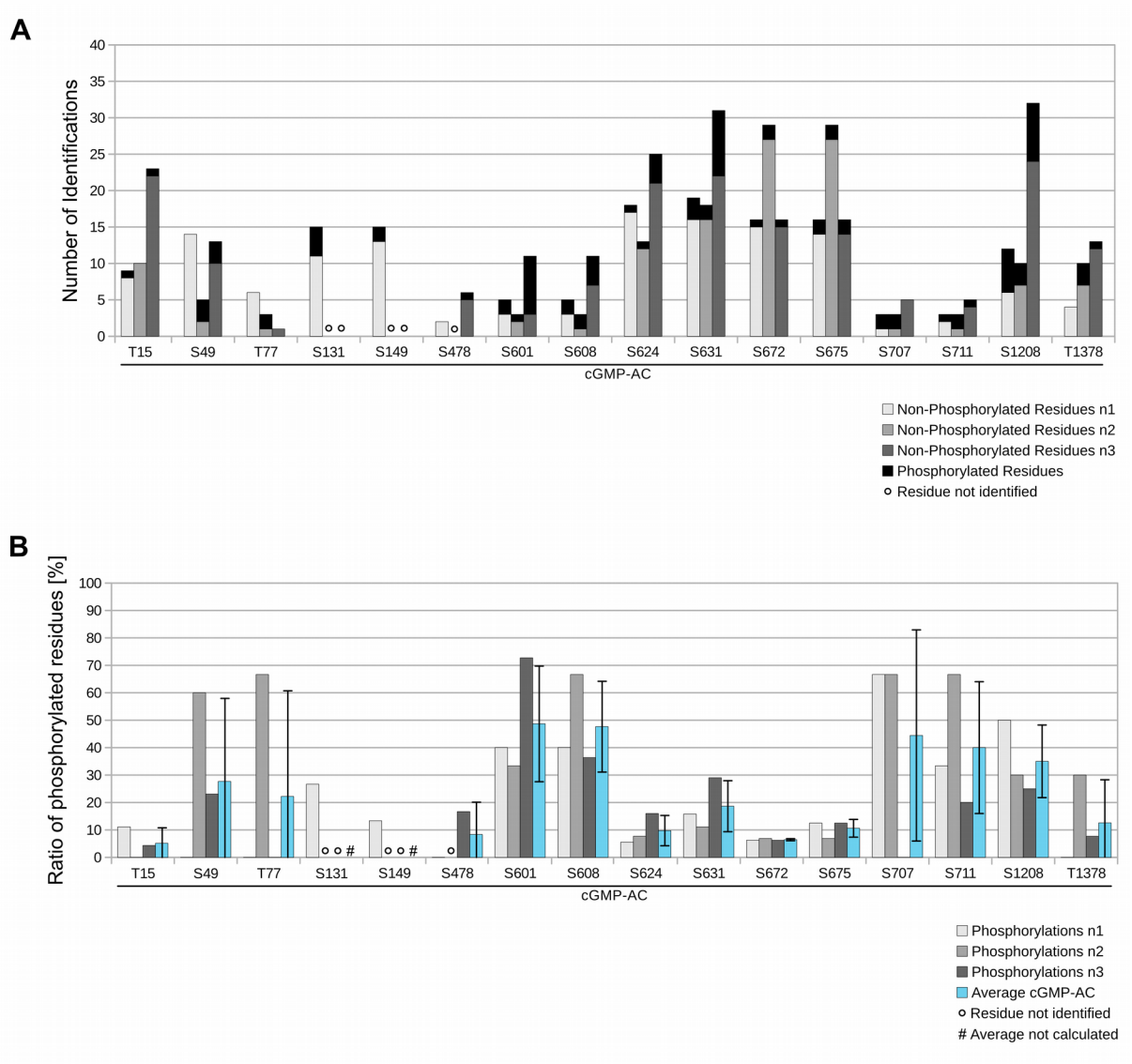

Figure 31: Detailed residue identification and phosphorylation status of CNGB1 subunits purified via cGMP affinity chromatography

Three independent biological replicates (n1, n2, n3) of CNG purified via cGMP-AC were analysed. Mass spectrometry analysis was performed to identify and determine the phosphorylation state of CNGB1 subunits. (A) Number of identified peptides containing the specified residue (x-axis), each bar is split between the number of non-phosphorylated (grey portion of the bar) and phosphorylated (black portion of the bar) residues. Residues that could not be identified are marked by a circle instead of a bar. (B) The ratio of phosphorylated residues of all identified residues was calculated and plotted for the three replicates (various grey values) and an average including the standard deviation, if applicable (light blue). Residues that could not be identified are marked by a circle, and when the average was not calculated, a '#' sign is shown.

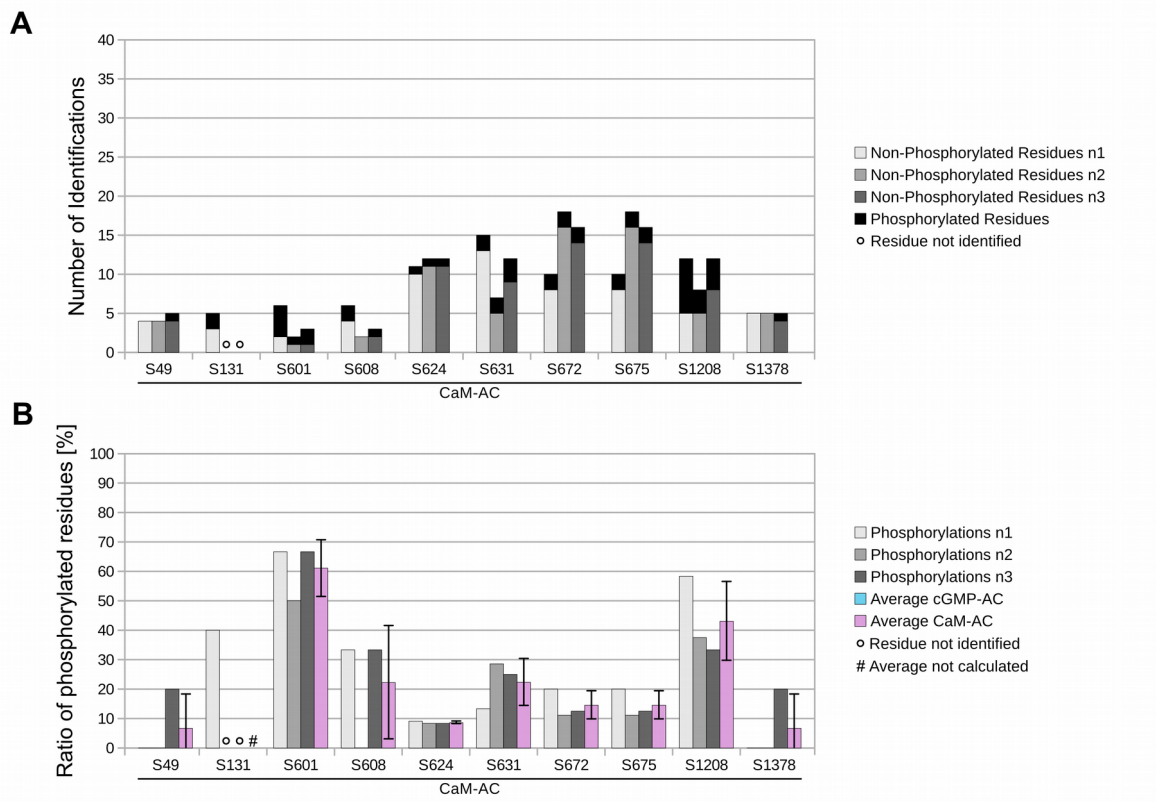

Figure 32: Detailed residue identification and phosphorylation status of CNGB1 subunits purified via CaM affinity chromatography

Three independent biological replicates (n1, n2, n3) of CNG purified via CaM-AC were analysed. Mass spectrometry analysis was performed to identify and determine the phosphorylation state of CNGB1 subunits. (A) Number of identified peptides containing the specified residue (x-axis), each bar is split between the number of non-phosphorylated (grey portion of the bar) and phosphorylated (black portion of the bar) residues. Residues that could not be identified are marked by a circle instead of a bar. (B) The ratio of phosphorylated residues of all identified residues was calculated and plotted for the three replicates (various grey values) and an average including the standard deviation, if applicable (light blue). Residues that could not be identified are marked by a circle, and when the average was not calculated, a '#' sign is shown.

4.4 Electron Microscopy-Based CNG Purification Assessment

Previous EM studies of the heteromeric CNG channel were performed in 2002 by Higgings and colleagues (Higgins et al., 2002). The resulting structure was termed “hanging gondola” and gave a first impression of the structural organisation of the channel. Although the CNG channels have become a subject of interest for structural investigations in recent years, this seems to be a challenging endeavor, and an atomic model is yet to be published. Nevertheless, some obstacles present in cryo-EM studies can be neglected when using negative staining techniques. Here, negative staining is used as a proof-of-principal to assess the sample purity, stability based on aggregation and verify the oligomeric state of the CNG channels.

With CNG channels, time is a crucial factor in the sample preparation for EM. Hence the channels were chemically cross-linked immediately after the purification (section 3.2.6). The negative-staining procedure was performed on the day of purification. First, a Quantifoil copper grid with holey carbon and a 2 nm continuous carbon layer (Cu R2/1 + 2 nm) was glow discharged with Argon plasma. Subsequently, the CNG sample was incubated on the grid and stained with 0,75 % uranyl formate solution (section 3.2.15). The single particle dataset was acquired manually on a JEOL JEM-2200 FS electron microscope at room temperature (section 3.2.16). Analysis and processing were performed using three software packages, SPHIRE, crYOLO, and RELION.

Figure 33 shows the processing steps from raw data to 2D classification of particles, while Figure 34 presents the density map and further information to assess the result.

Distinct particles were visible, and only a few aggregates were present in the raw data (Figure 33 A). Even though background contamination was observed, the particles did not seem to be obscured by it. In addition, the particle density was adequate, with only a minor proportion of particles too close to each other.

Fourier transforms are commonly used in calculations regarding EM micrographs. The contrast transfer function (CTF) describes aberrations introduced by the microscope and parameters used for acquisition that modulate these micrographs. Here, the CTF values were calculated by CTER in an automated way, along with an error assessment of the results (Penczek et al., 2014). The CTF assessment is part of the SPHIRE workflow but not shown in detail in the results section (Moriya et al., 2017). A power spectrum can be obtained by plotting the 2D squared average of the CTF (Thon, 1966). Such a power spectrum is shown in Figure 33 B and was obtained based on the micrograph shown in Figure 33 A. The power spectrum visualizes the intensity distribution of spatial frequencies and can be used to assess the quality of a micrograph.

Furthermore, the power spectrum is used in calculations during the processing of EM data to reverse the modulations of the micrographs, at least to some extent. The power spectrum

in Figure 33 B shows no obvious sign of astigmatism or sample movement. Furthermore, the first zero-crossings inform about the defocus, or more precisely under focus in this case, and is -1.9 µm for this representative micrograph. The extension of Thon rings indicates the highest resolution information present in the image (defocus frequency limit), here that limit is marked by a white circle and is positioned at 0.22 µm. In summary, the alignment of the EM appeared to be sufficient for SPA.

An automated approach was applied to identify the particles on the micrograph, using a neuronal network, trained to identify particles in negative stain EM micrographs (Figure 33 C). The confidence threshold was manually adjusted to 0.5, and 177 micrographs were subjected to the automated particle picking, which resulted in the identification of 76573 particles (Figure 33 E). The histogram in Figure 33 D shows the size distribution of particles identified by crYOLO, and the average diameter was 126 px. Finally, RELION was used for 2D classification, and the resulting 2D class averages were observed to be promising (Figure 33 F). 47327 particles were subjected to further reconstruction of a density map.

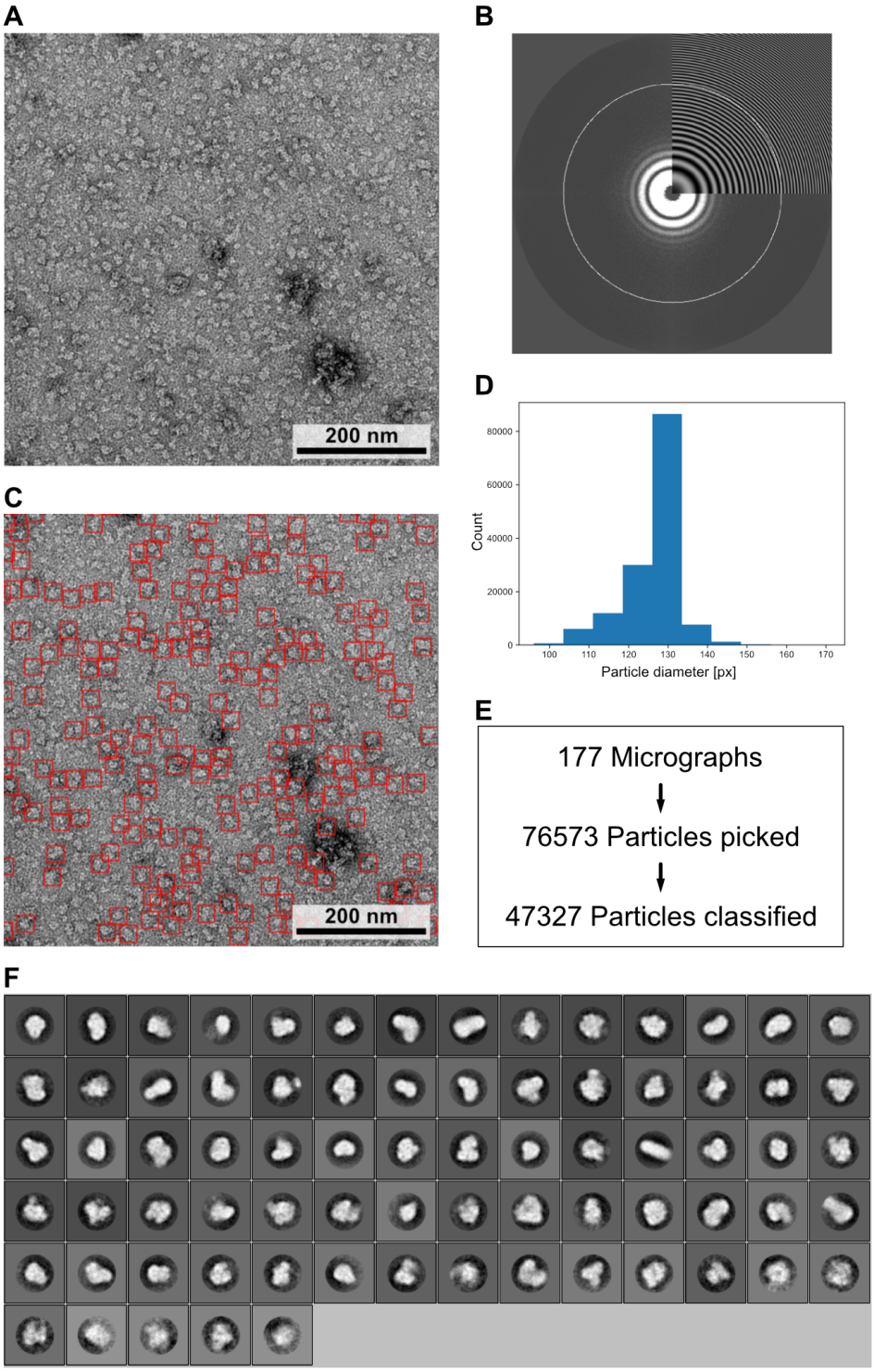

Figure 33: Raw data, particle selection, and classification of negative-stain EM data using single particle analysis

(A) A representative image of negative stained CNG sample purified via cGMP-AC, (B) corresponding 2D power spectrum with the Thon rings extending to about 0.22 µm as indicated by the white circle. (C) Particles were selected using a neuronal network (crYOLO, PhosaurusNet), the selected particles are indicated as red boxes. (D) The histogram shows the size distribution of selected particles. (E) Overview of acquired micrographs, particles picked, and particles participated in 2D classes used for reconstruction. (F) 2D class averages of CNG channel particles as determined by Relion (32.8 nm box size). Scale bars are equal to 200 Å.

For the reconstruction of the density map, a C4 symmetry was imposed in the initial model calculation because the additional density of CNGB1 is not expected to be visible under these conditions. The initial model was refined with a soft mask. The resulting density map is shown in Figure 34 A. Also, an atomic model of a CNGA1 homotetramer was fitted into the density using UCSF Chimera (Pettersen et al., 2004). Based on the fitting, the tip of the map represents the intracellular part, and the base corresponds to an integral part of the membrane protein. Figure 22 B shows the FSC curves of different density maps. The final resolution was reported to be 17.2 Å, but this seems to be an overestimation, a more likely resolution would be about 25 Å.

The structure and possible implications will be discussed later (section 5.1).

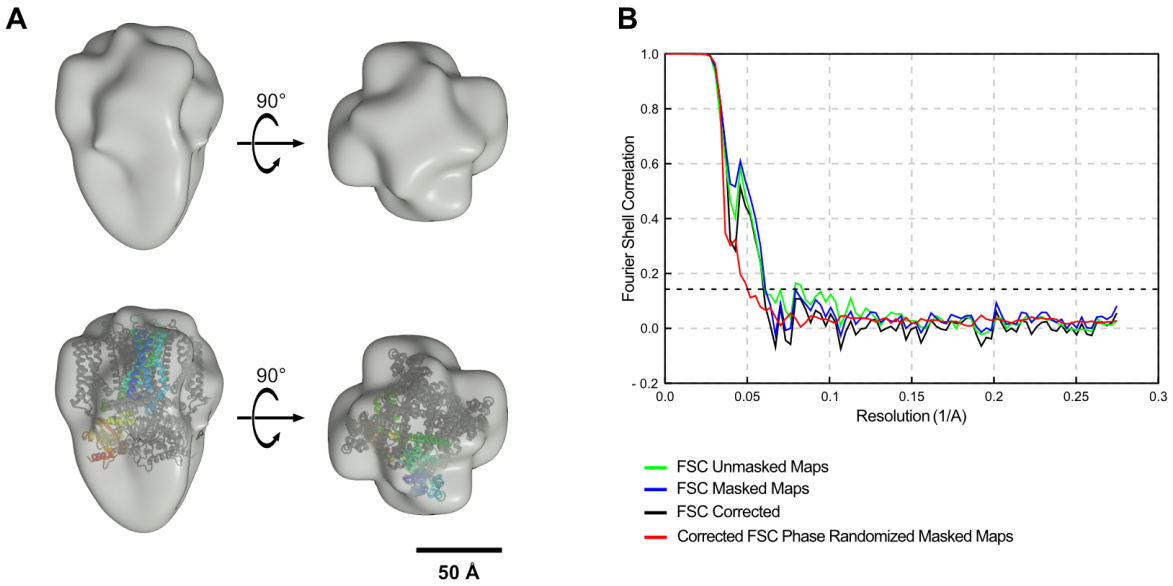

Figure 34: Overlay of the reconstructed CNG map with atomic model of CNGA1 homo-tetramer and the corresponding gold standard FSC curve of negative-stain EM single particle analysis

(A) Reconstruction of the CNG channel purified from bovine rod outer segments via cGMP-AC. A view parallel to the membrane (left) and extracellular space (right) are presented. The CNG reconstruction was fitted with the CNGA1 homomer (PDB 7LFX) for context. One subdomain of the model was rainbow-colored for orientation. (B) Fourier shell correlation (FSC) curves indicate the resolution of density maps at different processing steps. Scale bar is equal to 50 Å.

5 Discussion

5.1 Purification of Endogenous CNG Channels

The main approaches of the rod CNG channel purifications take advantage of the channel's binding affinity towards cGMP and CaM. While cGMP affinity is inherent to all CNG assemblies, CaM binding affinity relies on the presence of (at least one) CNGB1 subunit. Although many publications feature a homomeric protein, more detailed biochemical studies are often conducted on endogenous channels. The heteromeric arrangement with the reported three CNGA1 to one CNGB1 stoichiometry is crucial for in depth structural and functional studies because homomeric channels lack characteristic gating and modulating properties (Kaupp & Seifert, 2002; Körschen et al., 1995). For structural studies, using a native protein source is the exception, but whenever the native source was chosen, the decision was often required to analyse complex proteins (63 %, Figure 3). Native sources assure that the endogenous proteins did undergo all relevant post-transcriptional and post-translational steps and resemble functional states.

In this thesis, the CNG channels were purified from bovine ROS, following the established protocols (Jeyasankar, 2019) that exploit either the cGMP or the CaM affinity of CNG channels. The decision for affinity chromatography as polishing step takes several aspects into account. The endogenous protein lacks any specific purification tags or modifications that would improve the performance of other approaches and limits us to inherent properties/affinities of the CNG channels. Furthermore, CNG channels are expressed relatively low in ROS, rendering approaches that lower sample concentration even more (e.g., SEC) less appealing. Initial explorations using a HPLC system did not result in suitable separation of CNG channels from other proteins (data not shown), which may be due to the low concentration and the presence of detergent in the buffer.

Although previously established affinity chromatography protocols meet many of the requirements we have for the purification, we implemented additional optimisations and streamlining to improve the purification speed, decrease the requirement of a large amount of raw material (ROS), and preserve the phosphorylation status. The methodological modifications applied do not appear to impact purification results negatively.

Upon purification, antibodies specific for the CNG channel subunits were used successfully to demonstrate their presence in the eluates. The polyclonal antibody used for CNGB1 identification recognises the GARP domain of the subunit. Therefore, additional bands visible in the immunoblots against the CNGB1 subunit (Figure 17 and Figure 18) could be due to the soluble GARP1 and GARP2 protein in the samples, as previously observed (Batra-Safferling et al., 2006). Moreover, negative staining EM shows low amounts of contamination and few aggregates (Figure 34 A), and the sample appears relatively homogenous regarding particle size and shape (Figure 34 D). While the concentration of particles is sufficient for

negative staining EM, dilution of the sample was not required during sample preparation. In our experience, this indicates a low protein concentration in the elution. The notable decrease in abundance of CNG channel present in the solubilised compared to unbound sample (Figure 25) shows the efficient capturing process of the cGMP-AC. Moreover, the sample purity can be appreciated despite the reduced washing volume used as part of the (speed) optimisation.

Another parameter that is crucial for the characteristic behavior of CNG channels is their subunit stoichiometry. As discussed by Kaupp and Seifert in their review, the most likely arrangement of the native heterotetrameric CNG channels would be a three A1 to one B1 stoichiometry (Kaupp & Seifert, 2002). Later that year, this proposed stoichiometry was reported by H Zhong and colleagues, where they used Tryptophan residues to quantify the relative amount of subunits present in CNG samples purified from bovine rod outer segments (Zhong et al., 2002).

We expect a three CNGA1 to one CNGB1 ratio, as CNG channels are purified from a native source in this thesis. Therefore, the stoichiometry was analysed to verify our purification quality using two approaches, a TCE staining-based analysis, as used by H Zhong and colleagues in 2002, and a complex analysis based on MS data. After measuring the band intensity of TCE-soaked SDS-PAGE gels, the stoichiometry was calculated considering the number of Tryptophan residues in each subunit. For cGMP-AC, an average stoichiometry of 3.3 CNGA1 per CNGB1 and for CaM-AC, an average stoichiometry of 2.8 CNGA1 per CNGB1 was determined. The MS-based approach yielded an average stoichiometry of 2.4 CNGA1 per CNGB1 for cGMP-AC and 2.8 CNGA1 per CNGB1 for CaM-AC. While the approach based on TCE staining has already been published in the context of CNG stoichiometry analysis, the MS approach has not been used to determine CNG channel stoichiometry specifically until now. Both approaches have the common technical limitation that the composition of the complex is indirectly determined. The TCE staining-based approach uses the separation by SDS-PAGE, but as shown in (Figure 27), the bands also contain co-purified protein, and the assay assumes equal accessibility of TRP residues for A1 and B1. Besides, the MS methods applied here can only determine the ratio of subunits in a putative complex. The four CNG subunits (A1, A2, A3, and B1) used for the complex analysis are most likely not all part of one complex but members of different CNG channels. The resulting ratios are therefore representing the average among all CNG channels present in the sample. Nevertheless, this analysis aids in understanding the most probable CNG channel composition. Even though CNGA2 and CNGA3 are present, they only account for less than one percent of the total CNG protein, and their presence is likely due to contamination of the ROS.

Although the calculated values for CaM-AC samples are similar, the cGMP-AC samples show a weak significant difference ($p = 0.036$) in their determined stoichiometry between the TCE- and MS-based methods (Figure 39). This difference could be due to variations in the source material or varying purification qualities. Overall, the stoichiometry results presented here

show a three A1 to one B1 stoichiometry with an uncertainty similar to the 2002 published results by Zhong and colleagues and indicate a successful purification of endogenous CNG channels.

The TCE staining of the SDS-PAGE gels represents a reasonable approach to quickly and reliably determine the stoichiometry of CNG channels. This success initiated a further experiment to determine the CNG channel concentration based on the same chemical reaction between Tryptophan residues and TCE. In the control experiments, this method proves to be of limited informative value. While the determined concentration is in the correct range for Apoferritin, the BSA concentration was estimated about 15% below the applied amount (Figure 38). However, for the determination of the CNG channel concentration, the results from the TCE-assay were an improvement to the errant results from other approaches, in that the determined concentration was positive and roughly within the expected range based on the known copy number of the rod CNG channels (Milo et al., 2009). The primary constraints in measuring the concentration of this specific sample are one or a mixture of the following three: (1) the presence of the detergent CHAPS; (2) the concentration close to or below the detection limit; (3) a required sample volume, too big to be met with this purification.

As the concentration measurement is unspecific, any co-purified protein present in the sample will skew the results, and MS-based quantification experiments show that substantial amounts of the sample contain other proteins than CNG (Figure 33). Unfortunately, the measurement consumes about half of the elution volume that we obtain and thereby limits the use of the sample for other purposes. The results (cGMP-AC median 0.199 mg/ml, CaM-AC median 0.40 mg/ml) agree with observations made using electron microscopy. They are remarkable given the low amount of ROS source material used for each experiment. As concentration measurements are not included in former publications studying endogenous CNG, the established methodology and results in this work can be a reference for future studies.

These basic characterisations of the purified CNG channels are complemented by the structural investigation via negative staining EM, which was performed as a proof of principle on the CNG channels obtained from cGMP-AC. The acquired small dataset shows that more than half of the identified particles can be used for reconstructing a density map. Besides classes that represent the shape and size of CNG channels, several classes show averages with more density than expected. It is plausible that these classes show protein complexes, but we could not identify a specific arrangement because of insufficient particle numbers. The recently published (human) CNGA1 homomer (PDB 7LFX, Xue et al., 2021) could be fitted well in our obtained density map (Figure 34 A). Reconstruction without enforced symmetry fails to demonstrate the presence of the CNGB1 subunit (data not shown). However, in the shown reconstruction results, a C4 symmetry was applied, and the tetrameric organisation of the purified protein is apparent at a resolution of at least 25 Å.

Interestingly, the density in the intracellular tip of the protein extends the dimensions of the CNGA1 homomer, suggesting the presence of additional mass. In this study of the homomeric CNG channel (Xue et al., 2021), the intracellular N-term and C-term regions are truncated, but especially the C-term region of full length CNGA1 is known to contain alpha-helices (Zhong et al., 2002, 2003) that would explain the additional density we observe. Furthermore, the CNGB1 subunit is characterised by the large N-term GARP domain. However, the GARP is considered a largely disordered domain and would likely not result in a distinct density (Batra-Safferling et al., 2006). In comparison to the findings of Higgins and colleagues, which suspect the subunits to arrange in a “dimer of dimers”, the density map shown in this thesis agrees in general dimensions. However, we cannot see the “dimer of dimers” arrangement, likely due to the imposed symmetry during reconstruction (Higgins et al., 2002). Nevertheless, in light of the limited resolution, definitive conclusions are not reasonable at this time.

Besides evaluating purification results and protein integrity, the structural investigation by negative staining EM can also serve as the foundation for future structural investigations by cryo-EM. While the CNG channel appears intact and the contamination level sufficiently low, the protein concentration may pose a problem for cryo-EM. Compared to negative staining samples, the particle density on the grid is at least one magnitude lower in vitrified samples (Y. Cheng et al., 2015). Also, the concentration determined by the TCE protein assay is on average below 0.5 mg/ml for both purification strategies. The MS quantification analysis shows that CNG only accounts for roughly half of the protein content in the samples, further decreasing the number of useful particles in the data. In general, cryo-EM studies successfully investigating ion channels use about 1-5 mg/ml of proteins (Dang et al., 2018; Hite et al., 2015). Nevertheless, there have been exceptions, where low concentrations of 0.3 mg/ml have been used for structural determination (Liao et al., 2013). In our experience, concentration efforts with various spin concentrators have proven only marginally effective (data not shown).

Another step that will improve the relevance of structural investigations is using a membrane mimicking system such as MSP or polymer stabilised nanodisc (Knowles et al., 2009; Nath et al., 2007). Besides positive impact on stability, membrane mimicking systems provide a more native environment, including lipids. While several ion channel structures reconstituted in such a system are present, investigations performed in detergent often precede these studies and highlight pitfalls and challenges (Liao et al., 2013 followed by Gao et al., 2016).

Although several characteristics of the purified CNG channels were analysed, functional properties have not been actively monitored in this thesis. However, both purification strategies rely on binding affinity, and therefore the purified proteins indicate a functional binding site/pocket. The full functional status of the protein is unknown, and considering the presence of detergent and apparent instability of the protein, possible functional and

structural impairment cannot be ruled out. Therefore, all experiments were conducted immediately after the purification, or if applicable, the protein was preserved by flash freezing or cross-linking.

5.2 Distinct Sample Composition Revealed by Mass Spectrometry

In this thesis, mass spectrometry was performed on samples generated by cGMP-AC and CaM-AC. Although MS is considered a reliable and precise method, native source material introduces a biological variance. Therefore, the experiments were performed on three biological replicates, each (unless stated otherwise). The MS-based analysis applied in this thesis reveals the composition of samples by determining which proteins are present and how abundant the identified proteins are. While other methods like antibody-based proteomics rely on a pre-selection of proteins that can be detected and quantified, MS is a hypothesis-free approach that works on a small- and proteome-wide scale.

Figure 21 A and B shows the agreement of identified proteins within the biological replicates and between the two different experimental sources. The majority of proteins (223 in cGMP-AC and 222 in CaM-AC) are identified in all three replicates of the experiment. Nevertheless, the total numbers between the three replicates vary considerably for both purifications. Likely some samples have a higher overall protein concentration, which allows identification of more proteins with sufficient methodological certainty leading to higher numbers of identified proteins. Unfortunately, the high sample volume consumed for concentration determination and MS analysis did not permit further investigation of this connection. Proteins present in only one of the replicates will be regarded as not meaningful in the characterisation of the populations, although we are aware that this may exclude relevant proteins from the analysis. It is noteworthy that most MS studies are based on a single biological replicate, and therefore we are confident that our data is substantially above average.

(Figure 21 D) best represents the consistently identified proteins (present in all replicates) and how the populations differ between the purification strategies. An agreement of proteins identified in the two purification approaches is undoubtedly expected in samples arising from purifications of the same POI, using the same source material, and under similar experimental conditions. However, about 100 proteins consistently identified are unique to either purification. Compared to previous work by Becirovic and colleagues (Becirovic et al., 2014) and Cheng and Molday (C. L. Cheng & Molday, 2013), both used co-immunoprecipitation with antibodies against CNGB1 to obtain their protein sample, we consider that our protein sample compositions are similar. Of the 15 bovine proteins listed in Cheng and Molday, 11 (73 %) are present in all six experiments presented in this thesis (C. L. Cheng & Molday, 2013). Becirovic and colleagues performed their experiments with murine retina and provided a comprehensive list (< 200 entries) of identified proteins that include potential contaminants (e.g., Keratine). In this case, the agreement with our data is much

lower (38 %). This result is undoubtedly also influenced by the high amount of ribosomal proteins identified in their study. Moreover, the proteins untypical for ROS but present in surrounding cell compartments (e.g., nuclear pore proteins) and tissues (e.g., Beta-crystallin B3 from the eye lens) that are included in their dataset decrease the agreement between our data (Becirovic et al., 2014).

The protein quantification supports the observation of two distinct populations because severe differences exist even among highly abundant proteins (Figure 26). Proteins that are similar between the purification approaches include CNG, Rhodopsin, and Peripherin-2. Among CNG channel proteins, the subunits CNGA1 and CNGB1 are the most abundant, but surprisingly, other CNG subunits (CNGA2 and CNGA3) have been identified in low abundance. As mentioned above, a likely explanation is the contamination of the ROS source material, for example, with cone photoreceptors where CNGA3 is expressed (Bönigk et al., 1993).

It is noteworthy that soluble GARP1 and GARP2 proteins in the UniProt database are categorized as CNGB1 isoforms (Q28181-4 and Q28181-5), and therefore, they are included in the CNGB1 protein group. Hence, the isoform is not considered a separate protein, which may influence stoichiometry and quantification of (full length) CNGB1. However, peptide identifications of the GARP region are comparatively low, indicating properties that render them elusive in the MS approach we used. Furthermore, we have reason to believe that the concentration of soluble GARPs is reduced in comparison to the physiological state because, as performed in this thesis, hypotonic washing of the ROS has been reported to remove substantial amounts of GARP1 and GARP2 (Körschen et al., 1999).

Rhodopsin is an expected contamination that is most likely co-purified due to its high copy number in the source material but may also be part of a complex, as explained in the following section (see section 5.3). Peripherin-2 is also consistently present in both purifications and is suspected to be part of a protein cluster formed between proteins of the plasma membrane, soluble proteins, and disk-associated proteins (see section 5.3). The three most striking protein groups present in high abundance and unique to one of the purification approaches are Nucleoside Diphosphate Kinases (NDPK) in cGMP-AC, Ankyrin Repeat Domain 33B (ANKRD33B), and three catalytic subunit isozymes (PPP3CA, PPP3CB, and PPP3CC) of the Serine/Threonine-protein phosphatase (PPP3 or Calcineurin) in CaM-AC.

The comparison of quantification data in soluble CNG samples and Coomassie-stained SDS-PAGE of a representative sample (Figure 27) already provides some insight into the identity of visible bands. However, we decided to perform a gel excision followed by MS analysis to deepen our understanding (Figure 33).

The CNGB1 bands of both purification approaches and CNGA1 of cGMP-AC exhibit high purity support our results from Immunoblot analysis (Figure 17 and Figure 18). The three bands visible in the CaM-AC samples, close to the expected running height of CNGA1, show

unexpected results. While the Immunoblot (Figure 18) shows a distinct CNGA1 band, MS quantification returned contradicting results, with none of the visible bands containing a high quantity of CNGA1. Instead, CNGA1, ANKRD33B, and the PPP3C isozymes are the most abundant proteins in those three bands. However, the MS quantification of total elution samples shows that CNGA1 is the most abundant protein. Therefore, we assume that the CNGA1 containing gel piece was cut short, leaving the bulk of CNGA1 behind.

5.3 Direct and Indirect Interaction Partners

Observing high quantities of co-purified proteins in our samples led us to question why these proteins are present. The likely reasons for a protein other than the CNG channel being present in the elution are the following: (1) unspecific binding of the protein to the affinity resin, (2) the protein has an affinity towards the cGMP or CaM resin, or (3) the protein's interaction partner has an affinity towards the resin. The latter option may inform about putative interaction partners of CNG, which can lead to a more comprehensive understanding of complex formation or highlight the role of CNG in other functional processes of ROS.

For proteins that are part of signal transduction events, clustering has been observed in various cases, probably to increase speed, specificity, and sensitivity of the process (Cebecauer et al., 2010; Houtman et al., 2005; Zuker & Ranganathan, 1999). Such a macromolecular assembly has also been suspected and studied in the context of the phototransduction cascade (Kaupp & Seifert, 2002; Körschen et al., 1999; Robert S. Molday & Moritz, 2015; Pearring et al., 2021).

Figure 35 is a visual representation of a plausible protein-protein interaction network based on the literature and database research in combination with the analysis of our MS data (e.g., STRING protein-protein interaction database, string-db.org, (Szklarczyk et al., 2015) about potential interaction partners for the two CNG subunits of interest. The shown proteins do not necessarily interact with CNG at the time of purification but are listed because they have been reported (or are suggested) to interact with CNG during its life cycle. Furthermore, additional proteins identified in the respective purification and quantified in high abundance were selected for the representation. The respective compounds used to capture protein in the cGMP-AC and CaM-AC are also available interaction partners, and therefore, they are included in Figure 35 (triangular shape).

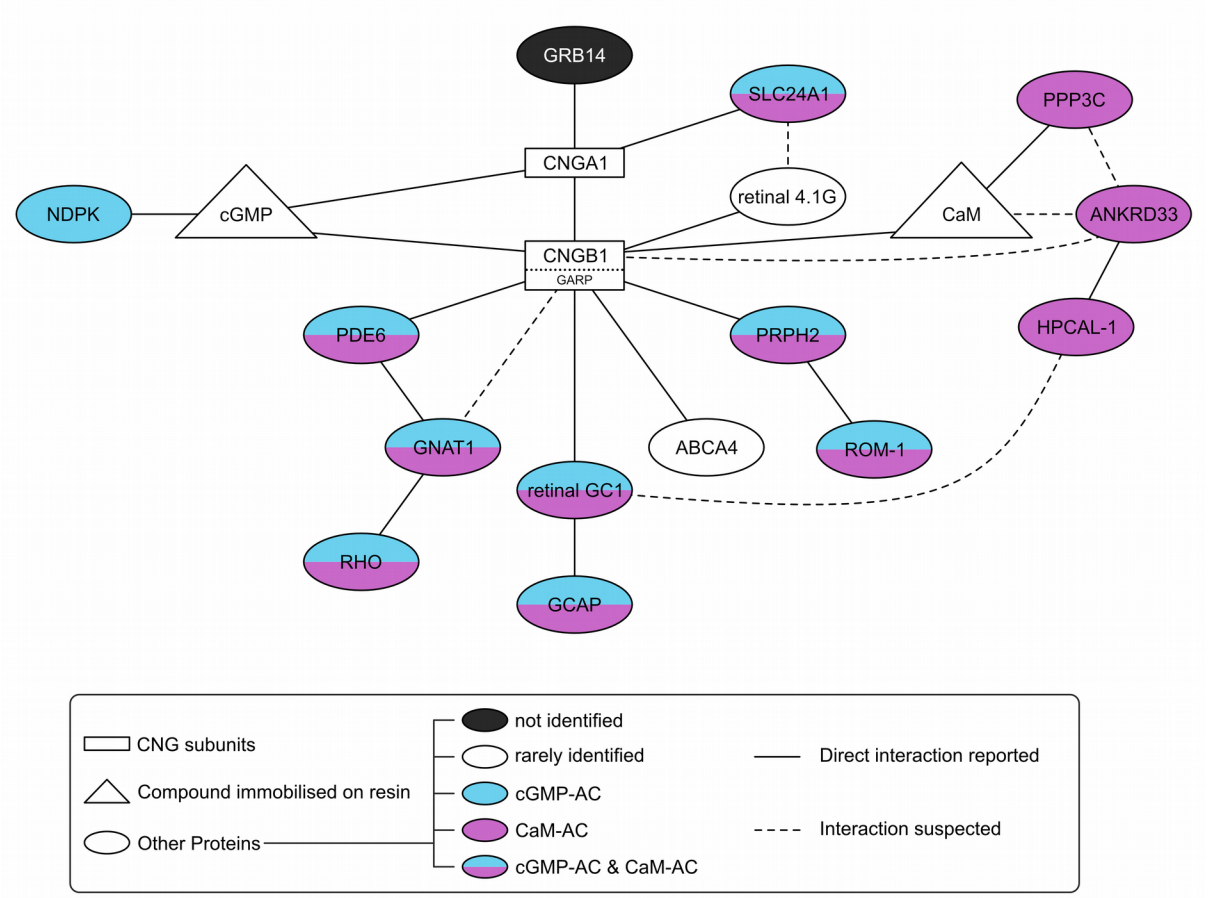

Figure 35: Overview of selected potential interactions

The diagram shows compounds used for affinity purification (triangular shape), CNG subunits (rectangular shapes, GARP'/1/2 separated by dotted line), and selected proteins (oval shape). The lines specify whether a direct interaction between network members has been reported (continuous line) or suspected (dashed line). Further information regarding the colour code is provided in the legend. Abbreviation for protein names are: CNGA1 = cyclic nucleotide-gated channel subunit alpha 1; CNGB1 = Cyclic Nucleotide-gated channel subunit beta 1; GARP = Glutamic Acid Rich Protein; GRB14 = Growth factor Receptor-Bound protein 14; SLC24A1 = Solute Carrier family 24 member 1; PPP3C = Serine/Threonine-protein phosphatase Calcineurin catalytic isozymes; ANKRD33B = Ankyrin Repeat Domain 33B; HPCAL-1 = Hippocalcin-like protein 1; PRPH2 = Peripherin-2; ROM-1 = Rod Outer segment Membrane protein 1; ABCA4 = ATP-binding cassette, sub-family A member 4; retinal GC = Guanylate Cyclase; GCAP = Guanylate Cyclase-Activating Protein; GNAT1 = Transducin α-subunits; RHO = Rhodopsin; PDE6 = Rod cGMP-specific 3',5'-cyclic Phosphodiesterase; NDPK = Nucleoside-Diphosphate Kinases NME1-2, NME2 and NME3

Most interactions of the CNG channel with other proteins occur due to the CNGB1 subunit (Körschen et al., 1999). The growth factor receptor-bound protein 14 (GRB14) has been reported to interact with the C-terminal region of CNGA1 (Gupta et al., 2010), and it functions as an adapter connecting the Insulin receptor kinase (IR kinase) to the CNG channel (Gua et al., 2012). However, according to our MS analysis, GRB14 is not observed in any of the samples.

The Na^+/Ca^{2+}-K^+ exchanger SLC24A1 (Solute carrier family 24 member 1, SLC24A1 also known as NCKX1) is responsible for Ca^{2+} efflux. In the dark, the Na^+/Ca^{2+}-K^+ exchanger is relevant for a balanced high intracellular Ca^{2+} concentration, and in light conditions, it is relevant for Ca^{2+} clearance and hyperpolarisation. Several studies reported a direct interaction of the Na^+/Ca^{2+}-K^+ exchanger and the CNGA1 subunit (Bauer & Drechsler, 1992; K. J. Kang et al., 2003; Robert S Molday & Molday, 1998). As the recovery time depends on a rapid Ca^{2+} efflux, the proximity of the Na^+/Ca^{2+}-K^+ exchanger and CNG channel is advantageous. Although we were able to identify the Na^+/Ca^{2+}-K^+ exchanger, the suggested two-fold ratio (Robert S Molday & Molday, 1998) can not be observed in any elution. The distinct band (~230 kDa) below the CNGB1 subunit visible after SDS-PAGE likely corresponds to the Na^+/Ca^{2+}-K^+ exchanger, but protein forming this band appears mainly in the unbound fraction (Figure 19). The hypotonic wash at the beginning of the purification probably disrupts the interaction, as was suggested previously (Robert S Molday & Molday, 1998).

The glutamic acid-rich part of the CNGB1 subunit (GARP') is intrinsically disordered and includes a negatively charged region and a proline-rich repeat region. Two splice variants of the same gene result in the soluble proteins GARP1 and GARP2. While GARP1 is identical to the GARP' domain of CNGB1, GARP2 is shorter and lacks part of the C-terminal (glutamic acid-rich) region (Colville & Molday, 1996; Körschen et al., 1995; Sugimoto et al., 1991). Under physiological conditions, soluble GARP proteins are closely associated with the membrane and were shown to be relatively abundant (Körschen et al., 1999). As the MS analysis performed in this thesis cannot distinguish between soluble GARP1/2 and the GARP' domain of CNGB1, in Figure 35, they are combined into one box separated by a dotted line.

Both soluble and membrane-bound PDE6 were reported to interact strongly with GARP2 (Körschen et al., 1999). From the soluble fraction of ROS, GARP1 and GARP2 have been observed to interact with the proline-rich repeat region present in all GARPs. Transducin α-subunits (GNAT1) have also been reported to bind the proline-rich repeat region of GARPs, but the interaction has been characterised as weak or is possibly mediated via another protein. From the membrane fraction, GC (retinal GC1) and photoreceptor-specific ATP-binding cassette transporter (ABCA4 or rim protein) are discussed as potential interaction partners with the same protein-rich repeat region. GC possibly only interacts with soluble GARP2 with the help of cytoskeletal proteins Tubulin and Actin. GARP2 has been reported interacting with GC and ABCA4 to assemble them at the disc margin near the CNG channels (Körschen et al., 1999). However, there is no clear experimental evidence that GARP' is involved in direct interactions with GC and ABCA4. Also, there is no experimental evidence of direct interaction between RHO and any of the CNG channel subunits but likely co-localisation due to clustering of the signaling proteins of rod photoreceptors.

Besides the functional components of the signaling cascade, the glutamic acid-rich region of GARP' has been observed to be essential for targeting the heterotetrameric channel to the plasma membrane of ROS (Becirovic et al., 2014; Pearring et al., 2021). In this context,

Peripherin-2 and ROM-1 have been reported to form an interaction complex at the disc rim with the CNG channel (Pearring et al., 2021). In additional experiments using immunoprecipitation and proteomic analysis, it has been observed that the retinal 4.1G protein is an interaction partner of the rod CNG channels. Furthermore, retinal 4.1G has been suggested to interact with the Na^{+}/Ca^{2+}-K^{+} exchanger 1 (C. L. Cheng & Molday, 2013).

In agreement with previously published work, we identified PDE6, GNAT1, retinal GC1, and Peripherin-2 in amounts that indicate a co-purification. Furthermore, proteins that are likely to be indirectly associated with CNG, such as Rhodopsin, GCAP (guanylyl cyclase-activating protein), and ROM-1, were identified in both purification approaches. In contrast, ABCA4 was identified in some experiments, but the low abundance suggests no strong interaction under our purification conditions.

Four proteins (NDPK PPP3C, HPCAL-1, ANKRD33B) were identified with no direct interaction indicated by any previous work. As the presence of these four proteins is limited to one specific purification approach, a methodological explanation is likely. Indeed, NDPK (Nucleoside-diphosphate kinases) are known to interact with nucleosides (Abdulaev et al., 1998b), and hence, a plausible interaction with the cGMP resin coincides with the observed identification that is limited to cGMP-AC. Furthermore, a membrane association has been reported explaining why (soluble) NDPKs were not removed during the hypotonic wash of the ROS (Mitchell et al., 2009). Given that Calcineurin (PPP3C) interacts in the presence of Ca^{2+} with CaM, a similar explanation would be feasible (Rusnak & Mertz, 2000). However, the possibility remains that CaM, while bound to CNG, recruits these proteins to the complex. In the case of the Serine/Threonine phosphatase Calcineurin, this would be a reasonable explanation for a Ca^{2+}-dependent phosphorylation mechanism (Creamer, 2020).

HPCAL-1 is also a Ca^{2+} binding protein, but further information relies on deductions from homologous proteins (Kobayashi et al., 1994). HPCAL-1 is a member of the EF-hand protein family, and the EF-hand motifs present are also found in Calcineurin and CaM (Yubin Zhou et al., 2006). While a direct binding to CaM or CNGB1 has not been reported, the structural similarity to CaM may explain the presence of HPCAL-1. Notably, an interaction with CaM-binding Calcineurin (Huttlin et al., 2017) and retinal GC (Krishnan et al., 2009) could be suggested.

Only little information is available about ANKRD33B, but it was identified by the MS analysis of Kwok and colleagues in 2008 in bovine ROS preparations (Kwok et al., 2008). A master thesis performed in the same lab revealed an interaction between ANKRD33B and HPCAL-1 attributed to the EF-motif, as mentioned previously (Rostamirad, 2010). This affinity of ANKRD33B towards EF-motifs suggests a binding affinity towards the CaM resin used in the CaM-AC.

The presence of proteins known or suspected to interact with CNG channels directly and indirectly further supports a successful purification of CNG channels alongside a naturally

occurring cluster of proteins. We were able to identify what proteins are purified through affinity to the respective purification resin and explain the presence of the most abundant proteins identified by MS. While most co-purified proteins are likely present due to physiological interactions with the CNG channels, we do not know whether they are present in one or several smaller multimeric protein complex(es). However, additional proteins in the elution samples should be considered for future studies, such as structural investigations by cryo-EM, because they introduce heterogeneity.

5.4 CNG channels Exhibit Various Phosphorylations

The phosphorylation of a protein is driven by kinases and entails a covalent addition of a phosphoryl group (PO_3^{2-}) to an amino acid residue. The vast majority of phosphorylated amino acids are Serine residues, followed by Threonine and Tyrosine residues (Olsen et al., 2006). Phosphorylation of the residues introduces a strong polarity, rendering the protein hydrophilic at the region and supporting the formation of hydrogen bonds and salt bridges. Phosphorylation of a functionally relevant residue causes conformational changes that often influence the activity or specificity of the phosphorylated protein (Nishi et al., 2014). For CNG channels, phosphorylations have also been discussed and considered likely, as some evidence has been published that phosphorylations play a role in the channel modulation (Kaupp & Seifert, 2002; Matulef & Zagotta, 2003). Gordon and colleagues show increased cGMP sensitivity of the CNG channels in rods over time due to Serine/Threonine phosphatase action (Gordon et al., 1992). Molokanova and colleagues reported that mutations of two specific Tyrosine residues diminish the CNG channel's ability to switch between high and low sensitivity states (Krajewski et al., 2003; Molokanova et al., 1997, 1999, 2003).

In (over-) expression-based protein purifications, the post-translational modifications are usually not or only partially present (Pandey et al., 2016). Furthermore, the status of post-translational modifications is not automatically preserved throughout the protein purification process. Therefore, we purified protein from a natural source that was endogenously expressed and subjected to *in vivo* post-transcriptional and post-translational modifications. As phosphorylation is a reversible process, a phosphatase inhibitor cocktail was used to preserve the phosphorylation status.

Immunoblots were performed using antibodies against phosphorylated Serine/Threonine residues and phosphorylated Tyrosine residues. The residues appear consistently modified between the input and the elution, indicating good preservation of the phosphorylation state throughout the purification. Phosphorylated proteins were detected in the correct running height for most CNGA1 and CNGB1 bands but with weak signals. The information from MS-driven identification of proteins shows a diverse population of proteins in the elution, and therefore a signal at expected height does not necessarily prove phosphorylated

CNG subunits. Overall, the immunoblots highlight the presence of phosphorylated protein but lack specific information.

In our analysis, only phosphorylations of Serine and Threonine residues were observed, even though only the phosphorylations of specific Tyrosine residues are discussed in the literature (Krajewski et al., 2003; Molokanova et al., 1997, 1999, 2003). We cannot determine whether this is due to a systemic or methodological phenomenon. The technique used here, by all means, can identify all phosphorylated residues and other PTMs, such as methylations of the amino-terminus. Indeed, the N-terminal methylation for example was detected across all analysed CNG samples (data not shown).

Overall CNG channels purified from cGMP-AC appear more frequently phosphorylated compared to the CaM purification strategy. This could indicate a connection between phosphorylation state and ligand binding affinity. However, we are not able to exclude a methodological reason, such as insufficient blocking or incomplete removal of phosphatases. The presence of Ca^{2+} ions in CaM-AC buffers could be sufficient to supports activity of Ca^{2+} dependent phosphatases, resulting in dephosphorylation of the proteins purified via CaM-AC.

Figure 36 shows a different representation of the observed phosphorylation sites presented in the results section 5.4 (see Figure 29 to Figure 32). Here the sites are annotated alongside the functional domains of the CNG subunits. The positions of domains were fetched from the UniProt database and the best of our literature knowledge. For CNGA1, all phosphorylation sites are located between the CNBD and the carboxy-terminus (Figure 36 A). In the samples from CaM-AC, only S630 was observed to be phosphorylated, while in cGMP-AC, two additional phosphorylation sites (S616 and S648) were observed. The previously reported potential phosphorylation site Y498 of CNGA1 was not observed in either purification approach (empty gear in Figure 36), although the peptides spanning this amino acid were identified.

The recently published atomic model of the human CNGA1 homotetramer (Xue et al., 2021) likely corresponds to the structural organisation of CNGA1 subunits present in the heterotetramer and could be helpful to assess the functional mechanism behind these phosphorylation sites. Unfortunately, the atomic model provided in the PDB database (7LFT) lacks amino acids 1-155 and 606-690, and we can not appreciate the structural context of any residue that we found phosphorylated.

Zhong and colleagues identified the C-terminal region containing the phosphorylation in question (S616, S630, and S648 of CNGA1) as a leucine-zipper-homology domain (CLZ) unique for CNGA1 subunits (Zhong et al., 2002). Subsequently, the CLZ has been reported to be crucial for assembling the heterotetrameric channel. They reveal an assembly of a trimeric CNGA1 that prefers to form a complex with CNGB1 instead of a fourth CNGA1 (Zhong et al., 2003). Studies on other proteins containing a Leucine zipper also show

phosphorylations in this domain (Wegner et al., 1992). Depending on the protein and the site, the phosphorylations stabilise (Szilák et al., 1997), impact activity, or support dimerisation of the protein (S. Lee et al., 2010). A similar supportive role could be present in CNG, but further experiments are required to determine relevance and mechanism.

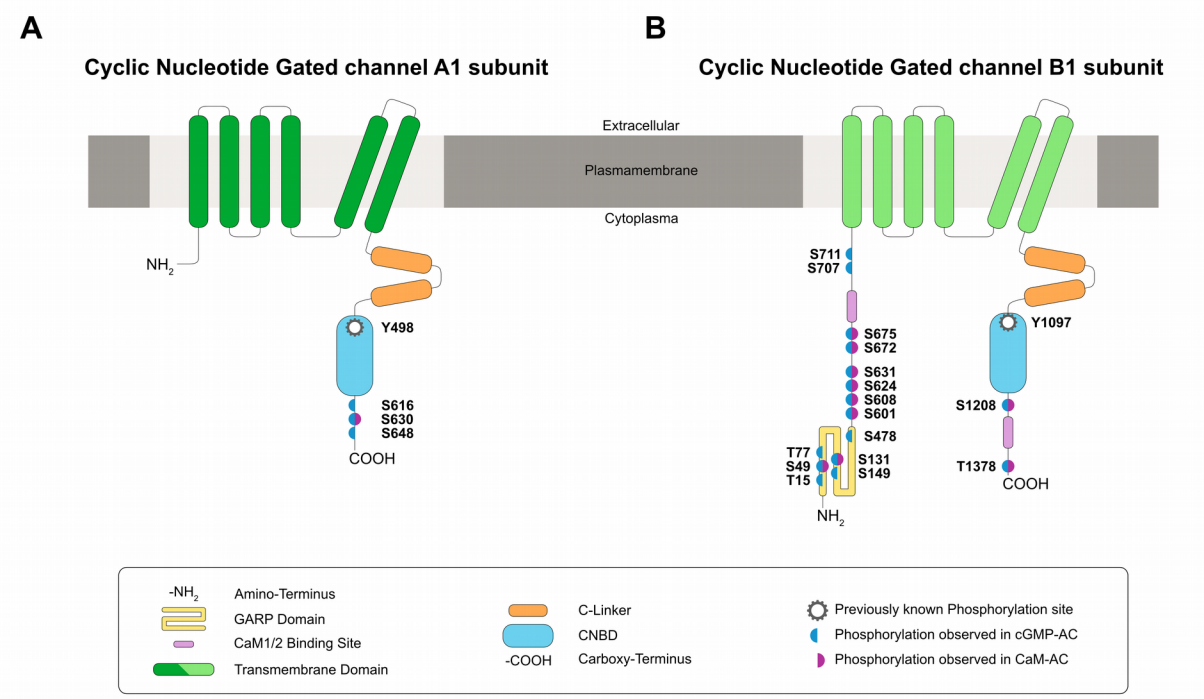

Figure 36: Schematic overview of CNG channel phosphorylation sites identified by Mass Spectrometry

Phosphorylation sites that have been observed at least once are annotated. Phosphorylation sites from literature are marked by a gear (Y498 in CNGA1 and Y1097 in CNGB1). Phosphorylation sites observed by the MS analysis of the samples obtained from cGMP-AC (blue half-circle) and CaM-AC (red half-circle) are marked in the schemes of CNGA1 (A) and CNGB1 (B). The modified amino acids (S = Serine, T = Threonine, Y = Tyrosine) and exact positions are specified on each marker's side.

For CNGB1, several clusters of phosphorylation sites were observed. The first six phosphorylation sites are located within the GARP domain (Figure 36 B), of which only two were observed in CaM-AC samples. The second cluster of phosphorylation sites (S601, S608, S624, S631, S672, S675) is located between the GARP domain and the first calmodulin-binding site (CaM1), and the majority of these phosphorylation sites was consistently phosphorylated. This region may interact with the CLZ of the CNGA1 subunits (Shuart et al., 2011). Here basal phosphorylation would support subunit interaction and therefore could be relevant for the assembly in the defined stoichiometry.

The subsequent cluster of phosphorylated sites was only present in cGMP-AC purified samples and is located after the CaM1. The previously reported potential phosphorylation site Y1097 of CNGB1 would have been located just at the beginning of CNBD, but similar to the Y498 of CNGA1 subunit, it was not observed in either purification approach (empty gear) (Krajewski et al., 2003; Molokanova et al., 1997, 1999, 2003). The consistently phosphorylated S1208 residue is located few amino acids after the CNBD and upstream of the second calmodulin-binding site (CaM2). Finally, T1378 was observed in both purification approaches and is located close to the carboxy-terminus. Lacking an atomic model of the heterotetrameric rod photoreceptor CNG channel, we cannot use a structural context to speculate on the relevance and role of the phosphorylation sites identified in the CNGB1 subunit.

In olfactory CNG channels, phosphorylation of a Serine residue in the flanking region next to the CaM binding site increased its cyclic nucleotide sensitivity (Müller et al., 1998). However, similar results are not published for rod photoreceptor CNG to our knowledge. We found both CaM binding sites flanked by phosphorylated residues. The CaM1 located at the amino-terminal region is essential for the Ca^{2+}/CaM mediated modulation of the channel, and the carboxy-terminal CaM2 is of minor importance (Weitz et al., 1998). While the CNG channels purified by both purification strategies exhibit phosphorylations at the N-terminal of CaM1, only cGMP-AC purified channels carry phosphorylations after the CaM1 domain. It could indicate that Ca^{2+}/CaM binding is only possible when S707 and S711 are not phosphorylated. This region was not well covered in our analysis for CaM-AC purified channels, and functional binding studies will be required for comprehensive understanding. Of the phosphorylations flanking CaM2, S1208 stands out because it has been observed to be consistently modified. As this may be a basal phosphorylation required for folding, additional studies need to be conducted to elucidate functional relevance.

Phosphorylations in the GARP may be relevant for switching between binding partners or regulate complex formation. Unfortunately, our data do not support conclusions regarding specific isoforms. Different phosphorylations between the GARP' of the full-length CNGB1 and soluble GARP1 and GARP2 could explain how different roles can be achieved.

In the disease context, defective CNG channels are known to cause some variations of Retinitis Pigmentosa (RP) (Giblin et al., 2016; Robert S. Molday & Moritz, 2015). In RP, the progressive photoreceptor degeneration leads to night blindness, and in advanced pathology, retinal degeneration generally results in total blindness (X. Chen et al., 2013; Hartong et al., 2006; Katagiri et al., 2014). We did not find an RP causing mutation in CNG subunits that connects directly to a phosphorylation site we identified (Dryja et al., 1995). However, most known CNG mutations leading to RP are located in CNGA1 subunits and cause a frameshift that results in severe truncation of the protein (Giblin et al., 2016).

In conclusion, we were able to show that phosphorylations are present as speculated by several other researchers investigating the CNG channel from bovine ROS (Kaupp & Seifert, 2002; Krajewski et al., 2003; Matulef & Zagotta, 2003; Molokanova et al., 1997, 1999, 2003). Furthermore, we identified in both subunits specific and novel phosphorylation sites. The identity of phosphorylated residues narrows down the group of protein kinases and phosphatases involved. However, additional experiments will be required to characterise each phosphorylation site and determine the mechanisms at work.

6 References

Abdulaev, N. G., Karaschuk, G. N., Ladner, J. E., Kakuev, D. L., Yakhyaev, A. V., Tordova, M., Gaidarov, I. O., Popov, V. I., Fujiwara, J. H., Chinchilla, D., Eisenstein, E., Gilliland, G. L., & Ridge, K. D. (1998a). Nucleoside diphosphate kinase from bovine retina: Purification, subcellular localization, molecular cloning, and three-dimensional structure. *Biochemistry*, *37*(40), 13958–13967. https://doi.org/10.1021/bi980853s

Abdulaev, N. G., Karaschuk, G. N., Ladner, J. E., Kakuev, D. L., Yakhyaev, A. V., Tordova, M., Gaidarov, I. O., Popov, V. I., Fujiwara, J. H., Chinchilla, D., Eisenstein, E., Gilliland, G. L., & Ridge, K. D. (1998b). Nucleoside diphosphate kinase from bovine retina: Purification, subcellular localization, molecular cloning, and three-dimensional structure. *Biochemistry*, *37*(40), 13958–13967. https://doi.org/10.1021/bi980853s

Aebersold, R., & Mann, M. (2003). Mass spectrometry-based proteomics. In *Nature* (Vol. 422, Issue 6928, pp. 198–207). Nature Publishing Group. https://doi.org/10.1038/nature01511

Ahmad, I., Leinders-Zufall, T., Kocsis, J. D., Shepherd, G. M., Zufall, F., & Barnstable, C. J. (1994). Retinal ganglion cells express a cGMP-gated cation conductance activatable by nitric oxide donors. *Neuron*, *12*(1), 155–165. https://doi.org/10.1016/0896-6273(94)90160-0

Alvarez, F. J. D., He, S., Perilla, J. R., Jang, S., Schulten, K., Engelman, A. N., Scheres, S. H. W., & Zhang, P. (2017). CryoEM structure of MxB reveals a novel oligomerization interface critical for HIV restriction. *Science Advances*, *3*(9). https://doi.org/10.1126/sciadv.1701264

Anderson, N. L., & Anderson, N. G. (1998). Proteome and proteomics: New technologies, new concepts, and new words. *Electrophoresis*, *19*(11), 1853–1861. https://doi.org/10.1002/elps.1150191103

Arike, L., Valgepea, K., Peil, L., Nahku, R., Adamberg, K., & Vilu, R. (2012). Comparison and applications of label-free absolute proteome quantification methods on Escherichia coli. *Journal of Proteomics*, *75*(17), 5437–5448. https://doi.org/10.1016/j.jprot.2012.06.020

Baker, D., & Sali, A. (2001). Protein structure prediction and structural genomics. In *Science*. https://doi.org/10.1126/science.1065659

Bartesaghi, A., Lecumberry, F., Sapiro, G., & Subramaniam, S. (2012). Protein secondary structure determination by constrained single-particle cryo-electron tomography. *Structure*, *20*(12), 2003–2013. https://doi.org/10.1016/j.str.2012.10.016

Bateman, A., Martin, M. J., Orchard, S., Magrane, M., Agivetova, R., Ahmad, S., Alpi, E., Bowler-Barnett, E. H., Britto, R., Bursteinas, B., Bye-A-Jee, H., Coetzee, R., Cukura, A., Silva, A. Da, Denny, P., Dogan, T., Ebenezer, T. G., Fan, J., Castro, L. G., … Zhang, J. (2021). UniProt: The universal protein knowledgebase in 2021. *Nucleic Acids Research*. https://doi.org/10.1093/nar/gkaa1100

Batra-Safferling, R., Abarca-Heidemann, K., Körschen, H. G., Tziatzios, C., Stoldt, M., Budyak, I., Willbold, D., Schwalbe, H., Klein-Seetharaman, J., & Kaupp, U. B. (2006). Glutamic acid-rich proteins of rod photoreceptors are natively unfolded. *Journal of Biological Chemistry*. https://doi.org/10.1074/jbc.M505012200

Bauer, P. J., & Drechsler, M. (1992). Association of cyclic GMP-gated channels and Na(+)-Ca(2+)-K+ exchangers in bovine retinal rod outer segment plasma membranes. *The Journal of Physiology*, *451*(1), 109–131. https://doi.org/10.1113/jphysiol.1992.sp019156

Baumann, M., & Meri, S. (2004). Techniques for studying protein heterogeneity and post-translational modifications. *Expert Review of Proteomics*, *1*(2), 207–217. https://doi.org/10.1586/14789450.1.2.207

Bayat, A. (2002). Science, medicine, and the future: Bioinformatics. In *British Medical Journal* (Vol. 324, Issue 7344, pp. 1018–1022). BMJ Publishing Group. https://doi.org/10.1136/bmj.324.7344.1018

References

Becirovic, E., Nguyen, O. N. P., Paparizos, C., Butz, E. S., Stern-Schneider, G., Wolfrum, U., Hauck, S. M., Ueffing, M., Wahl-Schott, C., Michalakis, S., & Biel, M. (2014). Peripherin-2 couples rhodopsin to the CNG channel in outer segments of rod photoreceptors. *Human Molecular Genetics*, *23*(22), 5989–5997. https://doi.org/10.1093/hmg/ddu323

Benedikt, J., Hecimovic, A., Ellerweg, D., & Von Keudell, A. (2012). Quadrupole mass spectrometry of reactive plasmas. *Journal of Physics D: Applied Physics*, *45*(40), 403001. https://doi.org/10.1088/0022-3727/45/40/403001

Berg, J. M., Tymoczko, J. L., Gatto, G. J., & Stryer, L. (2018). *Stryer Biochemie*. Springer Berlin Heidelberg. http://link.springer.com/10.1007/978-3-662-54620-8

Berman, H. M., Westbrook, J., Feng, Z., Gilliland, G., Bhat, T. N., Weissig, H., Shindyalov, I. N., & Bourne, P. E. (2000). The Protein Data Bank. In *Nucleic Acids Research* (Vol. 28, Issue 1, pp. 235–242). Oxford University Press. https://doi.org/10.1093/nar/28.1.235

Bernaudat, F., Frelet-Barrand, A., Pochon, N., Dementin, S., Hivin, P., Boutigny, S., Rioux, J. B., Salvi, D., Seigneurin-Berny, D., Richaud, P., Joyard, J., Pignol, D., Sabaty, M., Desnos, T., Pebay-Peyroula, E., Darrouzet, E., Vernet, T., & Rolland, N. (2011). Heterologous expression of membrane proteins: Choosing the appropriate host. *PLoS ONE*, *6*(12). https://doi.org/10.1371/journal.pone.0029191

Biel, M., & Michalakis, S. (2009). Cyclic Nucleotide-Gated Channels. In *Handbook of Experimental Pharmacology 191* (pp. 111–136).

Biemann, K. (2015). Structure Determination of Natural Products by Mass Spectrometry. In *Annual Review of Analytical Chemistry*. https://doi.org/10.1146/annurev-anchem-071114-040110

Bill, R. M., Henderson, P. J. F., Iwata, S., Kunji, E. R. S., Michel, H., Neutze, R., Newstead, S., Poolman, B., Tate, C. G., & Vogel, H. (2011). Overcoming barriers to membrane protein structure determination. In *Nature Biotechnology* (Vol. 29, Issue 4, pp. 335–340). Nat Biotechnol. https://doi.org/10.1038/nbt.1833

Black, D. L. (2000). Protein diversity from alternative splicing: A challenge for bioinformatics and post-genome biology. In *Cell* (Vol. 103, Issue 3, pp. 367–370). Elsevier B.V. https://doi.org/10.1016/S0092-8674(00)00128-8

Böer, E., Steinborn, G., Kunze, G., & Gellissen, G. (2007). Yeast expression platforms. In *Applied Microbiology and Biotechnology* (Vol. 77, Issue 3, pp. 513–523). Springer. https://doi.org/10.1007/s00253-007-1209-0

Bönigk, W., Altenhofen, W., Müller, F., Dose, A., Illing, M., Molday, R. S., & Kaupp, U. B. (1993). Rod and cone photoreceptor cells express distinct genes for cGMP-gated channels. *Neuron*, *10*(5), 865–877. https://doi.org/10.1016/0896-6273(93)90202-3

Bönigk, W., Bradley, J., Müller, F., Sesti, F., Boekhoff, I., Ronnett, G. V., Kaupp, U. B., & Frings, S. (1999). The native rat olfactory cyclic nucleotide-gated channel is composed of three distinct subunits. *Journal of Neuroscience*, *19*(13), 5332–5347. https://doi.org/10.1523/jneurosci.19-13-05332.1999

Bornert, O., Alkhalfioui, F., Logez, C., & Wagner, R. (2012). Overexpression of membrane proteins using Pichia pastoris. *Current Protocols in Protein Science*, *1*(SUPPL.67), 29.2.1-29.2.24. https://doi.org/10.1002/0471140864.ps2902s67

Bradley, J., Zhang, Y., Bakin, R., Lester, H. A., Ronnett, G. V., & Zinn, K. (1997). Functional expression of the heteromeric “olfactory” cyclic nucleotide- gated channel in the hippocampus: A potential effector of synaptic plasticity in brain neurons. *Journal of Neuroscience*, *17*(6), 1993–2005. https://doi.org/10.1523/jneurosci.17-06-01993.1997

Brenner, S., & Horne, R. W. (1959). A negative staining method for high resolution electron microscopy of viruses. *BBA - Biochimica et Biophysica Acta*. https://doi.org/10.1016/0006-3002(59)90237-9

Bright, S. R., Rich, E. D., & Varnum, M. D. (2007). Regulation of human cone cyclic nucleotide-gated channels by endogenous phospholipids and exogenously applied phosphatidylinositol 3,4,5-trisphosphate. *Molecular Pharmacology*, *71*(1), 176–183. https://doi.org/10.1124/mol.106.026401

Bruschi, M., Petretto, A., Caicci, F., Bartolucci, M., Calzia, D., Santucci, L., Manni, L., Ramenghi, L. A., Ghiggeri, G., Traverso, C. E., Candiano, G., & Panfoli, I. (2018). Proteome of Bovine Mitochondria and Rod Outer Segment Disks: Commonalities and Differences. *Journal of Proteome Research*, *17*(2), 918–925. https://doi.org/10.1021/acs.jproteome.7b00741

Burgess, R. R. (2009). Chapter 20 Protein Precipitation Techniques. In *Methods in Enzymology* (Vol. 463, Issue C, pp. 331–342). Academic Press Inc. https://doi.org/10.1016/S0076-6879(09)63020-2

Büyükköroğlu, G., Dora, D. D., Özdemir, F., & Hizel, C. (2018). Techniques for protein analysis. In *Omics Technologies and Bio-engineering: Towards Improving Quality of Life* (Vol. 1). https://doi.org/10.1016/B978-0-12-804659-3.00015-4

Callaway, E. (2020). "It will change everything": DeepMind's AI makes gigantic leap in solving protein structures. In *Nature* (Vol. 588, Issue 7837, pp. 203–204). NLM (Medline). https://doi.org/10.1038/d41586-020-03348-4

Camponova, P., Baud, S., Mattras, H., Duroux-Richard, I., Bonnafous, J. C., & Marie, J. (2007). High-level expression and purification of the human bradykinin B2 receptor in a tetracycline-inducible stable HEK293S cell line. *Protein Expression and Purification*, *55*(2), 300–311. https://doi.org/10.1016/j.pep.2007.04.020

Can, T. (2014). Introduction to bioinformatics. *Methods in Molecular Biology*, *1107*, 51–71. https://doi.org/10.1007/978-1-62703-748-8_4

Carlson, M. L., Young, J. W., Zhao, Z., Fabre, L., Jun, D., Li, J., Li, J., Dhupar, H. S., Wason, I., Mills, A. T., Beatty, J. T., Klassen, J. S., Rouiller, I., & Duong, F. (2018). The peptidisc, a simple method for stabilizing membrane proteins in detergent-free solution. *ELife*, *7*. https://doi.org/10.7554/eLife.34085

Carpenter, E. P., Beis, K., Cameron, A. D., & Iwata, S. (2008). Overcoming the challenges of membrane protein crystallography. In *Current Opinion in Structural Biology*. https://doi.org/10.1016/j.sbi.2008.07.001

Carroll, D. I., Dzidic, I., Stillwell, R. N., Haegele, K. D., & Horning, E. C. (1975). Atmospheric Pressure Ionization Mass Spectrometry. Corona Discharge Ion Source for use in a Liquid Chromatograph-Mass Spectrometer-Computer Analytical System. *Analytical Chemistry*. https://doi.org/10.1021/ac60364a031

Catterall, W. A. (2000). From ionic currents to molecular mechanisms: The structure and function of voltage-gated sodium channels. In *Neuron* (Vol. 26, Issue 1, pp. 13–25). Cell Press. https://doi.org/10.1016/S0896-6273(00)81133-2

Cebecauer, M., Spitaler, M., Sergé, A., & Magee, A. I. (2010). Signalling complexes and clusters: Functional advantages and methodological hurdles. In *Journal of Cell Science* (Vol. 123, Issue 3, pp. 309–320). The Company of Biologists. https://doi.org/10.1242/jcs.061739

Chalmel, F., & Rolland, A. D. (2015). Linking transcriptomics and proteomics in spermatogenesis. In *Reproduction*. https://doi.org/10.1530/REP-15-0073

Chelikani, P., Reeves, P. J., Rajbhandary, U. L., & Khorana, H. G. (2006). The synthesis and high-level expression of a β_2-adrenergic receptor gene in a tetracycline-inducible stable mammalian cell line. *Protein Science*, *15*(6), 1433–1440. https://doi.org/10.1110/ps.062080006

Chen, C. Y., Oppermann, H., & Hitzeman, R. A. (1984). Homologous versus heterologous gene expression in the yeast, Saccharomyces cerevisiae. *Nucleic Acids Research*, *12*(23), 8951–8970. https://doi.org/10.1093/nar/12.23.8951

Chen, J., Petrov, A., Tsai, A., O'Leary, S. E., & Puglisi, J. D. (2013). Coordinated conformational and compositional dynamics drive ribosome translocation. *Nature Structural and Molecular Biology*, *20*(6), 718–727. https://doi.org/10.1038/nsmb.2567

Chen, T. Y., Peng, Y. W., Dhallan, R. S., Ahamed, B., Reed, R. R., & Yau, K. W. (1993). A new subunit of the cyclic nucleotide-gated cation channel in retinal rods. *Nature*, *362*(6422), 764–767. https://doi.org/10.1038/362764a0

Chen, X., Zhao, K., Sheng, X., Li, Y., Gao, X., Zhang, X., Kang, X., Pan, X., Liu, Y., Jiang, C., Shi, H., Chen, X., Rong, W., Chen, L. J., Lai, T. Y. Y., Liu, Y., Wang, X., Yuan, S., Liu, Q., … Zhao, C. (2013). Targeted sequencing of 179 genes associated with hereditary retinal dystrophies and 10 candidate genes identifies novel and known mutations in patients with various

retinal diseases. *Investigative Ophthalmology & Visual Science*, *54*(3), 2186–2197. https://doi.org/10.1167/iovs.12-10967

Cheng, C. L., & Molday, R. S. (2013). Interaction of 4.1G and cGMP-gated channels in rod photoreceptor outer segments. *Journal of Cell Science*. https://doi.org/10.1242/jcs.137679

Cheng, Y. (2015). Single-Particle Cryo-EM at Crystallographic Resolution. *Cell*, *161*(3), 450–457. http://linkinghub.elsevier.com/retrieve/pii/S0092867415003694

Cheng, Y. (2018). Membrane protein structural biology in the era of single particle cryo-EM. *Current Opinion in Structural Biology*, *52*, 58–63. https://linkinghub.elsevier.com/retrieve/pii/S0959440X18300496

Cheng, Y., Grigorieff, N., Penczek, P. A., & Walz, T. (2015). A Primer to Single-Particle Cryo-Electron Microscopy. *Cell*, *161*(3), 438–449. http://dx.doi.org/10.1016/j.cell.2015.03.050

Chiu, P. L., Pagel, M. D., Evans, J., Chou, H. T., Zeng, X., Gipson, B., Stahlberg, H., & Nimigean, C. M. (2007). The Structure of the Prokaryotic Cyclic Nucleotide-Modulated Potassium Channel MloK1 at 16 Å Resolution. *Structure*, *15*(9), 1053–1064. https://doi.org/10.1016/j.str.2007.06.020

Chopra, A., Willmore, W. G., & Biggar, K. K. (2019). Protein quantification and visualization via ultraviolet-dependent labeling with 2,2,2-trichloroethanol. *Scientific Reports*, *9*(1), 1–8. https://www.nature.com/articles/s41598-019-50385-9

Chung, D., Young, J., Bomble, Y. J., Vander Wall, T. A., Groom, J., Himmel, M. E., & Westpheling, J. (2015). Homologous Expression of the Caldicellulosiruptor bescii CelA Reveals that the Extracellular Protein Is Glycosylated. *PLOS ONE*, *10*(3), e0119508. https://doi.org/10.1371/journal.pone.0119508

Coburn, C. M., & Bargmann, C. I. (1996). A putative cyclic nucleotide-gated channel is required for sensory development and function in C. elegans. *Neuron*, *17*(4), 695–706. https://doi.org/10.1016/S0896-6273(00)80201-9

Cohn, E. J., Strong, L. E., Hughes, W. L., Mulford, D. J., Ashworth, J. N., Melin, M., & Taylor, H. L. (1946). Preparation and Properties of Serum and Plasma Proteins. IV. A System for the Separation into Fractions of the Protein and Lipoprotein Components of Biological Tissues and Fluids. *Journal of the American Chemical Society*, *68*(3), 459–475. https://doi.org/10.1021/ja01207a034

Colville, C. A., & Molday, R. S. (1996). Primary structure and expression of the human β-subunit and related proteins of the rod photoreceptor cGMP-gated channel. *Journal of Biological Chemistry*, *271*(51), 32968–32974. https://doi.org/10.1074/jbc.271.51.32968

Cook, N. J., Hanke, W., & Kaupp, U. B. (1987). Identification, purification, and functional reconstitution of the cyclic GMP-dependent channel from rod photoreceptors. *Proceedings of the National Academy of Sciences*, *84*(2), 585–589. https://doi.org/10.1073/pnas.84.2.585

Cook, N. J., Molday, L. L., Reid, D., Kaupp, U. B., & Molday, R. S. (1989). The cGMP-gated channel of bovine rod photoreceptors is localized exclusively in the plasma membrane. *Journal of Biological Chemistry*, *264*(12), 6996–6999. https://doi.org/10.1016/s0021-9258(18)83530-x

Cook, N. J., Zeilinger, C., Koch, K. W., & Kaupp, U. B. (1986). Solubilization and functional reconstitution of the cGMP-dependent cation channel from bovine rod outer segments. *Journal of Biological Chemistry*, *261*(36), 17033–17039. https://doi.org/10.1016/s0021-9258(19)75995-x

Corin, K., & Bowie, J. U. (2020). How bilayer properties influence membrane protein folding. In *Protein Science* (Vol. 29, Issue 12, pp. 2348–2362). Blackwell Publishing Ltd. https://doi.org/10.1002/pro.3973

Cox, J., Hein, M. Y., Luber, C. A., Paron, I., Nagaraj, N., & Mann, M. (2014). Accurate proteome-wide label-free quantification by delayed normalization and maximal peptide ratio extraction, termed MaxLFQ. *Molecular and Cellular Proteomics*, *13*(9), 2513–2526. https://doi.org/10.1074/mcp.M113.031591

Cox, J., & Mann, M. (2008). MaxQuant enables high peptide identification rates, individualized p.p.b.-range mass accuracies and proteome-wide protein quantification. *Nature Biotechnology*. https://doi.org/10.1038/nbt.1511

Creamer, T. P. (2020). Calcineurin. *Cell Communication and Signaling*, *18*(1). https://doi.org/10.1186/s12964-020-00636-4

Crowther, R. A., Amos, L. A., Finch, J. T., De Rosier, D. J., & Klug, A. (1970). Three Dimensional Reconstructions of Spherical Viruses by Fourier Synthesis from Electron Micrographs. *Nature*, *226*(5244), 421–425. https://doi.org/10.1038/226421a0

Dang, S., van Goor, M. K., Wang, Y., Julius, D., Cheng, Y., & van der Wijst, J. (2018). Structural insight into TRPV5 channel function and modulation. *BioRxiv*, 434902. http://biorxiv.org/lookup/doi/10.1101/434902

De Rosier, D. J., & Klug, A. (1968). Reconstruction of three dimensional structures from electron micrographs. *Nature*, *217*(5124), 130–134. https://doi.org/10.1038/217130a0

DePristo, M. A., De Bakker, P. I. W., & Blundell, T. L. (2004). Heterogeneity and inaccuracy in protein structures solved by X-ray crystallography. *Structure*, *12*(5), 831–838. https://doi.org/10.1016/j.str.2004.02.031

Ding, X. Q., Matveev, A., Singh, A., Komori, N., & Matsumoto, H. (2014). Exploration of cone cyclic nucleotide-gated channel-interacting proteins using affinity purification and mass spectrometry. *Advances in Experimental Medicine and Biology*, *801*, 57–65. https://doi.org/10.1007/978-1-4614-3209-8_8

Dörr, J. M., Koorengevel, M. C., Schäfer, M., Prokofyev, A. V, Scheidelaar, S., van der Cruijsen, E. A. W., Dafforn, T. R., Baldus, M., & Killian, J. A. (2014). Detergent-free isolation, characterization, and functional reconstitution of a tetrameric K+ channel: The power of native nanodiscs. *Proceedings of the National Academy of Sciences*, *111*(52), 18607–18612. http://www.pnas.org/lookup/doi/10.1073/pnas.1416205112

Doudna, J. A., & Charpentier, E. (2014). The new frontier of genome engineering with CRISPR-Cas9. In *Science* (Vol. 346, Issue 6213). American Association for the Advancement of Science. https://doi.org/10.1126/science.1258096

Doyle, D. A., Cabral, J. M., Pfuetzner, R. A., Kuo, A., Gulbis, J. M., Cohen, S. L., Chait, B. T., & MacKinnon, R. (1998). The structure of the potassium channel: Molecular basis of K+ conduction and selectivity. *Science*, *280*(5360), 69–77. https://doi.org/10.1126/science.280.5360.69

Dryja, T. P., Finn, J. T., Peng, Y. W., Mcgee, T. L., Berson, E. L., & Yau, K. W. (1995). Mutations in the gene encoding the α subunit of the rod cGMP-gated channel in autosomal recessive retinitis pigmentosa. *Proceedings of the National Academy of Sciences of the United States of America*, *92*(22), 10177–10181. https://doi.org/10.1073/pnas.92.22.10177

Dubochet, J., & McDowall, A. W. (1981). Vitrification of pure water for electron microscopy. *Journal of Microscopy*. https://doi.org/10.1111/j.1365-2818.1981.tb02483.x

Dubochet, Jacques, Adrian, M., Chang, J.-J., Homo, J.-C., Lepault, J., McDowall, A. W., & Schultz, P. (1988). Cryo-electron microscopy of vitrified specimens. *Quarterly Reviews of Biophysics*, *21*(2), 129–228. https://doi.org/10.1017/S0033583500004297

Dunham, W. H., Mullin, M., & Gingras, A. C. (2012). Affinity-purification coupled to mass spectrometry: Basic principles and strategies. *Proteomics*, *12*(10), 1576–1590. https://doi.org/10.1002/pmic.201100523

Duquesne, K., Prima, V., & Sturgis, J. N. (2016). Heterologous Expression of Membrane Proteins. In I. Mus-Veteau (Ed.), *Methods in Molecular Biology* (2nd ed., Vol. 1432). Springer New York. https://doi.org/10.1007/978-1-4939-3637-3

Dyballa, N., & Metzger, S. (2009). Fast and Sensitive Colloidal Coomassie G-250 Staining for Proteins in Polyacrylamide Gels. *Journal of Visualized Experiments*, *30*, e1431. https://www.jove.com/video/1431/fast-sensitive-colloidal-coomassie-g-250-staining-for-proteins

Eguchi, Y., Makanae, K., Hasunuma, T., Ishibashi, Y., Kito, K., & Moriya, H. (2018). Estimating the protein burden limit of yeast cells by measuring the expression limits of glycolytic proteins. *ELife*, *7*. https://doi.org/10.7554/eLife.34595

Emmott, E., Jovanovic, M., & Slavov, N. (2019). Ribosome Stoichiometry: From Form to Function. In *Trends in Biochemical Sciences* (Vol. 44, Issue 2, pp. 95–109). Elsevier Ltd. https://doi.org/10.1016/j.tibs.2018.10.009

References

Endo, Y., & Sawasaki, T. (2006). Cell-free expression systems for eukaryotic protein production. In *Current Opinion in Biotechnology* (Vol. 17, Issue 4, pp. 373–380). Curr Opin Biotechnol. https://doi.org/10.1016/j.copbio.2006.06.009

Ersson, B., Rydén, L., & Janson, J. C. (2011). Introduction to Protein Purification. In *Protein Purification: Principles, High Resolution Methods, and Applications: Third Edition* (pp. 1–22). Wiley Blackwell. https://doi.org/10.1002/9780470939932.ch1

Fabre, L., Bao, H., Innes, J., Duong, F., & Rouiller, I. (2017). Negative stain single-particle em of the maltose transporter in nanodiscs reveals asymmetric closure of MalK2 and catalytic roles of ATP, MalE, and maltose. *Journal of Biological Chemistry*, *292*(13), 5457–5464. https://doi.org/10.1074/jbc.M116.757898

Fenn, J. B., Mann, M., Meng, C. K., Wong, S. F., & Whitehouse, C. M. (1989). Electrospray ionization for mass spectrometry of large biomolecules. In *Science*. https://doi.org/10.1126/science.2675315

Fenyö, D., & Beavis, R. C. (2003). A method for assessing the statistical significance of mass spectrometry-based protein identifications using general scoring schemes. *Analytical Chemistry*, *75*(4), 768–774. https://doi.org/10.1021/ac0258709

Fesenko, E. E., Kolesnikov, S. S., & Lyubarsky, A. L. (1985). Induction by cyclic GMP of cationic conductance in plasma membrane of retinal rod outer segment. *Nature*. https://doi.org/10.1038/313310a0

Franken, H., Mathieson, T., Childs, D., Sweetman, G. M. A., Werner, T., Tögel, I., Doce, C., Gade, S., Bantscheff, M., Drewes, G., Reinhard, F. B. M., Huber, W., & Savitski, M. M. (2015). Thermal proteome profiling for unbiased identification of direct and indirect drug targets using multiplexed quantitative mass spectrometry. *Nature Protocols*. https://doi.org/10.1038/nprot.2015.101

Frauenfeld, J., Löving, R., Armache, J.-P., Sonnen, A. F.-P., Guettou, F., Moberg, P., Zhu, L., Jegerschöld, C., Flayhan, A., Briggs, J. A. G., Garoff, H., Löw, C., Cheng, Y., & Nordlund, P. (2016). A saposin-lipoprotein nanoparticle system for membrane proteins. *Nature Methods*, *13*(4), 345–351. https://www.nature.com/articles/nmeth.3801

Frauenfelder, H., Sligar, S. G., & Wolynes, P. G. (1991). The energy landscapes and motions of proteins. *Science*, *254*(5038), 1598–1603. https://doi.org/10.1126/science.1749933

Gao, Y., Cao, E., Julius, D., & Cheng, Y. (2016). TRPV1 structures in nanodiscs reveal mechanisms of ligand and lipid action. *Nature*, *534*(7607), 347–351. http://www.nature.com/doifinder/10.1038/nature17964

Gasteiger, E., Hoogland, C., Gattiker, A., Duvaud, S., Wilkins, M. R., Appel, R. D., & Bairoch, A. (2005). Protein Identification and Analysis Tools on the ExPASy Server. In *The Proteomics Protocols Handbook*. https://doi.org/10.1385/1-59259-890-0:571

Giblin, J. P., Comes, N., Strauss, O., & Gasull, X. (2016). Ion Channels in the Eye: Involvement in Ocular Pathologies. In *Advances in Protein Chemistry and Structural Biology* (Vol. 104, pp. 157–231). Academic Press Inc. https://doi.org/10.1016/bs.apcsb.2015.11.006

Gileadi, O. (2017). Recombinant protein expression in E. coli : A historical perspective. In *Methods in Molecular Biology* (Vol. 1586, pp. 3–10). Humana Press Inc. https://doi.org/10.1007/978-1-4939-6887-9_1

Gingras, A. C., Gstaiger, M., Raught, B., & Aebersold, R. (2007). Analysis of protein complexes using mass spectrometry. In *Nature Reviews Molecular Cell Biology* (Vol. 8, Issue 8, pp. 645–654). Nature Publishing Group. https://doi.org/10.1038/nrm2208

Glaeser, R. M. (2013). Invited Review Article: Methods for imaging weak-phase objects in electron microscopy. *Review of Scientific Instruments*, *84*(11). https://doi.org/10.1063/1.4830355

Glish, G. L., & Vachet, R. W. (2003). The basics of mass spectrometry in the twenty-first century. In *Nature Reviews Drug Discovery*. https://doi.org/10.1038/nrd1011

Gold, L. (1990). Expression of heterologous proteins in Escherichia coli. In *Methods in Enzymology* (Vol. 185, pp. 11–14). Academic Press. https://doi.org/10.1016/0076-6879(90)85004-8

Gordon, S. E., Brautigan, D. L., & Zimmerman, A. L. (1992). Protein phosphatases modulate the apparent agonist affinity of the light-regulated ion channel in retinal rods. *Neuron*, *9*(4), 739–748. https://doi.org/10.1016/0896-6273(92)90036-D

Gräslund, S., Nordlund, P., Weigelt, J., Hallberg, B. M., Bray, J., Gileadi, O., Knapp, S., Oppermann, U., Arrowsmith, C., Hui, R., Ming, J., Dhe-Paganon, S., Park, H. W., Savchenko, A., Yee, A., Edwards, A., Vincentelli, R., Cambillau, C., Kim, R., … Gunsalus, K. C. (2008). Protein production and purification. *Nature Methods*, *5*(2), 135–146. https://doi.org/10.1038/nmeth.f.202

Graveley, B. R. (2001). Alternative splicing: Increasing diversity in the proteomic world. In *Trends in Genetics* (Vol. 17, Issue 2, pp. 100–107). Elsevier Current Trends. https://doi.org/10.1016/S0168-9525(00)02176-4

Griffiths, J. (2008). A brief history of mass spectrometry. In *Analytical Chemistry*. https://doi.org/10.1021/ac8013065

Grunwald, M. E., Yu, W. P., Yu, H. H., & Yau, K. W. (1998). Identification of a domain on the β-subunit of the rod cGMP-gated cation channel that mediates inhibition by calcium-calmodulin. *Journal of Biological Chemistry*, *273*(15), 9148–9157. https://doi.org/10.1074/jbc.273.15.9148

Gua, V. K., Rajala, A., & Rajala, R. V. S. (2012). Insulin receptor regulates photoreceptor CNG channel activity. *American Journal of Physiology - Endocrinology and Metabolism*, *303*(11), E1363. https://doi.org/10.1152/ajpendo.00199.2012

Gupta, V. K., Rajala, A., Daly, R. J., & Rajala, R. V. S. (2010). Growth factor receptor-bound protein 14: A new modulator of photoreceptor-specific cyclic-nucleotide-gated channel. *EMBO Reports*, *11*(11), 861–867. https://doi.org/10.1038/embor.2010.142

Haag, A. M. (2016). Mass analyzers and mass spectrometers. In *Advances in Experimental Medicine and Biology* (Vol. 919, pp. 157–169). Springer New York LLC. https://doi.org/10.1007/978-3-319-41448-5_7

Hackos, D. H., & Korenbrot, J. I. (1999). Divalent cation selectivity is a function of gating in native and recombinant cyclic nucleotide-gated ion channels from retinal photoreceptors. *Journal of General Physiology*, *113*(6), 799–817. https://doi.org/10.1085/jgp.113.6.799

Hamdi, F., Tüting, C., Semchonok, D. A., Visscher, K. M., Kyrilis, F. L., Meister, A., Skalidis, I., Schmidt, L., Parthier, C., Stubbs, M. T., & Kastritis, P. L. (2020). 2.7 Å cryo-EM structure of vitrified M. Musculus H-chain apoferritin from a compact 200 keV cryo-microscope. *PLoS ONE*, *15*(5), 1–18. https://doi.org/10.1371/journal.pone.0232540

Hamilton, S. R., Bobrowicz, P., Bobrowicz, B., Davidson, R. C., Li, H., Mitchell, T., Nett, J. H., Rausch, S., Stadheim, T. A., Wischnewski, H., Wildt, S., & Gerngross, T. U. (2003). Production of complex human glycoproteins in yeast. *Science*, *301*(5637), 1244–1246. https://doi.org/10.1126/science.1088166

Han, B., Tokay, T., Zhang, G., Sun, P., & Hou, S. (2017). Eag1 K+ Channel: Endogenous Regulation and Functions in Nervous System. In *Oxidative Medicine and Cellular Longevity* (Vol. 2017). Hindawi Limited. https://doi.org/10.1155/2017/7371010

Han, D. K., Eng, J., Zhou, H., & Aebersold, R. (2001). Quantitative profiling of differentiation-induced microsomal proteins using isotope-coded affinity tags and mass spectrometry. *Nature Biotechnology*, *19*(10), 946–951. https://doi.org/10.1038/nbt1001-946

Hartong, D. T., Berson, E. L., & Dryja, T. P. (2006). Retinitis pigmentosa. In *Lancet* (Vol. 368, Issue 9549, pp. 1795–1809). Elsevier B.V. https://doi.org/10.1016/S0140-6736(06)69740-7

Haslbeck, M., Schuster, I., & Grallert, H. (2003). GroE-dependent expression and purification of pig heart mitochondrial citrate synthase in Escherichia coli. *Journal of Chromatography B: Analytical Technologies in the Biomedical and Life Sciences*, *786*(1–2), 127–136. https://doi.org/10.1016/S1570-0232(02)00716-X

Haurowitz, F. (1979). Protein Heterogeneity: Its History, Its Bases, and Its Limits. *Annals of the New York Academy of Sciences*, *325*(1 The Origins o), 37–52. https://doi.org/10.1111/j.1749-6632.1979.tb14127.x

References

Hayat, M. A. (1986). Glutaraldehyde: Role in electron microscopy. *Micron And Microscopica Acta*. https://doi.org/10.1016/0739-6260(86)90042-0

Haynes, L. W., Kay, A. R., & Yau, K. W. (1986). Single cyclic GMP-activated channel activity in excised patches of rod outer segment membrane. *Nature*. https://doi.org/10.1038/321066a0

Heginbotham, L., Lu, Z., Abramson, T., & MacKinnon, R. (1994). Mutations in the K+ channel signature sequence. *Biophysical Journal*, *66*(4), 1061–1067. https://doi.org/10.1016/S0006-3495(94)80887-2

Heginbotham, Lise, Abramson, T., & MacKinnon, R. (1992). A functional connection between the pores of distantly related ion channels as revealed by mutant K+ channels. *Science*, *258*(5085), 1152–1155. https://doi.org/10.1126/science.1279807

Hellman, U., Wernstedt, C., Góñez, J., & Heldin, C. H. (1995). Improvement of an “in-gel” digestion procedure for the micropreparation of internal protein fragments for amino acid sequencing. *Analytical Biochemistry*. https://doi.org/10.1006/abio.1995.1070

Henderson, R., Chen, S., Chen, J. Z., Grigorieff, N., Passmore, L. A., Ciccarelli, L., Rubinstein, J. L., Crowther, R. A., Stewart, P. L., & Rosenthal, P. B. (2011). Tilt-pair analysis of images from a range of different specimens in single-particle electron cryomicroscopy. *Journal of Molecular Biology*, *413*(5), 1028–1046. https://doi.org/10.1016/j.jmb.2011.09.008

Henzel, W. J., Billeci, T. M., Stults, J. T., Wong, S. C., Grimley, C., & Watanabe, C. (1993). Identifying proteins from two-dimensional gels by molecular mass searching of peptide fragments in protein sequence databases. *Proceedings of the National Academy of Sciences of the United States of America*. https://doi.org/10.1073/pnas.90.11.5011

Higgins, M. K., Weitz, D., Warne, T., Schertler, G. F. X., & Kaupp, U. B. (2002). Molecular architecture of a retinal cGMP-gated channel: the arrangement of the cytoplasmic domains. *The EMBO Journal*, *21*(9), 2087–2094. http://emboj.embopress.org/cgi/doi/10.1093/emboj/21.9.2087

Hitchman, R. B., Possee, R. D., & King, L. A. (2011). Protein Expression in Insect Cells. In *Comprehensive Biotechnology, Second Edition* (Vol. 1, pp. 323–340). Elsevier Inc. https://doi.org/10.1016/B978-0-08-088504-9.00037-4

Hite, R. K., Yuan, P., Li, Z., Hsuing, Y., Walz, T., & MacKinnon, R. (2015). Cryo-electron microscopy structure of the Slo2.2 Na+-activated K+ channel. *Nature*, *527*(7577), 198–203. https://doi.org/10.1038/nature14958

Hollywood, K., Brison, D. R., & Goodacre, R. (2006). Metabolomics: Current technologies and future trends. In *Proteomics* (Vol. 6, Issue 17, pp. 4716–4723). John Wiley & Sons, Ltd. https://doi.org/10.1002/pmic.200600106

Houtman, J. C. D., Barda-Saad, M., & Samelson, L. E. (2005). Examining multiprotein signaling complexes from all angles: The use of complementary techniques to characterize complex formation at the adapter protein, linker for activation of T cells. *FEBS Journal*, *272*(21), 5426–5435. https://doi.org/10.1111/j.1742-4658.2005.04972.x

Hovmöller, S., Zhou, T., & Ohlson, T. (2002). Conformations of amino acids in proteins. *Acta Crystallographica Section D: Biological Crystallography*, *58*(5), 768–776. https://doi.org/10.1107/S0907444902003359

Hsu, Y. T., & Molday, R. S. (1994). Interaction of calmodulin with the cyclic GMP-gated channel of rod photoreceptor cells. Modulation of activity, affinity purification, and localization. *Journal of Biological Chemistry*, *269*(47), 29765–29770. http://www.jbc.org/content/269/47/29765.abstract

Hughes, C. S., Foehr, S., Garfield, D. A., Furlong, E. E., Steinmetz, L. M., & Krijgsveld, J. (2014). Ultrasensitive proteome analysis using paramagnetic bead technology. *Molecular Systems Biology*. https://doi.org/10.15252/msb.20145625

Hunter, M., Yuan, P., Vavilala, D., & Fox, M. (2019). Optimization of Protein Expression in Mammalian Cells. *Current Protocols in Protein Science*, *95*(1). https://doi.org/10.1002/cpps.77

Hurwitz, R., & Holcombe, V. (1991). Affinity purification of the photoreceptor cGMP-gated cation channel. *Journal of Biological Chemistry*, *266*(13), 7975–7977. http://www.jbc.org/content/266/13/7975.abstract

Hüttl, S., Michalakis, S., Seeliger, M., Luo, D. G., Acar, N., Geiger, H., Hudl, K., Mader, R., Haverkamp, S., Moser, M., Pfeifer, A., Gerstner, A., Yau, K. W., & Biel, M. (2005). Impaired channel targeting and retinal degeneration in mice lacking the cyclic nucleotide-gated channel subunit CNGB1. *Journal of Neuroscience*, *25*(1), 130–138. https://doi.org/10.1523/JNEUROSCI.3764-04.2005

Huttlin, E. L., Bruckner, R. J., Paulo, J. A., Cannon, J. R., Ting, L., Baltier, K., Colby, G., Gebreab, F., Gygi, M. P., Parzen, H., Szpyt, J., Tam, S., Zarraga, G., Pontano-Vaites, L., Swarup, S., White, A. E., Schweppe, D. K., Rad, R., Erickson, B. K., … Wade Harper, J. (2017). Architecture of the human interactome defines protein communities and disease networks. *Nature*, *545*(7655), 505–509. https://doi.org/10.1038/nature22366

Iost, I., Guillerez, J., & Dreyfus, M. (1992). Bacteriophage T7 RNA polymerase travels far ahead of ribosomes in vivo. *Journal of Bacteriology*, *174*(2), 619–622. https://doi.org/10.1128/jb.174.2.619-622.1992

Irwin, M. J., Gupta, R., Gao, X. Z., Cahill, K. B., Chu, F., & Cote, R. H. (2019). The molecular architecture of photoreceptor phosphodiesterase 6 (PDE6) with activated G protein elucidates the mechanism of visual excitation. *Journal of Biological Chemistry*, *294*(51), 19486–19497. https://doi.org/10.1074/jbc.RA119.011002

James, Z. M., Borst, A. J., Haitin, Y., Frenz, B., DiMaio, F., Zagotta, W. N., & Veesler, D. (2017). CryoEM structure of a prokaryotic cyclic nucleotide-gated ion channel. *Proceedings of the National Academy of Sciences of the United States of America*, *114*(17), 4430–4435. https://doi.org/10.1073/pnas.1700248114

Jensen, O. N. (2004). Modification-specific proteomics: Characterization of post-translational modifications by mass spectrometry. In *Current Opinion in Chemical Biology* (Vol. 8, Issue 1, pp. 33–41). Elsevier Ltd. https://doi.org/10.1016/j.cbpa.2003.12.009

Jewett, M. C., & Swartz, J. R. (2004). Mimicking the Escherichia coli Cytoplasmic Environment Activates Long-Lived and Efficient Cell-Free Protein Synthesis. *Biotechnology and Bioengineering*, *86*(1), 19–26. https://doi.org/10.1002/bit.20026

Jeyasankar, G. (2019). *Stable reconstitution of an endogenous ion channel for structural studies*. Rheinischen Friedrich-Wilhelms-Universität Bonn.

Kallberg, K., Johansson, H. O., & Bulow, L. (2012). Multimodal chromatography: An efficient tool in downstream processing of proteins. In *Biotechnology Journal* (Vol. 7, Issue 12, pp. 1485–1495). Biotechnol J. https://doi.org/10.1002/biot.201200074

Kang, D., Gho, Y. S., Suh, M., & Kang, C. (2002). Highly sensitive and fast protein detection with Coomassie brilliant blue in sodium dodecyl sulfate-polyacrylamide gel electrophoresis [5]. *Bulletin of the Korean Chemical Society*, *23*(11), 1511–1512. https://doi.org/10.5012/bkcs.2002.23.11.1511

Kang, E., Park, J. W., McClellan, S. J., Kim, J. M., Holland, D. P., Lee, G. U., Franses, E. I., Park, K., & Thompson, D. H. (2007). Specific adsorption of histidine-tagged proteins on silica surfaces modified with Ni2+/NTA-derivatized poly(ethylene glycol). *Langmuir*, *23*(11), 6281–6288. https://doi.org/10.1021/la063719e

Kang, K. J., Bauer, P. J., Kinjo, T. G., Szerencsei, R. T., Bönigk, W., Winkfein, R. J., & Schnetkamp, P. P. M. (2003). Assembly of retinal rod or cone Na+/Ca2+-K+ exchanger oligomers with cGMP-gated channel subunits as probed with heterologously expressed cDNAs. *Biochemistry*, *42*(15), 4593–4600. https://doi.org/10.1021/bi027276z

Kaniyappan, S., Tepper, K., Biernat, J., Chandupatla, R. R., Hübschmann, S., Irsen, S., Bicher, S., Klatt, C., Mandelkow, E. M., & Mandelkow, E. (2020). FRET-based Tau seeding assay does not represent prion-like templated assembly of Tau filaments. *Molecular Neurodegeneration*, *15*(1), 39. https://doi.org/10.1186/s13024-020-00389-1

Karas, M., Bachmann, D., & Hillenkamp, F. (1985). Influence of the Wavelength in High-Irradiance Ultraviolet Laser Desorption Mass Spectrometry of Organic Molecules. *Analytical Chemistry*. https://doi.org/10.1021/ac00291a042

Karas, M., & Hillenkamp, F. (1988). Laser Desorption Ionization of Proteins with Molecular Masses Exceeding 10 000 Daltons. In *Analytical Chemistry* (Vol. 60, Issue 20, pp. 2299–2301). Anal Chem. https://doi.org/10.1021/ac00171a028

References

Katagiri, S., Akahori, M., Sergeev, Y., Yoshitake, K., Ikeo, K., Furuno, M., Hayashi, T., Kondo, M., Ueno, S., Tsunoda, K., Shinoda, K., Kuniyoshi, K., Tsurusaki, Y., Matsumoto, N., Tsuneoka, H., & Iwata, T. (2014). Whole exorne analysis identifies frequent CNGA 1 mutations in japanese population with autosomal recessive retinitis pigmentosa. *PLoS ONE*, *9*(9). https://doi.org/10.1371/journal.pone.0108721

Kaufmann, W. (1906). Über die Konstitution des Elektrons. *Annalen Der Physik*. https://doi.org/10.1002/andp.19063240303

Kaupp, U. B., Niidome, T., Tanabe, T., Terada, S., Bönigk, W., Stühmer, W., Cook, N. J., Kangawa, K., Matsuo, H., Hirose, T., Miyata, T., & Numa, S. (1989a). Primary structure and functional expression from complementary DNA of the rod photoreceptor cyclic GMP-gated channel. *Nature*, *342*(6251), 762–766. https://doi.org/10.1038/342762a0

Kaupp, U. B., Niidome, T., Tanabe, T., Terada, S., Bönigk, W., Stühmer, W., Cook, N. J., Kangawa, K., Matsuo, H., Hirose, T., Miyata, T., & Numa, S. (1989b). Primary structure and functional expression from complementary DNA of the rod photoreceptor cyclic GMP-gated channel. *Nature*. https://doi.org/10.1038/342762a0

Kaupp, U. B., & Seifert, R. (2002). Cyclic Nucleotide-Gated Ion Channels. *Physiological Reviews*, *82*(3), 769–824. https://doi.org/10.1152/physrev.00008.2002

Kharche, S. A., & Sengupta, D. (2020). Dynamic protein interfaces and conformational landscapes of membrane protein complexes. *Current Opinion in Structural Biology*, *61*, 191–197. https://doi.org/10.1016/j.sbi.2020.01.001

Khoury, G. A., Baliban, R. C., & Floudas, C. A. (2011). Proteome-wide post-translational modification statistics: frequency analysis and curation of the swiss-prot database. *Scientific Reports*, *1*(1), 90. https://doi.org/10.1038/srep00090

Knowles, T. J., Finka, R., Smith, C., Lin, Y.-P., Dafforn, T., & Overduin, M. (2009). Membrane Proteins Solubilized Intact in Lipid Containing Nanoparticles Bounded by Styrene Maleic Acid Copolymer. *Journal of the American Chemical Society*, *131*(22), 7484–7485. https://pubs.acs.org/doi/10.1021/ja810046q

Kobayashi, M., Takamatsu, K., Fujishiro, M., Saitoh, S., & Noguchi, T. (1994). Molecular cloning of a novel calcium-binding protein structurally related to hippocalcin from human brain and chromosomal mapping of its gene. *BBA - Molecular Cell Research*, *1222*(3), 515–518. https://doi.org/10.1016/0167-4889(94)90062-0

Komatsu, H., Mori, I., Rhee, J. S., Akaike, N., & Ohshima, Y. (1996). Mutations in a cyclic nucleotide-gated channel lead to abnormal thermosensation and chemosensation in C. elegans. *Neuron*, *17*(4), 707–718. https://doi.org/10.1016/S0896-6273(00)80202-0

Komolov, K. E., Senin, I. I., Kovaleva, N. A., Christoph, M. P., Churumova, V. A., Grigoriev, I. I., Akhtar, M., Philippov, P. P., & Koch, K. W. (2009). Mechanism of rhodopsin kinase regulation by recoverin. *Journal of Neurochemistry*, *110*(1), 72–79. https://doi.org/10.1111/j.1471-4159.2009.06118.x

Körschen, H. G., Beyermann, M., Müller, F., Heck, M., Vantler, M., Koch, K. W., Kellner, R., Wolfrum, U., Bode, C., Hofmann, K. P., & Kaupp, U. B. (1999). Interaction of glutamic-acid-rich proteins with the cGMP signalling pathway in rod photoreceptors. *Nature*, *400*(6746), 761–766. https://doi.org/10.1038/23468

Körschen, H. G., Illing, M., Seifert, R., Sesti, F., Williams, A., Gotzes, S., Colville, C., Muller, F., Dose, A., Godde, M., Molday, L., Kaupp, U. B., & Molday, R. S. (1995). A 240 kDa protein represents the complete β subunit of the cyclic nucleotide-gated channel from rod photoreceptor. *Neuron*, *15*(3), 627–636. https://doi.org/10.1016/0896-6273(95)90151-5

Koster, A. J., Grimm, R., Typke, D., Hegerl, R., Stoschek, A., Walz, J., & Baumeister, W. (1997). Perspectives of molecular and cellular electron tomography. *Journal of Structural Biology*, *120*(3), 276–308. https://doi.org/10.1006/jsbi.1997.3933

Kowal, J., Biyani, N., Chami, M., Scherer, S., Rzepiela, A. J., Baumgartner, P., Upadhyay, V., Nimigean, C. M., & Stahlberg, H. (2018). High-Resolution Cryoelectron Microscopy Structure of the Cyclic Nucleotide-Modulated Potassium Channel MloK1 in a Lipid Bilayer. *Structure*, *26*(1), 20-27.e3. https://doi.org/10.1016/j.str.2017.11.012

Krajewski, J. L., Luetje, C. W., & Kramer, R. H. (2003). Tyrosine Phosphorylation of Rod Cyclic Nucleotide-Gated Channels Switches Off Ca2+/Calmodulin Inhibition. *Journal of Neuroscience*, *23*(31), 10100–10106. http://www.jneurosci.org/lookup/doi/10.1523/JNEUROSCI.23-31-10100.2003

Krishnan, A., Duda, T., Pertzev, A., Kobayashi, M., Takamatsu, K., & Sharma, R. K. (2009). Hippocalcin, new Ca2+ sensor of a ROS-GC subfamily member, ONE-GC, membrane guanylate cyclase transduction system. *Molecular and Cellular Biochemistry*, *325*(1–2), 1–14. https://doi.org/10.1007/s11010-008-0015-z

Kuhlbrandt, W. (2014). The Resolution Revolution. *Science*, *343*(6178), 1443–1444. http://www.sciencemag.org/cgi/doi/10.1126/science.1251652

Kuhlman, B., & Bradley, P. (2019). Advances in protein structure prediction and design. *Nature Reviews Molecular Cell Biology*, *20*(11), 681–697. https://doi.org/10.1038/s41580-019-0163-x

Kwan, T. O. C., Axford, D., & Moraes, I. (2020). Membrane protein crystallography in the era of modern structural biology. In *Biochemical Society Transactions*. https://doi.org/10.1042/BST20200066

Kwok, M. C. M., Holopainen, J. M., Molday, L. L., Fosteer, L. J., & Molday, R. S. (2008). Proteomics of photoreceptor outer segments identifies a subset of SNARE and rab proteins implicated in membrane vesicle trafficking and fusion. *Molecular and Cellular Proteomics*, *7*(6), 1053–1066. https://doi.org/10.1074/mcp.M700571-MCP200

Labrou, N. E. (2014). Protein purifi cation: An overview. *Methods in Molecular Biology*, *1129*, 3–10. https://doi.org/10.1007/978-1-62703-977-2_1

Ladner, C. L., Yang, J., Turner, R. J., & Edwards, R. A. (2004). Visible fluorescent detection of proteins in polyacrylamide gels without staining. *Analytical Biochemistry*, *326*(1), 13–20. http://linkinghub.elsevier.com/retrieve/pii/S0003269703008017

Laemmli, U. K. (1970). Cleavage of structural proteins during the assembly of the head of bacteriophage T4. *Nature*. https://doi.org/10.1038/227680a0

Lee, C. H., & MacKinnon, R. (2017). Structures of the Human HCN1 Hyperpolarization-Activated Channel. *Cell*, *168*(1–2), 111-120.e11. https://doi.org/10.1016/j.cell.2016.12.023

Lee, P., & Hruby, D. E. (1997). Detection of recombinant protein based on reporter enzyme activity: chloramphenicol acetyltransferase. *Methods in Molecular Biology (Clifton, N.J.)*, *63*, 31–40. https://doi.org/10.1385/0-89603-481-x:31

Lee, S., Shuman, J. D., Guszczynski, T., Sakchaisri, K., Sebastian, T., Copeland, T. D., Miller, M., Cohen, M. S., Taunton, J., Smart, R. C., Xiao, Z., Yu, L.-R., Veenstra, T. D., & Johnson, P. F. (2010). RSK-Mediated Phosphorylation in the C/EBPβ Leucine Zipper Regulates DNA Binding, Dimerization, and Growth Arrest Activity. *Molecular and Cellular Biology*, *30*(11), 2621–2635. https://doi.org/10.1128/mcb.00782-09

Leitner, A., Faini, M., Stengel, F., & Aebersold, R. (2016). Crosslinking and Mass Spectrometry: An Integrated Technology to Understand the Structure and Function of Molecular Machines. *Trends in Biochemical Sciences*, *41*(1), 20–32. https://doi.org/10.1016/j.tibs.2015.10.008

Li, M., Zhou, X., Wang, S., Michailidis, I., Gong, Y., Su, D., Li, H., Li, X., & Yang, J. (2017). *Structure of a eukaryotic cyclic-nucleotide-gated channel*. 1–20. papers3://publication/doi/10.1038/nature20819

Liao, M., Cao, E., Julius, D., & Cheng, Y. (2013). Structure of the TRPV1 ion channel determined by electron cryo-microscopy. *Nature Publishing Group*, *504*(7478), 107–112. https://www.nature.com/articles/nature12822

Liu, Y., Huynh, D. T., & Yeates, T. O. (2019). A 3.8 Å resolution cryo-EM structure of a small protein bound to an imaging scaffold. *Nature Communications*, *10*(1), 1–7. https://doi.org/10.1038/s41467-019-09836-0

Lodish, H., Berk, A., Zipursky, S. L., Matsudaira, P., Baltimore, D., & Darnell, J. (2000). *Overview of the Secretory Pathway*. https://www.ncbi.nlm.nih.gov/books/NBK21471/

Lowe, R., Shirley, N., Bleackley, M., Dolan, S., & Shafee, T. (2017). Transcriptomics technologies. *PLoS Computational Biology*. https://doi.org/10.1371/journal.pcbi.1005457

Lucy, C. A. (2003). Evolution of ion-exchange: From Moses to the Manhattan Project to Modern Times. In *Journal of Chromatography A* (Vol. 1000, Issues 1–2, pp. 711–724). Elsevier. https://doi.org/10.1016/S0021-9673(03)00528-4

Ludwig Reimer, & Helmut Kohl. (2008). *Transmission Electron Microscopy: Vol. Springer Series in …* (5th ed.). Springer New York. https://doi.org/10.1007/978-0-387-40093-8

Lundstrom, K. (2004). Structural genomics on membrane proteins: The MePNet approach. In *Current Opinion in Drug Discovery and Development*.

Luo, D. G., Su, C. Y., & Yau, K. W. (2009). Photoreceptors: Physiology. *Encyclopedia of Neuroscience*, 677–686. https://doi.org/10.1016/B978-008045046-9.00913-X

Maity, S., Mazzolini, M., Arcangeletti, M., Valbuena, A., Fabris, P., Lazzarino, M., & Torre, V. (2015). Conformational rearrangements in the transmembrane domain of CNGA1 channels revealed by single-molecule force spectroscopy. *Nature Communications*, *6*. https://doi.org/10.1038/ncomms8093

Makarov, A. (2000). Electrostatic axially harmonic orbital trapping: A high-performance technique of mass analysis. *Analytical Chemistry*, *72*(6), 1156–1162. https://doi.org/10.1021/ac991131p

Manghwar, H., Lindsey, K., Zhang, X., & Jin, S. (2019). CRISPR/Cas System: Recent Advances and Future Prospects for Genome Editing. In *Trends in Plant Science* (Vol. 24, Issue 12, pp. 1102–1125). Elsevier Ltd. https://doi.org/10.1016/j.tplants.2019.09.006

Mann, M., Højrup, P., & Roepstorff, P. (1993). Use of mass spectrometric molecular weight information to identify proteins in sequence databases. *Biological Mass Spectrometry*. https://doi.org/10.1002/bms.1200220605

Martens, L. (2011). Bioinformatics challenges in mass spectrometry-driven proteomics. In *Methods in Molecular Biology* (Vol. 753, pp. 359–371). https://doi.org/10.1007/978-1-61779-148-2_24

Mastronarde, D. N. (2005). Automated electron microscope tomography using robust prediction of specimen movements. *Journal of Structural Biology*. https://doi.org/10.1016/j.jsb.2005.07.007

Matos, M. J. B., Trovão, F., Gonçalves, J., Rothbauer, U., Freire, M. G., Barbosa, A. M. J. B., Pina, A. S., & Roque, A. C. A. (2021). A purification platform for antibodies and derived fragments using a de novo designed affinity adsorbent. *Separation and Purification Technology*, *265*, 118476. https://doi.org/10.1016/j.seppur.2021.118476

Matthiesen, R. (Ed.). (2020). *Mass Spectrometry Data Analysis in Proteomics* (Vol. 2051). Springer New York. https://doi.org/10.1007/978-1-4939-9744-2

Matulef, K., & Zagotta, W. N. (2003). Cyclic Nucleotide-Gated Ion Channels. *Annual Review of Cell and Developmental Biology*, *19*, 23–44. https://doi.org/10.1146/annurev.cellbio.19.110701.154854

McNaught, A. D., & Wilkinson, A. (2019). The IUPAC Compendium of Chemical Terminology (the “Gold Book”). In *The IUPAC Compendium of Chemical Terminology* (2nd Editio). International Union of Pure and Applied Chemistry (IUPAC). https://doi.org/10.1351/goldbook

Mergulhão, F. J. M., Summers, D. K., & Monteiro, G. A. (2005). Recombinant protein secretion in Escherichia coli. In *Biotechnology Advances* (Vol. 23, Issue 3, pp. 177–202). Elsevier Inc. https://doi.org/10.1016/j.biotechadv.2004.11.003

Mesdaghi, S., Murphy, D. L., Sánchez Rodríguez, F., Burgos-Mármol, J. J., & Rigden, D. J. (2021). In silico prediction of structure and function for a large family of transmembrane proteins that includes human Tmem41b. *F1000Research*, *9*, 1395. https://doi.org/10.12688/f1000research.27676.2

Michalski, A., Damoc, E., Lange, O., Denisov, E., Nolting, D., Müller, M., Viner, R., Schwartz, J., Remes, P., Belford, M., Dunyach, J. J., Cox, J., Horning, S., Mann, M., & Makarov, A. (2012). Ultra high resolution linear ion trap orbitrap mass spectrometer (orbitrap elite) facilitates top down LC MS/MS and versatile peptide fragmentation modes. *Molecular and Cellular Proteomics*, *11*(3). https://doi.org/10.1074/mcp.O111.013698

Migneault, I., Dartiguenave, C., Bertrand, M. J., & Waldron, K. C. (2004). Glutaraldehyde: behavior in aqueous solution, reaction with proteins, and application to enzyme crosslinking. *Doi.Org*, *37*(5), 790–802. https://www.future-science.com/doi/10.2144/04375RV01

Mikami, S., Kobayashi, T., Masutani, M., Yokoyama, S., & Imataka, H. (2008). A human cell-derived in vitro coupled transcription/translation system optimized for production of recombinant proteins. *Protein Expression and Purification*, *62*(2), 190–198. https://doi.org/10.1016/j.pep.2008.09.002

Millington, D. S., Kodo, N., Norwood, D. L., & Roe, C. R. (1990). Tandem mass spectrometry: A new method for acylcarnitine profiling with potential for neonatal screening for inborn errors of metabolism. *Journal of Inherited Metabolic Disease*. https://doi.org/10.1007/BF01799385

Millington, David S., Norwood, D. L., Kodo, N., Roe, C. R., & Inouet, F. (1989). Application of fast atom bombardment with tandem mass spectrometry and liquid chromatography/ mass spectrometry to the analysis of acylcarnitines in human urine, blood, and tissue. *Analytical Biochemistry*, *180*(2), 331–339. https://doi.org/10.1016/0003-2697(89)90441-7

Milo, R., Jorgensen, P., Moran, U., Weber, G., & Springer, M. (2009). BioNumbers The database of key numbers in molecular and cell biology. *Nucleic Acids Research*, *38*(SUPPL.1), D750. https://doi.org/10.1093/nar/gkp889

Mitchell, K. A. P., Szabo, G., & de S. Otero, A. (2009). Direct binding of cytosolic NDP kinases to membrane lipids is regulated by nucleotides. *Biochimica et Biophysica Acta - Molecular Cell Research*, *1793*(3), 469–476. https://doi.org/10.1016/j.bbamcr.2008.12.009

Moffitt, J. R., Bambah-Mukku, D., Eichhorn, S. W., Vaughn, E., Shekhar, K., Perez, J. D., Rubinstein, N. D., Hao, J., Regev, A., Dulac, C., & Zhuang, X. (2018). Molecular, spatial, and functional single-cell profiling of the hypothalamic preoptic region. *Science*. https://doi.org/10.1126/science.aau5324

Mogk, A., & Bukau, B. (2006). Protein quality control systems: Mechanisms and applications. *Microbial Cell Factories*, *5*(Suppl 1), 1–1. https://doi.org/10.1186/1475-2859-5-S1-S8

Molday, R. S., & Molday, L. L. (1987). Differences in the protein composition of bovine retinal rod outer segment disk and plasma membranes isolated by a ricin-gold-dextran density perturbation method. *Journal of Cell Biology*, *105*(6 I), 2589–2601. https://doi.org/10.1083/jcb.105.6.2589

Molday, R. S., Molday, L. L., Dose, A., Clark-Lewis, I., Illing, M., Cook, N. J., Eismann, E., & Kaupp, U. B. (1991). The cGMP-gated channel of the rod photoreceptor cell characterization and orientation of the amino terminus. *Journal of Biological Chemistry*. https://doi.org/10.1016/s0021-9258(18)54724-4

Molday, Robert S., & Molday, L. L. (1999). Purification, characterization, and reconstitution of cyclic nucleotide- gated channels. *Methods in Enzymology*, *294*, 246–260. https://doi.org/10.1016/S0076-6879(99)94015-6

Molday, Robert S., & Moritz, O. L. (2015). Photoreceptors at a glance. *Journal of Cell Science*, *128*(22), 4039–4045. https://doi.org/10.1242/jcs.175687

Molday, Robert S, & Molday, L. L. (1998). Molecular properties of the cGMP-gated channel of rod photoreceptors. *Vision Research*, *38*(10), 1315–1323. http://linkinghub.elsevier.com/retrieve/pii/S0042698997004094

Molokanova, E., Krajewski, J. L., Satpaev, D., Luetje, C. W., & Kramer, R. H. (2003). Subunit contributions to phosphorylation-dependent modulation of bovine rod cyclic nucleotide-gated channels. *Journal of Physiology*, *552*(2), 345–356. https://doi.org/10.1113/jphysiol.2003.047167

Molokanova, E., Savchenko, A., & Kramer, R. H. (1999). Noncatalytic inhibition of cyclic nucleotide-gated channels by tyrosine kinase induced by genistein. *Journal of General Physiology*, *113*(1), 45–56. https://doi.org/10.1085/jgp.113.1.45

Molokanova, E., Trivedi, B., Savchenko, A., & Kramer, R. H. (1997). Modulation of Rod Photoreceptor Cyclic Nucleotide-Gated Channels by Tyrosine Phosphorylation. *Journal of Neuroscience*, *17*(23), 9068–9076. http://www.jneurosci.org/lookup/doi/10.1523/JNEUROSCI.17-23-09068.1997

Morbœuf, O., Borgel, D., Aiach, M., Kaabache, T., Gandrille, S., & Gaussem, P. (2000). Expression and characterization of recombinant protein S with the Ser 460 Pro mutation. *Thrombosis Research*, *100*(1), 81–88. https://doi.org/10.1016/S0049-3848(00)00296-6

Moriya, T., Saur, M., Stabrin, M., Merino, F., Voicu, H., Huang, Z., Penczek, P. A., Raunser, S., & Gatsogiannis, C. (2017). High-resolution Single Particle Analysis from Electron Cryo-microscopy Images Using SPHIRE. *Journal of Visualized Experiments*, *123*, 1–11. https://www.jove.com/video/55448/high-resolution-single-particle-analysis-from-electron-cryo

Müller, F., Bönigk, W., Sesti, F., & Frings, S. (1998). Phosphorylation of mammalian olfactory cyclic nucleotide-gated channels increases ligand sensitivity. *Journal of Neuroscience*, *18*(1), 164–173. https://doi.org/10.1523/jneurosci.18-01-00164.1998

Narayanan, A., Ridilla, M., & Yernool, D. A. (2011). Restrained expression, a method to overproduce toxic membrane proteins by exploiting operator-repressor interactions. *Protein Science*, *20*(1), 51–61. https://doi.org/10.1002/pro.535

Nath, A., Atkins, W. M., & Sligar, S. G. (2007). Applications of phospholipid bilayer nanodiscs in the study of membranes and membrane proteins. *Biochemistry*, *46*(8), 2059–2069. https://doi.org/10.1021/bi602371n

Nathans, J. (1992). Rhodopsin : Structure, Function, and Genetics. *Biochemistry*, *31*(21), 4923–4931. https://doi.org/10.1021/bi00136a001

Nikolov, M., Schmidt, C., & Urlaub, H. (2012). Quantitative mass spectrometry-based proteomics: An overview. In *Methods in Molecular Biology* (Vol. 893, pp. 85–100). Methods Mol Biol. https://doi.org/10.1007/978-1-61779-885-6_7

Nishi, H., Shaytan, A., & Panchenko, A. R. (2014). Physicochemical mechanisms of protein regulation by phosphorylation. In *Frontiers in Genetics* (Vol. 5, Issue AUG). Frontiers Research Foundation. https://doi.org/10.3389/fgene.2014.00270

Noble, A. J., Wei, H., Dandey, V. P., Zhang, Z., Tan, Y. Z., Potter, C. S., & Carragher, B. (2018). Reducing effects of particle adsorption to the air–water interface in cryo-EM. *Nature Methods*, *15*(10), 793–795. https://doi.org/10.1038/s41592-018-0139-3

Novák, M. (1994). Truncated tau protein as a new marker for Alzheimer's disease. In *Acta virologica* (Vol. 38, Issue 3, pp. 173–189). https://europepmc.org/article/MED/7817900

Nussinov, R., Tsai, C. J., Shehu, A., & Jang, H. (2019). Computational structural biology: Successes, future directions, and challenges. In *Molecules* (Vol. 24, Issue 3). MDPI AG. https://doi.org/10.3390/molecules24030637

Nwanochie, E., & Uversky, V. N. (2019). Structure Determination by Single-Particle Cryo-Electron Microscopy: Only the Sky (and Intrinsic Disorder) is the Limit. *International Journal of Molecular Sciences*, *20*(17), 4186. https://www.mdpi.com/1422-0067/20/17/4186/htm

Ohi, M., Li, Y., Cheng, Y., & Walz, T. (2004). Negative staining and image classification - Powerful tools in modern electron microscopy. *Biological Procedures Online*. https://doi.org/10.1251/bpo70

Okada, T., Le Trong, I., Fox, B. A., Behnke, C. A., Stenkamp, R. E., & Palczewski, K. (2000). X-ray diffraction analysis of three-dimensional crystals of Bovine Rhodopsin obtained from mixed micelles. *Journal of Structural Biology*, *130*(1), 73–80. https://doi.org/10.1006/jsbi.1999.4209

Okada, T., Takeda, K., & Kouyama, T. (1998). Highly Selective Separation of Rhodopsin from Bovine Rod Outer Segment Membranes Using Combination of Divalent Cation and Alkyl(thio)glucoside. *Photochemistry and Photobiology*, *67*(5), 495–499. https://doi.org/10.1111/j.1751-1097.1998.tb09084.x

Olsen, J. V., Blagoev, B., Gnad, F., Macek, B., Kumar, C., Mortensen, P., & Mann, M. (2006). Global, In Vivo, and Site-Specific Phosphorylation Dynamics in Signaling Networks. *Cell*, *127*(3), 635–648. https://doi.org/10.1016/j.cell.2006.09.026

Olsen, J. V., Macek, B., Lange, O., Makarov, A., Horning, S., & Mann, M. (2007). Higher-energy C-trap dissociation for peptide modification analysis. *Nature Methods*, *4*(9), 709–712. https://doi.org/10.1038/nmeth1060

Ong, S. E., Blagoev, B., Kratchmarova, I., Kristensen, D. B., Steen, H., Pandey, A., & Mann, M. (2002). Stable isotope labeling by amino acids in cell culture, SILAC, as a simple and accurate approach to expression proteomics. *Molecular & Cellular Proteomics : MCP*, *1*(5), 376–386. https://doi.org/10.1074/mcp.M200025-MCP200

Palczewski, K., Kumasaka, T., Hori, T., Behnke, C. A., Motoshima, H., Fox, B. A., Le Trong, I., Teller, D. C., Okada, T., Stenkamp, R. E., Yamamoto, M., & Miyano, M. (2000). Crystal structure of rhodopsin: A G protein-coupled receptor. *Science*. https://doi.org/10.1126/science.289.5480.739

Pandey, A., Shin, K., Patterson, R. E., Liu, X. Q., & Rainey, J. K. (2016). Current strategies for protein production and purification enabling membrane protein structural biology. *Biochemistry and Cell Biology*, *94*(6), 507–527. https://doi.org/10.1139/bcb-2015-0143

Pappin, D. J. C., Hojrup, P., & Bleasby, A. J. (1993). Rapid identification of proteins by peptide-mass fingerprinting. *Current Biology*. https://doi.org/10.1016/0960-9822(93)90195-T

Parker, C. E., Mocanu, V., Mocanu, M., Dicheva, N., & Warren, M. R. (2009). Mass spectrometry for post-translational modifications. In *Neuroproteomics* (pp. 93–113). CRC Press. https://doi.org/10.1201/9781420076264.ch6

Paul, W. (1990). Electromagnetic Traps for Charged and Neutral Particles (Nobel Lecture). In *Angewandte Chemie International Edition in English* (Vol. 29, Issue 7, pp. 739–748). John Wiley & Sons, Ltd. https://doi.org/10.1002/anie.199007391

Pearring, J. N., Martínez-Márquez, J., Willer, J. R., Lieu, E. C., Salinas, R. Y., & Arshavsky, V. Y. (2021). The GARP domain of the rod CNG channel s β1-subunit contains distinct sites for outer segment targeting and connecting to the photoreceptor disk rim. *Journal of Neuroscience*, *41*(14), 3094–3104. https://doi.org/10.1523/JNEUROSCI.2609-20.2021

Penczek, P. A. (2010). Fundamentals of Three-Dimensional reconstruction from projections. In *Methods in Enzymology* (Vol. 482, Issue C, pp. 1–33). Academic Press Inc. https://doi.org/10.1016/S0076-6879(10)82001-4

Penczek, P. A., Fang, J., Li, X., Cheng, Y., Loerke, J., & Spahn, C. M. T. (2014). CTER—Rapid estimation of CTF parameters with error assessment. *Ultramicroscopy*, *140*(C), 9–19. http://dx.doi.org/10.1016/j.ultramic.2014.01.009

Penczek, P. A., Zhu, J., & Frank, J. (1996). A common-lines based method for determining orientations for N greater than 3 particle projections simultaneously. *Ultramicroscopy*, *63*(3–4), 205–218. https://doi.org/10.1016/0304-3991(96)00037-X

Perkins, D. N., Pappin, D. J. C., Creasy, D. M., & Cottrell, J. S. (1999). Probability-based protein identification by searching sequence databases using mass spectrometry data. *Electrophoresis*, *20*(18), 3551–3567. https://doi.org/https://doi.org/10.1002/(SICI)1522-2683(19991201)20:18%3C3551::AID-ELPS3551%3E3.0.CO;2-2

Perry, R. H., Cooks, R. G., & Noll, R. J. (2008). Orbitrap mass spectrometry: Instrumentation, ion motion and applications. *Mass Spectrometry Reviews*, *27*(6), 661–699. https://doi.org/10.1002/mas.20186

Peter J. Goodhew, John Humphreys, & Richard Beanland. (2001). *Electron Microscopy and Analysis* (3rd ed.). Taylor & Francis.

Pettersen, E. F., Goddard, T. D., Huang, C. C., Couch, G. S., Greenblatt, D. M., Meng, E. C., & Ferrin, T. E. (2004). UCSF Chimera - A visualization system for exploratory research and analysis. *Journal of Computational Chemistry*, *25*(13), 1605–1612. https://doi.org/10.1002/jcc.20084

Poetsch, A., Molday, L. L., & Molday, R. S. (2001). The cGMP-gated Channel and Related Glutamic Acid-rich Proteins Interact with Peripherin-2 at the Rim Region of Rod Photoreceptor Disc Membranes. *Journal of Biological Chemistry*, *276*(51), 48009–48016. https://doi.org/10.1074/jbc.M108941200

Popot, J.-L. (2010). Amphipols, Nanodiscs, and Fluorinated Surfactants: Three Nonconventional Approaches to Studying Membrane Proteins in Aqueous Solutions. *Annual Review of Biochemistry*, *79*(1), 737–775. http://www.annualreviews.org/doi/10.1146/annurev.biochem.052208.114057

Pratt, J. M., Simpson, D. M., Doherty, M. K., Rivers, J., Gaskell, S. J., & Beynon, R. J. (2006). Multiplexed absolute quantification for proteomics using concatenated signature peptides encoded by QconCAT genes. *Nature Protocols*, *1*(2), 1029–1043. https://doi.org/10.1038/nprot.2006.129

Pugh, E. N., & Lamb, T. D. (2000). Phototransduction in vertebrate rods and cones: Molecular mechanisms of amplification, recovery and light adaptation. In *Handbook of Biological Physics* (Vol. 3, Issue C, pp. 183–255). North-Holland. https://doi.org/10.1016/S1383-8121(00)80008-1

Punjani, A., Rubinstein, J. L., Fleet, D. J., & Brubaker, M. A. (2017). CryoSPARC: Algorithms for rapid unsupervised cryo-EM structure determination. *Nature Methods*. https://doi.org/10.1038/nmeth.4169

Radivojac, P., Obradovic, Z., Smith, D. K., Zhu, G., Vucetic, S., Brown, C. J., Lawson, J. D., & Dunker, A. K. (2004). Protein flexibility and intrinsic disorder. *Protein Science*, *13*(1), 71–80. https://doi.org/10.1110/ps.03128904

Ramachandran, G. N., Ramakrishnan, C., & Sasisekharan, V. (1963). Stereochemistry of polypeptide chain configurations. *Journal of Molecular Biology*, *7*(1), 95–99. https://doi.org/10.1016/S0022-2836(63)80023-6

Rapoport, T. A. (2007). Protein translocation across the eukaryotic endoplasmic reticulum and bacterial plasma membranes. In *Nature* (Vol. 450, Issue 7170, pp. 663–669). Nature Publishing Group. https://doi.org/10.1038/nature06384

Rehm, H., & Letzel, T. (2016). Der Experimentator: Proteinbiochemie/Proteomics. In *Der Experimentator: Proteinbiochemie/Proteomics*. Springer Berlin Heidelberg. https://doi.org/10.1007/978-3-662-48851-5

Rheinberger, J., Gao, X., Schmidpeter, P. A. M., & Nimigean, C. M. (2018). Ligand discrimination and gating in cyclic nucleotide-gated ion channels from apo and partial agonist-bound cryo-EM structures. *ELife*, *7*, 1–25. https://doi.org/10.7554/eLife.39775

Roh, S. H., Hryc, C. F., Jeong, H. H., Fei, X., Jakana, J., Lorimer, G. H., & Chiu, W. (2017). Subunit conformational variation within individual GroEL oligomers resolved by Cryo-EM. *Proceedings of the National Academy of Sciences of the United States of America*, *114*(31), 8259–8264. https://doi.org/10.1073/pnas.1704725114

Root, M. J., & MacKinnon, R. (1993). Identification of an external divalent cation-binding site in the pore of a cGMP-activated channel. *Neuron*, *11*(3), 459–466. https://doi.org/10.1016/0896-6273(93)90150-P

Roque, A. C. A., Silva, C. S. O., & Taipa, M. Â. (2007). Affinity-based methodologies and ligands for antibody purification: Advances and perspectives. In *Journal of Chromatography A* (Vol. 1160, Issues 1–2, pp. 44–55). J Chromatogr A. https://doi.org/10.1016/j.chroma.2007.05.109

Rosenheck, K., & Doty, P. (1961). The far ultraviolet absorption spectra of polypeptide and protein solutions and their dependence on conformation. *Proceedings of the National Academy of Sciences of the United States of America*, *47*(11), 1775–1785. https://doi.org/10.1073/pnas.47.11.1775

Ross, P. L., Huang, Y. N., Marchese, J. N., Williamson, B., Parker, K., Hattan, S., Khainovski, N., Pillai, S., Dey, S., Daniels, S., Purkayastha, S., Juhasz, P., Martin, S., Bartlet-Jones, M., He, F., Jacobson, A., & Pappin, D. J. (2004). Multiplexed protein quantitation in Saccharomyces cerevisiae using amine-reactive isobaric tagging reagents. *Molecular and Cellular Proteomics*, *3*(12), 1154–1169. https://doi.org/10.1074/mcp.M400129-MCP200

Rostamirad, S. (2010). *Identification and characterization of a novel retinal protein, ANKRD33, and its interacting partner HPCAL-1* [University of British Columbia]. https://doi.org/10.14288/1.0071124

Rusnak, F., & Mertz, P. (2000). Calcineurin: Form and function. *Physiological Reviews*, *80*(4), 1483–1521. https://doi.org/10.1152/physrev.2000.80.4.1483

Sandin, M., Teleman, J., Malmström, J., & Levander, F. (2014). Data processing methods and quality control strategies for label-free LC-MS protein quantification. *Biochimica et Biophysica Acta - Proteins and Proteomics*, *1844*(1 PART A), 29–41. https://doi.org/10.1016/j.bbapap.2013.03.026

Sassenfeld, H. M. (1990). Engineering proteins for p purification. *Trends in Biotechnology*, *8*(C), 88–93. https://doi.org/10.1016/0167-7799(90)90145-N

Savitski, M. M., Lemeer, S., Boesche, M., Lang, M., Mathieson, T., Bantscheff, M., & Kuster, B. (2011). Confident phosphorylation site localization using the mascot delta score. *Molecular and Cellular Proteomics*, *10*(2), S1–S12. https://doi.org/10.1074/mcp.M110.003830

Savitski, M. M., Reinhard, F. B. M., Franken, H., Werner, T., Savitski, M. F., Eberhard, D., Molina, D. M., Jafari, R., Dovega, R. B., Klaeger, S., Kuster, B., Nordlund, P., Bantscheff, M., & Drewes, G. (2014). Tracking cancer drugs in living cells by thermal profiling of the proteome. *Science*, *346*(6205). https://doi.org/10.1126/science.1255784

Scarff, C. A., Fuller, M. J. G., Thompson, R. F., & Iadaza, M. G. (2018). Variations on negative stain electron microscopy methods: Tools for tackling challenging systems. *Journal of Visualized Experiments*. https://doi.org/10.3791/57199

Scheres, S. H.W. (2016). Processing of Structurally Heterogeneous Cryo-EM Data in RELION. In *Methods in Enzymology* (Vol. 579, pp. 125–157). Academic Press Inc. https://doi.org/10.1016/bs.mie.2016.04.012

Scheres, Sjors H.W. (2012). RELION: Implementation of a Bayesian approach to cryo-EM structure determination. *Journal of Structural Biology*. https://doi.org/10.1016/j.jsb.2012.09.006

Schiffner, T., Pallesen, J., Russell, R. A., Dodd, J., de Val, N., LaBranche, C. C., Montefiori, D., Tomaras, G. D., Shen, X., Harris, S. L., Moghaddam, A. E., Kalyuzhniy, O., Sanders, R. W., McCoy, L. E., Moore, J. P., Ward, A. B., & Sattentau, Q. J. (2018). Structural and immunologic correlates of chemically stabilized HIV-1 envelope glycoproteins. *PLoS Pathogens*. https://doi.org/10.1371/journal.ppat.1006986

Schindelin, J., Arganda-Carreras, I., Frise, E., Kaynig, V., Longair, M., Pietzsch, T., Preibisch, S., Rueden, C., Saalfeld, S., Schmid, B., Tinevez, J. Y., White, D. J., Hartenstein, V., Eliceiri, K., Tomancak, P., & Cardona, A. (2012). Fiji: An open-source platform for biological-image analysis. In *Nature Methods*. https://doi.org/10.1038/nmeth.2019

Schneider, M. V., & Orchard, S. (2011). Omics technologies, data and bioinformatics principles. In *Methods in Molecular Biology (Methods and Protocols), vol 719. Humana Press*. https://doi.org/10.1007/978-1-61779-027-0_1

Schnetkamp, P. P. M., & Kaupp, U. B. (1985). Calcium-Hydrogen Exchange in Isolated Bovine Rod Outer Segments. *Biochemistry*, *24*(3), 723–727. https://doi.org/10.1021/bi00324a028

Schwanhüusser, B., Busse, D., Li, N., Dittmar, G., Schuchhardt, J., Wolf, J., Chen, W., & Selbach, M. (2011). Global quantification of mammalian gene expression control. *Nature*. https://doi.org/10.1038/nature10098

Scopes, R. K. (1974). Measurement of protein by spectrophotometry at 205 nm. *Analytical Biochemistry*, *59*(1), 277–282. https://doi.org/10.1016/0003-2697(74)90034-7

Scopes, R.K. (1995). Protein Purification Flow Charts. *Current Protocols in Protein Science*, *00*(1), 1–7. https://doi.org/10.1002/0471140864.ps0103s00

Scopes, R.K. (2001). Strategies for Protein Purification. In *Current Protocols in Protein Science* (Issue 1995, p. 167).

Scopes, R.K. (2002). Overview of Protein Purification and Characterization. *Current Protocols in Food Analytical Chemistry*, *3*(1), B4.1.1-B4.1.9. https://doi.org/10.1002/0471142913.fab0401s03

Scopes, Robert K. (1994). Separation by Adsorption—Affinity Techniques. In *Protein Purification* (pp. 187–237). Springer New York. https://doi.org/10.1007/978-1-4757-2333-5_7

Scott, S. P., Weber, I. T., Harrison, R. W., Carey, J., & Tanaka, J. C. (2001). A functioning chimera of the cyclic nucleotide-binding domain from the bovine retinal rod ion channel and the DNA-binding domain from catabolite gene-activating protein. *Biochemistry*, *40*(25), 7464–7473. https://doi.org/10.1021/bi002804x

Seifert, R., Eismann, E., Ludwig, J., Baumann, A., & Kaupp, U. B. (1999). Molecular determinants of a Ca2+-binding site in the pore of cyclic nucleotide-gated channels: S5/S6 segments control affinity of intrapore glutamates. *EMBO Journal*, *18*(1), 119–130. https://doi.org/10.1093/emboj/18.1.119

Shendure, J., & Aiden, E. L. (2012). The expanding scope of DNA sequencing. In *Nature Biotechnology*. https://doi.org/10.1038/nbt.2421

Shi, X., & Jarvis, D. (2007). Protein N-Glycosylation in the Baculovirus-Insect Cell System. *Current Drug Targets*, *8*(10), 1116–1125. https://doi.org/10.2174/138945007782151360

Shigematsu, H., Sokabe, T., Danev, R., Tominaga, M., & Nagayama, K. (2010). A 3.5-nm structure of rat TRPV4 cation channel revealed by zernike phase-contrast cryoelectron microscopy. *Journal of Biological Chemistry*. https://doi.org/10.1074/jbc.M109.090712

Shiloach, J., & Fass, R. (2005). Growing E. coli to high cell density - A historical perspective on method development. In *Biotechnology Advances* (Vol. 23, Issue 5, pp. 345–357). Biotechnol Adv. https://doi.org/10.1016/j.biotechadv.2005.04.004

Shuart, N. G., Haitin, Y., Camp, S. S., Black, K. D., & Zagotta, W. N. (2011). Molecular mechanism for 3:1 subunit stoichiometry of rod cyclic nucleotide-gated ion channels. *Nature Communications*, *2*(1). https://doi.org/10.1038/ncomms1466

Sigworth, F. J. (2015). Principles of cryo-EM single-particle image processing. *Microscopy*, *65*(1), 57–67. https://doi.org/10.1093/jmicro/dfv370

Simon J. Gaskell. (1997). Electrospray: Principles and Practice. *Journal of Mass Spectrometry*, *32*(7), 677–688. https://analyticalsciencejournals.onlinelibrary.wiley.com/doi/abs/10.1002/%28SICI%291096-9888%28199707%2932%3A7%3C677%3A%3AAID-JMS536%3E3.0.CO%3B2-G

Sitarska, A., Skora, L., Klopp, J., Roest, S., Fernández, C., Shrestha, B., & Gossert, A. D. (2015). Affordable uniform isotope labeling with 2H, 13C and 15N in insect cells. *Journal of Biomolecular NMR*, *62*(2), 191–197. https://doi.org/10.1007/s10858-015-9935-6

Smith, P. K., Krohn, R. I., Hermanson, G. T., Mallia, A. K., Gartner, F. H., Provenzano, M. D., Fujimoto, E. K., Goeke, N. M., Olson, B. J., & Klenk, D. C. (1985). Measurement of protein using bicinchoninic acid. *Analytical Biochemistry*, *150*(1), 76–85. https://doi.org/10.1016/0003-2697(85)90442-7

Sokolova, O., Kolmakova-Partensky, L., & Grigorieff, N. (2001). Three-dimensional structure of a voltage-gated potassium channel at 2.5 nm resolution. *Structure*, *9*(3), 215–220. https://doi.org/10.1016/S0969-2126(01)00578-0

Stark, H. (2010). GraFix: Stabilization of fragile macromolecular complexes for single particle Cryo-EM. In *Methods in Enzymology*. https://doi.org/10.1016/S0076-6879(10)81005-5

Stoebel, D. M., Dean, A. M., & Dykhuizen, D. E. (2008). The Cost of Expression of *Escherichia coli lac* Operon Proteins Is in the Process, Not in the Products. *Genetics*, *178*(3), 1653–1660. https://doi.org/10.1534/genetics.107.085399

Strijbos, P. J. L. M., Pratt, G. D., Khan, S., Charles, I. G., & Garthwaite, J. (1999). Molecular characterization and in situ localization of a full-length cyclic nucleotide-gated channel in rat brain. *European Journal of Neuroscience*, *11*(12), 4463–4467. https://doi.org/10.1046/j.1460-9568.1999.00893.x

Sugimoto, Y., Yatsunami, K., Tsujimoto, M., Gobind Khorana, H., & Ichikawa, A. (1991). The amino acid sequence of a glutamic acid-rich protein from bovine retina as deduced from the cDNA sequence. *Proceedings of the National Academy of Sciences of the United States of America*, *88*(8), 3116–3119. https://doi.org/10.1073/pnas.88.8.3116

Sułkowska, J. I., Morcos, F., Weigt, M., Hwa, T., & Onuchic, J. N. (2012). Genomics-aided structure prediction. *Proceedings of the National Academy of Sciences of the United States of America*. https://doi.org/10.1073/pnas.1207864109

Syage, J. A., Short, L. C., & Cai, S.-S. (2008). APPI: The second source for LC-MS. *LC GC Magazine*.

Szilák, L., Moitra, J., & Vinson, C. (1997). Design of a leucine zipper coiled coil stabilized 1.4 kcal mol-1 by phosphorylation of a serine in the e position. *Protein Science*, *6*(6), 1273–1283. https://doi.org/10.1002/pro.5560060615

Szklarczyk, D., Franceschini, A., Wyder, S., Forslund, K., Heller, D., Huerta-Cepas, J., Simonovic, M., Roth, A., Santos, A., Tsafou, K. P., Kuhn, M., Bork, P., Jensen, L. J., & Von Mering, C. (2015). STRING v10: Protein-protein interaction networks, integrated over the tree of life. *Nucleic Acids Research*, *43*(D1), D447–D452. https://doi.org/10.1093/nar/gku1003

Takizawa, Y., Binshtein, E., Erwin, A. L., Pyburn, T. M., Mittendorf, K. F., & Ohi, M. D. (2017). While the revolution will not be crystallized, biochemistry reigns supreme. *Protein Science*, *26*(1), 69–81. https://doi.org/10.1002/pro.3054

Tang, G., Peng, L., Baldwin, P. R., Mann, D. S., Jiang, W., Rees, I., & Ludtke, S. J. (2007). EMAN2: An extensible image processing suite for electron microscopy. *Journal of Structural Biology*. https://doi.org/10.1016/j.jsb.2006.05.009

Tao, S. X., Chan, H. W., & Van Der Graaf, H. (2016). Secondary electron emission materials for transmission dynodes in novel photomultipliers: A review. In *Materials* (Vol. 9, Issue 12, p. 1017). MDPI AG. https://doi.org/10.3390/ma9121017

Taylor, W. R., & Baylor, D. A. (1995). Conductance and kinetics of single cGMP-activated channels in salamander rod outer segments. *The Journal of Physiology*. https://doi.org/10.1113/jphysiol.1995.sp020607

Thomson, J. J. (1912). Further experiments on positive rays. *The London, Edinburgh, and Dublin Philosophical Magazine and Journal of Science*. https://doi.org/10.1080/14786440808637325

Thon, F. (1966). Zur defokussierungsabhängigkeit des phasen- kontrastes bei der elektronenmikroskopischen abbildung. *Zeitschrift Fur Naturforschung - Section A Journal of Physical Sciences*, *21*(4), 476–478. https://doi.org/10.1515/zna-1966-0417

Torre, V., Straforini, M., Sesti, F., & Lamb, T. D. (1992). Different channel-gating properties of two classes of cyclic GMP-activated channel in vertebrate photoreceptors. *Proceedings of the Royal Society B: Biological Sciences*. https://doi.org/10.1098/rspb.1992.0151

Towbin, H., Staehelin, T., & Gordon, J. (1979). Electrophoretic transfer of proteins from polyacrylamide gels to nitrocellulose sheets: Procedure and some applications. *Proceedings of the National Academy of Sciences of the United States of America*. https://doi.org/10.1073/pnas.76.9.4350

Tribet, C., Audebert, R., & Popot, J. L. (1996). Amphipols: Polymers that keep membrane proteins soluble in aqueous solutions. *Proceedings of the National Academy of Sciences of the United States of America*, *93*(26), 15047–15050. https://doi.org/10.1073/pnas.93.26.15047

Uchański, T., Masiulis, S., Fischer, B., Kalichuk, V., López-Sánchez, U., Zarkadas, E., Weckener, M., Sente, A., Ward, P., Wohlkönig, A., Zögg, T., Remaut, H., Naismith, J. H., Nury, H., Vranken, W., Aricescu, A. R., Pardon, E., & Steyaert, J. (2021). Megabodies expand the nanobody toolkit for protein structure determination by single-particle cryo-EM. *Nature Methods*, *18*(1), 60–68. https://doi.org/10.1038/s41592-020-01001-6

Uhlen, M., & Ponten, F. (2005). Antibody-based proteomics for human tissue profiling. *Molecular and Cellular Proteomics*, *4*(4), 384–393. https://doi.org/10.1074/mcp.R500009-MCP200

Uversky, V. N. (2016). Dancing protein clouds: The strange biology and chaotic physics of intrinsically disordered proteins. *Journal of Biological Chemistry*, *291*(13), 6681–6688. https://doi.org/10.1074/jbc.R115.685859

Vlastaridis, P., Papakyriakou, A., Chaliotis, A., Stratikos, E., Oliver, S. G., & Amoutzias, G. D. (2017). The pivotal role of protein phosphorylation in the control of yeast central metabolism. *G3: Genes, Genomes, Genetics*, *7*(4), 1239–1249. https://doi.org/10.1534/g3.116.037218

Wagner, T., Merino, F., Stabrin, M., Moriya, T., Antoni, C., Apelbaum, A., Hagel, P., Sitsel, O., Raisch, T., Prumbaum, D., Quentin, D., Roderer, D., Tacke, S., Siebolds, B., Schubert, E., Shaikh, T. R., Lill, P., Gatsogiannis, C., & Raunser, S. (2019). SPHIRE-crYOLO is a fast and accurate fully automated particle picker for cryo-EM. *Communications Biology*. https://doi.org/10.1038/s42003-019-0437-z

Wallin, E., & Von Heijne, G. (1998). Genome-wide analysis of integral membrane proteins from eubacterial, archaean, and eukaryotic organisms. *Protein Science*. https://doi.org/10.1002/pro.5560070420

Walz, J., Typke, D., Nitsch, M., Koster, A. J., Hegerl, R., & Baumeister, W. (1997). Electron tomography of single ice-embedded macromolecules: Three- dimensional alignment and classification. *Journal of Structural Biology*, *120*(3), 387–395. https://doi.org/10.1006/jsbi.1997.3934

Wang, W., & MacKinnon, R. (2017). Cryo-EM Structure of the Open Human Ether-à-go-go-Related K+ Channel hERG. *Cell*, *169*(3), 422-430.e10. https://doi.org/10.1016/j.cell.2017.03.048

Wang, Y., Katyal, P., & Montclare, J. K. (2019). Protein-Engineered Functional Materials. In *Advanced Healthcare Materials* (Vol. 8, Issue 11). Wiley-VCH Verlag. https://doi.org/10.1002/adhm.201801374

Wang, Z., Jiang, Y., Lu, L., Huang, R., Hou, Q., & Shi, F. (2007). Molecular Mechanisms of Cyclic Nucleotide-Gated Ion Channel Gating. *Journal of Genetics and Genomics*. https://doi.org/10.1016/S1673-8527(07)60052-6

Ward, W. (2012a). The Art of Protein Purification. In *Protein Purification*. InTech. https://doi.org/10.5772/27106

Ward, W. (2012b). The Isolation of Invertase from Baker's Yeast – An Introduction to Protein Purification Strategies. In *Protein Purification*. InTech. https://doi.org/10.5772/27543

Warren, R., & Molday, R. S. (2002). Regulation of the rod photoreceptor cyclic nucleotide-gated channel. *Advances in Experimental Medicine and Biology*, *514*, 205–223. https://doi.org/10.1007/978-1-4615-0121-3_12

Wegner, M., Cao, Z., & Rosenfeld, M. G. (1992). Calcium-regulated phosphorylation within the leucine zipper of C/EBPβ. *Science*, *256*(5055), 370–373. https://doi.org/10.1126/science.256.5055.370

Weissenberger, G., Henderikx, R. J. M., & Peters, P. J. (2021). Understanding the invisible hands of sample preparation for cryo-EM. *Nature Methods*, *18*(5), 463–471. https://doi.org/10.1038/s41592-021-01130-6

Weitz, D., Ficek, N., Kremmer, E., Bauer, P. J., & Kaupp, U. B. (2002). Subunit Stoichiometry of the CNG Channel of Rod Photoreceptors. *Neuron*, *36*(5), 881–889. http://linkinghub.elsevier.com/retrieve/pii/S089662730201098X

Weitz, D., Zoche, M., Müller, F., Beyermann, M., Körschen, H. G., Kaupp, U. B., & Koch, K.-W. (1998). Calmodulin controls the rod photoreceptor CNG channel through an unconventional binding site in the N-terminus of the β-subunit. *The EMBO Journal*, *17*(8), 2273–2284. http://emboj.embopress.org/cgi/doi/10.1093/emboj/17.8.2273

Weller, M., Virmaux, N., & Mandel, P. (1975). Light stimulated phosphorylation of rhodopsin in the retina: the presence of a protein kinase that is specific for photobleached rhodopsin. *Proceedings of the National Academy of Sciences of the United States of America*, *72*(1), 381–385. https://doi.org/10.1073/pnas.72.1.381

Wensel, T. G., Zhang, Z., Anastassov, I. A., Gilliam, J. C., He, F., Schmid, M. F., & Robichaux, M. A. (2016). Structural and molecular bases of rod photoreceptor morphogenesis and disease. In *Progress in Retinal and Eye Research* (Vol. 55, pp. 32–51). Elsevier Ltd. https://doi.org/10.1016/j.preteyeres.2016.06.002

Werner, T., Sweetman, G., Savitski, M. F., Mathieson, T., Bantscheff, M., & Savitski, M. M. (2014). Ion coalescence of neutron encoded TMT 10-plex reporter ions. *Analytical Chemistry*, *86*(7), 3594–3601. https://doi.org/10.1021/ac500140s

Whicher, J. R., & MacKinnon, R. (2016). Structure of the voltage-gated K+ channel Eag1 reveals an alternative voltage sensing mechanism. *Science*, *353*(6300), 664–669. https://doi.org/10.1126/science.aaf8070

Wilm, M., Shevchenko, A., Houthaeve, T., Breit, S., Schweigerer, L., Fotsis, T., & Mann, M. (1996). Femtomole sequencing of proteins from polyacrylamide gels by nano-electrospray mass spectrometry. *Nature*. https://doi.org/10.1038/379466a0

Wiśniewski, J. R., & Rakus, D. (2014). Quantitative analysis of the Escherichia coli proteome. *Data in Brief*, *1*, 7–11. https://doi.org/10.1016/j.dib.2014.08.004

Wohlfart, P., Haase, W., Molday, R. S., & Cook, N. J. (1992). Antibodies against synthetic peptides used to determine the topology and site of glycosylation of the cGMP-gated channel from bovine rod photoreceptors. *Journal of Biological Chemistry*, *267*(1), 644–648. https://doi.org/10.1016/s0021-9258(18)48542-0

Wrapp, D., Wang, N., Corbett, K. S., Goldsmith, J. A., Hsieh, C.-L., Abiona, O., Graham, B. S., & McLellan, J. S. (2020). Cryo-EM Structure of the 2019-nCoV Spike in the Prefusion Conformation. *Science*, *367*(6483), 1260–1263. https://doi.org/10.1101/2020.02.11.944462

Xue, J., Han, Y., Zeng, W., Xue, J., Han, Y., Zeng, W., Wang, Y., & Jiang, Y. (2021). Structural mechanisms of gating and selectivity of human rod CNGA1 channel. *Neuron*, *109*, 1–12. https://doi.org/10.1016/j.neuron.2021.02.007

Yao, Q., Weaver, S. J., Mock, J.-Y., & Jensen, G. J. (2018). Fusion of DARPin to aldolase enables visualization of small protein by cryoEM. *BioRxiv*, 455063. http://biorxiv.org/lookup/doi/10.1101/455063

Yarmush, M. L., & Jayaraman, A. (2002). Advances in proteomic technologies. *Annual Review of Biomedical Engineering*, *4*, 349–373. https://doi.org/10.1146/annurev.bioeng.4.020702.153443

Yau, K. W. (1994). Phototransduction mechanism in retinal rods and cones. The Friedenwald lecture. *Investigative Ophthalmology and Visual Science*, *35*(1), 9–32.

Yau, K. W., & Baylor, D. A. (1989). Cyclic GMP-activated conductance of retinal photoreceptor cells. *Annual Review of Neuroscience*, *12*, 289–327. https://doi.org/10.1146/annurev.ne.12.030189.001445

Yip, K. M., Fischer, N., Paknia, E., Chari, A., & Stark, H. (2020). Atomic-resolution protein structure determination by cryo-EM. *Nature*, *587*(7832), 157–161. https://doi.org/10.1038/s41586-020-2833-4

Young, C. L., Britton, Z. T., & Robinson, A. S. (2012). Recombinant protein expression and purification: A comprehensive review of affinity tags and microbial applications. In *Biotechnology Journal* (Vol. 7, Issue 5, pp. 620–634). Biotechnol J. https://doi.org/10.1002/biot.201100155

Yu, F. H., & Catterall, W. A. (2004). The VGL-chanome: a protein superfamily specialized for electrical signaling and ionic homeostasis. In *Science's STKE : signal transduction knowledge environment* (Vol. 2004, Issue 253). Sci STKE. https://doi.org/10.1126/stke.2532004re15

Yu, G., Vago, F., Zhang, D., Snyder, J. E., Yan, R., Zhang, C., Benjamin, C., Jiang, X., Kuhn, R. J., Serwer, P., Thompson, D. H., & Jiang, W. (2014). Single-step antibody-based affinity cryo-electron microscopy for imaging and structural analysis of macromolecular assemblies. *Journal of Structural Biology*, *187*(1), 1–9. https://doi.org/10.1016/j.jsb.2014.04.006

Zagotta, W. N., Olivier, N. B., Black, K. D., Young, E. C., Olson, R., & Gouaux, E. (2003). Structural basis for modulation and agonist specificity of HCN pacemaker channels. *Nature*, *425*(6954), 200–205. https://doi.org/10.1038/nature01922

Zeleny, J. (1917). Instability of electrified liquid surfaces. *Physical Review*. https://doi.org/10.1103/PhysRev.10.1

Zemlin, F. (1994). Expected contribution of the field-emission gun to high-resolution transmission electron microscopy. *Micron*, *25*(3), 223–226. https://doi.org/10.1016/0968-4328(94)90026-4

Zhang, Y. V., Wei, B., Zhu, Y., Zhang, Y., & Bluth, M. H. (2016). Liquid Chromatography–Tandem Mass Spectrometry: An Emerging Technology in the Toxicology Laboratory. *Clinics in Laboratory Medicine*, *36*(4), 635–661. https://doi.org/10.1016/j.cll.2016.07.001

Zhao, F. Q., & Craig, R. (2003). Capturing time-resolved changes in molecular structure by negative staining. *Journal of Structural Biology*, *141*(1), 43–52. https://doi.org/10.1016/S1047-8477(02)00546-4

Zheng, X., Fu, Z., Su, D., Zhang, Y., Li, M., Pan, Y., Li, H., Li, S., Grassucci, R. A., Ren, Z., Hu, Z., Li, X., Zhou, M., Li, G., Frank, J., & Yang, J. (2020). Mechanism of ligand activation of a eukaryotic cyclic nucleotide–gated channel. *Nature Structural and Molecular Biology*, *27*(7), 625–634. https://doi.org/10.1038/s41594-020-0433-5

Zhong, H., Lai, J., & Yau, K. W. (2003). Selective heteromeric assembly of cyclic nucleotide-gated channels. *Proceedings of the National Academy of Sciences of the United States of America*, *100*(9), 5509–5513. https://doi.org/10.1073/pnas.0931279100

Zhong, H., Molday, L. L., Molday, R. S., & Yau, K.-W. (2002). The heteromeric cyclic nucleotide-gated channel adopts a 3A:1B stoichiometry. *Nature*, *420*(6912), 193–198. http://www.nature.com/doifinder/10.1038/nature01201

Zhou, Y., Morais-Cabral, J. H., Kaufman, A., & Mackinnon, R. (2001). Chemistry of ion coordination and hydration revealed by a K+ channel-Fab complex at 2.0 Å resolution. *Nature*, *414*(6859), 43–48. https://doi.org/10.1038/35102009

References

Zhou, Yubin, Yang, W., Kirberger, M., Lee, H. W., Ayalasomayajula, G., & Yang, J. J. (2006). Prediction of EF-hand calcium-binding proteins and analysis of bacterial EF-hand proteins. *Proteins: Structure, Function and Genetics*, *65*(3), 643–655. https://doi.org/10.1002/prot.21139

Zi Tan, Y., Baldwin, P. R., Davis, J. H., Williamson, J. R., Potter, C. S., Carragher, B., & Lyumkis, D. (2017). Addressing preferred specimen orientation in single-particle cryo-EMthrough tilting. *Nature Methods*, *14*(8), 793–796. https://doi.org/10.1038/nmeth.4347

Zivanov, J., Nakane, T., Forsberg, B., Kimanius, D., Hagen, W. J. H., Lindahl, E., & Scheres, S. H. W. (2018). RELION-3: new tools for automated high-resolution cryo-EM structure determination. *BioRxiv*, 421123. http://biorxiv.org/lookup/doi/10.1101/421123

Zuker, C. S., & Ranganathan, R. (1999). The path to specificity. In *Science* (Vol. 283, Issue 5402, pp. 650–651). American Association for the Advancement of Science. https://doi.org/10.1126/science.283.5402.650

7 Appendix

7.1 Index of Figures

7.2 Index of Tables

7.3 List of Abbreviations

ABCA4	ATP-binding cassette, sub-family A member 4
AC	Affinity Chromatography
ANKRD33B	Ankyrin repeat domain 33B
ATP2B4	Plasma membrane calcium-transporting ATPase 4
AUC	Area Under the Curve
Ca^{2+}/CaM	Calcium ion bound to Calmodulin
CaM	Calmoduline
Ca_v	Voltage-Gated Calcium Channel
CBB	Coomassie Brilliant Blue
CBS	Coomassie Brilliant Blue Stain
cGMP	Cyclic Guanosine Monophosphate
CID	Collision Induced Dissociation
CIPP	Capture, Intermediate Purification, Polishing purification strategy
CMC	Critical Micelle Concentration
CNG channel	Cyclic Nucleotide-Gated ion channel
CNGA1	Cyclic Nucleotide-Gated Channel subunit Alpha 1
CNGB1	Cyclic Nucleotide-Gated Channel subunit Beta 1
DDA	Data-Dependent Acquisition
ESI	Electrospray Ionization
GARP	Glutamic-Acid Rich Part
GC	Guanylate Cyclase
HCD	Higher-Energy C-trap Dissociation
HIC	Hydrophobic Interaction Chromatography
HPCAL1	Hippocalcin-like protein 1
iBAQ	intensity-Based Absolute Quantification
IDP	Intrinsically Disordered Protein
IEX	Ion-Exchange Chromatography
IMAC	Immobilized Metal Affinity Chromatography
IS	Inner Segment
kDa	kilo Dalton
K_v	Voltage-Gated Potassium Channel
LC-MS	Liquid Chromatography Mass Spectrometry
m/z	Mass-to-Charge Ratio
mM	milli Molar
MS	Mass Spectrometry
MS/MS	Tandem Mass Spectrometry

MSP	Membrane Scaffolding Proteins
Na_v	Voltage-Gated Sodium Channel
NDPK	Nucleoside Diphosphate Kinases
OS	Outer Segment
OSN	Olfactory Sensory Neurons
PDB	Protein Data Bank
PDE6	Phosphodiesterase
PMF	Peptide Mass Finger-Printing
POI	Protein Of Interest
PPP3	Serine/Threonine-protein phosphatase Calcineurin
PRPH2	Peripherin-2
PSM	Peptide-Spectrum Matches
PTM	Post-Translational Modifications
RHO	Rhodopsin
ROM-1	Rod outer segment membrane protein 1
ROS	Rod Outer Segment
SIL	Stable Isotope Labelling
SILAC	Stable Isotope Labelling by Amino Acids in Cell Culture
SMA	Styrene-Maleic Acid
SNR	Signal-to-Noise Ratio
SP3	Single-Pot Solid-Phase-enhanced Sample Preparation
TEM	Transmission Electron Microscopy
TOF	Time-of-Flight
TRP	Transient Receptor Potential
VGIC	Voltage-Gated Ion Channel
VSLD	Voltage-Sensor-Like Domain
µl	Microliter

7.4 Control Experiments for TCE Stoichiometry Determination

For the TCE-assays, the number of Tryptophan residues of BSA and Apoferritin (ApoF) was considered to normalize the data because the signal used depends on the amount of Tryptophan residues reacting with TCE. Based on the sequence provided by the UniProt database (uniprot.org, entry P02769 and P02794), the number of Tryptophan residues was determined to be 3 for BSA and 24 for a complete assembly of ApoF (24 subunits, 1 TRP each) (see Table 7).

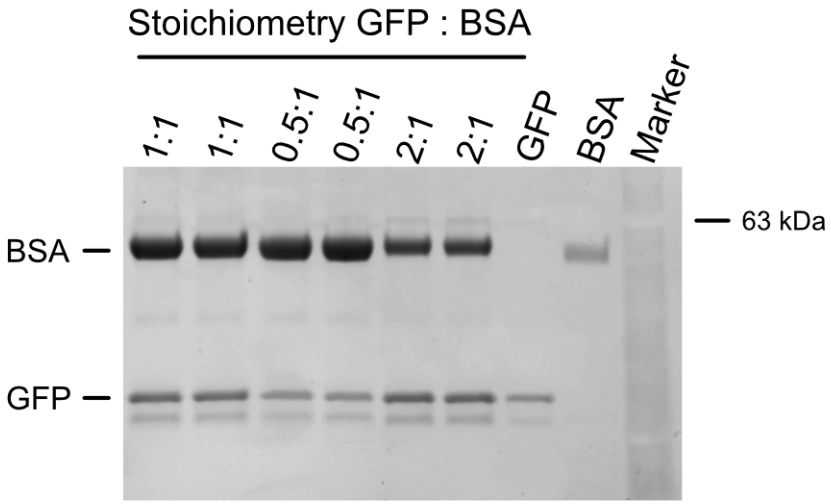

Stoichiometry GFP : BSA	
Expected	Observed
1 : 1	0.89 : 1
0.5 : 1	0.46 : 1
2 : 1	1.73 : 1

Figure 37: Control Experiment for Determining Stoichiometry-based on TCE Staining of SDS-PAGE Gels

Commercially obtained 4-20% gradient SDS-PAGE gels were used to determine the stoichiometry of different samples after TCE staining. Known mixtures of BSA and GFP in three different ratios were used for this experiment. The following ratios of GFP:BSA was loaded twice in lanes next to each other: 1:1, 0.5:1, and 2:1. After SDS-PAGE, the gels were stained with TCE and imaged under UV conditions described in the method (section 3.2.8). Using the Fiji image processing package of ImageJ, the bands corresponding to BSA and GFP were quantified as described in the method (section 3.2.10). The band intensity values of the duplicates were averaged, and the control samples from the lanes loaded with a known concentration of BSA and GFP respectively were used to normalize the measure intensity values. The calculated stoichiometry was observed to be close to the expected stoichiometry of the sample, as shown in the table. The result indicates that TCE staining-based band intensity measurement helps in the reliable stoichiometry calculation in protein samples.

7.5 Control Experiments for TCE Concentration Determination

The estimated protein concentration for both BSA and ApoF-based on the BCA assay was lower than expected. The mean reported concentration of BSA was determined to be 0.196 mg/ml, 2 % below the deployed concentration. The mean reported concentration of ApoF was determined to be 0.178 mg/ml, about 11 % below the deployed concentration (Figure 38 orange bars).

Measuring the absorption at 280 nm wavelength determined a BSA concentration of 0.175 mg/ml, 12 % below the deployed concentration. However, the ApoF concentration was measured as 0.233 mg/ml, 17 % above the expected concentration (Figure 38 blue bars).

The protein concentration determined by the TCE assay reported an average BSA concentration of 0.165, which deviates from the BSA concentration by -17.5 %. In contrast, the ApoF concentration was measured as 0.211 mg/ml, 5.7% above the expected value (Figure 38 dark red bars).

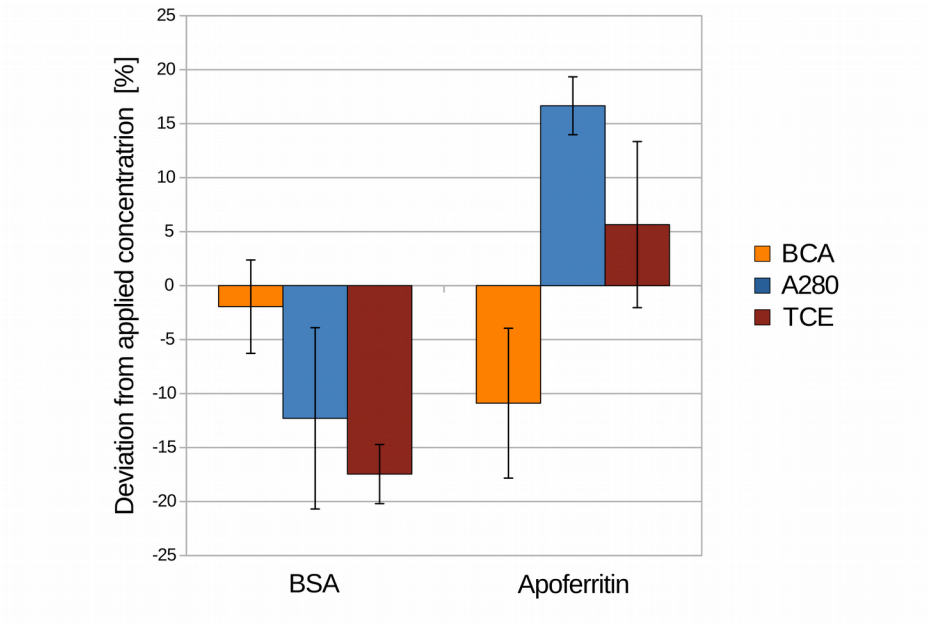

Figure 38: Assessment of concentration determination by BCA protein assay, Absorption at 280 nm and TCE protein assay

BCA protein assay (orange bars), absorption at 280 nm (blue bars), and TCE protein assay (dark red bars) were performed as control experiments. A known protein concentration of BSA (0.2 mg/ml) and Apoferritin (0.2 mg/ml) was used to be determined. The difference between the deployed and the reported protein concentration was calculated for each of the assays. In the TCE-based assay, the number of individual tryptophan residues was considered to calculate protein concentration. All experiments were performed three times independently (n=3).

7.6 Comparison of Methods Determining Stoichiometry

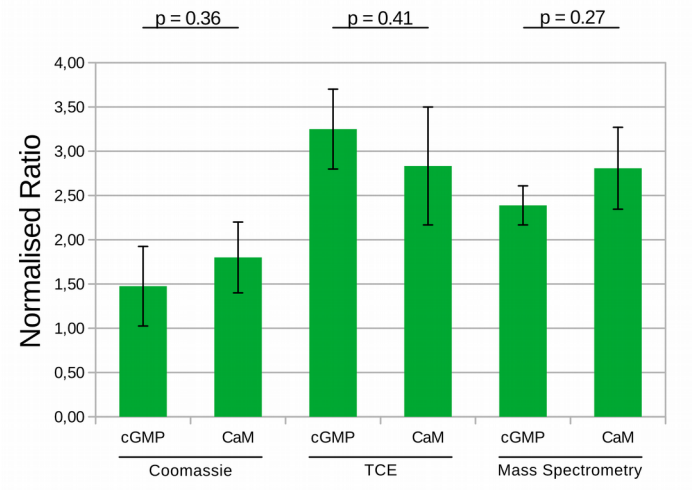

		CBS		TCE		MS	
		cGMP	CaM	cGMP	CaM	cGMP	CaM
CBS	cGMP						
	CaM	0.362					
TCE	cGMP	0.001					
	CaM		0.097	0.412			
MS	cGMP	0.030		0.036			
	CaM		0.047		0.959	0.271	

Figure 39: Comparison of methods employed in CNG channel subunit stoichiometry determination

(A) Bar diagram shows the CNGA1 ratio per CNGB1 subunit as determined by the different approaches for cGMP-AC and CaM-AC purified protein samples. Band intensity measured after Coomassie blue staining or 2,2,2-Trichloroethanol (TCE, corrected for TRP residues) and complex analysis by mass spectrometry. (B) Overview of p-values as follows: red $p > 0.05$ (not significant); yellow $p < 0.05$; $p < 0.01$.

7.7 Enrichment of CNG by affinity purification

The TCE staining of SDS-PAGEs was also used to determine the enrichment ratio of CNG channels in comparison to Rhodopsin. For the calculation, the number of Tryptophan residues was considered (see Table 7), and only CNGB1 was used to determine the CNG channel because the CNGA1 subunit can not be identified unequivocally in the Input sample.

	cGMP-AC	CaM-AC
Sample	Rhodopsin : CNG	Rhodopsin : CNG
Input	225 : 1	264 : 1
E1A	25 : 1	68 : 1
E2A	1.2 : 1	4 : 1
E1B	32 : 1	35 : 1
E2B	4.2 : 1	8 : 1

Table 9: Ratio of CNG channels

7.8 Mass Spectrometry Identification Data

The following list contains all proteins identified by Mass Spectrometry in alphabetical order for each of the experiments performed. All proteins have unique peptide matches (upm) > 1 and a total score ≥ 100.

cGMP-AC			CaM-AC		
P1342_cGMP_E2	**P1426_cGMP**	**P1475_cGMP_E2A**	**P1342_CaM_E2**	**P1426_CaM_I**	**P1426_E2CaM_II**
A0A0A0MP90	A0A0A0MP97	A0A0A0MP90	A0A0A0MP97	A0A0A0MP97	A0A0A0MP97
A0A0A0MP97	A0A140T827	A0A0A0MP97	A1A4J8	A0A0A0MPA4	A0A140T827
A0A0A0MPA2	A0A140T842	A0A0A0MPA2	A1L528	A0A140T832	A0A140T832
A0A140T827	A0A140T871	A0A140T871	A4IFM2	A0A140T842	A0A140T871
A0A140T897	A0A140T889	A0A140T897	A5D7T5	A0A140T871	A0A140T889
A0JNA3	A0A140T894	A1A4J1	A5D984	A0A140T894	A0A140T894
A1A4J1	A0A140T897	A1A4Q9	A5D9F0	A0A140T897	A0A140T897
A1A4R1	A0A140T8B8	A1A4R1	A5PJS1	A0A140T8B8	A0A140T8B8
A3KN04	A0JNA3	A1L528	A6H7H3	A1A4J1	A0JNA3
A4FUZ0	A1A4J1	A2VE06	A6QLL8	A1A4J8	A1A4J1
A4IFU5	A2VE06	A4IFU5	A6QLU1	A1L528	A1A4J8
A5D7Q4	A3KN04	A5D7Q4	A6QNM9	A2VDQ0	A1L528
A5D7T5	A4FUD7	A5D984	A6QQZ0	A3KN04	A4FUZ5
A5D984	A4FUZ5	A5D9F0	A6QR07	A4FUZ5	A4FV54
A5D9F0	A4FV54	A5PJS1	A7MB35	A4FV54	A4IFM2
A5PJS1	A4IFC3	A5PK70	A7YY46	A4IF97	A5D7E8
A5PK70	A5D783	A6H769	A8KC65	A4IFM2	A5D7J6
A6H783	A5D7E8	A6H783	D3K0R6	A5D7E8	A5D7T5
A6H7H3	A5D7J6	A6QLG5	D3K0R6-2	A5D7J6	A5D984
A6QLG5	A5D7Q4	A6QLL5	E1B717	A5D7T5	A5D9F0
A6QLL5	A5D7T5	A6QLL8	E1B7B1	A5D984	A5PJA6
A6QLL8	A5D984	A6QLS9	E1B8C7	A5D9F0	A5PJQ6
A6QNM9	A5D989	A6QNM9	E1B8K6	A5PJQ6	A5PJS1
A6QP55	A5D9F0	A6QP55	E1B919	A5PJS1	A5PK61
A6QQP0	A5PJA6	A6QPY0	E1B9K1	A5PKL1	A6H783
A6QQZ0	A5PJQ6	A6QQP0	E1B9Y5	A6H783	A6H7H3
A7YWU6	A5PJS1	A6QR07	E1BA21	A6H7H3	A6QLG5
A7YY46	A5PK70	A7MBI5	E1BAK0	A6QLG5	A6QLL5
A7Z066	A5PKL1	A7YY55	E1BBB4	A6QLL5	A6QLL8
C7EXK4	A6H707	A7Z066	E1BBP7	A6QLL8	A6QLS9
E1B722	A6H797	C7EXK4	E1BCW3	A6QLS9	A6QLU1
E1B898	A6H7H3	E1B717	E1BDB0	A6QLU1	A6QLY7
E1B8K6	A6H7J6	E1B871	E1BE36	A6QLY7	A6QNM9
E1B9K1	A6QLF9	E1B8G9	E1BEL7	A6QNM9	A6QP55
E1B9M9	A6QLG5	E1B9K1	E1BFB0	A6QNX5	A6QQZ0
E1BAZ9	A6QLL5	E1B9M9	E1BHT9	A6QP55	A6QR07

E1BB71	A6QLL8	E1BA21
E1BBP7	A6QLS9	E1BAT6
E1BCW3	A6QLY7	E1BAZ9
E1BDB0	A6QLZ1	E1BB71
E1BEK9	A6QNM9	E1BBP7
E1BHJ5	A6QP55	E1BCW3
E1BHK2	A6QQP0	E1BD64
E1BHT9	A6QQZ0	E1BDB0
E1BII3	A6YK35	E1BEK9
E1BIS4	A7E344	E1BEL7
E1BJA2	A7MB35	E1BGR7
E1BK63	A7MBI0	E1BGW2
E1BK80	A7MBI5	E1BHJ5
E1BKY3	A7YSY7	E1BHT9
E1BL87	A7YWU6	E1BII3
E1BLC2	A7YY55	E1BIS4
E1BM97	A7Z057	E1BJA2
E1BME9	A7Z066	E1BK63
E1BMW9	A8KC65	E1BK80
E1BN32	C7EXK4	E1BKT9
E1BN34	E1B717	E1BL87
E1BN97	E1B770	E1BLC2
E1BPU1	E1B7S3	E1BM97
E1BQ20	E1B844	E1BME9
F1MAZ1	E1B8C7	E1BMW9
F1MAZ3	E1B8K6	E1BN34
F1MBN0	E1B978	E1BN97
F1MD39	E1B9K1	E1BPU1
F1MDL3	E1B9M9	E1BQ20
F1ME65	E1B9Y5	F1MAZ1
F1MEZ3	E1BA21	F1MAZ3
F1MI44	E1BAT6	F1MB08
F1MK30	E1BAZ9	F1MBN0
F1MK52	E1BB14	F1MC11
F1MKZ5	E1BB71	F1MD39
F1MLB8	E1BBC4	F1MDK1
F1MLU7	E1BBP7	F1MDL3
F1MMU4	E1BCW3	F1MDN4
F1MNI8	E1BD64	F1ME65
F1MPR3	E1BDB0	F1MFT4
F1MQJ8	E1BDX8	F1MGC0
F1MR06	E1BDY3	F1MI32
F1MRI0	E1BE36	F1MIN1
F1MSQ7	E1BEK9	F1MJH2
F1MTS7	E1BEN2	F1MJQ1
E1BHZ3	A6QPY0	A6YK35
E1BIX6	A6QQZ0	A7MB35
E1BJ15	A6QR07	A7MBI5
E1BJ48	A6YK35	A7YWC4
E1BJS1	A7E344	A7YY46
E1BK80	A7MB35	A7YY55
E1BLC2	A7MBH9	A7Z057
E1BM93	A7MBI0	A7Z066
E1BMJ5	A7MBI5	A8KC65
E1BMN5	A7YSY7	A8NN94
E1BN34	A7YWT7	C7EXK4
E1BN97	A7YY46	D3K0R6
E1BPK6	A7Z057	D3K0R6-2
E1BPU1	A7Z066	E1B717
E1BQ20	A8KC65	E1B770
F1MB08	A8NN94	E1B7B1
F1MB46	C7EXK4	E1B7S3
F1MBN0	D3K0R6	E1B8C7
F1MBR9	D3K0R6-2	E1B8K6
F1MC11	E1B717	E1B919
F1MCU4	E1B722	E1B983
F1MCY0	E1B770	E1B9K1
F1MD39	E1B7B1	E1B9Y5
F1MD60	E1B7L9	E1BA21
F1MDL3	E1B7S3	E1BAK0
F1MDN4	E1B7U1	E1BAT6
F1ME65	E1B8C7	E1BAY0
F1MEL5	E1B8K6	E1BB71
F1MG86	E1B919	E1BBB4
F1MHK2	E1B9K1	E1BBP7
F1MHU1	E1B9M9	E1BCW3
F1MI32	E1B9Y5	E1BD64
F1MI44	E1BA21	E1BDB0
F1MIN1	E1BAK0	E1BDY3
F1MJ26	E1BAT6	E1BE36
F1MJX9	E1BAY0	E1BEC7
F1MK30	E1BB36	E1BEL7
F1MK52	E1BB71	E1BEM1
F1MKE9	E1BBB4	E1BFB0
F1MLB8	E1BBP7	E1BGH0
F1MLW4	E1BCW3	E1BGN3
F1MM17	E1BD64	E1BH82
F1MN60	E1BDB0	E1BHA5
F1MNI8	E1BDG4	E1BHD3
F1MNT3	E1BDY3	E1BHJ5

F1MU26	E1BF20	F1MK30
F1MUD2	E1BFB0	F1MK52
F1MUP3	E1BH82	F1ML72
F1MW86	E1BHJ5	F1MLB8
F1MWM0	E1BHK2	F1MLU7
F1MWU9	E1BHT9	F1MLW4
F1MX88	E1BII3	F1MMU4
F1MXG6	E1BIP2	F1MN04
F1MXX0	E1BIS4	F1MNI8
F1MXY8	E1BJA2	F1MPS1
F1MY40	E1BK63	F1MQJ8
F1MY44	E1BKY3	F1MR06
F1MY73	E1BL12	F1MRI0
F1MZC9	E1BL87	F1MS25
F1MZU2	E1BLC2	F1MSE1
F1MZV1	E1BM93	F1MSQ7
F1MZW1	E1BM97	F1MTS7
F1N0J0	E1BM98	F1MU26
F1N0J2	E1BME6	F1MUZ9
F1N0W3	E1BME9	F1MW86
F1N0X5	E1BMW9	F1MWM0
F1N1S2	E1BMX0	F1MWU9
F1N1W1	E1BN32	F1MX88
F1N4X0	E1BN34	F1MXX0
F1N5H8	E1BN97	F1MXY8
F1N6T4	E1BNG8	F1MY40
F2Z4D5	E1BP18	F1MY44
F2Z4E8	E1BP30	F1MY73
F2Z4F9	E1BPK6	F1MZ92
F2Z4G5	E1BPU1	F1MZC9
F2Z4I6	E1BPX9	F1MZU2
F2Z4J1	E1BQ20	F1N0J0
F6PWD5	F1MAZ1	F1N0J2
F6Q9S4	F1MAZ3	F1N0X5
F6R0H3	F1MB08	F1N1S2
F6RDE3	F1MB46	F1N405
F6RM11	F1MB52	F1N453
G1K1B4	F1MBF6	F1N4X0
G1K237	F1MBN0	F1N5H8
G3MXA9	F1MBS4	F1N632
G3MYW9	F1MBT8	F1N6C0
G3MZT0	F1MC11	F1N6T4
G3N0W8	F1MCQ1	F2Z4D5
G3N1F6	F1MCU4	F2Z4G5
G3N288	F1MD39	F2Z4I6
F1MR06	E1BE36	E1BHK2
F1MRE1	E1BEL7	E1BHT9
F1MRI0	E1BFB0	E1BII3
F1MS16	E1BGH0	E1BIP2
F1MTR1	E1BGU2	E1BIP3
F1MTS7	E1BH82	E1BIX6
F1MU26	E1BHA5	E1BJ48
F1MU48	E1BHD3	E1BJA2
F1MUD2	E1BHJ5	E1BK63
F1MUI9	E1BHT9	E1BK80
F1MUZ9	E1BHZ3	E1BKY5
F1MVF1	E1BII3	E1BL12
F1MVH6	E1BIP2	E1BLC2
F1MWM0	E1BIX6	E1BM93
F1MWU9	E1BJ48	E1BM98
F1MX88	E1BJA2	E1BME9
F1MY22	E1BJS1	E1BMJ5
F1MY40	E1BK63	E1BMN5
F1MY73	E1BK80	E1BMW9
F1MYC9	E1BKB8	E1BN34
F1MZC9	E1BKI3	E1BN97
F1MZU2	E1BKT9	E1BNT8
F1N063	E1BKY3	E1BPU1
F1N0X5	E1BL12	E1BQ12
F1N1S2	E1BLC2	E1BQ20
F1N1W1	E1BM93	F1MAZ1
F1N2C7	E1BM98	F1MAZ3
F1N2P1	E1BME6	F1MB08
F1N301	E1BME9	F1MB46
F1N377	E1BMJ5	F1MB52
F1N3A5	E1BMN5	F1MBF6
F1N4Q6	E1BMW9	F1MBN0
F1N5S7	E1BN34	F1MBN2
F1N650	E1BN97	F1MBR9
F1N6B7	E1BNT8	F1MBS4
F1N7J2	E1BP00	F1MCU4
F2Z4E8	E1BP30	F1MCU7
F2Z4F9	E1BPK6	F1MCY0
F6QVC9	E1BPU1	F1MD39
F6R0H3	E1BPY0	F1MD60
F6RM11	E1BQ12	F1MDK1
F6RX10	E1BQ20	F1MDL3
G1K1B4	F1MAZ1	F1MDN4
G3MWX5	F1MAZ3	F1ME65
G3MXA9	F1MB08	F1MEL5

G3N2B8	F1MD60	F2Z4J1
G3N2H8	F1MDC1	F6PWD5
G3N2R1	F1MDK1	F6Q9S4
G3N3U9	F1MDL3	F6R0H3
G3X807	F1MDL6	F6RDE3
G5E686	F1MDN4	G1K1B4
G8JKV5	F1ME65	G1K1X0
G8JKX9	F1MEN8	G1K237
G8JKY0	F1MEQ3	G3MXA9
G8JL00	F1MEW3	G3MZC1
M5FJR2	F1MEZ3	G3N0K3
O46469	F1MF34	G3N1F6
O77784	F1MF38	G3N288
P00514	F1MF42	G3N2B8
P00515	F1MFB7	G3N2H8
P00516	F1MFT4	G3N3U9
P00516-2	F1MGC0	G3N3X4
P00639	F1MGJ7	G3X7S2
P00760	F1MH44	G3X807
P00767	F1MHM5	G5E686
P00829	F1MI32	G8JKX9
P02699	F1MI44	G8JKY0
P02722	F1MIH2	G8JL00
P02769	F1MIN1	G8JL06
P04272	F1MJH2	M5FJW2
P04695	F1MJQ1	O02740
P04696	F1MK30	O18789
P05631	F1MK52	O46469
P05631-2	F1MKH6	P00423
P06623	F1MKN3	P00514
P08168	F1MLG1	P00515
P0C0S9	F1MLU7	P00516
P0CG53	F1MM57	P00516-2
P0CH28	F1MM79	P00829
P10096	F1MME6	P02253
P11541	F1MMJ2	P02548
P12234	F1MMK8	P02699
P12234-2	F1MMU4	P02722
P13619	F1MN04	P02769
P15103	F1MN74	P04272
P15690	F1MNG3	P04695
P17810	F1MNG7	P04696
P19120	F1MNI4	P05631
P19483	F1MNI8	P05631-2
P20072	F1MPS1	P06623

G3MYK1	F1MB46	F1MEW3
G3N1F6	F1MB52	F1MF34
G3N2R1	F1MBF6	F1MF38
G3N348	F1MBN0	F1MF42
G3X6L2	F1MBR9	F1MFT4
G3X7S2	F1MC11	F1MG05
G3X807	F1MCF1	F1MG20
G5E6T3	F1MCU4	F1MG86
G8JKV5	F1MCU7	F1MGC0
G8JKY0	F1MCY0	F1MH43
O02740	F1MCY2	F1MHK2
O46469	F1MD39	F1MHU1
P00829	F1MD60	F1MI32
P02699	F1MDC9	F1MIN1
P02722	F1MDK1	F1MJ26
P02769	F1MDL3	F1MJQ1
P04272	F1MDN4	F1MJV0
P04409	F1ME65	F1MK30
P04695	F1MEL5	F1MK52
P05631	F1MEN8	F1MKB0
P08168	F1MEW3	F1MKE9
P08168-2	F1MEZ3	F1MKH6
P0CG53	F1MF34	F1ML72
P0CH28	F1MF38	F1MLB8
P10096	F1MF42	F1MLG1
P10103	F1MFT4	F1MLU7
P11541	F1MG20	F1MME6
P12234	F1MG86	F1MN60
P12234-2	F1MGC0	F1MN74
P12661	F1MGJ7	F1MNG3
P13214	F1MHU1	F1MNG7
P15103	F1MI32	F1MNI4
P16386	F1MI44	F1MNI8
P17810	F1MIN1	F1MNJ2
P19120	F1MIW8	F1MNT3
P19483	F1MJ26	F1MP30
P19754	F1MJQ1	F1MPR3
P20072	F1MJX9	F1MPS1
P21457	F1MK30	F1MPT3
P22292	F1MK52	F1MR06
P23439	F1MKB0	F1MRE1
P27674	F1MKE9	F1MRI0
P28327	F1MKH6	F1MS16
P29105	F1MLE8	F1MS25
P32007	F1MLG1	F1MSE1

P21457	F1MPU0	P08168	P34943	F1MLU7	F1MTS7
P22292	F1MQ37	P08239	P39872	F1MM17	F1MTV6
P23439	F1MQJ8	P0C0S9	P42899	F1MME6	F1MTV9
P27674	F1MR06	P0CG53	P45879	F1MMJ2	F1MU26
P28327	F1MRI0	P0CH28	P46193	F1MN60	F1MU48
P29105	F1MS25	P10096	P48018	F1MN74	F1MUI9
P31322	F1MSE1	P10103	P48452	F1MNG3	F1MUP3
P32007	F1MSJ9	P11023	P48452-2	F1MNI4	F1MUZ9
P34933	F1MSQ7	P11541	P49410	F1MNI8	F1MWA2
P34943	F1MTS7	P12234	P52205	F1MNS8	F1MWM0
P36225	F1MTV6	P12234-2	P59837	F1MNT3	F1MWU9
P36225-2	F1MU26	P12344	P60712	F1MPR3	F1MWX4
P36225-3	F1MUD2	P12661	P61257	F1MPS1	F1MX05
P39872	F1MUP3	P13619	P61267	F1MPU0	F1MX88
P42899	F1MUT6	P15103	P61284	F1MR06	F1MXX6
P45879	F1MUZ9	P15690	P61602	F1MR28	F1MY22
P48018	F1MW86	P17694	P61763	F1MRE1	F1MY40
P48452	F1MWM0	P17810	P62157	F1MRI0	F1MY73
P48452-2	F1MWU9	P19120	P62261	F1MRI2	F1MYC9
P49410	F1MWV0	P19483	P62803	F1MS16	F1MYX4
P52175	F1MWX4	P19632	P62808	F1MS25	F1MZ92
P52205	F1MX88	P19858	P62871	F1MS45	F1MZC9
P59837	F1MXB4	P20004	P62992	F1MSC2	F1MZU2
P60712	F1MXX0	P21457	P63048	F1MSE1	F1MZV1
P61257	F1MXY8	P22292	P63099	F1MSJ9	F1N063
P61284	F1MY22	P23004	P63258	F1MSQ7	F1N0J2
P61286	F1MY40	P23439	P68103	F1MTR1	F1N0X5
P61356	F1MY44	P23709	P79103	F1MTS7	F1N1I4
P61763	F1MY73	P25708	P81287	F1MTV6	F1N1S2
P62157	F1MYC9	P27674	Q00194	F1MTV9	F1N206
P62803	F1MZ92	P28327	Q01321	F1MU26	F1N2C7
P62808	F1MZC9	P29105	Q03041	F1MU48	F1N2J9
P62871	F1MZU2	P31322	Q08DA1	F1MUI9	F1N2P1
P62992	F1MZV1	P31800	Q08DK8	F1MUP3	F1N2P6
P63048	F1N0J0	P32007	Q08E32	F1MUV1	F1N3A5
P63258	F1N0X5	P34943	Q08E45	F1MUZ9	F1N405
P68002	F1N1S2	P36225	Q0II87	F1MWA2	F1N4X0
P68103	F1N1W1	P36225-2	Q0IIG5	F1MWM0	F1N5S7
P79110	F1N206	P36225-3	Q0IIG8	F1MWU9	F1N650
P80724	F1N2J9	P39872	Q0IIL1	F1MWX4	F1N690
P81948	F1N2N5	P42899	Q0V8E7	F1MX05	F1N6B7
P84080	F1N301	P45879	Q0VCL5	F1MX88	F1N7J2
Q00194	F1N3A5	P46411	Q0VCX2	F1MXX0	F2Z4D5
Q01321	F1N3M8	P47803	Q148D3	F1MY22	F6R0H3
Q03041	F1N3R4	P48018	Q17QL4	F1MY40	F6RM11

Q05927	F1N405	P49410
Q08DK4	F1N4X0	P52174
Q08E32	F1N548	P52175
Q0IIG5	F1N5H8	P52205
Q0IIG8	F1N690	P59837
Q0VCL5	F1N6C0	P60712
Q0VCX2	F1N6T4	P61223
Q148H4	F1N7J2	P61257
Q17QQ3	F1N7T2	P61284
Q1JQ97	F1N7X3	P61286
Q24JY1	F2Z4E8	P61356
Q27965	F2Z4F9	P61585
Q27975	F2Z4I5	P61763
Q27979	F6Q9S4	P62157
Q28030	F6RDE3	P62261
Q28139	F6S1Q0	P62803
Q28139-2	G1K1B4	P62833
Q28181	G1K1L9	P62871
Q29441	G1K1X0	P62992
Q2HJ26	G1K237	P63026
Q2HJ92	G3MWI1	P63048
Q2HJ97	G3MWR4	P63258
Q2HJF7	G3MXA9	P67808
Q2HJF8	G3MXT4	P68002
Q2KI62	G3MY34	P68103
Q2KII5	G3MY67	P68530
Q2KJI7	G3MYJ0	P79103
Q2M2T1	G3MYP5	P79110
Q2T9S0	G3MYW9	P80724
Q2TA29	G3MZ22	P81948
Q2TBG5	G3MZC1	Q00194
Q2TBQ5	G3MZT0	Q01321
Q32L35	G3N0K2	Q03041
Q32S29	G3N0K3	Q04467
Q3MHP2	G3N1F6	Q08DA1
Q3MHW6	G3N288	Q08DK4
Q3SWX4	G3N2B8	Q08E32
Q3SYR7	G3N2H8	Q0II87
Q3SZ86	G3N2K4	Q0IIG5
Q3SZ90	G3N3U9	Q0IIG8
Q3SZA4	G3N3X4	Q0VCX2
Q3SZI6	G3X6W0	Q148D5
Q3SZQ6	G3X7M4	Q17QQ3
Q3T003	G3X807	Q1JQ97
Q3T025	G3X8E2	Q1RMJ6
Q17QQ3	F1MY73	F6RX10
Q17QS4	F1MYC9	G1K1X0
Q1JQ97	F1MZ92	G3MXA9
Q1LZH1	F1MZC9	G3MY34
Q27955	F1MZU2	G3MYD7
Q27965	F1MZV1	G3MYK1
Q27975	F1N063	G3MZT0
Q27979	F1N0J2	G3N0K2
Q28036	F1N0X5	G3N0K3
Q28139	F1N1I4	G3N0S6
Q28139-2	F1N1S2	G3N0S9
Q28181	F1N1W1	G3N1F5
Q29441	F1N1W7	G3N1F6
Q2HJ97	F1N206	G3N262
Q2KII5	F1N2C7	G3N2K4
Q2KJ28	F1N2J9	G3N2P2
Q2KJD0	F1N2N5	G3N2R1
Q2M2T1	F1N2P1	G3N2Z0
Q2NKS2	F1N301	G3N348
Q2TBM9	F1N3A5	G3N354
Q2TBQ5	F1N405	G3X6L2
Q32PB9	F1N4Q6	G3X807
Q32S29	F1N4X0	G5E5P6
Q3MHW6	F1N5I2	G5E686
Q3SZ13	F1N5S7	G5E6T3
Q3SZ90	F1N626	G8JKY0
Q3T087	F1N632	M5FHL5
Q3T0R1	F1N650	O46469
Q3T0W9	F1N690	O77784
Q3T149	F1N6B7	O77784-2
Q3T165	F1N7J2	P00125
Q3ZBI7	F6QVC9	P00130
Q3ZBU2	F6RDE3	P00366
Q3ZBX0	F6RM11	P00423
Q3ZBX6	F6RX10	P00829
Q3ZCH0	G1K192	P02253
Q3ZCK2	G1K1B4	P02699
Q3ZKN0	G1K1X0	P02722
Q4PJK1	G3MWR4	P02769
Q56JX8	G3MWX5	P04272
Q56JZ1	G3MXA9	P04409
Q56K03	G3MXE1	P04695
Q58DQ3	G3MY67	P04696
Q58DT1	G3MYK1	P05631
Q58DW0	G3MZP2	P06623

Q3T040	G5E523	Q1RMR8
Q3T076	G5E5P6	Q24JY1
Q3T0D5	G5E675	Q24JZ4
Q3T0L7	G8JKX9	Q27965
Q3T0Q4	G8JKY0	Q27975
Q3T0R1	L7R5X3	Q27979
Q3T0S6	M5FHL5	Q28030
Q3T0U2	M5FJR2	Q28056
Q3T0U5	M5FJW2	Q28139
Q3T0W9	O02675	Q28139-2
Q3T0X6	O02691	Q28181
Q3T165	O18789	Q29441
Q3T169	O46469	Q2HJ26
Q3T171	O46629	Q2HJ92
Q3ZBU2	O77784	Q2HJ94
Q3ZBX9	P00125	Q2HJ97
Q3ZCH0	P00130	Q2HJF8
Q56JV9	P00423	Q2KID9
Q56JX3	P00514	Q2KJD0
Q56JY1	P00515	Q2KJI7
Q56JZ1	P00516	Q2T9S0
Q56K03	P00516-2	Q2TA29
Q58DQ3	P00639	Q2TBG5
Q58DT1	P00760	Q2TBQ5
Q58DW0	P00766	Q32LG3
Q58DW5	P00767	Q32PD5
Q5E958	P00829	Q3MHM7
Q5E973	P02253	Q3MHP2
Q5E988	P02548	Q3MHW6
Q5E995	P02699	Q3SWX4
Q5E9E6	P02722	Q3SYR7
Q5E9I6	P02769	Q3SZ00
Q5E9M8	P04272	Q3SZ62
Q5EAD6	P04409	Q3SZ86
Q5W5U3	P04695	Q3SZ90
Q6B856	P04696	Q3SZQ6
Q76LV1	P05131	Q3SZR8
Q76LV2	P05131-2	Q3T003
Q861S4	P05307	Q3T025
Q8MJG0	P05631	Q3T076
Q8SQH5	P05631-2	Q3T087
Q95140	P06623	Q3T0B6
Q95M18	P08168	Q3T0D5
Q95MP1	P08239	Q3T0F5
Q9BGI7	P09867	Q3T0L7

Q5E958	G3MZT0	P08168
Q6B856	G3N0K2	P08239
Q76LV2	G3N0K3	P0CG53
Q8MJ05	G3N0S6	P0CH28
Q8MJG0	G3N0T8	P10096
Q8MJN0	G3N1F5	P10103
Q8SQH5	G3N1F6	P10279
Q8WN91	G3N262	P10949
Q95140	G3N2B8	P11019
Q9BGI7	G3N2H8	P11023
Q9N126	G3N2K4	P11024
Q9N179	G3N2R1	P11541
Q9TTK8	G3N2Y5	P11966
Q9XSJ4	G3N2Z0	P12234
	G3N348	P12234-2
	G3N354	P12344
	G3X6L2	P12661
	G3X6W0	P13214
	G3X7G4	P13619
	G3X807	P13621
	G5E686	P15103
	G5E6M7	P15690
	G5E6T3	P16386
	G8JKY0	P17694
	M0QVY0	P17810
	M5FHL5	P19120
	O46469	P19483
	O46629	P19632
	O77784	P19754
	O77784-2	P19858
	P00125	P20004
	P00130	P21398
	P00423	P21457
	P00829	P22292
	P02253	P22439
	P02699	P23004
	P02722	P23439
	P02769	P23709
	P04038	P25708
	P04272	P27674
	P04409	P28327
	P04695	P29105
	P04696	P31404
	P05126	P31408
	P05126-2	P31800

Q9N126	P0C0S4	Q3T0P6	P05631	P32007
Q9XSI3	P0CG53	Q3T0Q4	P05631-2	P34933
	P0CH28	Q3T0R1	P06623	P34942
	P10096	Q3T0S6	P08168	P34943
	P10103	Q3T0U2	P08168-2	P36225
	P10123	Q3T0U5	P08239	P36225-2
	P10279	Q3T0W9	P09867	P36225-3
	P11019	Q3T0X6	P0CG53	P38657
	P11023	Q3T145	P0CH28	P39872
	P11024	Q3T149	P10096	P40673
	P11179	Q3T165	P10103	P43249
	P11541	Q3T169	P10123	P45879
	P11966	Q3T171	P10279	P46193
	P12234	Q3ZBG1	P10949	P46411
	P12234-2	Q3ZBH8	P11023	P47803
	P12344	Q3ZBU2	P11024	P48018
	P12624	Q3ZBU7	P11541	P48452
	P12661	Q3ZBX0	P11966	P48452-2
	P13271	Q3ZBX9	P12234	P48616
	P13619	Q3ZBY4	P12234-2	P49410
	P13620	Q3ZCH0	P12344	P51490
	P13621	Q3ZCJ6	P12624	P52193
	P15103	Q56JV9	P12661	P52205
	P15690	Q56JX3	P13214	P59837
	P17694	Q56JX5	P13619	P60712
	P17810	Q56JX8	P13621	P61267
	P19120	Q56JY1	P15690	P61286
	P19483	Q56JZ1	P16386	P61356
	P19632	Q56K03	P16586	P61585
	P19858	Q56K10	P17694	P61602
	P20000	Q58DQ3	P17810	P61763
	P20004	Q58DT1	P19120	P62157
	P20072	Q58DW0	P19483	P62261
	P20488	Q58DW5	P19632	P62803
	P21457	Q5E958	P19754	P62833
	P22292	Q5E973	P19858	P62871
	P23004	Q5E988	P20000	P62894
	P23439	Q5E995	P20004	P62992
	P23709	Q5E9B1	P20072	P62998
	P25708	Q5E9E6	P21398	P63026
	P27674	Q5E9M8	P21457	P63048
	P28327	Q5EA61	P22292	P63099
	P29105	Q5EAD6	P22439	P63103
	P31039	Q5XQN5	P23004	P63258
	P31322	Q76LV2	P23439	P67808

P31404	Q7JAT3
P31408	Q7YRW9
P31800	Q861S4
P31836	Q862I1
P31976	Q8MJG0
P32007	Q8MJN0
P33097	Q95140
P34942	Q9BGI7
P34943	Q9MZ13
P36225	Q9N126
P36225-3	Q9TTK8
P38657	Q9XSI3
P39872	Q9XSJ4
P40673	
P42899	
P43249	
P45879	
P46411	
P47803	
P48018	
P48452	
P48452-2	
P48616	
P49410	
P49951	
P51177	
P51490	
P52175	
P52193	
P52205	
P59837	
P60712	
P61257	
P61267	
P61284	
P61286	
P61356	
P61763	
P62157	
P62261	
P62803	
P62808	
P62871	
P62894	
P62992	

P23709	P68002
P25708	P68103
P27674	P68250
P28327	P68250-2
P29105	P68252
P31039	P68399
P31404	P68432
P31408	P68509
P31800	P79103
P31836	P80311
P31976	P80724
P32007	P81948
P34942	P82913
P34943	P84227
P36225	Q00194
P36225-2	Q01061
P36225-3	Q02368
P38657	Q02373
P39872	Q02375
P40673	Q02379
P45879	Q02827
P46065	Q03041
P46193	Q04467
P46411	Q05927
P47803	Q08DA1
P48018	Q08DB4
P48452	Q08DF4
P48452-2	Q08DK4
P48616	Q08DK8
P49410	Q08E32
P49951	Q08E34
P51122	Q08E45
P51490	Q0II87
P52193	Q0IIG5
P52205	Q0IIG7
P59837	Q0IIG8
P60712	Q0IIL1
P61257	Q0V8E7
P61267	Q0VC89
P61284	Q0VCW5
P61356	Q0VCX2
P61602	Q148D3
P61763	Q148D5
P62157	Q148L0
P62261	Q148N0

P62998		P62803	Q17QL5
P63009		P62833	Q17QQ3
P63026		P62871	Q17QS4
P63048		P62894	Q17QW3
P63103		P62935	Q1JQ97
P63258		P62992	Q1LZH1
P67808		P62998	Q24JY1
P68002		P63009	Q24JY6
P68103		P63026	Q24JZ4
P68250		P63048	Q27955
P68250-2		P63099	Q27965
P68252		P63103	Q27975
P68399		P63258	Q27979
P68509		P67808	Q28030
P68530		P68002	Q28036
P79103		P68103	Q28056
P79110		P68250	Q28139
P79134		P68250-2	Q28139-2
P80311		P68252	Q28175
P80724		P68399	Q28181
P81948		P79103	Q29397
P82649		P80311	Q29441
P82670		P80724	Q29455
P82922		P81287	Q29455-2
P82925		P81948	Q29466
P83095		P84080	Q29466-2
Q00194		P84081	Q29RK1
Q01321		Q00194	Q29RK2
Q02369		Q00361	Q29S11
Q02373		Q02368	Q2HJ86
Q02375		Q02369	Q2HJ94
Q02379		Q02373	Q2HJ97
Q02827		Q02375	Q2HJF7
Q03041		Q02379	Q2HJH2
Q04467		Q02399	Q2KIV7
Q05927		Q03041	Q2KJD0
Q08DA1		Q03763	Q2KJG3
Q08DB4		Q04467	Q2KJI7
Q08DF4		Q05927	Q2M2S4
Q08DH7		Q08DA1	Q2NKS2
Q08DK4		Q08DB4	Q2TA29
Q08DS7		Q08DC9	Q2TBM9
Q08DU9		Q08DF4	Q2TBQ5
Q08DW1		Q08DK4	Q32LG3
Q08E32		Q08DK8	Q32LL2

Q08E34
Q0II87
Q0IIG5
Q0IIG7
Q0IIG8
Q0VC89
Q0VCA3
Q0VCK5
Q0VCX2
Q0VCY1
Q148D5
Q148H0
Q148J4
Q148L0
Q148N0
Q17QL5
Q17QQ3
Q17QU4
Q1JQ97
Q24JY1
Q24JZ4
Q27965
Q27975
Q27979
Q27991
Q28030
Q28139
Q28139-2
Q28175
Q28181
Q28851
Q29441
Q29455
Q29455-2
Q29465
Q29RK1
Q29RK2
Q29RV1
Q2HJ26
Q2HJ55
Q2HJ60
Q2HJ92
Q2HJ94
Q2HJ97
Q2HJF8
Q08DS7
Q08E32
Q08E34
Q08E45
Q0II87
Q0IIG5
Q0IIG7
Q0IIG8
Q0IIL1
Q0V8E7
Q0VC89
Q0VCV6
Q0VCX2
Q0VCY1
Q0VD07
Q148D3
Q148D5
Q148H0
Q148L0
Q148N0
Q17QL5
Q17QQ3
Q17QS4
Q17QW3
Q1JQ97
Q1LZH1
Q1RMT5
Q24JY1
Q24JY6
Q24JZ4
Q27955
Q27965
Q27975
Q27979
Q27991
Q28030
Q28056
Q28139
Q28139-2
Q28175
Q28181
Q29397
Q29441
Q29455
Q29RK1
Q32LP4
Q32PB9
Q32PD5
Q3MHE8
Q3MHJ9
Q3MHP2
Q3MHW6
Q3MIC0
Q3SWZ3
Q3SZ00
Q3SZ13
Q3SZ62
Q3SZ86
Q3SZC6
Q3SZV3
Q3T001
Q3T067
Q3T087
Q3T0P6
Q3T0W9
Q3T0X6
Q3T145
Q3T149
Q3T160
Q3T165
Q3ZBD7
Q3ZBG1
Q3ZBI7
Q3ZBL4
Q3ZBU2
Q3ZBX0
Q3ZBY4
Q3ZCH0
Q3ZCK2
Q3ZKN0
Q3ZRW9
Q4PJK1
Q56JV9
Q56JX5
Q56JX8
Q56JZ1
Q58DQ3
Q58DR7
Q58DT1
Q58DW0

Q2HJH2
Q2KHX4
Q2KI07
Q2KII5
Q2KJD0
Q2KJG3
Q2KJI7
Q2M2T1
Q2NKY8
Q2T9V8
Q2TA40
Q2TBG5
Q2TBQ5
Q2YDF6
Q32LA7
Q32LG3
Q32LG5
Q32LL2
Q32LP4
Q32PA1
Q32PB9
Q32PD5
Q32S29
Q3MHM7
Q3MHP2
Q3MHW6
Q3MIC0
Q3SWX4
Q3SWY9
Q3SWZ3
Q3SX47
Q3SYR2
Q3SYR7
Q3SZ00
Q3SZ62
Q3SZ86
Q3SZ90
Q3SZI6
Q3SZQ6
Q3T003
Q3T025
Q3T040
Q3T076
Q3T087
Q3T0B6
Q29RK2
Q29RV1
Q29S11
Q2HJ60
Q2HJ86
Q2HJ92
Q2HJ94
Q2HJ97
Q2HJH2
Q2KJ64
Q2KJD0
Q2KJG3
Q2KJH5
Q2KJI7
Q2M2S4
Q2NKS2
Q2TBM9
Q2TBQ5
Q2TBW6
Q32LG3
Q32LG5
Q32LP4
Q32PB9
Q32PD5
Q3MHP2
Q3MHW6
Q3MIC0
Q3SWZ3
Q3SYR2
Q3SYR7
Q3SZ00
Q3SZ13
Q3SZ47
Q3SZ62
Q3SZC6
Q3SZF2
Q3SZQ6
Q3SZV6
Q3T001
Q3T054
Q3T067
Q3T087
Q3T0D5
Q3T0L7
Q3T0P6
Q58DW5
Q58HC3
Q5E956
Q5E958
Q5E995
Q5E9A1
Q5E9B1
Q5E9E6
Q5E9F1
Q5E9F8
Q5E9M8
Q5EA61
Q5EAD6
Q5W5U3
Q66LN0
Q6B856
Q76LV1
Q76LV2
Q7YRW9
Q8MJG0
Q8WN91
Q95114
Q95140
Q95M18
Q9BGI7
Q9MZ13
Q9N126
Q9N179
Q9TTK8
Q9XSJ4
V6F7T1

Q3T0D5
Q3T0F5
Q3T0L7
Q3T0P6
Q3T0Q4
Q3T0R1
Q3T0S6
Q3T0U1
Q3T0U2
Q3T0U5
Q3T0W9
Q3T0X6
Q3T145
Q3T165
Q3T168
Q3T169
Q3T171
Q3ZBD7
Q3ZBG1
Q3ZBH5
Q3ZBL4
Q3ZBU2
Q3ZBU7
Q3ZBV2
Q3ZBV8
Q3ZBX0
Q3ZBY4
Q3ZC13
Q3ZCD7
Q3ZCH0
Q3ZCK2
Q3ZRW9
Q56JV9
Q56JX3
Q56JX5
Q56JX8
Q56JY1
Q56JZ1
Q56K03
Q58DE5
Q58DG6
Q58DG6-2
Q58DQ3
Q58DQ5
Q58DR7
Q3T0S6
Q3T0U2
Q3T0U5
Q3T0W9
Q3T0X6
Q3T145
Q3T149
Q3T160
Q3T165
Q3T169
Q3ZBD7
Q3ZBG1
Q3ZBI7
Q3ZBL4
Q3ZBU2
Q3ZBU7
Q3ZBX0
Q3ZBY4
Q3ZC09
Q3ZC50
Q3ZCD7
Q3ZCH0
Q3ZCK2
Q3ZKN0
Q56JV9
Q56JX3
Q56JX5
Q56JX8
Q56JZ1
Q56K03
Q58DG6
Q58DG6-2
Q58DQ3
Q58DS9
Q58DT1
Q58DW0
Q58DW5
Q59HJ6
Q5E956
Q5E958
Q5E9A1
Q5E9B1
Q5E9D3
Q5E9E2
Q5E9E6

Q58DS9	Q5E9F1
Q58DT1	Q5E9I6
Q58DW0	Q5E9M8
Q58DW5	Q5EAD6
Q5E954	Q5W5U3
Q5E958	Q66LN0
Q5E973	Q76LV1
Q5E988	Q76LV2
Q5E993	Q861S4
Q5E995	Q865S1
Q5E9A3	Q8MJ05
Q5E9B1	Q8MJG0
Q5E9D3	Q8MJG1
Q5E9E6	Q8SPJ1
Q5E9F1	Q8WN91
Q5E9M8	Q95140
Q5EA61	Q95M18
Q5EAD6	Q95MP1
Q5W5U3	Q9BGI7
Q6B856	Q9N126
Q6B860	Q9N179
Q6Q137	Q9TTK8
Q76LV1	Q9XSJ4
Q76LV2	V6F7T1
Q7JAT3	
Q861S4	
Q8MJ05	
Q8MJG0	
Q8MJN0	
Q8WMV0	
Q8WN91	
Q95140	
Q95KV7	
Q95M18	
Q95MP1	
Q9BGI0	
Q9BGI7	
Q9N0H5	
Q9N126	
Q9TTK8	
Q9XSI3	
Q9XSJ4	
V6F7T1	

Table 10: Mass Spectrometry Identification Data

8 Acknowledgments

Ohne Unterstützung wäre dieser Ausflug in die Unwägbarkeiten der Wissenschaft ein Albtraum gewesen – vielen Dank and alle, die mir eine lehrreiche und unterhaltsame Zeit im Labor und außerhalb der Arbeit beschert haben!

Zuerst danke ich Prof. Dr. Elmar Behrmann mich in Zeiten der Not in seiner Gruppe willkommen zu heißen und mir ein gleichermaßen herausforderndes und inspirierendes Projekt zu überlassen.

Außerdem bedanke ich mich bei Prof. Dr. Günter Schwarz und Prof. Dr. Stephanie Kath-Schorr für ihr Engagement in meiner Prüfungskommission und die Bewertung meiner Arbeit.

Prof. Dr. U. Benjamin Kaupp danke ich für konstruktive Gespräche nach denen ich stets motiviert und inspiriert war.

Für Anleitung und Unterstützung in allen Bereichen der Elektronenmikroskpie und das entgegengebrachtes Vertrauen danke ich Dr. Stephan Irsen. Auch allen Mitgliedern der EMA, die wissenschaftlichen Support und Menschlichkeit wunderbar vereinen, möchte ich herzlich danken.

Ein großer Dank gebührt Mandy Rettel, die mir Tatkräftig und bei meinen unendlichen Fragen zur Massenspektrometrie geduldig und kompetent geholfen hat.

Dr. Gayathri Jeyasankar hat mich durch die Höhen und Tiefen des Projekes begleitet und durch unschätzbaren Beitrag und geduldige Korrektur meine Arbeit zweifelsohne aufgewertet. Vielen Dank für gemeinsam verbrachte Zeit, egal ob im Labor oder den zahlreichen Aktivitäten außerhalb.

Allen Mitgligern der Arbeitsgruppe und des Institutes – vielen Dank für das Arbeitsklima und Hilfsbereitschaft. Insbesondere Alexandra Schneider hat dieses Projekt bereichert und verdient ausdrücklichen Dank. Aber auch all die anderen Momente sind wertvoll für mich – egal ob Badminton, Bouldern, Klettern, Grillen, Ausgehen, Lachen, im Garten sitzen, Wandern, Spiele spielen, gemeinsame Mittagspausen oder Zeit “in the air” verbringen – vielen Dank an euch alle.

Nils und seine kleine Familie haben mir stehts Geborgenheit gegeben – für deine Freundschaft bin ich außerordentlich dankbar. Auch allen anderen Freunden die mich immer mit offenen Armen empfangen oder zu einer nötigen Pause überredet haben danke ich herzlich.

Und schließlich gilt ein besonderer Dank meiner Familie die stehts interessiert und liebevoll an meiner Seite steht.